

**TWO DIMENSIONAL DISPLACEMENT OF OIL BY GAS AND  
SURFACTANT SOLUTION UNDER FOAMING CONDITIONS**

**Supri TR-58**

**By**

**Syed Mohammad Mahmood and W.E. Brigham  
Stanford University Petroleum Research Institute  
Stanford, California 94305-4042**

**H.J. Lechtenberg, *Technical Project Officer*  
San Francisco Operations Office  
Fossil, Geothermal and Solar Division  
1333 Broadway  
Oakland, California 94612**

**Date published--June 1987**

**Work Performed for the Department of Energy  
Under Contract No. DE-AC03-81SF11564**

**UNITED STATES DEPARTMENT OF ENERGY**

## TABLE OF CONTENTS

	<i>Page</i>
List of Tables .....	iv
List of Figures .....	v
Acknowledgments .....	vi
Abstract .....	vii
<b>1. INTRODUCTION AND RESEARCH OBJECTIVES .....</b>	<b>1</b>
1.1 Introduction.....	1
1.2 Research Objectives.....	3
<b>2. LITERATURE REVIEW .....</b>	<b>4</b>
2.1 Rheology and Factors Affecting It .....	4
2.2 Foam Flow Mechanisms .....	8
2.3 Oil Recovery by Foam Drive .....	9
2.4 Selection of Injection Method.....	12
2.5 Darcy's Law and its Limitations for Foam Flow .....	13
2.6 Mathematical Description of Foam Flow .....	18
<b>3. DESCRIPTION OF THE APPARATUS .....</b>	<b>24</b>
3.1 Important Design Features.....	24
3.2 Description of the Coreholder.....	26
3.3 Experimental Procedure .....	37
<b>4. QUALITATIVE ANALYSIS OF FOAM DISPLACEMENT .....</b>	<b>39</b>
4.1 Definition of Foam .....	39
4.2 Effect of Operating Conditions on Foam Flow .....	42
4.3 Frontal Behavior and Recovery .....	46
4.4 Slug Design .....	54
<b>5. MATHEMATICAL FORMULATIONS FOR RECOVERY AND PRESSURE DROP ..</b>	<b>63</b>
5.1 Onset of Foam Generation.....	63
5.2 Description of the Combination-Drive Model .....	66
5.3 Recovery for Combination-Drive Displacement .....	67
5.4 Pressure History for Combination-Drive Displacement.....	83
5.5 Recovery for Displacement other than Combination-Drive.....	88
<b>6. RESULTS AND DISCUSSION .....</b>	<b>91</b>
6.1 Rheology of Foam .....	91
6.2 Scaled-Model Studies .....	93
6.3 Effect of Mode of Injection .....	99
6.4 Effect of Mobility Ratios .....	107
6.5 Effect of Surfactant Concentration .....	113
6.6 Effect of Injection Rate .....	117
6.7 Effect of Gas/Surfactant Solution Volume Ratio .....	123
6.8 Gravity-Dominated Displacement with a Long Shut-in .....	128
6.9 Pressure History Matching.....	128
<b>7. CONCLUSIONS AND RECOMMENDATIONS .....</b>	<b>139</b>
7.1 Conclusions .....	139
7.2 Recommendations .....	140
<b>8. NOMENCLATURE.....</b>	<b>141</b>
<b>9. REFERENCES .....</b>	<b>142</b>
<b>APPENDICES .....</b>	<b>151</b>
A: Analytical Solution of the Recovery Equation .....	151
B: Application of Scaling and Modeling Laws .....	153
C: Operational Details of Flow Lines Used in the Glass Sandpack.....	162

## LIST OF TABLES

	<i>Page</i>
2.1 A Survey of the Rheological Behavior Reported in Literature .....	5
2.2 A Survey of Flow Mechanisms Reported in the Literature.....	10
2.3 Core Permeabilities for Newtonian Macro-Emulsions.....	16
3.1 Basic Sandpack Parameters .....	28
4.1 Proposed Classification of Foam .....	40
4.2 Required Conditions for Different Flow Mechanisms.....	43
6.1 Run #8. Operating Conditions and Predictive Equations for Single Slug of Surfactant Solution Followed by Gas .....	100
6.2 Run #6. Operating Conditions for Alternate Slugs of Gas and Surfactant Solution.....	103
6.3 Run #10, Operating Conditions and Predictive Equations for Preformed Foam Injection.....	106
6.4 Run #9. Operating Conditions and Predictive Equations for Simultaneous Injection of Gas and Surfactant Solution.....	108
6.5 Run #11, Operating Conditions and Predictive Equations for Favorable Mobility Ratio Between Oil and Surfactant Solution .....	109
6.6 Run #13, Operating Conditions and Predictive Equation for Viscous-Dominated Surfactant Solution Front .....	111
6.7 Run #16, Operating Conditions for Low Concentration Displacement in which Surfactant Concentration was near CMC .....	114
6.8 Run #17, Operating Conditions for Low Concentration Displacement in which Surfactant Concentration was Much Below CMC .....	115
6.9 Run #20, Operating Conditions and Predictive Equations for Displacement in which Surfactant Concentration was Slightly Higher Than CM .....	118
6.10 Run #21, Operating Conditions and Predictive Equations for Displacement in which Surfactant Concentration was Quite Higher Than CMC .....	119
6.11 Run #19, Operating Conditions and Predictive Equations for Surfactant Solution Rate of 24 cm <sup>3</sup> /min .....	120
6.12 Run #18, Operating Conditions and Predictive Equations for Surfactant Solution Rate of 124 cm <sup>3</sup> /min .....	121
6.13 Run #14, Operating Conditions and Predictive Equations for High Gas to Surfactant Solution Volumetric Ratio .....	125
6.14 Run #12, Operating Conditions and Predictive Equations for Variable Gas to Surfactant Solution Volumetric Ratio .....	126
6.15 Run #15, Operating Conditions and Predictive Equations for Gravity-Dominated Displacement with Long Shut-in .....	129

## LIST OF FIGURES

	Page
2.1 Pressure-Flow Rate Characteristics of Work Hardened Emulsions .....	17
2.2 Effect of Shear <del>Stress</del> on Slip Coefficient.....	19
3.1 Schematic Diagram of Two-Dimensional Sandpack .....	27
3.2 Details of the Two-Dimensional Glass Sandpack Vertical Cross <del>Section</del> .....	29
3.3 Details of the Two-Dimensional Glass Sandpack: Horizontal Cross Section .....	30
3.4 Details of the Two-Dimensional <del>Glass</del> Sandpack: Front and Back Views .....	31
3.5 Bolt-Tightening Sequence.....	31
4.1 The Classification of Foam on the Basis of Physical Appearance .....	41
4.2 Idealized Frontal Behavior of Linear Oil Displacement by Gadsurfactant Solution under Partially Foaming Conditions.....	47
4.3 Idealized Frontal Behavior of a Combination-Drive Displacement .....	49
4.4 Idealized Pressure Profiles of Different Zones for a Combination-Drive <del>Floo</del> .....	49
4.5 An Idealized Diagram for a Run with Favorable Mobility Ratio Between Surfactant Solution and <del>Oil</del> .....	51
4.6 Effect of Injection Rate on Frontal Behavior of Surfactant Solution.....	51
4.7 Effect of Location of Injection and Production Interval for <del>the</del> Simultaneous Injection of Gas and Surfactant Solutio.....	52
4.8 Effect of Surfactant Concentration on Frontal Behavior of Gas and Surfactant Solution .....	53
4.9 Effect of Gadsurfactant Solution Volume <del>ratio</del> on Frontal Behavior .....	55
4.10 Idealized Front Profiles for Alternate Slug Injection: Large Slugs .....	56
4.11 Idealized Front Profiles for Alternate Slug Injection: Small Slugs .....	56
4.12 <del>An</del> Idealized Diagram of Front Profiles During <del>Preformed</del> Foam Injection .....	58
4.13 Idealized Front Profiles for Different Stages of a Typical Gadsurfactant Solution Simultaneous Injection .....	60
5.1 Effect of Surfactant concentration on <del>the</del> Onset of Foam Generation .....	65
5.2 Effect of Surfactant Solution Rate on the Onset of Foam Generation .....	65
5.3 Front Profiles of a Combination-Drive Displacement During Stage III .....	74
5.4 Enlarged View of the Surfactant Tongue at <del>the</del> Cross-section Encircled in Fig. 5.3 ....	74
6.1 Effect of Time and <del>Shear</del> History for a Two-Dimensional <del>Flow</del> .....	92
6.2 Effect of Rate on <del>the</del> Effective Mobility of Two-Dimensional Flow .....	94
6.3 Typical Performance Chart Based on Bond Number .....	96
6.4 Typical Performance Chart Based on Capillary Number .....	97
6.5 Typical Performance Chart Based on Oil Viscosity <del>Alone</del> .....	98
6.6 Comparison of Predicted and Experimental Recovery for Single <del>slug</del> of Surfactant Solution Followed by Gas .....	102
6.7 Experimental Recovery Data for Alternate Slugs of Gas and Surfactant Solution .....	102
6.8 Comparison of Predicted and Experimental Recovery for Preformed Foam Injection.....	105
6.9 Comparison of Predicted and Experimental Recovery for Simultaneous Injection of Gas <del>and</del> Surfactant Solution.....	105
6.10 Comparison of Predicted and Experimental Recovery for Favorable Mobility Ratio Between Oil and Surfactant Solution .....	112
6.11 Comparison of Predicted and Experimental Recovery for Viscous-Dominated Surfactant Solution Front .....	112
6.12 Experimental Recovery Data for a Low Concentration Displacement in which Surfactant Concentration was at CMC .....	116

6.13	Experimental Recovery Data for a Low Concentration Displacement in which Surfactant Concentration was Much Below CMC .....	.116
6.14	Comparison of Predicted and Experimental Recovery for Displacement in which Surfactant Concentration was Slightly Higher Than CMC .....	129
6.15	Comparison of Predicted and Experimental Recovery for Displacement in which Surfactant Concentration was Quite Higher Than CMC .....	122
<del>6.16</del>	<del>Comparison of Predicted and Experimental Recovery</del> Favorable Mobility Ratio Between Oil and Surfactant Solution.....	135
6.26	Comparison of Predicted and Experimental Pressure Drops for Viscous-Dominated Surfactant Solution Front .....	136
6.27	Comparison of Predicted and Experimental Pressure Drops for a Low Concentration Displacement in which Surfactant Concentration was at CMC .....	136
6.28	Comparison of Predicted and Experimental Pressure Drops for a Low Conc. Displacement in which Sufactant Concentration was much below CMC .....	138
6.29	Comparison of Predicted and Experimental Pressure Drops for Gravity-Dominated Displacement with Long Shut-in .....	.138
6.30	Comparison of Predicted and Experimental Pressure Drops for High Gas to Surfactant Solution Volumetric Ratio.....	139
6.31	Comparison of Predicted and Experimental Pressure Drops for Variable Gas to Surfactant Solution Volumetric Ratio .....	139

#### ACKNOWLEDGMENTS

The author gratefully acknowledges the financial support received from Stanford University Petroleum Research Institute, under DOE contract DEACO-381SF-11564.

## ABSTRACT

Gas displacement in the presence of surfactant under foaming conditions has been shown to enhance oil recovery. But it is a complex process because surface phenomenon is involved in it. The lack of understanding is a barrier for its commercial-scale testing and application.

A major difficulty in analyzing the production performance of such displacement is in deciding whether to treat gas and surfactant solution as a two phase mixture or as a single phase homogeneous fluid (foam). Another uncertainty is in determining the rheological behavior of gas and surfactant solution mixture flowing in the porous media. The problem is further complicated if two-dimensional flow is taking place, since the frontal geometry may also influence the performance significantly.

This study was performed to investigate these problems. Flow was visually observed through a two-dimensional (x,z) sandpack of four feet length and one foot height, having 14 darcies permeability and 35% porosity. Since analytical treatment of the flow and oil recovery data has not been possible, the objectives were to get a basic understanding of the flow behavior under foaming conditions, devise conceptual models with the help of flow processes seen, and then analyze the data quantitatively using semi-analytical approaches. A model meeting these objectives was developed and successfully matched with experimental data obtained in the two-dimensional sandpack.

## 1. INTRODUCTION AND RESEARCH OBJECTIVES

The various techniques used for increasing oil production from reservoirs are briefly examined in this section. The potential of foam drive is also discussed in relation to these methods. The research objectives of this study are also described.

### 1.1. INTRODUCTION

The producing life of a typical oil reservoir goes through several changes. In the early life the reservoir is being depleted by its own energy, and displacement is due to the difference in pressure that exists between the higher reservoir pressure and the lower wellhead pressure. As the reservoir is depleted, the pressure declines and so does the production rate. This recovery is called primary recovery; it is usually only a small fraction of the total oil in place. The average primary recovery is in the range of 5-25% of the total oil in place.

Additional recovery is usually obtained by providing mechanical energy to the reservoir, generally in the form of gas or water injection. This is done by converting some of the producing wells to injection wells, or drilling new wells for injection. This technique is called secondary recovery and often recovers approximately 5-25% more oil. The most widely applied secondary recovery technique is waterflooding. However, there are instances when gas injection is considered more favorable; e.g., in high dip reservoirs where gravity forces may help in displacement, or in reservoirs with such low permeability that water is difficult to inject.

Secondary recovery techniques are not always efficient because of the incompatibilities between the injected fluid and reservoir oil properties, such as the density and mobility ( $k/\mu$ ) differences. The density difference may tend to segregate the fluids, forming gravity tongues, whereas the high mobility of injected fluid may cause it to by-pass the reservoir oil through low-resistance channels present in most reservoirs.

The movement of the front between injected fluid and oil is governed by the ratio of their mobilities, and by the ratios of viscous, gravity and capillary forces induced by the fluid injection. When gravity forces are dominant as compared to viscous forces, gravity segregation takes place. If viscous forces are much higher than capillary forces, channeling and fingering may be severe. Both fingering and gravity segregation are also promoted by higher mobility ratios.

Gas drives are characterized by high gravity forces and high mobility ratios since gas has lower density and viscosity by an order of magnitude compared to reservoir oils. Thus gas drives are prone to gravity segregation, channeling and fingering, which cause early breakthrough with much of the oil unswept behind the displacing front.

Waterflooding is also affected by channeling and fingering, especially in heavy oil reservoirs, where oil has considerably lower mobility than the water. The displacement may be improved to some extent by lowering the injection rates, and thus adjusting the viscous to capillary force ratio, but this is not usually very effective. The capillary forces cannot be easily increased in a reservoir, and similarly, the gravity forces can not be easily adjusted. The parameter which is the easiest to change is the mobility ratio.

Reduction in mobility is important in a sense that vertical sweep efficiency is determined by the stability of the boundary between injected fluid and oil (front). In a stable displacement process, the front may have a piston-like profile and theoretically all recoverable fluids could be recovered. In a nonstable displacement, the front is distorted by fingers and channels, and also by gravity segregation if the fluid densities are dissimilar as well. Once fingers are formed, they tend to grow in size, and early in the injection process they reach the producing well and break through. After breakthrough of the injected fluids, a less resistant passage is created and most of the injected fluid flows without effectively contributing to further oil recovery. The oil recovery at breakthrough is a direct function of the mobility ratio at the front.

Several techniques are currently used to improve front profiles by reducing the mobility ratio. These methods increase the viscosity of the injected fluid, decrease the viscosity of reservoir oil, or change the effective permeability of the reservoir. These techniques are called tertiary or enhanced oil recovery processes, and include steam-drives, fire-flooding, polymer flooding, alternating water and gas slugs (WAG), and simultaneous injection of water with gas to reduce the gas permeability.

There is another class of enhanced oil recovery process in which the interfacial tension is lowered (low-tension or micellar floods) or reduced to zero (miscible-flooding) so that the entrapped oil droplets may be released easily, or mass transfer between phases can help in oil production. While the earlier class of enhanced oil recovery processes increases oil recovery by improving the front profile and obtaining a greater invaded area, the latter class obtains high recovery due to better scavenging at the pore level. The majority of the enhanced oil recovery processes employ more than one aspect of these recovery improvement mechanisms.

A common reservoir practice is to apply tertiary or enhanced recovery techniques only after oil production by secondary recovery methods has become uneconomical. This practice is due to economic reasons, since the enhanced recovery techniques tend to be expensive. The application of enhanced recovery techniques earlier in the life of flood can generally yield higher ultimate recovery. When started at a later stage, the fluid distribution in the reservoir has become so uneven that full exploitation of enhanced recovery techniques becomes difficult. The injected fluids tend to invade the already swept zone causing an uneven distribution of the heat or chemicals.

The enhanced oil recovery techniques currently employed are far from satisfactory, and better methods are constantly being sought. The possibility of using a combination of water, surfactant solution and gas as enhanced recovery fluids under foaming conditions is currently under active investigation in laboratories as well as in field tests.

The use of foam seems promising when one considers its unique physical properties. The apparent viscosity of the foam is usually higher than the viscosities of either of its constituents, and thus it has a lower mobility ratio than gas and water. Foam has also shown other interesting behavior in laboratory experiments; it can totally block the displacement, or it can selectively block flow through the gas zone, making it a useful driving fluid. The control of mobility ratio alone could theoretically eliminate the fingering problem, but it may only partially improve channeling for many reservoirs in which permeability variation is high. Because of selective blocking, foam would appear to have potential for this improvement. In the injection of steam or gas, often the displacement takes place through tongues or fingers caused by gravity segregation. The reduced mobility of foam can reduce these instabilities and thereby can considerably increase the recovery.

Despite experimental and pilot demonstrations that show its potential, the foam drive process has not consistently been found to improve recovery. Some laboratory experiments

have demonstrated higher recoveries attributed to foam, but others have demonstrated lower recoveries. One observation made by almost all investigators is the dramatic reduction in calculated mobility when foam is introduced or generated in-situ, even though there is some disagreement as to how foam accomplishes this reduction. The field projects conducted using surfactant-gas mixtures have shown increased recovery, but have generally been inconclusive in explaining the flow behavior.

Much of the petroleum engineering research on foam rheology and the mechanism of foam flow through porous media is somewhat controversial due to differing conclusions drawn. The controversies come from the difficulties in applying the scaling laws to laboratory models due to the lack of basic equations describing foam flow. Whereas the physical properties of foam not confined in pores are well-described, foam flow through porous media is not well understood. Consequently, foam flooding has not gained as much popularity as perhaps it could have.

The expectation of higher recoveries whenever a surfactant is added to a gas/water drive has not always proven to be true. The presence of a surfactant in a porous medium can also have some harmful effects, e.g. it can reduce the magnitude of capillary forces. For flow dominated by capillary forces, this may increase channeling and gravity segregation, which can reduce both vertical and area coverage if the surfactant slug is not well designed. In addition, the surfactant may cause in-situ emulsification which could leave more residual oil behind.

The commonly employed methods to predict recovery are based on the Buckley-Leverett or Dietz theories. Both of these theories assume the injection of a single phase homogeneous fluid, whereas foam does not always meet this criterion. No predictive methods have been developed to estimate the production performance of foam flooding.

## 1.2. RESEARCH OBJECTIVES

The main directions and objectives of this research are as follows. From the inconsistent results in the literature, it is clear that the mechanisms of foam flow in porous media are not well understood. Thus it appeared necessary to operate experiments in a model in which the various flowing fluids could be visually tracked. Also, since gravity forces often play a dominant role in the flow of gases and liquids, it was felt that the model should be similar to an  $x-z$  slice of a reservoir so that the interplay between gravity and other forces could be seen.

The goal was to use these visual observations as guides concerning the nature of the flow in such a system, and from these observations to develop conceptual flow models, and then try to match them with the observed behavior. If such conceptual models are appropriate, both the recovery and the pressure drop/flow rate behavior of the physical model could be matched under various operating conditions. As will be seen later, this goal was accomplished.

This study is far from complete since it was limited in scope to a specific flow geometry and specific fluids. It is hoped, however, that this study will give some insight into the complications involved in foam flooding, and will provide a solid foundation for future research and more comprehensive prediction methods.

## 2 LITERATURE REVIEW

The flow of gas and water in the presence of surface active agents is complex, since these fluids can generate foam whose behavior is non-Newtonian. The rheology of foam can not be adequately described by a single property called Viscosity. Unlike simple fluids, the rheology of foam has been found to be a function of several parameters. The generation of foam itself is conditional on operating conditions and foam generation may sometimes be delayed or may never occur. This complex behavior is examined in the following discussion where many pertinent studies on foam for oil recovery are reviewed. This literature review, however, is not meant to be complete, since several literature and state-of-technology reviews have been recently published (Zirritz and Rancel, 1983; Marsden, 1986), and the interested reader can refer to these publications.

### 21. RHEOLOGY AND FACTORS AFFECTING IT

The non-Newtonian nature of foam has been known for a long time, but perhaps the first published account traces back to Sibree (1943), where he reported the viscosity of foam to be much higher than either of its components, and found this viscosity to be shear rate dependent.

The early work (e.g., Plateau, 1869) on physical properties of foam was performed mainly by surface chemists. Foam has been used since the late 1950's for petroleum operations such as drilling and workovers, but the idea of using foam as a recovery fluid was first published by Bond and Holbrook (1958) in which it was suggested that foam generated in porous media will improve the mobility ratio of gas drives. This idea was soon followed by Fried (1961), with an extensive investigation on the physical properties of foam, especially foam rheology. He reported high viscosities measured in both rotational and static capillary-tube viscometers.

In the following few years, many petroleum engineering studies were performed with the goal of understanding this unique fluid for recovery operations. Most of these studies started with basic viscometry in simplified systems. Viscosity values of foam were measured by many investigators during this stage by using standard viscometers such as Fann V-G meters and capillary tubes. Some of the findings reported during this stage confirmed what surface chemists had described in their fundamental studies many decades earlier.

The viscosity values for foam flowing through porous media were rarely reported, probably because it was not clearly understood how to measure Viscosity during core flooding. Marsden and Khan (1966) assumed that Darcy's law is applicable to foam flow, and thus calculated the effective mobility,  $k_e/\mu$ , of the foam using this law. The viscosity was then inferred using the experimentally determined effective permeability values. Due to the uncertainties involved in indirect measurements, they termed this viscosity "apparent viscosity;" this terminology has been used commonly in the literature to mean Darcy's law derived viscosity, and will also be used in the same context in this section.

Early studies on foam rheology assumed that foam could be described by one of the rheological models used for other non-Newtonian fluids, and the investigators tended to fit their results to one of these models. As a result, several rheological models were proposed which are listed in Table 2.1.

TABLE 2.1

A Survey *Of* The Rheological Behavior Reponed *In Literature*

Authors	Flow Medium	Rheology
Sibree (1943)	viscometer	Pseudoplastic
Wise (1951)	half in. dia. pipe	"
Stenuf (1953)	half in. dia. pipe	"
Fried (1961)	capillary viscometer	"
Khan (1965)	porous media and Fann rheometer	"
Raza and Marsden (1967)	glass tubes	"
David and Marsden (1969)	capillary tubes	"
David and Marsden (1969)	<del>short</del> porous medium	"
Amiyan (1971)	rotational viscometer	"
Aizad and Okandan (1977)	sandpack	"
Holbrook et al. (1981)	capillary tubes	"
Patton et al. (1983)	capillary tubes	"
Ali et al. (1985)	2.7 cm dia. sandpack	"
Penny and Blackman (1943)	two parallel plates	Bingham Plastic
Evgenev and Turnier (1969)	2 mm glass beads	"
Evgenev and Turnier (1969)	0.7 mm glass tubes	"
David (1969)	capillary tubes	"
Mitchel (1970)	capillary tubes	"
Blauer et al. (1974)	capillary viscometer	"
Blauer et al. (1974)	field tubular data	"
Starkey (1975)	pipes	"
Evgenev and Turnier (1969)	2 mm glass beads	Time-dependent
Evgenev and Turnier (1969)	0.7 mm glass tubes	Time-dependent
Evgenev and Turnier (1969)	2 mm. glass beads	Pseudo-solid
Fried (1961)	capillary viscometer	Plastic
Richman (1966)	rotational viscometer	Plastic
Grove (1951)	drag viscometer	Newtonian

Whereas numerous models have **been** proposed, the two most commonly used were the pseudoplastic (power law) and Bingham fluid models. Marsden and Khan (1966) realized **this** disagreement between the independent studies and suggested **the** dual nature of foam, *i.e.* **some** foams behave like a pseudoplastic while others behave like a Bingham Plastic, but also indicated that **there is no known reason** for **this** dual behavior.

However, some earlier investigators had observed foam to behave like a complex fluid **which** changes its rheological behavior at some critical point. Sibree (1943) observed pseudo-plastic behavior changing to Newtonian at higher shear rates. **In** a **concurrent** study, Penny and Blackman (1943) observed just the opposite, *i.e.*, at low shear rates the behavior was Newtonian which changed to a plug-like flow at higher shear. Rug-type flow is typically characterized by pseudoplastic behavior. Later, Raza and Marsden (1967) **also** observed similar behavior.

The next stage could be considered a "descriptive stage," when **the** investigators realized that foam flow through **porous** medium is complex, and could not be adequately described by **known** rheological models. Raza (1970) attempted to resolve **this** controversy and performed exhaustive laboratory **tests**, but the results could not be described either in **terms** of apparent viscosity or any other **known** method, and he declared that the existing theories explaining foam rheology **are** **inadequate**.

**The** role of threshold pressure, which is related to yield value, **has not been** clearly defined in the literature. Evgenev and Turnier (1969) observed a strong threshold pressure when flowing through both glass **tubes** and unconsolidated sandpacks, and found **this** to **be** time dependent. David and **Marsden** (1969) also found a yield value. They corrected the apparent viscosity values for slip, which reduced the yield values to some **extent**, but the values were still **finite**. **They** found yield value **to be** a function of foam **quality** instead of time, when foam quality is **the** volume percent gas. **This** result is opposite to that found in **an** earlier study (Evgenev and Turnier, 1969). **On** the other hand, the earlier investigators had not noticed the presence of a yield value.

**One** complication found in describing the rheology of foam was its dependence **on** the geometry **and the** dimensions of the medium through which it was flowing. Fried (1961) observed a considerable increase in apparent viscosity of foam with an increase in capillary diameter. Raza and Marsden (1967) reported similar **results** in glass tubes, but surmised that **this** might have been due to slip. Later David and Marsden (1969) corrected for slippage, but the corrected apparent viscosities still increased with an increase in diameter. Khan (1965) observed **that** the apparent viscosities obtained from a **Fann** V-G meter, Bendix Ultra-Viscoson and capillary tube viscometers were considerably different for the same foam under similar conditions. **The** same differing behavior was found for porous media, **as** Marsden and Khan (1966) observed an apparent viscosity which was dependent **on the** permeability.

Another **uncertainty** in describing foam is the disagreement found **in the** literature in deciding which parameters **are** important and how they affect the foam rheology. The two parameters which **are** widely believed **to affect the** behavior **are** the quality and the surfactant concentration; but again how they **affect** it, or why they affect it, is not clearly described in the literature. The observations made by different investigators are outlined in the following two paragraphs..

Grove (1951) reported a fifteen-fold increase in viscosity with less **than** three-fold reduction in foam density (inverse of foam quality). Fried (1961) reported similar behavior for flow through porous media. Other investigators also observed similar behavior such **as** Marsden and Khan (1966), Abernathy and Eerligh (1966), Raza and Marsden (1967), Aizad and Okandan

(1977), and Holbrook *et al.* (1981). However, when David and Marsden (1969) corrected for the slippage, the apparent viscosity for their study became independent of quality. Minssieux (1974) also studied the effect of quality and found it to be just the opposite when oil is present in the porous medium, *i.e.* the apparent viscosity decreased four times when the quality was increased from 50 to 96%.

Like quality, the role of surfactant concentration is not clearly defined in the literature. Marsden and Khan (1966) and Richman (1966) reported that the apparent viscosity of foam increased with an increase in surfactant concentration. Abernathy and Earlich (1966) observed opposite behavior, *i.e.* the apparent viscosity decreased with an increase in concentration. They also observed a dramatic decrease in mobility, which occurred, according to their estimates, when the bubble size became smaller than the pore openings. Clark (1947) found considerable concentration dependence for some foams and minor dependence for others. Amiyan (1971) observed that a concentration range between 0.5 to 2.0% had only a small effect on foam viscosity. Holcomb *et al.* (1980) also observed similar behavior for four different types of foam, that the role of concentration ceased above around 0.5%. Badalov and Khasaev (1966) concluded that viscosity through capillary viscometers increased with concentration only at high pressures.

The unusually high apparent viscosities of some foams have attracted the attention of many investigators. Fried (1961) explained this on the basis of electrokinetic potential. He observed this phenomenon during foam flow and noticed that it could block the flow completely in some cases. He also discovered that this blockage could be suppressed by using an electrolyte. Later Raza and Marsden (1967) measured the values of streaming potential for foam flowing through tubes and unconsolidated porous media, and also related streaming potential to pressure drop mathematically in terms of important parameters.

Many studies have instead focused on mobility reduction during foam flooding. Bernard and Holm (1970) observed that foam flooding was 99% successful in blocking the flow. Minssieux (1974) observed total blocking in unconsolidated sandpicks of 50 Darcies. Mast (1972) observed in etched glass cells that the flow through portions of the porous network was temporarily blocked which resulted in a decrease in gas permeability. Similar results were obtained by Gangoli and Thudos (1977). It has been claimed that this reduction in mobility could completely stop the flow. This phenomenon has been termed "blockage." Several laboratory experiments have shown that gas flow could be stopped by foam, and the use of foam to stop gas leakage from pipes and reservoirs has indeed shown some success.

It has been further reported that this blockage is selective, *i.e.* foam preferentially blocks high permeability channels. The permeability blockage of Bernard and Holm's (1964) consolidated and unconsolidated porous media in the presence of foam was greater for loose sands. Similar results were observed by Heller (1980) where a one-hundred-fold decrease was reported for higher permeabilities. Smith *et al.* (1969) used two parallel packed columns of different permeabilities and observed that blocking was more significant in a higher permeability pack. Albrecht and Marsden (1970), Sharma *et al.* (1982) and Fried (1961) have reported similar behavior.

To summarize the above discussion, one could say that a single generally accepted theory does not exist which could describe the flow of foam. The several theories presented have been

experimentally supported for specific conditions, but are not universally valid. However, the following observations have been reported by many authors:

- (1) Foam reduces the permeability. This can eventually lead to complete blocking for a given operating pressure.
- (2) The degree of blocking depends on the pore openings or permeability such that blocking is more pronounced for higher permeability. Also the apparent viscosity values inferred from Darcy's law are higher for higher permeability.
- (3) Apparent viscosity values calculated from different types of viscometer are significantly different from each other and sometimes are an order of magnitude different than the ones derived from flow through porous media.
- (4) The duration and history of injection have a pronounced effect on foam rheology under certain conditions.

## 22 FOAM FLOW MECHANISMS

An overview of the literature gives an impression that the description of foam flow is still controversial. An understanding of foam flow through the intricate flow paths of a porous medium is crucial for the advancement of foam technology. This importance has been realized in recent years and a better understanding of foam flow mechanism has been actively sought.

Many theories have been proposed describing the flow mechanism, some of which are based on physical observations during foam flow, and others are logically inferred from production performance. These theories sometimes differ slightly, but in essence can be represented by the following seven behavioral patterns.

- (1) **Bubble Flow:** Foam flows as a homogeneous fluid with gas uniformly dispersed in the surfactant solution. The implicit assumption in this theory is that the size of bubbles is small compared to the pore or capillary constrictions so that the bubbles need not distort when passing through. It is also implicitly assumed that the velocity of the gas is the same as the liquid flow.
- (2) **Intermittent Flow:** Foam flows in such a way that liquid is transported through a continuous network of liquid membranes acting as a free phase, while gas flows as a discontinuous phase through breaking and reforming of bubbles.
- (3) **Plug Flow:** Foam flows as plugs characterized by high shear rates near the boundary between the foam and the conduit (the container).
- (4) **Trapped-Gas Flow:** Foam flows in such a manner that it traps some gas in the porous medium while the remainder flows as a free phase following Darcy's law. The fraction of gas flowing as a continuous phase is generally small compared to the trapped gas saturation.

- (5) **Segregated Flow:** Foam flows only through gas channels carrying a small amount of surfactant solution with it. The majority of the liquid flows through separate channels, the number and distribution of which depend upon liquid saturation; these channels would be the same whether or not surfactant is present or foam is generated. Most of the liquid flows as free phase described by Darcy's law. Nahid (1971) suggested that gas can also be treated by Darcy's law if a correction factor is used for the change in permeability due to foam generation.
- (6) **Membrane Flow:** Foam is generated as lamellae at specific locations in a porous medium which have specific pore constrictions that help in its generation. The foam propagation is conditional to the favorable conditions and the geometry of the pores.
- (7) **Tubular-Channel Flow:** Foam flows through channels consisting of tubular bubbles moving along and extending over several pore spaces. These tubes cause trapping of gas or liquid by making them discontinuous. The volume trapped depends upon the operating conditions and pore geometries.

A survey of the studies supporting these theories is given in Table 2.2. Most of the theories are able to explain the individual observations quite well, but they are not general, and often contradict the observations made by other independent studies.

This point could perhaps be made clear by examples showing the contradictory nature. Gurbanov *et al.* (1970) showed that foam did not penetrate through his linear sandpack column more than a few centimeters. Minssieux (1974) found similar results by X-ray absorption and showed that foam did not penetrate very far into his sandpack. Both of these observations contradict the bubble flow theory. He also observed a uniform saturation throughout the pack and surmised that it could not possibly be bubble flow since in that case the gas saturation should have gradually changed due to the high compressibility and pressure gradients involved. Similarly, Handy (1971) showed by a gas tracer technique that a certain portion of the gas is trapped during flow, and this gas does not participate in the flow process.

Raza (1965) found more than one flow behavior by visual observations of capillary tubes. He was able to identify five distinct flow regimes by changing the quality of foam. Owete (1982) observed most of the previously described seven mechanisms taking place concurrently in different combinations, and the role of each mechanism was influenced by experimental parameters. These observations were made microscopically at different operating conditions through an etched silicon wafer with artificially produced uniform and nonuniform pore openings.

## 23. OIL RECOVERY BY FOAM DRIVE

The notion that a gas drive under foaming conditions will improve the secondary recovery performance of oil displacement was presented by Bond and Holbrook (1958), and was substantiated by extensive investigation of Fried (1961) that demonstrated a superiority of foam drive over any other conventional secondary recovery mechanism. He also claimed that foam drive can be used effectively for tertiary or enhanced recovery as well. In his tests the unconsolidated sandpicks and consolidated cores were saturated with 78 to 850 cp oils and were gas driven, waterflooded or surfactant flooded. Then the foam drive followed which reduced the oil saturation by 44 to 70% of what had been left by secondary methods. His work was comprehensive and convincing enough to become a landmark in the development of foam technology.

**TABLE 2.2**

**A Survey Of Flow Mechanisms Reported In The Literature**

<b>Authors</b>	<b>Flow Medium</b>	<b>Flow Mechanism</b>
Fried (1961)	glass tube sandpack	Bubble flow
Marsden and Khan (1966)	capillary tubes	"
Sharma (1965)	glass beads cell	"
Mast (1972)	etched glass cell	"
Alizad and Okandan (1977)	unc. porous media	"
Fried (1961)	glass tube sandpack	Intermittent flow
Bernard and Holm (1964)	cons. and uncons. p.m.	"
Bernard, et al. (1965)	porous media	"
Holm (1968)	tracers in p.m.	"
Holm (1968)	sand in cap. tube	"
Handy (1971)	tracers in p.m.	"
Mast (1972)	etched glass cell	"
Penny and Blackman (1943)		Plug flow
Fried (1961)	capillary and unc. p.m.	"
Raza and Marsden (1967)	large cap. tubes	"
Hoffer and Rubin (1969)	vertical columns	"
Kolb (1964)		Trapped Gas flow
Bernard and Holm (1964)	porous media	"
Bernard et al. (1965)		"
Nahid (1971)	tracer in p.m.	"
Handy (1971)	tracers in p.m.	"
Mast (1972)	etched glass cell	"
Nahid (1971)	tracer in p.m.	Segregated flow
Bond and Bernard (1966)		"
Minssieux (1974)	porous media	"
Mendez (1975)		"
Sharma (1965)	glass bead cell	Membrane flow
Owete et al. (1982)	etched silicon cell	
Owete et al. (1982)	etched silicon cell	Tubular-channel flow

However, some of the subsequent studies (Wang *et al.*, 1982 and G.C. Wang, 1984) revealed that recovery could be lower in some cases than with conventional methods. This raised another issue, *i.e.* whether or not foam drive increases the oil recovery over conventional methods, and if it does, then to what extent and under what circumstances.

The laboratory studies mentioned here addressed this issue. Bernard (1963) found that, at breakthrough, foam drive was three times more efficient in displacing oil through linear unconsolidated sandpacks than an ordinary gas drive. Bernard, Holm and Jacobs (1965) inferred that foam flooding should recover more oil than waterflooding, at least through a predominantly water-wet system, since foam flooding increases trapped gas saturation which is known to cause an increase in oil recovery. Roszelle (1971) recovered 86% of O.I.P. by foam drive from a 0.187 Darcy core saturated with 7 cp crude and which was already waterflooded. Al-Attar (1976) recovered appreciably more oil from a 0.14 Darcy Berea core as compared to a gas drive by injecting an oil-based foam. This improvement was 19% better in a dipping system than in horizontal tests. Chiang *et al.* (1980) also reported an increase in oil recovery from a two dimensional visual ( $x, z$ ) sandpack which was initially saturated with white mineral oil and residual surfactant solution. A surfactant solution slug (0.2 pore volumes, 1% active) was then injected and was pushed by  $N_2$  to generate foam in-situ. The recovery was doubled over the recovery when the same oil was driven by nitrogen only.

These studies have generally tried to compare the performance of foam drive with gas drive secondary recovery, or have studied the performance of foam drive for tertiary recovery. One of the few studies that directly compare foam's performance with waterflooding is by Aizad and Okandan (1977) who found by displacing oil through unconsolidated porous media that foam flooding is better than waterflooding.

Some studies confirm that foam drive improves recovery over a gas drive, but to a reduced magnitude. Minssieux (1974) observed that the recovery by foam injection is not appreciably greater than a waterflooding, but is definitely greater than a gas drive.

There have even been some studies that find no change or even a lower recovery by foam drives. Kanda and Schechter (1976) reported that the presence of oil adversely affects the foam displacement performance. Wang (1984) observed only slight improvement in oil recovery in most runs but also observed that sometimes a lower recovery was obtained, especially when high surfactant concentrations were used. He attributed this result to the formation of a rigid foam or the presence of emulsions. A more drastic observation was made by Mendez (1975) that a conventional waterflood recovered more oil than did either externally generated or internally generated oil-based foam at any throughput, *e.g.* 15% pore volume more oil was recovered by waterflood at 1.0 pore volume throughput.

Despite numerous successful laboratory tests, the application of foam flooding on a pilot field-test scale was not seriously considered for some time. The first field test was conducted by Union Oil Company in the Siggins Field, Illinois, and the results were published by Holm (1970). The field was shallow and highly permeable with a wide permeability distribution ( $h = 30-50$  ft,  $\mu_o = 8$  cp @ reservoir temperature of  $65^\circ$  F,  $p = 75-200$  psig,  $k = 10-300$  md, with an average permeability of 56-75 md). It was waterflooded before a foam injection test was started. There were two highly permeable channels, each 5 ft thick, one at the center and one near the bottom of the formation. The producing interval was mainly composed of a fine-grained sandstone with several thin shale streaks. A modified ammonium lauryl sulfate solution was injected to generate foam. Concentration of this foaming agent was gradually increased in the aqueous phase. Both cyclic slug injection and preformed foam injection methods were tried in this test. Compressed air was used as the gaseous phase. No effective foam was seen at the producing well below 1% surfactant concentration, but apparent mobilities of gas and

water were reduced to less than half of the original values when foam was believed to have been generated. At least 0.06 pore volumes of the foaming agent had to be injected before lasting mobility control was achieved. Severe channeling of gas to one production well was stopped, and foam caused a more uniform water injection profile and reduced slightly the average water-oil-ratio of the surrounding wells.

In the early 1980's foam flooding in steam drives was field-tested in pilots conducted by Chevron (Ploeg and Duerksen, 1985), the CLD group (Doscher and Hammershaimb, 1981), Corco (Eson *et al.*, 1985), Shell (Dilgren *et al.*, 1982) and Stanford (Brigham *et al.*, 1985), all of them indicating improved recovery. The operators of these tests demonstrated improvement in front profile due to steam diversion which resulted in an increase in oil production rate, reduction in injectivity and reduction in steam-oil-ratio. These pilot field-tests have also been described in detail by Zirritz and Rancel (1983).

During the same time period when foam was under investigation in laboratories of the Western hemisphere, the potential of foam was tested in USSR in a different context. Foam was used to treat high water-cut wells by injecting a surfactant solution followed by gas. On resumption, the production from these treated wells generally showed improvement by reducing water-cut. This treatment was operationally similar to a cyclic steam injection sometimes used to treat wells. These tests have not been described here in detail because the author feels that the few papers translated have been unscientifically selected, showing only successful results; and also the accuracy of translation is doubtful. A chronological description of these tests was given earlier by Mahmood (1983).

#### 2.4. SELECTION OF INJECTION METHOD

Several schemes have been used in the past to inject surfactant solution with gas and production behavior was seen to differ from one technique to another. The following three injection methods have been used by many investigators with slight modifications:

- (1) Slug injection, in which gas and surfactant solution are injected alternately in separate slugs.
- (2) Preformed foam injection, in which foam is generated outside the porous medium and this externally generated foam is injected.
- (3) Simultaneous injection, in which gas and surfactant solution are injected concurrently and foam is expected to generate in-situ.

When the idea of using foam for enhancing oil recovery was first presented by Bond and Holbrook (1958), the use of a single slug of surfactant solution followed by a standard gas drive was recommended. In the following years, many refinements took place which are outlined below.

Raza (1968) introduced the idea of dividing the surfactant solution into several small batches which were alternated with small batches of gas to form a more effective foam. The volume of the batches of gas were very small to avoid foam collapse between the treatments. Root (1971) suggested a similar idea of using alternate slugs of gas and surfactant solution for multiple porosity reservoirs, so that the foam could block the high porosity layers and the recovery of oil could come from low porosity layers. He surmised that this process would be especially useful in reservoirs where much of the oil is in a dense matrix.

Bernard (1969) suggested the injection of a miscible slug between the surfactant solution slug and gas injection to improve the profile. He also reported obtaining high recoveries (64.4%) from an oil saturated Boise core (sandstone) when a foam bank was generated in-situ by surfactant solution and gas injection which was then driven by water-alternated gas slugs (WAG). The alternating slugs of gas and water had a volumetric ratio (WAG ratio) of 5-15 volumes of gas per volume of water.

In the Siggins Field, Illinois field test, Holm (1970) reported that the mobility reduction was not significant when alternate slugs of 0.02 pore volumes were injected, whereas pre-formed foam injection showed promising results. In the other three field tests mentioned earlier, the surfactant solution was injected continuously by Shell (Dilgren *et al.*, 1982); in small alternating slugs by Chevron (Duerksen, 1984); and in three large slugs by SUPRI (Brigham *et al.*, 1984). All three injection schemes showed successful results.

## 25. DARCY'S LAW AND ITS LIMITATIONS FOR FOAM FLOW

Darcy's law is the most commonly used relationship to characterize the flow of fluids through porous media. It is based on the assumption of the flow of nonreactive Newtonian fluids, and thus can not be directly used to describe the flow of non-Newtonian fluids such as foam. However, several attempts have been made in the past to extend this law for foam flow.

The application of Darcy's law for foam flood is examined in the following sub-sections. Its several forms, the implicit assumptions and the complex nature of foam are reviewed. The attempts to describe foam flow by other classical approaches are also mentioned briefly.

### 25.1. Development and Extensions of Darcy's Law

Darcy's law was first formulated empirically (Darcy, 1856) in its integrated form:

$$q = k \frac{A}{\mu} \frac{\Delta p}{L} \quad (2.1)$$

where

$q$  = flow rate,  $\text{cm}^3/\text{s}$

$k$  = permeability, Darcys

$A$  = cross-sectional area,  $\text{cm}^2$

$L$  = core length, cm

$\mu$  = fluid viscosity, cp

$\Delta p$  = pressure drop across the porous medium, atm

This law is valid only if one Newtonian fluid is flowing through a porous medium at flow rates low enough to cause laminar flow. First presented in this simple form as an empirical relationship, this law has since been extended to characterize many other types of flow. It has been done by deriving the fundamental form of the differential equation whose solution is

represented by **Darcy's original** equation. This partial differential equation is:

$$q = - \frac{k}{\mu} A \frac{\partial p}{\partial x} \quad (2.2)$$

The differential form of **Darcy's law** is universally accepted and used as the basic flow equation for displacement through porous media. Due to its usefulness, this equation has been extended to a variety of flow conditions.

It has also been written in potential form; for example Hubbert (1953) has suggested this form:

$$u_0 = - \frac{k \rho}{\mu} \Delta \phi \quad (2.3)$$

where

$\rho$  = fluid density, g/cm<sup>3</sup>

$\Delta \phi$  = flow potential gradient in the flow direction, atm-cm<sup>2</sup>/g

$u_0$  = macroscopic or Darcian velocity, cm/s

The term,  $\phi$ , is called the Hubbert flow potential and is defined as:

$$\phi = \int_{p_0}^p \frac{dp}{\rho} + \frac{g z}{g_c} \quad (2.4)$$

where

- $p_0$  = base pressure taken at an arbitrary plane
- $z$  = height above the arbitrary plane
- $g$  = acceleration due to gravity
- $g_c$  = the conversion constant for Newton's second law

This and other potential forms of Darcy's Law have use for multi-dimensional, gravity segregated flows frequently encountered in reservoirs.

**Darcy's Law** has also been extended to the flow of one phase in the presence of other fluids, and to the simultaneous flow of more than one phase. This has been done by modeling porous media to be composed of bundles of capillary tubes (Kozeny, 1927) where each phase flows in different capillaries; the number of tubes containing each phase depends upon its saturation. Thus it is assumed that Darcy's Law can be applied to each phase if the absolute permeability,  $k$ , is replaced by an effective permeability to that phase.

There have been attempts to derive Darcy's law analytically; for example an expression describing the laminar flow of a Newtonian fluid through packed beds was proposed by Kozeny (1927):

$$u_0 = \frac{D_p^2 \phi^3 \Delta p}{150 \mu (1 - \phi)^2 L} \quad (2.5)$$

where

- $u_0$  = superficial velocity
- $D_p$  = particle diameter
- $\phi$  = porosity
- $\mu$  = Newtonian viscosity

Using this formulation, the permeability of the medium is defined as follows:

$$k = \frac{D_p^2 \phi^3}{150 (1 - \phi)^2} \quad (2.6)$$

However, this equation still remains semi-empirical since pore diameter distribution in porous media is indeterminate. Attempts to develop an analytical flow equation have not been successful.

## 25.2. Validity of Darcy's Law for Foam Flow

One of the limitations of Darcy's Law is its empirical nature. The absolute permeability,  $k$ , a parameter in Darcy's Law, is merely a proportionality constant. It is an average macroscopic property of each porous medium and does not provide any insight into the microscopic nature. Like restrictions in other empirical relationships, it is logical to infer that Darcy's Law will not hold under any of the following conditions:

- (1) For samples not containing enough pores that can represent a reliable statistical average of the true microscopic properties.
- (2) For reactive fluids that may change the surface characteristics.
- (3) For fluids whose rheological properties are sensitive to the tortuosity or surface characteristics.
- (4) For fluids whose properties are sensitive to the pore geometry (e.g. grain structure and pore constrictions).

A good example of such cases where Darcy's Law may not be applicable is the flow of emulsions through porous media. For stable emulsions, some droplets may be larger than the pores causing constriction to flow. For the flow of unstable emulsions, the size and distribution of the droplets generated or sustained in-situ depend upon the tortuosity and pore geometry of the porous medium. Since the size and distribution affect rheology, the permeability for the flow of such emulsion may not be constant.

Alvarado (1975) noticed this characteristic for flow of macro-emulsions through porous media. He observed that flow of **O/W** emulsions of low quality (less than 50 percent) through capillary tubes strictly followed Newtonian behavior. However, when he flowed the same emulsions through porous media, the **Darcy** equation did not hold. The flow still exhibited Newtonian behavior, since the viscosity remained constant at different rates used in his experiments. He attributed this discrepancy to permeability reduction due to partial plugging of smaller channels, and used modified permeabilities as indicated in the following table.

**TABLE 2 3**  
**CORE PERMEABILITIES FOR NEWTONIAN MACRO-EMULSIONS**  
**FLOWING THROUGH POROUS MEDIA**

Core No.	Emulsion Quality $\Gamma$ (%)	Initial Perm. $k$ (md)	Flowing Perm. $k_f$ (md)
-			
Be6 A(5)	10	200	182
Be4 A(3)	20	653	434
Be4 a(1)	40	847	523

[After Alvarado (1975), Table 5, p. 1431

Nonconstant flow behavior has also been seen for High-Internal-Phase-Ratio (**HIPR**) emulsions by Mannheim (1972). In his experiments, the flow of **HIPR** emulsions (98% liquid hydrocarbon dispersed in water) was examined in capillary tubes of different diameters and wettabilities. He observed complex rheological behavior including reversible work hardening (increase of yield value by agitation) for which relaxation took several days, and apparent slip-flow anomalies. He also observed a strong influence of surface wettability. For stainless steel tubes of hydrophilic wettability, a discontinuity in the flow curve was observed at higher stresses, whereas this discontinuity was absent for polytetrafluoroethylene tubes of hydrophobic wettability (Fig. 2.1). The critical stress at which a discontinuity was observed depended on tube diameters. The different types of tubes produced entirely different results. All these observations suggest flow is also dependent on wettability characteristics.

His efforts to characterize the flow properties of these systems in cylindrical tubes were confronted with a problem of poor experimental reproducibility. In some cases, the flow suddenly increased or became erratic.

**HIPR** emulsions and high quality ( $\Gamma$ ) foams have many physical properties in common which are important in flow through porous media. Both contain continuous interfaces of fixed structure and fixed relative positions which are not free to move randomly. Due to the similarity in surface forces involved, the author expects that a high quality foam will act in a fashion similar to an **HIPR** emulsion.

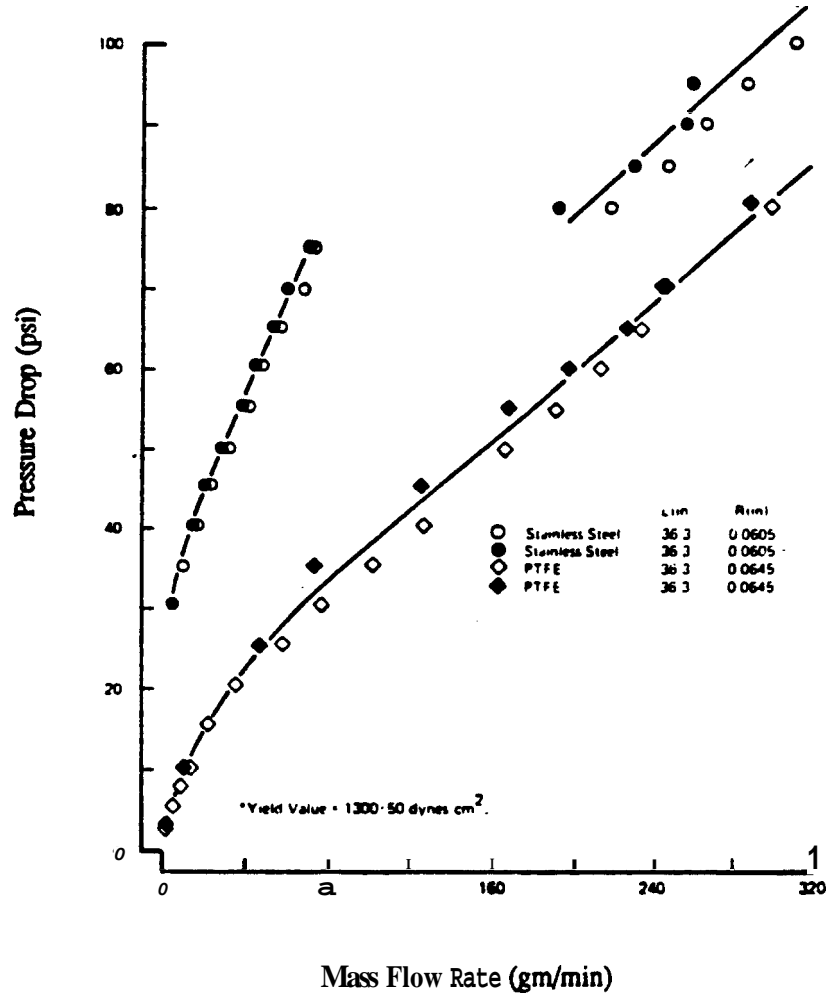


Figure 2.1 Pressure-Flow Rate Characteristics of Work hardened Emulsions in Stainless Steel and PTFE Tubes of Approximately the Same Size. (Duplicate Experiments) [After: Mannheim (1972), Fig. 4].

Another interesting phenomenon, called slip, occurs when a larger size foam bubble is forced by high driving forces through a smaller pore causing partial deformation. David (1969) has observed slip during foam flow through capillary tubes. He found that the slip coefficient,  $\beta$  (defined in Fig. 2.2) had a general tendency to increase with an increase in shear stress.

David also observed that the apparent viscosity of foam depended on the capillary tube diameter even after due correction for slip had been applied. He did not, however, notice any discontinuity in rheological behavior as seen by Mannheimer (1972). This was perhaps because the maximum quality ( $\Gamma$ ) of his foam was 0.96, not high enough to act the same as an HIPR emulsion, whereas this discontinuity is expected to be seen only at the boundary of transition from one configuration to the other.

Another complexity in foam flow which defies Darcy's law is the generation of an electrical potential, which is substantially higher than for liquid flow, and which is a function of many parameters (Fried, 1961; Raza, 1965). This electrical potential is generated due to electrokinetic effects at the sand-liquid interface and is called the streaming potential. Fried (1961) surmised that this electrical potential exerts a resistance to flow and is at least partially responsible for blockage. Raza (1965) observed that the magnitude of streaming potential depends upon many parameters such as the electrochemical nature of the surfactant, pressure differential, dimensions of the flow channel and the quality of the foam.

In the author's opinion, attempts to force Darcy's law to fit foam flow will not be fruitful in the foreseeable future. This is because the concept of Darcy permeability is not applicable to foam flow, nor can the rheology of foam be universally described without taking into account the detailed geometry of the porous medium and defining the physico-chemical properties of the surface active agent. The attempts to modify Darcy's Law by either redefining apparent viscosities or permeabilities do not seem to have general applicability. There is a need for a more basic and fundamental approach, but for the present, an effort to empirically adapt existing laws is still desirable.

## 2.6. MATHEMATICAL DESCRIPTION OF FOAM FLOW

Darcy's law and its limitation for foam flow have been discussed in Section 2.5. The classical approaches of modifying the equations of fluid flow through pores will be reviewed here. Some fundamental properties related to foam flow will also be discussed.

Despite the appearance of many papers, there is still no satisfactory mathematical description of the static and dynamic properties of foam. Most of the work was done for the flow of foam through pipes. General expressions were derived for homogeneous non-Newtonian fluids, and foam flow was treated as an extension of these general developments.

But foam is unique because it is a compressible non-Newtonian fluid, and thus its flow is more complicated. Several investigators have assumed that foam flowing through capillaries can be treated as an incompressible single phase fluid without serious error (Khan, 1965; Raza, 1965; Hooker and Marsden, 1972; Aizad and Okandan, 1977). The only support for this assumption comes from an x-ray study of in-situ fluid saturations performed by Minssieux (1974). The shadow-graphs taken after foam injection revealed a uniform distribution of fluids throughout the entire porous medium. It was thus inferred that the compressibility effects were not pronounced, else a uniform fluid distribution could not have been achieved.

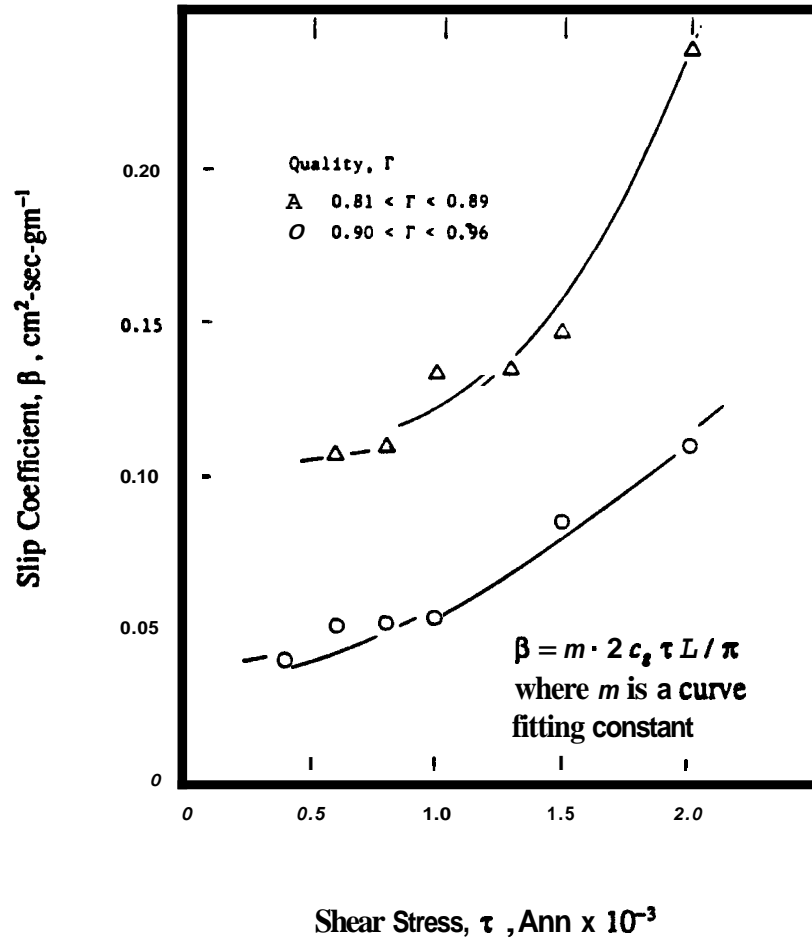


Figure 2.2 The Effect of Shear Stress on Slip Coefficient [After: David (1969). Fig. 8].

Another common practice has been to assume foam generation and propagation automatically in the presence of surfactant solution and gas. Some studies have suggested that foam will penetrate the formation only a short distance, e.g. **Gurbanov et al. (1970)** injected foam into unconsolidated sand columns (26-32 Darcies) and developed analytical and graphical relationships between system parameters which confirmed that foam could not have penetrated more than a few centimeters into their 80 cm long sandpack.

With this brief background information on the two general assumptions, some important studies are mentioned below which include equations of state and foam flow through pipes as they may be useful for promoting fundamental understanding; but expressions on foamability and foam stability are excluded, for the effect of these parameters on characterization of foam is not yet understood on a quantitative basis.

Many equations have been proposed to describe the static behavior of foam. Some of them will be mentioned here. Marsden and Khan (1966) defined foam quality as:

$$\Gamma_{foam} = \frac{V_g}{V_g + V_l} \quad (2.7)$$

where

- $V_g$    ▪ volume of gas
- $V_l$    ▪ volume of liquid

Raza and Marsden (1965) have also expressed the quality,  $\Gamma_p$ , as a function of pressure assuming Boyle's law is applicable:

$$\Gamma_p = \frac{p_i \Gamma_i}{(1 - \Gamma_i) p + p_i \Gamma_i} \quad (2.8)$$

where subscript,  $i$  indicates injection conditions. Ross (1969) has proposed the following equation:

$$(p_s - p_{gf}) V_F + (2/3) \sigma a = n R T_{gf} \quad (2.9)$$

Where

- $p$     = absolute pressure
- $V$     = volume
- $\sigma$    = surface tension
- $a$     = interfacial surface area
- $n$     = moles of gas within the foam
- $R$     = gas constant
- $T$     = absolute temperature

The subscripts,  $s$ ,  $gf$  and  $F$  indicate surroundings, gas in foam, and total foam, respectively. This equation contains parameters which need to be determined empirically, and thus is not very useful.

An equation of state was also developed by Kopalinsky and Bryant (1976) for foam flow through pipes assuming bubbly two-phase flow and using ideal gas laws to describe the gaseous phase:

$$p = \left[ \frac{1}{\rho_F} - \frac{1}{1 + \beta} \cdot \frac{1}{\rho_L} \right] = \frac{\beta R g}{(1 + \beta)} \quad (2.10)$$

where

- $\rho_F, \rho_L$  = mass densities of foam and liquid, respectively
- $\beta$  = foam gas to liquid mass ratio
- $R$  = gas constant

Similarly, Lord (1981) has developed an equation of state on a mass basis:

$$\frac{p}{\rho_F} = \frac{(1 - W_g) p}{\rho_L} + \frac{(W_g z R T)}{M} \quad (2.11)$$

where

- $W_g$  = mass fraction of gas
- $z$  = gas compressibility factor
- $M$  = molecular weight of gas

The other terms are defined in Eqs. (2.9) and (2.10).

An expression based on the definition of isothermal compressibility and pressure dependent foam quality has been proposed to be used as an equation of state if the quality remains constant (David and Marsden, 1969; Ikoku, 1978):

$$c_{foam} = \Gamma_{foam} c_{gas} \quad (2.12)$$

The above equation was obtained by assuming that the liquid component of the foam is incompressible compared to the gas, and then reducing the general expression for the compressibility of gas. It was derived for constant quality, but it can also be used for variable quality if the pressure-volume dependence of both quality and compressibility are known and substituted.

Foam's dynamic behavior has also been studied by several investigators. This was essentially done for foam flow through circular pipes under steady state conditions in an attempt to predict the wellhead pressure during foam injection. Krug and Mitchell (1972) used a modified Buckingham-Reiner equation developed for a particular rheological model (Bird *et al.*, 1960) and solved it numerically. Beyer *et al.* (1972) used a semi-empirical flow equation based on the results of bench and pilot-scale experiments. In their development, the total flow was separated in two components, the fluidity which was correlated using Buckingham-Reiner equation, and the slip which was correlated with foam quality in a fashion suggested by Mooney and later used by David and Marsden (1969).

Some investigators (Blauer *et al.*, 1974; Blauer and Kohlhaas, 1974; Holditch and Plummer, 1976) have used the concept of "effective viscosity" in which an effective or equivalent Newtonian viscosity is calculated for a fixed rate by comparing it with a non-Newtonian rheological model. Foam is then treated as an incompressible Newtonian fluid.

Quite different from the above two approaches, Lord (1981) proposed a foam flow equation which is based on a unique solution to the differential form of the mechanical energy balance. His equation cannot be solved explicitly for pressure and requires a numerical solution.

In the classical approach of Aizad and Okandan (1977), the Navier-Stokes equation yielded a highly complex, nonlinear partial differential equation, which was found difficult to solve. Some investigators have tried to manipulate the classical Darcy's law and have simply related the foam flow rate to the pressure gradient across the porous medium (Marsden and Khan, 1966; Minssieux, 1974). Evgenev (1973) proposed that Darcy's law could be applied directly assuming a homogeneous gas if it was used conditionally for low pressure gradients. Ikoku (1978) has suggested the following modification of Darcy's law for foam flow:

$$(u_0)^n = - \frac{k_r}{\mu_{eff}} \left[ \frac{dp}{dr} \right] \quad (2.13)$$

Where

- $u_0$  = superficial velocity in the radial (horizontal) direction
- $n$  = consistency index

This expression was obtained by modifying Kozeny's (1927) semi-empirical equation for the laminar flow of power law fluids through packed beds, and using empirical relationships for both effective permeability and the viscosity of foam.

After finding Navier-Stokes equation difficult to solve, Aizad and Okandan (1977) applied a momentum-balance for the flow of an incompressible fluid through capillary tubes, and derived a semiempirical relationship. A power-law model similar to Eq. (2.13) was used to define the momentum flux for a non-Newtonian fluid. The experimental data of foam flowing through unconsolidated porous media showed good agreement with the equation.

Independent measurements of the viscosity of foam flowing through porous media can not be taken. Laboratory measurements by rotational or similar viscometers are not directly applicable since the ability of these devices to generate foam is quite different than a porous medium. Also, the capillary forces are involved in porous media. Both of these factors strongly influence the effective viscosity.

Generally, the equations for the viscosity of foam have been derived using Darcy's law or Poiseuille's law, and treating the foam as a single fluid (Minssieux, 1974; Holcomb *et al.*, 1980). Experimental data, however, indicate that the apparent viscosity calculated from Darcy's law is valid only for low pressures. For higher pressures, apparent viscosity values fall with increasing pressure. Some other equations for viscosity have been developed using a similar approach (Hatschek, 1911; Mitchell, 1970). An attempt to determine viscosity for foam flowing through porous media has also been described by Aizad and Okandan (1977). A few dissertations (Richman, 1966; Augsburg, 1967; David, 1969; Mitchell, 1970) have appeared on viscosity of foam using the concept of capillary tubes and verifying experimental results with theory.

Some studies have emphasized friction losses encountered during foam flow in pipes. A method to predict pipe friction losses for different flow regimes has been presented by Krug (1975). It was found that the relationship between Fanning friction factor and Reynold's number was identical to that of a single phase fluid when apparent viscosity of foam was used. Graphical solution of pressure loss calculations showed the critical parameters to be the foam density for turbulent flow and effective viscosity for laminar flow. A prediction of friction coefficient for bubbly two-phase flow in horizontal pipes has also been described by Kopalinsky and Bryant (1976). Since the quality values were as high as 0.73, many of their flowing fluids could be considered to be foams, although no surfactant was used in their study. For foam flowing through porous media, relationship for Fanning friction factor,  $f_f$ , and modified Reynold's number,  $R_e$ , have been proposed by Aizad and Okandan (1977) with references to other similar work

Several papers have appeared in the literature which provide methods for predicting well-head pressures during foam injection (Beyer *et al.*, 1972; Blauer *et al.*, 1974; Blauer and Kohlhaas, 1974; Krug, 1975; Holditch and Plummer, 1976). The total pressure drop from top to bottom in flowing foam is the resultant of frictional and hydrostatic pressure drops. Since foam is a compressible fluid, friction and hydrostatic pressure drops influence each other and iterative methods have been employed. These iterative techniques are based on dividing the wellbore into segments or taking fixed pressure intervals and changing important parameters for each segment. Generally, the Buckingham-Reiner equation (Bird *et al.*, 1960) or some experimentally derived semi-empirical equations were used in determining well string pressure drop (Beyer *et al.*, 1972; Blauer and Kohlhaas, 1974; Krug, 1975). Some noniterative techniques have also been used by estimating an effective or equivalent Newtonian viscosity and foam density, and then treating foam as an incompressible Newtonian fluid (Blauer *et al.*, 1974). Lord (1981) has described a procedure for predicting pressure distribution of both static and dynamic foam which is based on a unique solution to the differential form of the mechanical energy balance. However, his equations are nonlinear and need iterative numerical solutions.

A nonlinear partial differential equation for the radial flow of foam through porous media has been derived by Ikoku (1978). This equation was derived for a homogeneous reservoir assuming ideal gas, neglecting the specific weight of the gas, and assuming constant permeability and porosity. This equation considers the compressibility and pressure-dependent quality of foam and assumes that a power law modification of Darcy's law applies (Eq. 2.13). It was suggested that this nonlinear partial differential equation can be linearized by using pseudo-parameters, can be written in dimensionless form, and can be used for transient well test analysis during foam injection.

### 3. DESCRIPTION OF THE APPARATUS

Displacement experiments are often conducted on unscaled models of cylindrical geometries, with standard design features that are simple to fabricate and operate. Rectangular models, especially with visual capabilities, are difficult to fabricate and operate, as pointed out by Rojas and Farouq Ali (1985) who said, "It has been impossible to fabricate a rectangular model free of mechanical problems."

The apparatus designed for this study has been found to perform well in terms of its simplicity, rigidity to moderate pressures (50 psig), ease of cleaning, inertness to cleaning chemicals, and resistance to sand settling and migration, the problems commonly encountered in rectangular sandpacks. The design and fabrication process of this apparatus is described in this section in some detail.

#### 3.1. IMPORTANT DESIGN FEATURES

Two-dimensional displacement models have been used frequently, but the presence of surfactant in a model causes some unique problems which have to be overcome before any meaningful results can be expected. In this section, some of the considerations given to the design of the experimental system are discussed.

##### 3.1.1. Visual versus Indirect Observation

The frontal behavior could possibly be traced in a displacement model by connecting the porous medium with a network of pressure taps, and then estimating and reconstructing the saturation or pressure profiles. This method offers an advantage that core holders can withstand high working pressures, but has a disadvantage that the results can be ambiguous in multiphase flow. In the presence of a complex rheological fluid like foam, the saturation determination becomes difficult. Another disadvantage of this method is the lengths of lines needed to monitor pressure, which add to the total dead volume, making material balance calculations inaccurate and cleaning difficult.

The standard practice of following the front profiles using a known frontal advance mechanism is not applicable when foam is present, since the foam flow mechanism is not known. There have been experiments performed in which anomalous recovery behavior was observed and a unique interpretation of the results was not possible. Another common method of tracing the fronts is to use tracers. This method was not considered appropriate for this study.

Since a primary objective of this study was to get a qualitative insight of the flow process, it was decided to make the model visual, so that the frontal behavior could be observed directly to avoid any misinterpretation.

### 3.12 Repacking versus Reusing the Same Sandpack

It was considered appropriate to use the same sandpack repeatedly for **this** study, instead of **repacking** for every run. **This** decision **was** made on the basis **of** past experience in which it was found difficult to duplicate **the** sandpack properties, especially the minor inhomogeneities which are random and inevitable in **a** manual packing **process**.

The **repacking** practice could have **been** adopted by applying a correction factor sometimes used to account for any difference in properties, but for flow of surfactants and foams, these effects **are** neither understood nor established.

Reusing the same sandpack **also** has some drawbacks, since thorough cleaning is generally difficult. In addition, the surfactants tend to change the surface properties of the sandpack. The effects of the changes in surface properties could, however, be minimized by pretreating the model, as will be described later in **this** section.

### 3.13 Uniformity and Homogeneity in Packing

One important consideration was to pack the model with sand as uniformly and homogeneously as possible. Sand settling and sand migration **are** difficult to control. **A** frequent problem with **this** model was **the** expansion and increase! in bulk volume at high pressures, despite efforts to make **the** model rigid. **Thus, at** higher pressures, channels would sometimes appear in **the** sandpack. The same effect would **also** be observed if **the** model was **not** tightly packed, or if **the** sand was allowed to **become bone dry**.

These small channels, sometimes not even large enough to **be** visible by naked eye, can have a substantial effect on performance, since they behave much like fractures, offering **very** little resistance to **flow**. In **our** experience, the effect of these otherwise small and sometimes invisible channels is **so** drastic that it may completely overwhelm the performance, resulting in **a** situation where the effect of changes in other parameters will **be** masked completely. In the case of waterflooding, **the** effect of these channels may not **be** pronounced, since the **strong** capillary forces suppress channeling; but, in the presence of gas, channeling **can** be **serious**.

### 3.14 Wet Packing versus Dry Packing

It is also important **to** decide which packing method is suitable for a particular use, since the properties of the pack **are** affected by **the** packing methods. In previous **dry** packing attempts, a **screen** was used to distribute the sand going in the core holder. The presence of **a** screen helped in **getting** a uniform pack, but the pack **was** not compact, and sand settling was still a problem. The same was **true** for wet packing in which considerable sand subsidence occurred after the model had been dried. In the wet-packing procedure, both water and sand **are** added gradually such that the water level always is maintained slightly above the sand. **After** many experiments, pressurizing the model after **dry** packing and then shaking it vigorously using industrial vibrators proved to be **the** best method. All the expansion of the **model** that **takes** place due **to** high **pressure** had already taken place and the model was under a prestressed condition. Thus **this** procedure offered conditions closest **to** **the** experimental operating conditions.

### 3.1.5. Prestressing versus No Stressing

The rectangular coreholder expands when moderate pressures (up to 50 psig) are applied. Since sandgrain expansion is negligible, a gap or discontinuity is developed at the sand/metal or the sand/glass contact areas, which provides paths of low resistance to flow.

This problem could be overcome by prestressing the model as described in Section 3.3.5. However, prestressing slightly changes the vertical cross-sectional area from a true rectangle. This small change in area must be taken into account in quantitative analysis.

The question of how much prestressing is appropriate, if it is needed at all, must be answered after due consideration is given to possible effects. For this study, it was considered more important to achieve proper frontal behavior than to obtain an exactly constant areal cross-section, therefore, the sandpack was prestressed to 50 psig.

### 3.1.6. Ease of Cleaning

Another important consideration in the design of this model was to make cleaning simple. The presence of surfactant causes potential problems in cleaning. Surfactants tend to absorb on sand grain surfaces, altering their properties. Even a very small concentration of surfactant is enough to reduce surface and interfacial tensions, therefore affecting the displacement process.

The materials used for construction were selected on the basis of their non-reactive nature to the chemicals used for cleaning. Therefore, all the metals in contact with the core fluids were stainless steel, and the visible side of the model was made of thick glass. The use of glass as a material of construction posed some limitations on the applied pressure, as will be discussed later, but past experiences using Plexiglas have been quite disappointing (Chiang, 1979). Plexiglas has been seen to react with solvents, and also is flexible enough that on application of pressure, a discontinuity appeared at the contact surface with sand.

### 3.1.7. Minimizing the Dead Volume

One other consideration in designing the model was to keep the dead volume as low as possible. With the addition of each metering device or flow circuit, considerable length of tubing must be used. Whereas these devices help in gathering more data and reduce the operational time and manual work, they tend to increase the dead volume inaccuracies and make the operation prone to experimental mistakes. Judgement must be exercised in deciding what is essential for interpreting the results. The apparatus for this study was designed to reduce the dead volume to 5% of the pore volume.

## 3.2. DESCRIPTION OF THE COREHOLDER

The coreholder used in this study has been referred to in this study as "the glass model" or "the two-dimensional sandpack" and is shown in Fig. 3.1 as component A. This was an aluminum, stainless steel and Neoprene rubber construction holding a thick glass plate in front of it, and was set-up vertically to hold unconsolidated sand. The sandpack after final assembly was approximately four feet long, one foot high and one quarter of an inch thick. The sand was loaded from the top where the cross-sectional area was about four feet by one quarter inch and the top was then sealed using a combination of rubber cement and room temperature



vulcanizer (RTV). The mechanical drawings of the model are shown in Figs. 3.2 through 3.4. This sandpack is an extensive modification of a similar sandpack used by Chiang (1979). The specifications of the sandpack are given in Table 3.1.

TABLE 3.1  
BASIC SANDPACK PARAMETERS

Height	1 ft
<b>Length</b>	<b>4 ft</b>
Width	0.25 in.
Porosity	35-38%
Permeability	14 darcies
Sand	Ottawa
Grain size	180-220 mesh

The use of glass plate in this model for moderate working pressures (up to 50 psig) made the system quite fragile; the glass has been broken several times whenever extreme care was not exercised in handling the model.

Fluid bypassing was another problem which needed to be eliminated before meaningful results could be obtained. Bypassing is generally caused by expansion of the model, drying of the sealing material or sand migration. The most probable areas for bypassing are the planes of discontinuity between sand and the other construction materials in contact with the sand. Bypassing was checked for routinely as well as whenever anomalous behavior was observed.

The following section points out some of the important precautions found critical to the proper functioning of the model, and describes some of the frequently occurring problems.

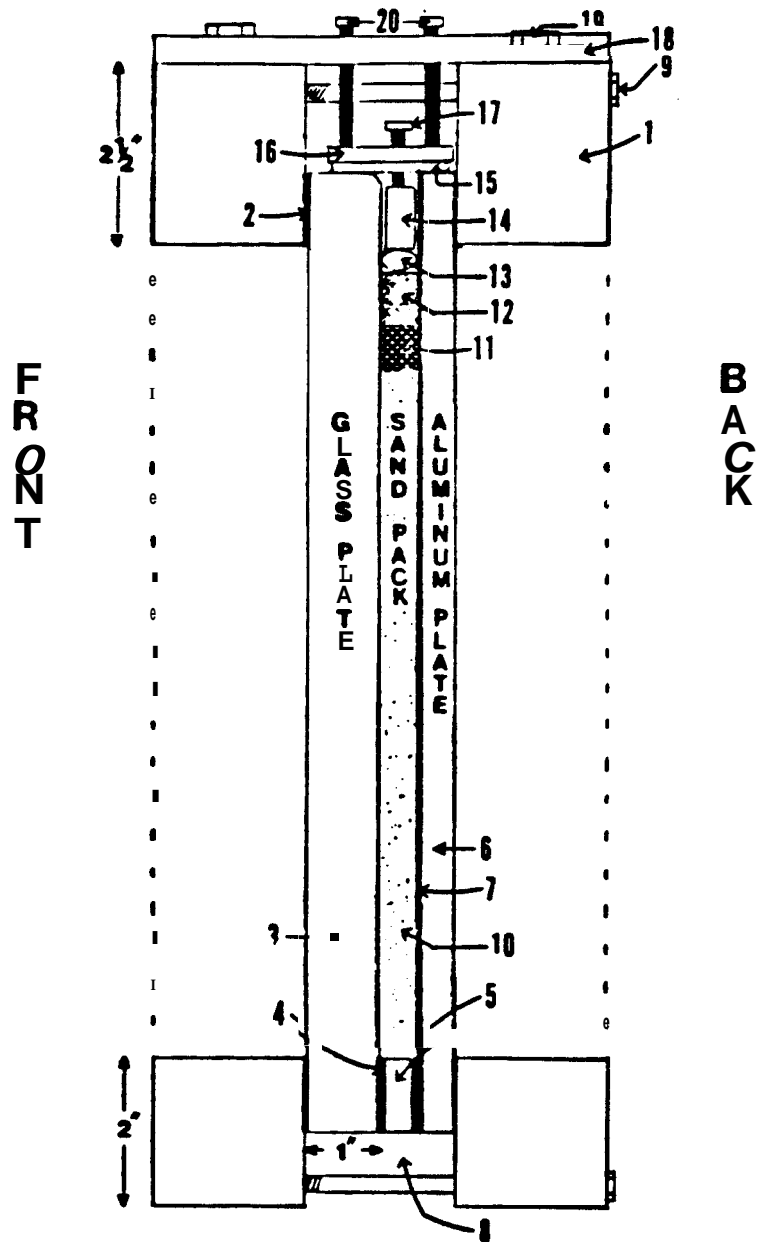
### 3.2.1. Preparation for Assembly

The most important point in assembling the model was to check the flatness of the front frame (1) [the numbers in this section refer to Fig. 3.2]. It was sometimes found after disassembly that the frame had been warped due to excessive pressure or mishandling. An error of 1/16th in. was enough to break the glass. If a greater error was found, the frame was machined again.

A Neoprene rubber cushion (2) was glued by 3M-brand spray-on adhesive on the inward side of this frame. An uncut rubber sheet of 1/16 in. thickness and large enough to cover the entire frame was used. The sheet was thoroughly cleaned with household detergent and was sprayed lightly with acetone to de-nature the rubber surface before gluing. The glue was applied only on the frame and then the rubber sheet was placed on it. The extra rubber from those areas which would not contact the glass was cut off later after the glue had been properly cured. If the rubber sheet was cut first and then glued, the sheet was often improperly placed.

The next step was to prepare the insert (5) by tack-welding a new screen of #300 mesh stainless steel to the insert. It was found to be a good idea to replace the screen whenever the model was disassembled, since normal wear and tear weakened the screen, and it broke a few times after assembly.

## VERTICAL CROSS SECTION



**LEGEND:**

- |                                  |  |   |
|----------------------------------|--|---|
| 1. The Front and Back Frames     | 9. Side Bolts                              | 14. Driving Bar                         |
| 2. Rubber Gasket Between 1 & 3   | 10. Sand                                   | 15. Rubber Gasket Between 16 and 3,6,14 |
| 3. Glass Plate                   | 11. Buffer Zone Between 10 & 12            | 16. Top Sealing Plate                   |
| 4. Rubber Gasket Between 5 & 3/6 | 12. Room Temperature Vulcanizer (RTV)      | 17. Driving Bolts                       |
| 5. U-Shaped Insert               | 13. Tygon Tube with Both End Closed by RTV | 18. Top Driving Plate                   |
| 6. Aluminum plate                |  | 19. Top Side Bolts                      |
| 7. Steel Lining Between 6 & 10   |  | 20. Top Center Bolts                    |
| 8. Bottom Insert                 |  |   |

Figure 3.2 Details of the Two-Dimensional Glass Sandpack: Vertical Cross Section.

### HORIZONTAL CROSS SECTION

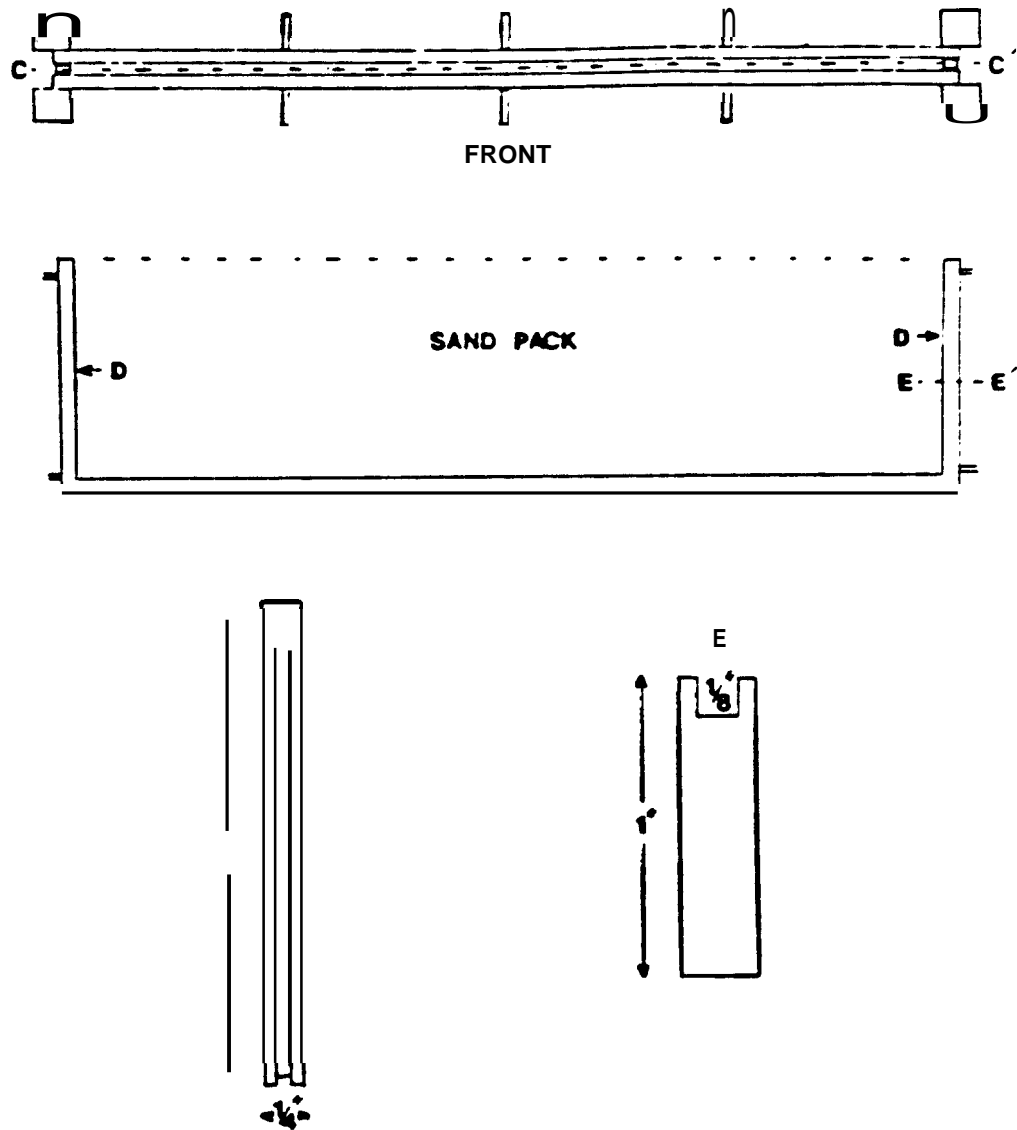


Figure 3.3 Details of the Two-Dimensional Glass Sandpack: Horizontal Cross Section.

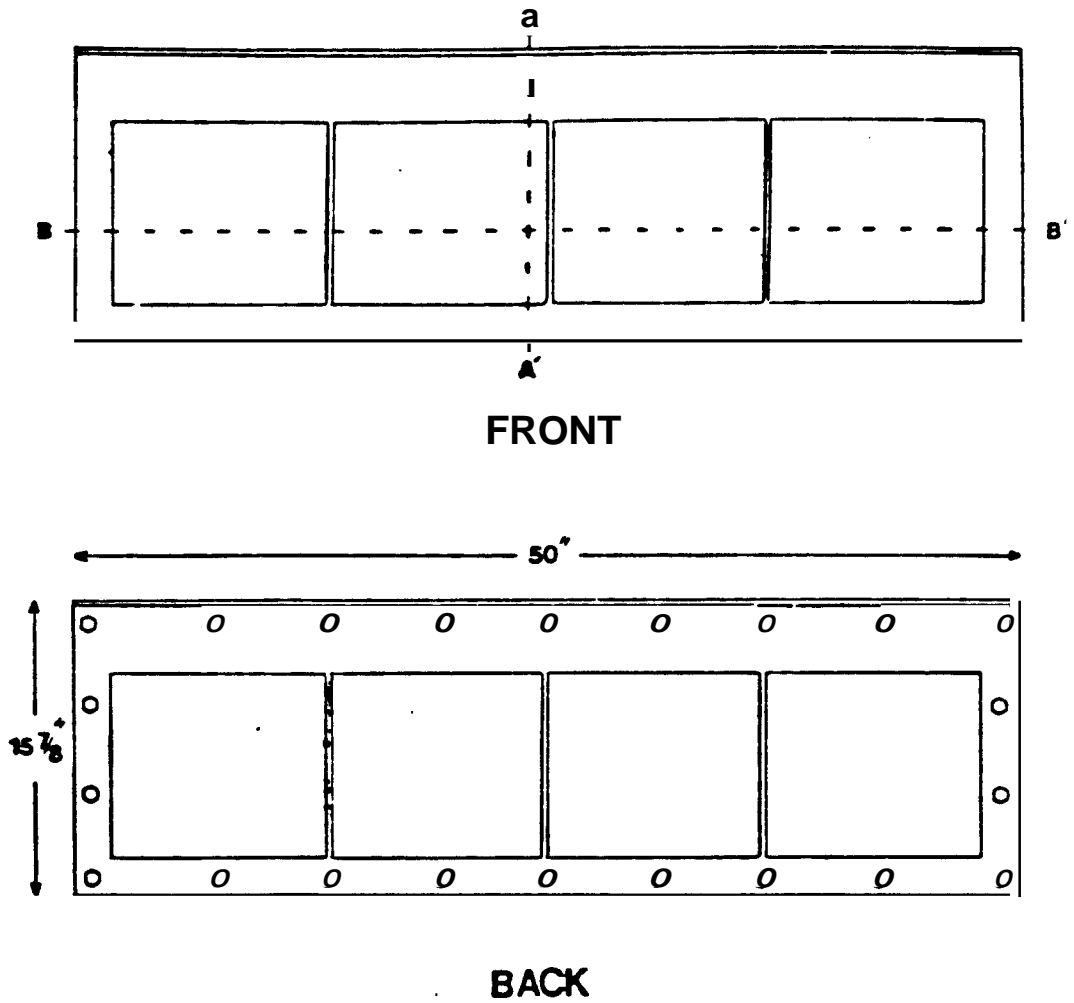


Figure 3.4 Details of the Two-Dimensional Glass Sandpack: Front and Back Views.

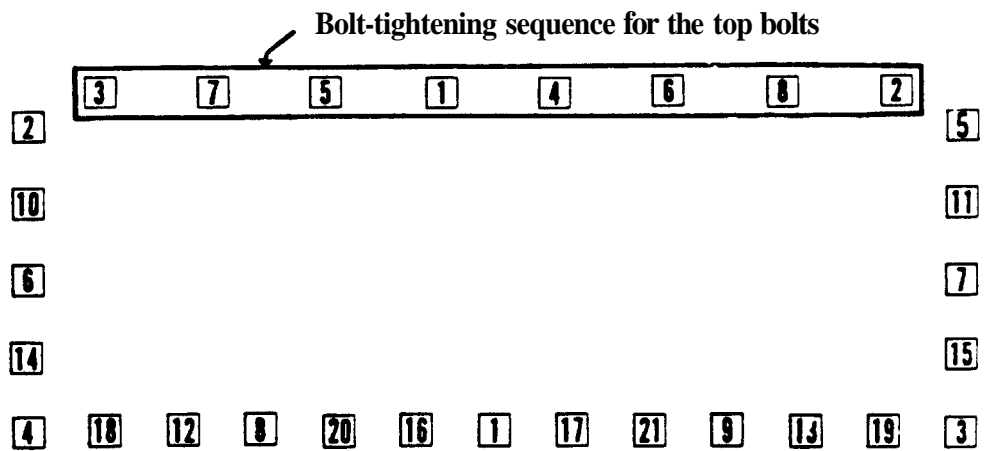


Figure 3.5 Bolt-Tightening Sequence.

After the screen had been properly welded, a Neoprene rubber gasket (4) was glued on both sides of the insert. This was done in a manner similar to that described for gluing the gasket to the frame. After proper curing, the excess rubber was cut off from both sides.

Since this insert had to be placed inside the model, the excess rubber which extruded due to the model compression was impossible to cut off. This squeezed rubber not only blocked the view, but also provided empty pockets which were hard to fill with sand. Therefore, the rubber was cut approximately 1/16th in. undersize to allow for this expansion.

The U-shape of the insert made it necessary to use some temporary inserts along the top with the permanent inserts at the time frame bolts were tightened. This was done to support the open end so that the glass would not break due to an uneven distribution of stresses. Once the model had been filled with sand, the sandpack provided uniform support.

These temporary inserts (not shown in figures) were eight pieces of metal, 1 in. x 1 in. x 1/4 in. in size, with rubber gaskets glued on both larger sides of each piece to give the same thickness as the permanent insert. These inserts had holes drilled and threaded on them, so that they could be easily pulled out of the model by screwing in appropriate size bolts and using these bolts as handles.

Another part prepared before the final assembly was the top sealing plate (16), which was done by gluing a 3/16th in. thick Neoprene rubber gasket (15) on one of its larger sides. The holes through the gasket were not punched at this stage, since this plate was used several times for temporarily sealing the model before final assembly.

### 3.2.2 Assembling the Core Holder

The following sequence was found satisfactory for an efficient assembly:

- (a) The front frame (1) was placed horizontally on a flat surface with the rubber gasket side facing up,
- (b) All the bolts (9) on the sides and bottom of the frame were inserted, and also the bottom insert (8) was placed temporarily to position the glass plate (3).
- (c) The glass plate (3) was placed horizontally on the front frame (1), its sides evenly spaced from the side bolts (9) and its longitudinal bottom side touching the bottom insert (8).
- (d) The U-shaped insert (5) was placed horizontally on top of the glass plate with the open end away from the bottom insert, and was positioned symmetrically with the glass plate. Also the eight temporary inserts (described earlier) were placed in the open end of the U-shaped insert, with their threaded holes facing out, and the temporary inserts located just below each of the side bolts (9), in order to provide support under the bolts and still be easily removable.
- (e) The steel-lined aluminum plate (6) was placed horizontally on top of the U-shaped insert with the stainless steel lining facing toward the glass plate, and was positioned accurately above the glass plate. It was imperative to make sure that the top ends of the glass plate, the insert and the aluminum plate were perfectly aligned. A slight discrepancy resulted in improper seating for the top sealing plate (16), and caused problems in sealing properly.

- (f) The bolts (9) were then unscrewed, and the back aluminum frame (1) was placed horizontally on top of the aluminum plate (6), such that the rubber gasket faced the aluminum plate. The holes of the front and back frames (1) were aligned and the bolts (9) were inserted again. All the bolts were tightened by hand. Extreme care was exercised not to dislocate the previously assembled parts, because the alignment of top edges was crucial for proper sealing. Before tightening the bolts, the top edge alignment was checked again.
- (g) The bolts were tightened to 100 in.-lb torque, in increments of 20 in.-lb, in a sequence shown in Fig. 3.5. However, this initial torque of 100 in.-lb was generally not enough to provide adequate sealing to 50 psig pressure, and additional torque was required for final sealing as will be described next. The torque at this stage was found enough, however, to hold all the parts together.
- (h) The model was now ready for inspection and leak testing, so it was placed upright with the glass side facing the operator. All the plumbing was done at this stage as shown in Fig. 3.1.

### 3.23. Testing the Coreholder for Leaks

It was necessary to test the coreholder for leaks at this stage, since stopping leaks at later stages was found difficult. For testing the coreholder for leaks, it was temporarily sealed by placing the top sealing plate (16) with its rubber gasket side facing the end of glass and aluminum plates (3) and (6). Then the top driving plate (18) was fastened with bolts (19). The bolts (20) were screwed in until they touched the top sealing plate (16). Sealing was completed by tightening the bolts (20) to 50 in.-lb torque.

The model was filled with water under pressure, as described in Appendix C (section C.1.2), and was checked for leaks. If any leak was found, the bolts were tightened an additional 10 in.-lb in the same rotational order described in Fig. 3.5. The torque was increased in increments of 10 in.-lb until the leak was stopped. The injection pressure was increased slightly until a leak was observed, or pressure had reached 50 psig, whichever came first. If a leak was observed before the recommended pressure was reached, additional torque was applied on the bolts (9). However, if the leak was not stopped up to 200 in.-lb torque, the model was disassembled and reworked.

The final check for leaks was made by draining the model and injecting gas at the prescribed pressure, then isolating the model by closing all valves and observing the pressure changes through the pressure transducer. Minor fluctuations were always observed due to temperature changes, but no significant decline in pressure over several days indicated good sealing.

After assuring a good seal, the pressure was released slowly. Before dismantling the top sealing arrangement, the bulk volume of the model under pressurized condition was determined for later use in calculation of the porosity and the pore volume. This was done by pouring a known volume of water in the water slug container (L) [Fig. 3.1] and injecting it in the model at various pressures, and noting the bulk volume by material balance. The systematic procedure to carry out this step is described in Section 3.2.9. The model was now ready for packing.

### 3.2.4. Packing the Coreholder

The first step was to decide the size of the sand to be used, which affected the permeability of the sandpack after assembly. The size was estimated by using the Kozeny-Carman equation.

The sand used in this core holder was mixture of different sizes. It was sieved within a close limit of specified sizes and then mixed in the desired proportion. About 4000 cc of sand was found enough for this coreholder.

The sand was thoroughly cleaned with petroleum ether, dried in open air at atmospheric conditions and washed with tap water. It was then dried in an oven at moderate temperatures (around 100°C) to avoid firing. It was finally cooled down to room temperature and the density and the total weight of the available sand were determined. The sand filling apparatus was simply a large glass funnel mounted on a tall stand, with its lower end connected to a Tygon tubing with a clamp to control the flow. When the clamp was opened, the sand would flow like a liquid. After filling the sand to the top edge, the sealing plate (16) was placed, and the top driving plate was fastened by screwing the bolts (19). Then the driving bolts (20) were inserted and tightened to 50 in.-lb torque. This step sealed the model temporarily.

### 3.3.5. Prestressing the Coreholder

To prestress the coreholder with sand, the model was pressurized to 50 psig by injecting nitrogen. Three vibrators were attached at even spacing on the top of the model with bolts. The model was vibrated until sand stopped settling. When no more settling was observed, the pressure was bled off, and the top sealing arrangement was opened by removing the top driving (18) and top sealing (16) plates. More sand was added and the procedure was repeated until there was virtually no more settling.

The next step was to presettle the sand by water flowing at 50 psig injection pressure. The vibrators were removed and the model was exposed to constant water flow for a few days. The procedure of opening the top seal, adding more sand and remounting the sealing system was repeated. One precaution taken was to inject gas in the model at a slow rate, since gas entering the model under high pressure tended to move some of the sand toward the producing well. However, when the model was near the final packing stage, gas was injected at high velocity so that any sand migration could take place before the model was permanently sealed. After a sequence of pressurizing, vibrating and adding sand at both gas and water flowing conditions, the sandpack became quite rigid.

After performing the above steps the model had become prestressed, and for our working pressures of up to 25 psig, the model did not show any significant expansion. The sand in the model was now compact enough to take care of any compression due to tightening the bolts, so the temporary inserts were removed.

Some loose sand was occasionally found on the top of the sandpack during the packing process; this was removed without disturbing the compact sand. An easy way to do it was by using a small vacuum pickup probe. The top of the sandpack was not tampered with in any way, nor was sand added at this stage because doing so could have altered the permeability at the top and caused channeling.

### 3.2.6. Permanently Sealing the Coreholder

The model was thoroughly tested for acceptable performance before permanently sealing. A good seal was crucial, since even a hairline crack caused erroneous results. This was difficult to achieve. The common reasons for the development of these channels were sand settling, the discontinuity between sand grains and the smooth sealing materials, and contraction of the sealing materials after curing.

Good sealing was obtained by using the following procedure established by trial and error over a period of time. To eliminate the upper sand surface discontinuity, the top half inch of sand was soaked with liquid rubber (Devcon). After curing for several days, this rubber cemented the top of the sandpack and completely blocked the pores providing a buffer zone (11). This buffer zone alone was not strong enough to take high pressures, so it was supported mechanically. This support was provided by pouring room temperature vulcanizing rubber (RTV) on top of the buffer zone to form about a quarter inch thick layer (12), and let it cure for several days.

For providing additional strength, a 3/8th in. diameter Tygon tube (13) was placed on top of the RTV. This tube was exactly as long as the top of the sandpack and its ends had been closed by RTV. The driving bar (14) was inserted and set at even spacing from the sides, so that it could evenly support the sandpack. Now the holes were punched in the rubber gasket (15) of the sealing plate (16), and the bolts (17) were screwed in on the plate. The sealing plate was placed on the top and it was made sure that the ends of the bolts touched the center axis of the driving bar. The top driving plate (18) was then placed and the bolts (19) tightened to 150 in.-lb torque. The driving bolts (20) were inserted and tightened to 50 in.-lb. The final step was to drive the sealing bolts (17) slightly, starting from the center bolts and moving towards the end bolts of each side. Hand tightening was found to be enough. Tightening too much helped initially in getting a good seal but left little provision for future tightening that was sometimes needed to combat leakage if it began later in the runs.

RTV can act as an antifoaming agent, and also dissolves slightly in some solvents. Thus it is a potential source of trouble if it came in contact with the sandpack. The presence of the buffer zone (11) generally provided adequate isolation, but before starting each run the seal had to be inspected for leaks and for the integrity of the buffer zone. If a problem was detected in early stages, it was corrected simply by driving the driving bar (14) further, or by opening the top and reworking the buffer zone. This was much easier than repacking the model.

### 3.2.7. Pretreating the Coreholder

The virgin sandpack, immediately after packing and before the injection of any surfactant, showed different characteristics than in later runs, perhaps because the surfactant permanently altered the surface properties of the pores. The model was, therefore, pretreated before any run was made. This pretreatment consisted of injecting surfactant solution (1% active Suntech 4) into the model and giving enough residence time for all the possible changes to take place. Then a large quantity of surfactant solution was injected over a period of time to further complete the treatment process.

To account for the possible changes caused by the cleaning materials, a cleaning run was made under normal operating conditions. The model was saturated with oil at irreducible water saturation, and then this oil was displaced by injection of gas and surfactant solution. After that the standard cleaning procedure was followed to clean the model. The results of this cleaning run were discarded, because they were not found to be the same as later runs.

### 3.2.8. Disassembling the Model

Before undertaking a disassembling job, it was made sure that disassembly was warranted. Sometimes minor adjustments were able to correct the problem. For example, if the sandpack was degraded, it was easier to remove all sand and repack it without the need to completely dismantle. The sand was removed by vacuuming it through a water trap in which the sand settled due to gravity and was retrieved. Before vacuuming the sand, however, the temporary inserts used during assembly operation had to be inserted to avoid glass breakage.

If disassembly could not be avoided, it was carried out carefully so as not to lose the preserved sand. To save the sand, the sandpack had to be thoroughly cleaned and dried before dismantling the model. Absolutely clean and dried sand was required for a compact pack, and for a problem-free packing process.

To prevent the glass from breaking, the stresses on the glass were relieved before dismantling. This was done by pressurizing the model to 30 psig and vibrating with commercial vibrators in exactly the same way as was done for assembly. The bolts were also loosened in small increments following the same sequence as described for assembly.

### 3.2.9. Determination of Sandpack Parameters

The porosity and permeability of the sandpack were two important parameters needed for material balance calculations and for the indication of the integrity of the sandpack. An increase in porosity generally meant a sand production problem indicating a broken Screen or a leak from the model. A decrease in permeability signalled the presence of foreign particles blocking the pore spaces, and an increase meant channels were formed in the sandpack. A large increase in permeability was caused by improper sealing and the presence of a crack. The porosity and permeability readings were, therefore, taken frequently, normally before every run.

The bulk volume of the model under pressurized condition could be determined only before the model was packed. This was done by pouring a known volume of water in the aqueous slug container (L) and injecting it in the model at various pressures. The model was then sealed off by closing the injection well valves (16 through 20 in Fig. 3.1) and the producing well valves (21 through 25). The water remaining in the aqueous slug container was recovered by opening the injection well valve (20) towards the drain. This recovered volume was metered, and the bulk volume calculated by material balance taking into account the known dead volume. The pore volume was directly measured using the same procedure used for measuring bulk volume, and it was also calculated using the standard values of quartz matrix density, and by measuring the weight of sand put in the model. The porosity calculated by both methods was in reasonable agreement ( $\pm 1.5\%$ ). The absolute permeability was measured by flowing water under steady state conditions using Darcy's law. The absolute permeability was also obtained by flowing gas. Several readings at various flow rates were performed to ensure that non-Darcy effects were not present. After the permeability calculated by both methods was found close ( $\pm 0.5$  Darcies); an average value was used for quantitative interpretations.

### 33. EXPERIMENTAL PROCEDURE

The procedure used for cleaning, saturating and running the model is described here in some detail. The operating procedure for the flow lines and auxiliary equipment is described in Appendix C.

#### 3.3.1. Cleaning the Model

For cleaning the sandpack, alternate slugs of  $CO_2$ , water, mineral spirits (petroleum distillate) and tertiary butyl alcohol (TBA) were injected. The TBA was found better than any other chemical tried, because of its three phase miscibility with water, mineral spirits and oils. The slight solubility of  $CO_2$  in water was also quite helpful in reducing the gas saturation to zero.

The model was cleaned every time before making a run, by injecting the cleaning fluids at 20 psig inlet pressure. The slug volumes and sequence of each slug is described below:

(a) $CO_2$ injection	1 hour
(b) Distilled Water	5 pore volumes
(c) Mineral Spirits	2 pore volumes
(d) Distilled Water	2 pore volumes
(e) Mineralspirits	1 pore volume
(f) Distilled Water	1 pore volume
(g) Mineral Spirits	1 pore volume
(h) Distilled Water	2 pore volumes
(i) TBA	4 pore volumes
(j) Distilled Water	3 pore volumes

The dead volume fluids were drained every time a different slug was injected to assure no contamination occurred.

#### 3.3.3. Saturating the Model

After cleaning, the model was saturated completely with dyed distilled water (Schilling, containing food color and propylene glycol) by injecting about four pore volumes. If it was an oil run, a white mineral oil was injected at 20 psig to displace the water from the model. Oil injection was stopped when no traces of water were found in the oil being produced. The total volume of oil injection required to displace movable water varied from one oil to another. Typically, for an oil of 180 cp viscosity, around five pore volumes of oil injection were sufficient.

It is appropriate to emphasize here the importance of having the model fully saturated with liquids only. Any gas remaining at the end of the saturation process provides easy channels for fluids injected during a run and affects the performance. If there was any indication of the presence of gas at any time during the liquid saturation process, the cleaning procedure was aborted and restarted again from Step (a) above.

### 33.3. Making a Run

After the model had been adequately cleaned and saturated with oil and irreducible water, final arrangements were made before starting a run. These arrangements included calibrating the chart recorder and pressure transducer, setting up the gas regulator to the desired pressure, starting the fraction collector and setting up the camera. The runs were started by opening the valves as described in Appendix C (Section C.3).

During the runs, photographs were taken frequently, more often at early times, very often just after breakthrough and then at ever increasing intervals of time later in the runs.

The time interval setting on the fraction collector needed adjustment from time to time, so as to maximize the volume collected in each collecting tube. The fewer the number of tubes used for collecting produced fluids, the less was the metering error. The number of tubes were minimized by adjusting the interval time according to the expected liquid production rates. Any change in the time interval had to be recorded for follow up calculations.

### 33.4. Measuring Results

During the saturation process, material balance calculations were performed on volumes of oil injected and produced to determine the volume of oil remaining in the model. Knowing the pore volume (1257 cc at 5 psig), the oil and water saturations were calculated.

After completing a run, collecting tubes were removed from the fraction collector and stored in a closed container, which was saturated with the vapors of the same oil, to avoid evaporation losses. Once the emulsions had been broken, the tubes were removed and the volumes of both water and oil in each tube were read volumetrically and recorded on the chart at corresponding time intervals.

These readings were summed to give cumulative production. The photographs were used to measure the swept area, which was in turn used to calculate the saturation behind the front and the sweep efficiency. These photographs were also used for qualitative understanding of the frontal behavior. The volume of gas injected during each time interval was obtained by graphical integration of the flow rate curve on the chart, since this method was found to give the best results. However, the values were checked with the readings of the cumulative gas mass counter after due correction for operating pressures.

## 4. QUALITATIVE ANALYSIS OF FOAM DISPLACEMENT

The literature review on physical properties of foam pertaining to flow through porous media indicated that the conclusions drawn are not always in agreement with each other. An attempt is made in this section to review the state of knowledge and present some possible explanations and suggestions. A number of these ideas are based on visual observations of the many experiments performed for this study, and appear to be solidly based. But a few ideas are also based on inference from previous studies and need further testing.

### 4.1. DEFINITION OF FOAM

The studies in past have used many different terminologies for the classification of foam. The lack of standard definitions for various types of foam has resulted in some confusion when comparing the results of these studies with each other.

Foam is defined commonly as a uniform dispersion of gas in a liquid such that most of the phase volume is gas. Two types of foam have been frequently mentioned, wet foam and dry foam; distinguishing them on the basis of volume ratios of gas and surfactant solution.

The author feels that this classification is inadequate, since the physical appearance of foam is more important in determining its properties than the volume ratio of gas and surfactant solution.

For example, foam in which gas is dispersed in the form of spherical bubbles, which are free to move around relative to each other, will be characterized by low apparent viscosity and low static stability. On the other hand, foam in which gas is dispersed between liquid films (lamellae) having fixed geometrical structure, will have just the opposite behavior. There seems to be an approximate relationship between the physical appearance of foam and the gas to surfactant volume ratio. But strictly speaking, the structure of foam at any given instant is a function of the molecular structure of its constituents, and the amount of free energy contained in the system. The following classification (Sections 4.1.1 to 4.1.3) is based on physical appearance rather than merely on volume ratios of gas and surfactant. A summary of this classification is also given in Table 4.1.

#### 4.1.1. Emulsion Foam

This type of foam is characterized by discrete spherical bubbles. Since these bubbles are separate entities, there is no continuous interface and little mass transfer takes place between the bubbles. These bubbles are free to move around randomly with little interaction, and therefore, they do not have any fixed relative position. This type of foam is expected at lower quality. A typical emulsion foam is shown in Fig. 4.1(a).

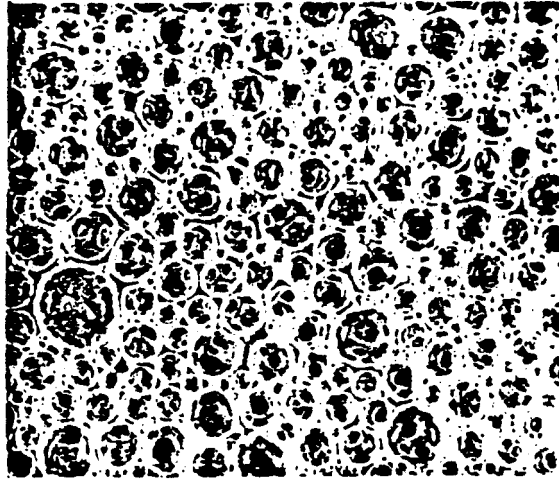
#### 4.1.2. Transitional Foam

A distinct feature of transitional foam is the close proximity between bubbles. This type of foam has properties in between emulsion foam and HIPR foam (described in next section). The bubbles are discrete as in emulsion foam, but are deformed elliptically. Since bubbles have separate entities, the interface between them has a variable thickness. The smaller

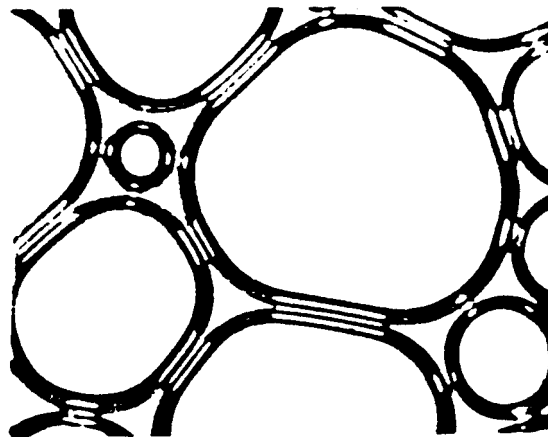
TABLE 4.1  
Proposed Classification of Foam

Class of Foam	Characteristics
Emulsion <b>Foam</b>	<ul style="list-style-type: none"> <li>(1) spherical bubbles having separate entities,</li> <li>(2) minor interaction or mass transfer across bubbles,</li> <li>(3) no fixed relative position and free to move randomly,</li> <li>(4) discontinuous interfaces,</li> <li>(5) lower quality, <math>\Gamma</math>.</li> </ul>
Transitional <b>Foam</b>	<ul style="list-style-type: none"> <li>(1) bubbles having separate entities but are deformed due to compression,</li> <li>(2) some interaction or mass transfer across bubbles,</li> <li>(3) no fixed position but offer resistance in movement,</li> <li>(4) discontinuous interfaces,</li> <li>(5) intermediate quality, <math>\Gamma</math>.</li> </ul>
<b>HIPR</b> Foam	<ul style="list-style-type: none"> <li>(1) fixed geometrical structure of lamellae.</li> <li>(2) mass transfer occurs across bubbles,</li> <li>(3) fixed relative position and not free to move randomly,</li> <li>(4) continuous, nearly linear, interfaces,</li> <li>(5) higher quality, <math>\Gamma</math>.</li> </ul>

(a) Emulsion Foam



(b) Transitional foam



(c) HIPR foam

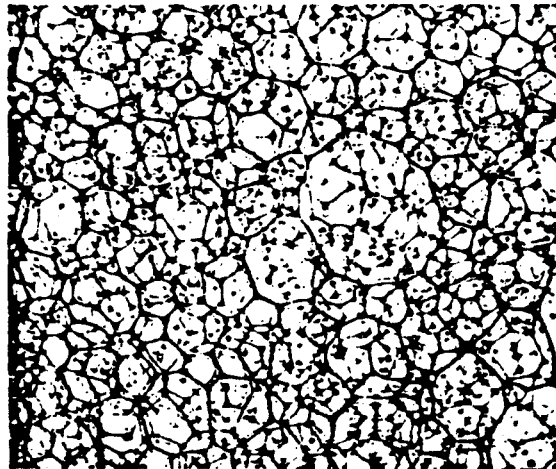


*Figure 4.1* The Classification of Foam on the Basis of Physical Appearance: (a) Emulsion Foam, (b) Transitional foam, (c) HIPR foam.

bubbles are at higher pressure than the larger bubbles and thus gas diffusion takes place between adjacent bubbles, causing the smaller bubbles to disappear gradually and the larger bubbles to grow further. These bubbles do not have any fixed relative position and can move around under shearing force strong enough to overcome resistance. An example of transitional foam is shown in Fig. 4.1(b) and it is generally observed at intermediate values of foam quality.

#### 4.13. HIPR Foam

The term HIPR (high-internal-phase-ratio) is commonly used to describe liquid-liquid emulsions in which the volume of discontinuous phase is much higher than the continuous phase. The term HIPR foam is introduced here due to its many similarities with HIPR emulsions. HIPR foam is distinguished by a continuous web-like structure of lamellae. Each film has a fixed relative position, and is not free to move randomly. Gas diffusion across the films is significant. No convective mass transfer can take place without deforming and breaking the foam structure. This type of foam is encountered at high quality after severe agitation and is shown in Fig. 4.1(c).

## 4.2. EFFECT OF OPERATING CONDITIONS ON FOAM FLOW

Foam is thermodynamically unstable due to the surface free energy. Its physical properties change continuously. When foam flow is taking place under constant operating conditions, a state of dynamic equilibrium can be reached. Thus a variety of flow mechanisms and rheological models are expected from one set of conditions to the other. The past attempts to propose a unique foam flow mechanism and rheological behavior has resulted in controversies. Almost all of the reported mechanisms are possible under differing circumstances. Logical explanations for much of this behavior are given in the following two sections.

### 4.2.1. Effect of Operating Conditions on Foam Flow Mechanism

A number of mechanisms have been proposed for foam propagation through porous media, most of which have been observed microscopically through transparent tubes and cells. Foam generation and rupture are influenced by the geometry of the generator, the composition of gas and liquid, and the interaction of these fluids with the medium in which it is flowing. A unique mechanism can not describe flow for the diverse systems encountered in laboratory experiments. For a given flow condition, some of these mechanisms may be correct, while others may be invalid. However, it is possible that several different mechanisms may simultaneously be active at the same time. These mechanisms were described briefly in Section 2.2. The conditions at which each of these mechanisms are expected is described in the following paragraphs and these conditions are also summarized in Table 4.2.

In the bubble flow mechanism, the bubbles are discrete, stable and small compared to the pore openings so that they can pass through the pores without deformation or rupture. These conditions can generally be met when a uniformly dispersed foam composed of small bubbles is externally generated with a concentrated surfactant solution, and the foam is injected through a uniform conduit such as a capillary tube or cells loosely packed with uniform beads or sands, or made up of uniform etches. These conditions are generally not met in real or simulated cores and tight sandpacks.

TABLE 4.2  
Required Conditions For Different Flow Mechanisms

Mechanism	Conditions	Applicability
Bubble Flow	(1) emulsion foam, (2) high stability, (3) bubble diameter smaller than conduit or pores.	cap. tubes, loosely-packed or etched uniform cells.
Intermittant Flow	(1) transitional foam, (2) high stability, (3) high foamability.	tight cells, heterogeneous cells, cons. and uncons. porous media.
Segregated Flow	(1) low stability, (2) low foamability.	tight cores or packs with oil or brines.
Trapped-gas Flow	(1) <del>HIER</del> foam, (2) high stability, (3) high foamability.	heterogen. tight glass cells cons. and unconsolidated porous media.
Plug, Membrane or Tubular-Channel Flow	(1) high stability, (2) low foamability, (3) high rates.	cap. tubes, vertical columns, uniformly etched cells, specific-geometry cells to generate <i>in situ</i> lamellae.

In Intermittant Flow, **the** bubbles or films are ruptured while passing through pore throats but new bubbles or films **an** constantly regenerated. Thus **this** mechanism requires that the system should have low stability and high foamability. **The** heterogeneities in pore openings play an important role in **both** breaking and **reforming** foam, since some **geometric** configurations cause the foam to **rupture** and others cause regeneration. Higher surfactant concentrations (above CMC) and little or no oil or electrolyte in the system improve foamability. These conditions are generally found **with** transitional foam and in **heterogeneous cores** or sandpacks, but **are** not common in simple and highly regular systems such as capillary tubes. **A** transitional foam is also likely **to** cause **this** flow due to its low stability and nonuniform bubbles which are ruptured during flow.

Sometimes the system might have **both** low stability and low foamability **so** that foam breaks down when entering **the pores** and there is little foam regeneration. Under these **conditions**, Segregated Flow is expected such that each phase is flowing in different channels. Low stability is generally associated with low surfactant concentration and **can also occur** in the presence of oil, brine or other foamicidal agents. Low foamability is caused by tight pore openings, improper type of surfactant, **and/or** surfactant concentration **well** below the CMC.

If HIPR foam is internally generated and **the** stability of foam is high, the trapped-gas flow mechanism is expected. These conditions **are** found when the surfactant **has** high foamability, the surfactant concentration is high, the foam quality is high and oil, brine or other foamicidal agents **are** absent. In addition, **the** porous medium **has** high permeability or heterogeneity to aid in foam generation **These** conditions **are** not met in highly **regular** and simplified systems such **as** capillary tubes **and** cells.

The Plug Flow, Membrane Flow and **the** Tubular-Channel Flow mechanisms **are** all found under **high** foam stability and low foamability conditions in highly Uniform models such **as** capillary tubes and etched cells. Membrane Flow could **be** expected **at** low **rates**, Plug Flow at moderate **rates**, **and** Tubular-Channel flow at very high rates. Due to low foamability, only a few discrete films **are** generated, whereas due to high stability, **these** films **are** able **to** **propagate** without collapsing. Even though the conditions of low foamability and high stability could **be** found in real or simulated cores, **the** highly irregular geometry of **the** pores will not allow the lamellae to propagate for a long distance without rupturing.

#### **4.2.2. Effect of Operating Conditions on the Rheology of Foam**

Many types of rheological behavior have been observed in experimental studies. **A** survey of rheological behavior reported in **the** literature was presented in Section 2.1 (Table 2.1). The most likely reason for **the** disagreement among different investigators is the different operating conditions at which they performed **these** runs, such **as** **the** method of foam generation, the type of porous medium, **the** surfactant properties and concentration, and **the** range of shear rates involved. The results of one study **can** not always **be** directly compared with the others.

Many of these disagreements come from assuming the flow of foam **to** **be** homogeneous **and** steady state. **Both** of **these** conditions **are** **hard** to reach, since at early time foam may break **down** when entering a porous medium, **and** the in-situ foam generation is only gradual. **Most** of the **foam** studies have analyzed **the** results assuming a **linear** and stable flow, whereas in reality, **the** **low** capillary forces due to the presence of surfactant tend **to** **make** flow unstable and segregated. **The** flow is further complicated if foam blocking takes place changing **the** permeability. Furthermore, foam rheology is strongly dependent on flowing time **and** flow history.

The blockage and hysteresis effects have been generally ignored in most foam studies. The reported flow behaviors have been analyzed in the following paragraph to see under what circumstances they could be expected.

Pseudoplastic behavior, in which the apparent viscosity decreases with an increase in shear rate, is typically observed in polymers or suspensions where molecules or particles have a tendency to form aggregates which can break down or reform due to a change in shear rate. A transitional foam flowing by a bubble flow mechanism closely approximates these conditions and could show pseudoplastic behavior. The conditions under which a bubble flow mechanism is expected have been described in Section 4.2.1.

Plug flow or bubble flow with slippage is likely to exhibit pseudoplastic behavior with gel strength, i.e. the deformation or flow takes place only after the shear stress exceeds a critical value. Only a few studies have reported this behavior even though the foam flow mechanisms for which it is expected are quite commonly observed in experimental studies. This is perhaps because foam sometimes has low yield values which are hard to notice. David and Marsden (1969) observed pseudoplastic behavior with low gel strength. Their description describes exactly a yield pseudoplastic foam of low gel strength.

The physical characteristics of a Bingham fluid, which show Newtonian behavior but have gel strength, are seldom described in the literature, perhaps because there are very few fluids that are truly Bingham plastic. Plug flow or bubble flow with slippage are likely to approximate Bingham fluid behavior, because in each of these mechanisms, major shearing takes place at the contact boundary of the solid and liquid surface. Bingham fluid behavior is not expected because the generation of uniformly sized bubbles in-situ is unlikely. These conditions, however, are found in laboratory experiments. Nevertheless, foam flow has been fit to the Bingham fluid model by more than one study. But both pseudoplastic and yield pseudoplastic fluids resemble Bingham fluids over low ranges of shear rates, thus there is also a possibility of misinterpretation.

Many of the simple fluids found in nature are Newtonian due to their homogeneity and small molecular structure, whereas emulsions, on the other hand, do not have these properties and thus are generally non-Newtonian. Foam is not expected to show Newtonian behavior since it acts like a special class of emulsions due to its inhomogeneity. It could, however, closely approximate Newtonian behavior at very low or very high shear rates, or when the quality is very low.

The time dependency is a characteristic of those dispersions or colloidal suspensions in which the size and orientation of particles is important, but the ability to rearrange the orientation is rather slow. The dependence of foam rheology on time and shear history has not been emphasized in the literature, even though foam belongs to this type of dispersion. A few studies have reported thixotropy, i.e., a decrease in apparent viscosity with time at a given shear rate. This type of behavior can be typically expected in HIPR foams, since their foaminess is gradually decreased with time, due to film-thinning caused by gravity drainage of surfactant solution. A complex rheology was observed by Mannheimer (1972) during the flow of HIPR oil-in-water emulsions through capillary tubes, which was found to be function of both time and shear history.

The gel strength of a HIPR foam is also a function of shear rate and history, especially the last rate before the flow ceases. This yield value has been seen to increase with an increase of shear rate, but to decrease with time, a phenomenon called reversible work-hardening. The relaxation time observed in some runs on the two-dimensional sandpack was

about a week in **this** study, whereas others have reported **this time to be as long as** two months.

The characteristics of porous media **also** affect foam **rheology**. One such effect is the ability of some **pores** to **be** plugged by foam. Several investigators have reported **this** blockage, which is sometimes selective, but few have attempted to explain it. Blockage **has** been attributed to: (1) a reduction in **gas** permeability due to gas entrapment (Bernard and Holm, 1964); (2) the **Jamin** effect resulting from a unique change in phase distribution in the **pores** (Mast, 1972); (3) a **sharp** increase in apparent viscosity caused by an in-situ increase in foam quality due to **gas** accumulation (Minssieux, 1974); (4) the bubbles subdividing into smaller bubbles while passing **through** the pore **constrictions** and then blocking them (Fried, 1961); and (5) the resistance exerted by the **electrokinetic potential** (Fried, 1961; Albrecht and Marsden, 1970).

Whereas the above studies have attempted to explain blockage, none **has** explained the **reason** for the selective **nature** of **this** blockage. To understand **this** important foam phenomenon, the controversy **should be** resolved whether blockage is caused by the static or the dynamic surfaces. The indication is strong that the dramatic reductions in mobility frequently found during foam flow **are** perhaps due to the formation of **static films** or bubbles. Otherwise, complete blocking for extended periods of time is difficult to explain on the basis of a dynamic process. **Further research** is **needed** to explain blocking behavior.

### 43. FRONTAL BEHAVIOR AND RECOVERY

The studies on the **frontal** behavior in presence of **foam** are still in a **speculative** stage. A difficulty in describing the **frontal** behavior is the complexity of propagation mechanisms involved in foam flow through porous media.

Frontal advance theories such as the Buckley-Leverett or Dietz models assume the injection of a single phase, homogeneous, and nonreactive fluid, whereas the simultaneous injection of gas and surfactant **does not meet this** criterion. In early stages of displacements **through the** two-dimensional sandpack used in **this** study, the gas and surfactant solution were seen to dissociate and segregate, flowing separately. **This** collapse of foam was attributed to the **losses** by adsorption, partitioning, degradation and **other thermodynamic** instabilities. **The** in-situ generation of foam did not **seem** to initiate until a **certain** mass of surfactant had been flushed through to **counter these** foamicidal effects (see Section 5.1 for further description).

In the absence of well established theories applicable to foam flow, the **frontal** advance behavior was described with the help of simplified models. The models proposed here were inferred from direct observation through the two-dimensional visual sandpack.

#### 43.1. Linear Flow

**When** gas and surfactant **solution mixture** or preformed foam is injected in a porous **medium**, the foam tends to break down and the injected fluid enters the formation as a **two-phase mixture**. The surfactant **solution** loses most of the surfactant **mass to the surroundings**. It does not advance as fast as the **gas** due to the lower injection **rate** and lower mobility, thus the liquid front lags behind the **gas front**. **Gas** is able to, however, propagate through the

liquid bank. After the mass of surfactant flushed through the injection end is enough to overcome the losses, foam generation starts at this end, and the foam then forms a third front. The idealized diagram for this linear flow model behavior is shown in Fig. 4.2.

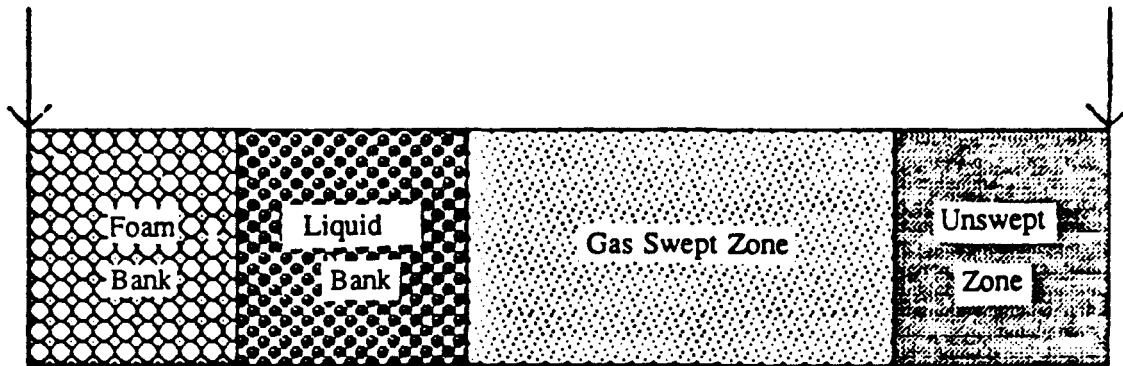


Figure 4.2 Idealized Frontal Behavior of Linear Oil Displacement by Gas/Surfactant Solution under Partially Foaming Conditions.

The recovery could be approximated by the superposition of these individual drives. The recovery due to gas drive can be approximated by the Buckley-Leverett advance mechanism. The recovery due to liquid drive can be obtained by assuming a piston-like displacement with only residual oil left behind the liquid front. The recovery due to foam could be neglected since foam is advancing through the zone where movable oil has already been displaced by the liquid drive.

It is also possible to speculate with the help of this simplified model, on the circumstances under which a foam drive will improve recovery. If foam is generated or able to persist, there would be no free gas or free liquid, and thus the gas-swept and the liquid-swept zones would not develop. In this case, foam would displace oil in a piston-like manner with only residual oil left in the swept zone. The recovery, given by the material balance, would be higher than either a gas flood or water flood because of the displacement of all the movable oil through the swept zone, as opposed to the Buckley-Leverett gradual saturation change. Also the front will be more stable because of an increase in apparent viscosity of foam, and thus the recovery would be higher than for an unstable surfactant flood.

On the other extreme, it can be assumed that foam will not generate or persist in the porous medium during the useful productive life of the flood, in which case only gas-swept and liquid-swept zones would advance. The recovery would be higher than the gas drive by an amount equal to the liquid drive through a gas-swept zone.

If foam flow starts somewhere during the useful productive life, which is generally the case, the performance will be between the two conditions described above.

## 43.2. Two-Dimensional Flow

Unlike linear oil displacement by foam, a two-dimensional displacement involves two nonlinear **fronts** of the gas and surfactant solution. **The** profiles of these fronts **are** sensitive to the operating conditions, especially to the rates and the **ratios** of fluids injected. **A** broad range of flow behavior **has** been observed through the visual two-dimensional sandpack. These various flow behaviors **are** shown in **Figs. 4.3** through **4.13**, and **are** explained in **this and next sections**.

In most **cases** the behavior was found to closely approximate a combination flood in which the top zone is under gas injection and the bottom zone is under surfactant solution drive (**Fig. 4.3**). In each of **the** two zones, fluid advance is by gravity tongues which grow in size and eventually interfere with each other. The behavior becomes complex after their interference, since by that time foam **has** propagated through the entire gas zone up to the producing end. The practical ultimate recovery is obtained by **this time so** the flow behavior at **this** stage is not important to **the** recovery.

Foam does not propagate with gas at early times due to losses. **A** surfactant solution bank is formed which meets two important criterion of the Dietz Model; *i.e.*, gravity tonguing and a sharp saturation gradient across the front. Foam generation is started after the losses are overcome, and thereafter, foam advances in the form of a third **front**. **This front** has a piston-like **shape** and it advances more slowly than either **gas** or surfactant fronts; and only through the gas-swept **zone**. **This** idealized behavior is shown in **Fig. 4.3**. The **total pressure** drop across **the** gas-swept **zone** is due to the composite effect of **the pressure drops** in the two zones; *i.e.*, **the foam zone** near **the** injection well and **the gas-only zone** near **the** producing well. The idealized pressure profiles are **shown** in **Fig. 4.4**.

The foam advances through **the zone** already swept by large volumes of gas throughout, where oil saturation **has** become low and **the** amount of oil left to be displaced by foam is insignificant. Nevertheless, **the** contribution of **the** foam to overall recovery is significant, **since** it creates vertical pressure gradients and thereby results in cross-flow. Thus **the** gas sweeps downward and the surfactant solution sweeps upward improving the sweep efficiency.

The combination flood described above **was** not **the** only behavior observed in **this** study, but it was obtained for **many** experimental **conditions**. **A** series of laboratory **tests** were performed to identify the important factors affecting the **frontal** behavior, and **the** following were found to be the most important **ones**:

- (a) Mode of injection
- (b) Mobility ratios
- (c) Location of injection and production intervals
- (d) Surfactant concentration
- (e) **The injection rate**
- (f) **The gas/surfactant solution volume ratio**

**Runs** were performed to understand the effect of each of these factors and **the** results are presented in Section **6** where simplified conceptual **models** and **the** experimental observations **are compared**. The effects of these parameters **are** discussed qualitatively in **the** following paragraphs and in Section **4.4**.

For gas/surfactant injection, **the** mobility **ratio** between in-situ oil and surfactant solution being injected is more important than between injected gas and in-situ oil. **This** is because the

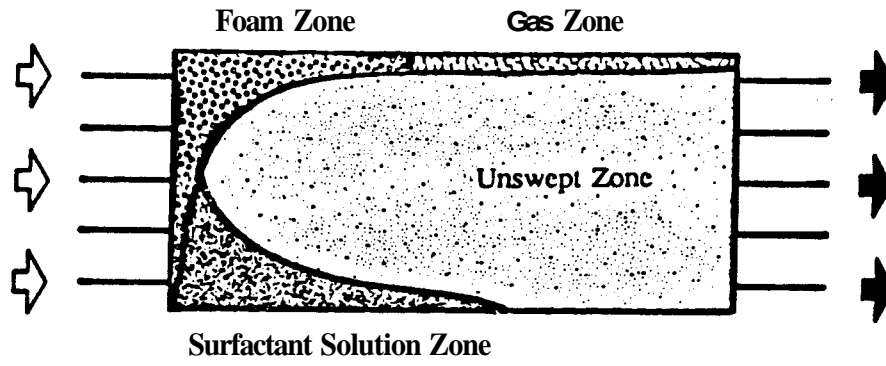


Figure 4.3 Idealized Frontal Behavior of a Combination-Drive Displacement

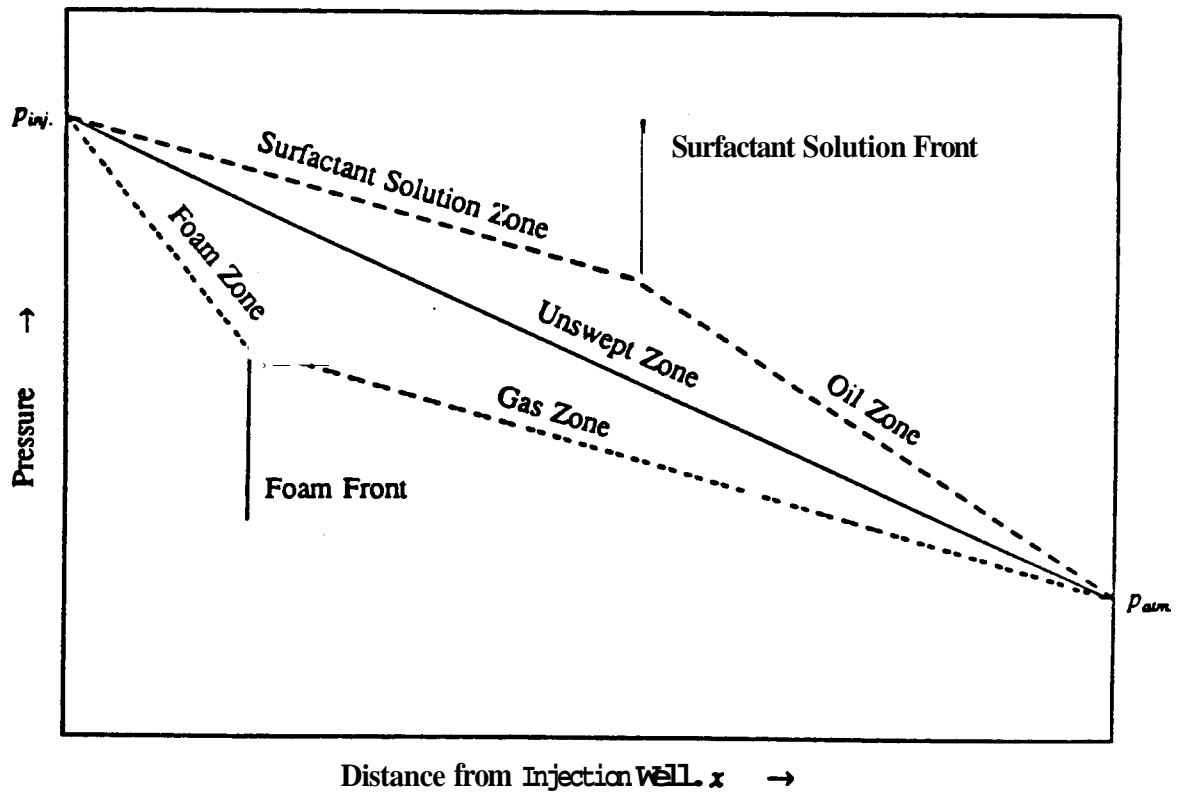


Figure 4.4 Idealized Pressure Profiles of Different Zones for a Combination-Drive Flood.

mobility ratios between gas and oil are always high, and within practical limits of mobility ratios, no appreciable change in gas behavior is expected. However, the mobility ratio between surfactant solution and oil can be favorable, in which case the surfactant bank will advance in a piston-like manner, as shown in Fig. 4.5.

The injection rate of surfactant solution also affects the frontal behavior. At higher rates, the flow could be viscous-dominated in which surfactant solution advances in the form of viscous fingers [see Fig. 4.6(a)]. At low rates, gravity-dominated behavior could be expected where gas and surfactant solution are fully segregated and are flowing in separate tongues [see Fig. 4.6(b)]. The tongues are initially thin but their thickness increases with the total throughput. Foam generation is considerably delayed since the volume of surfactant that comes in direct contact with the gas is small due to the gravity segregation.

The location of the injection and production ports had little effect on the performance of a preformed foam injection or an alternate slug injection, but had a pronounced effect on simultaneous injection. The effect of port locations during the simultaneous injection of gas and surfactant solution is shown in Fig. 4.7. The two-dimensional sandpack had five injection and five producing intervals. The location effect was more pronounced on the behavior of the surfactant front than it was on the gas front. Gas overrode quickly in all runs.

Injection from the bottom interval increased gravity segregation of the surfactant tongue because the bottom injection location increased surfactant underdrive [Fig. 4.7(a)]. Injection from the top reduced surfactant tonguing because some of the surfactant also entered the gas-swept zone [Fig. 4.7(b)], therefore the losses were overcome earlier and foam generation was quicker. The gas broke through somewhat sooner in this case, since the top injection location also furthered gas segregation, but this effect on the recovery or pressure behavior was small as compared to the improvement in surfactant profile.

Production from the bottom location increased gravity tonguing of the surfactant bank and reduced gas tonguing, whereas production from the top location had just the opposite effect. Production from all ports increased gravity tonguing for both the gas and surfactant solution fingers. When both the injection and production were from the entire formation, the behavior [Fig. 4.7(c)] was somewhere in between the behavior shown in Figs. 4.7(a) and (b).

The concentration of surfactant in the solution is also important, since it affects the onset of foam generation, the rate of foam front advance and the stability of the surfactant front. The behavior of a low concentration run (below critical micellar concentration) is shown in Fig. 4.8(a). The surfactant-oil interface was not very sharp due to the pronounced imbibition effects, and the vertical profile of the surfactant front was also improved. Due to the losses of surfactant, the generation of foam was delayed, and the presence of foam was noticed only late in the life of the flood. In some low concentration runs foam was not generated at all during the flood. However, once foam generation started, the physical properties of foam (*i.e.*, stability, mobility etc.) were seen to be quite independent of concentration.

The frontal behavior of a higher concentration surfactant solution run is shown in Fig. 4.8(b). The losses were overcome earlier because of higher concentration of surfactant in the solution and the foam bank could be seen early in the flood. Surfactant underdriving was severe due to the reduction of capillary forces, but the gas overriding was insensitive to the concentration until foam generation began, after which the foam front advanced faster for a higher concentration surfactant solution displacement which resulted in a rapid increase in gas tongue thickness.

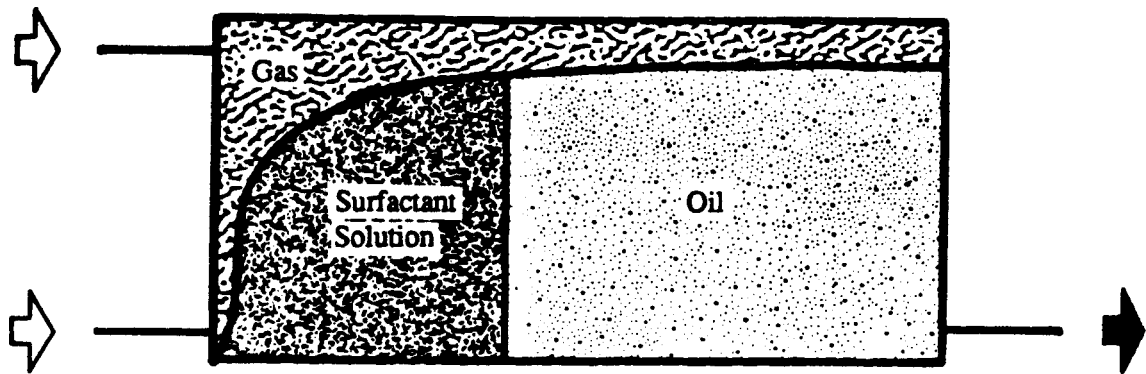


Figure 4.5 An Idealized Diagram for a Run with Favorable Mobility Ratio Between Surfactant Solution and Oil.

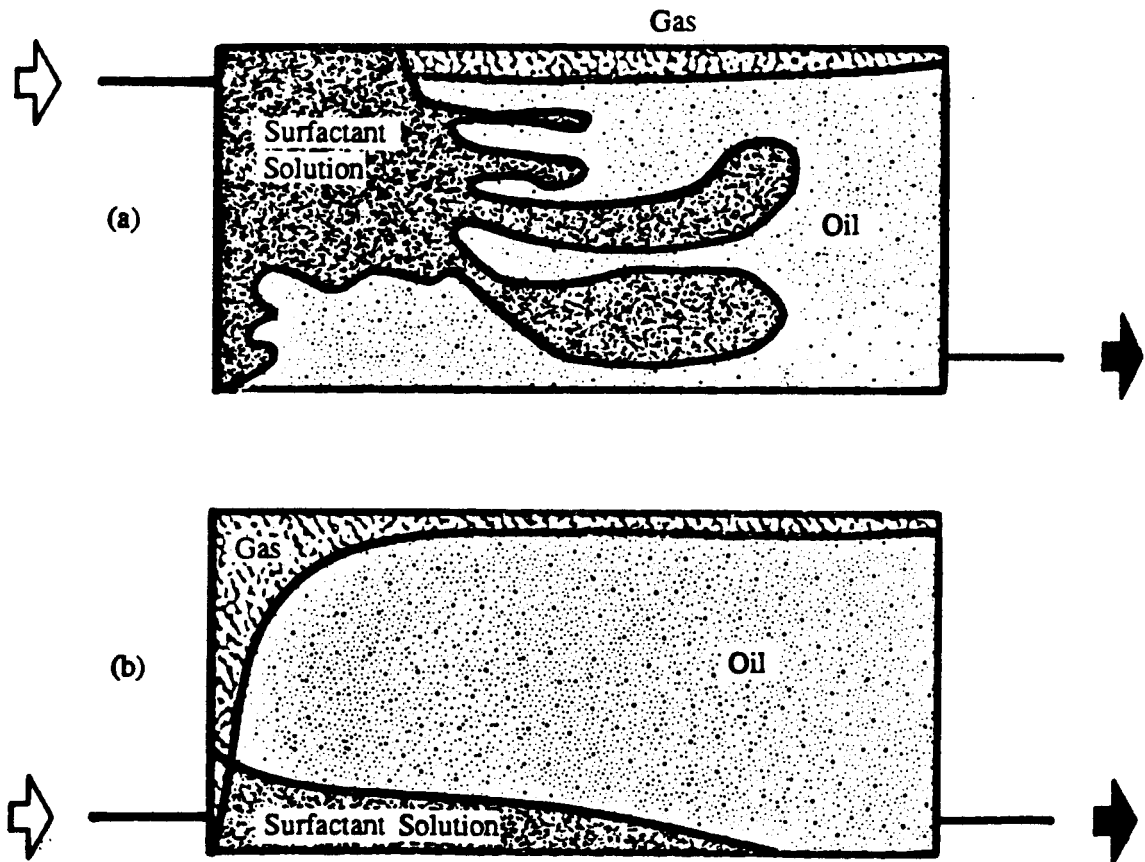
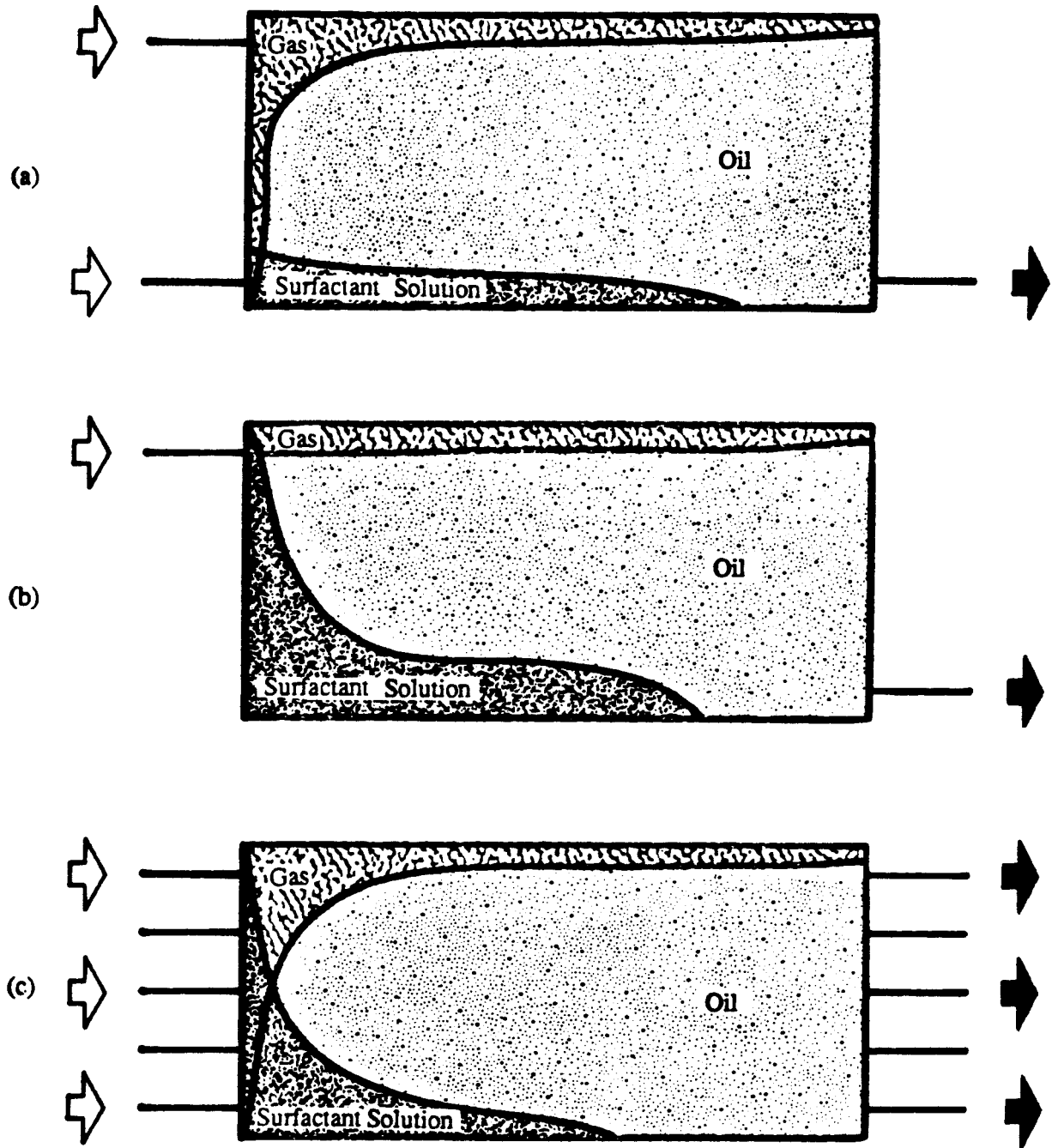
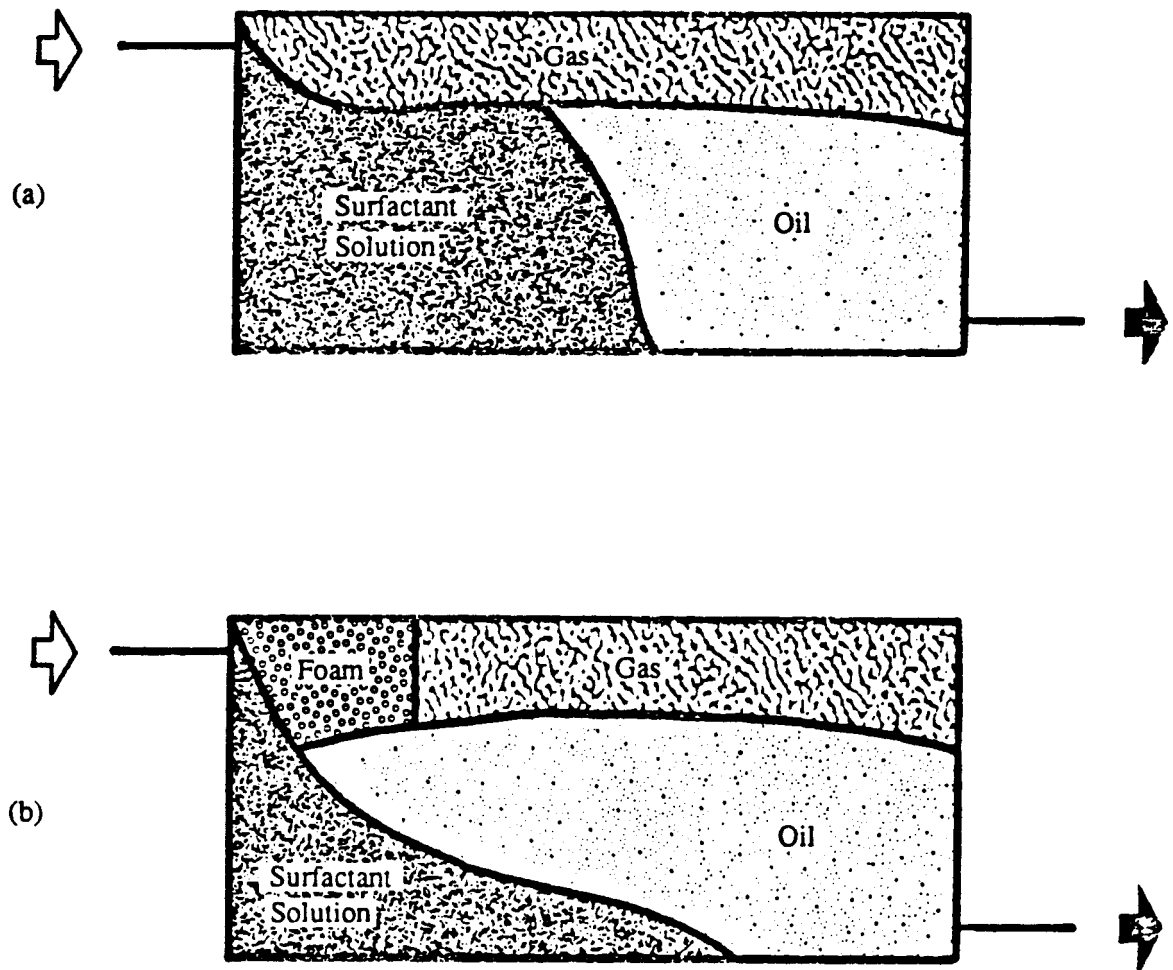


Figure 4.6 Effect of Injection Rate on Frontal Behavior of Surfactant Solution: (a) Viscous-Dominated Flow, (b) Gravity-Dominated Flow.



*Figure 4.7* Effect of Location of Injection and Production Interval for the Simultaneous Injection of Gas and Surfactant Solution:  
(a) Both Injection and Production from Bottom,  
(b) Injection from Top and Production from Bottom,  
(c) Injection and Production for Entire Formation.



*Figure 4.8* Effect of Surfactant Concentration on Frontal Behavior of Gas and Surfactant Solution: (a) Low Concentration, (b) High Concentration.

Another parameter which had a substantial effect on **frontal** behavior was the gas/surfactant volume ratio. If the gas/surfactant solution volume ratio was high, the gas-surfactant mixture entering the formation collapsed as it contacted the newly invaded formation due to the foamicidal effects of reservoir rock and fluids. This collapsed surfactant drained **down** and formed a gravity finger as shown in Fig. 4.9(a). This finger grew in size and eventually acquired the shape of a typical gravity tongue undemding the **oil**. For an injection in which the gas/surfactant solution volume ratio was low, the excess surfactant segregated within the wellbore, and invaded the formation from the bottom in the form of a thin channel. Meanwhile, the surfactant entering the formation with gas moved in exactly the same manner as in the high gas-surfactant ratio runs shown in Fig. 4.9(b).

#### 4.4. SLUG DESIGN

The proper method of placing surfactant in a porous medium to optimize oil recovery is still more of an art than a science. No theories at this time exist that can be used to get unique answers. The key factor in designing a slug is to reduce the time required for foam to be formed in-situ. The following are the important design parameters:

- (1) The mode of injection.
- (2) The type of surfactant-
- (3) The concentration of surfactant-
- (4) The volume of surfactant solution.
- (5) The injection location.
- (6) The injection rate.

The likely effects of each of these factors are described in the following paragraphs.

##### 4.4.1. Mode of Injection

There are three common methods of injecting surfactant to generate foam in-situ:

- (1) Alternate slug injection,
- (2) Preformed foam injection, and
- (3) Simultaneous injection of gas and surfactant solution.

Generally speaking, the performance of simultaneous injection was superior in the experiments performed in this study, to either slug injection or preformed foam injection. It had the lowest tendency for gravity segregation and there was a better control on the volume and concentration of the surfactant solution entering the sandpack with gas. This observation is limited to this particular experimental apparatus, since there are certain instances where other methods may prove to be more promising. Each of these methods are discussed below:

**Alternate Slug Injection:** The gas and surfactant slugs were injected alternately in this method. When a single large surfactant slug was injected first, it underrode, and broke through before the start of gas injection. When gas was injected subsequently, it overrode and flowed through the top channel, having very little contact with the surfactant solution. The sandpack behaved as if the lower part was under a surfactant solution flood, and the upper part was under gas injection (Fig. 4.10).

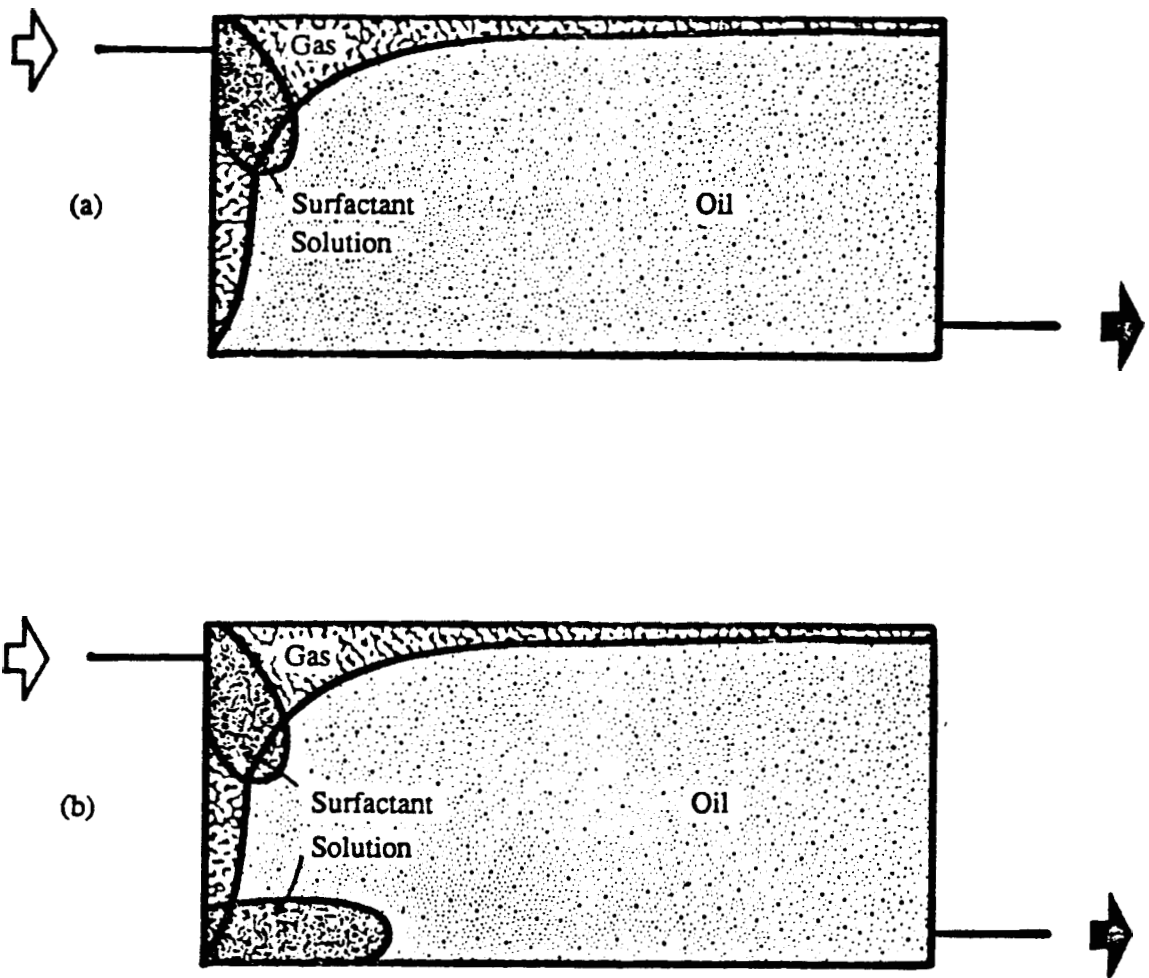


*Figure 4.9* Effect of Gas/Surfactant Solution Volume Ratio on **Frontal** Behavior:  
(a) High Gas to Surfactant Solution Volumetric Ratio,  
(b) Low Gas to Surfactant Solution Volumetric Ratio.

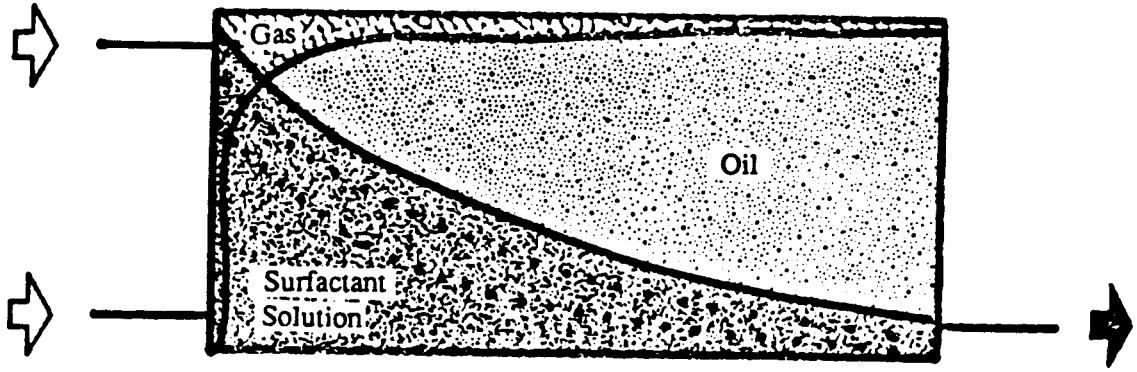


Figure 4.10 Idealized Front Profiles for Alternate Slug Injection: Large Slugs.

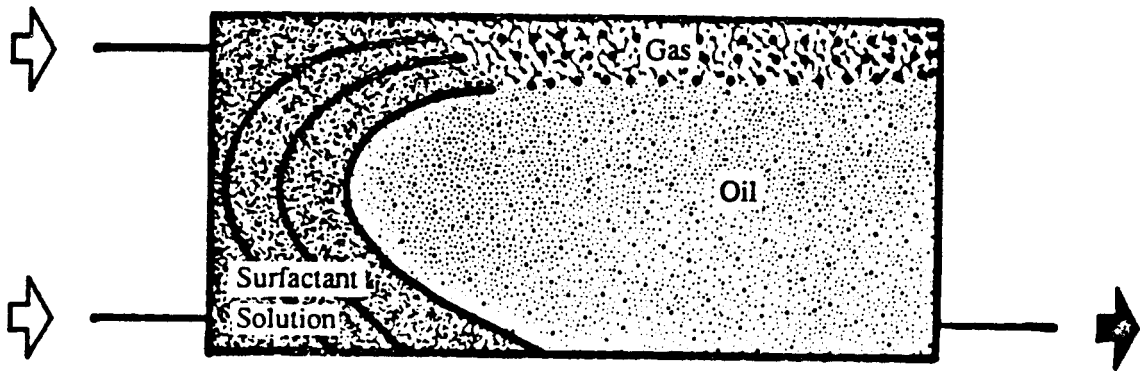


Figure 4.11 Idealized Front Profiles for Alternate Slug Injection: Small Slugs.

When a large number of small slugs were injected alternately, the gas injection started before the preceding surfactant slug broke through. Subsequent surfactant solution slugs also invaded the gas-swept top area (Fig. 4.11). Gravity segregation of surfactant solution seemed to be influenced by the size of surfactant slugs, such that smaller slugs showed less undemde. Therefore, it seemed beneficial to maintain the sizes of the slugs as small as practical limitations permitted.

Due to a greater delay in foam generation because of severe gravity segregation between gas and surfactant solution, the slug-type injection method was found not to be promising. A surfactant slug injected before gas injection would help in early foam generation if excessive underride could be controlled. This method may provide better vertical sweep efficiency in a reservoir with a permeability distribution which favors gravity override.

**Preformed Foam Injection:** Most of the preformed foam injected broke down at early time when it contacted the sandpack. The gas flowed in a thin gravity tongue on the top and broke through early. The size of this finger increased with an increase in gas throughput. Later in the life of the flood, a surfactant Solution bank was formed below the gas tongue, but adjacent to it (Fig. 4.12).

A serious problem in this method was the gravity drainage at the injection end which limited the volume of surfactant solution entering the sandpack to what could be sustained by the foam body. Excess surfactant drained down within the wellbore and underrode the formation, which, for practical purposes, made the displacement a case of dual injection with gas injection from the top and surfactant injection from the bottom.

Another problem in this method was the limitation on the concentration of surfactant solution entering the gas swept zone of the sandpack. The concentration of surfactant in the films of foam bubbles tends to be at the critical micelle concentration (CMC), quite independent of the concentration of the bulk phase. Since the surfactant was entering the gas-swept zone in the form of lamellae and bubbles only, the concentration of surfactant entering the gas swept zone was near the CMC.

The problem of the limited concentration and the limited volume of surfactant described in the two previous paragraphs, made the foamicidal action of the oil difficult to overcome, and large volumes of preformed foam had to be injected before it could survive in the porous medium. It should be emphasized here again that these observations are not general. Reformed foam could have potential if the problem of wellbore segregation and excessive collapse of foam could be solved by designing a better technique of injection and by discovering a surfactant of high CMC which could generate foam of low film thinning rate. This method could also be used if it is preceded by a large surfactant slug to overcome losses.

**Simultaneous Slug Injection:** Simultaneous injection appeared to be the best mode of injection because it did not have a surfactant solution undemde problem as severe as a slug type injection, nor was there any limitation on the concentration and volume of surfactant solution injected with gas. Foam was generated in-situ by the porous medium itself.

In this type of injection, a considerable volume of surfactant solution invaded the gas-swept zone in the form of a gas/surfactant mixture and gravity segregation was not severe as compared to the other two methods. Foam was generated earlier in this method because a greater volume of surfactant was entering the gas-swept zone, and the concentration of this surfactant was higher.

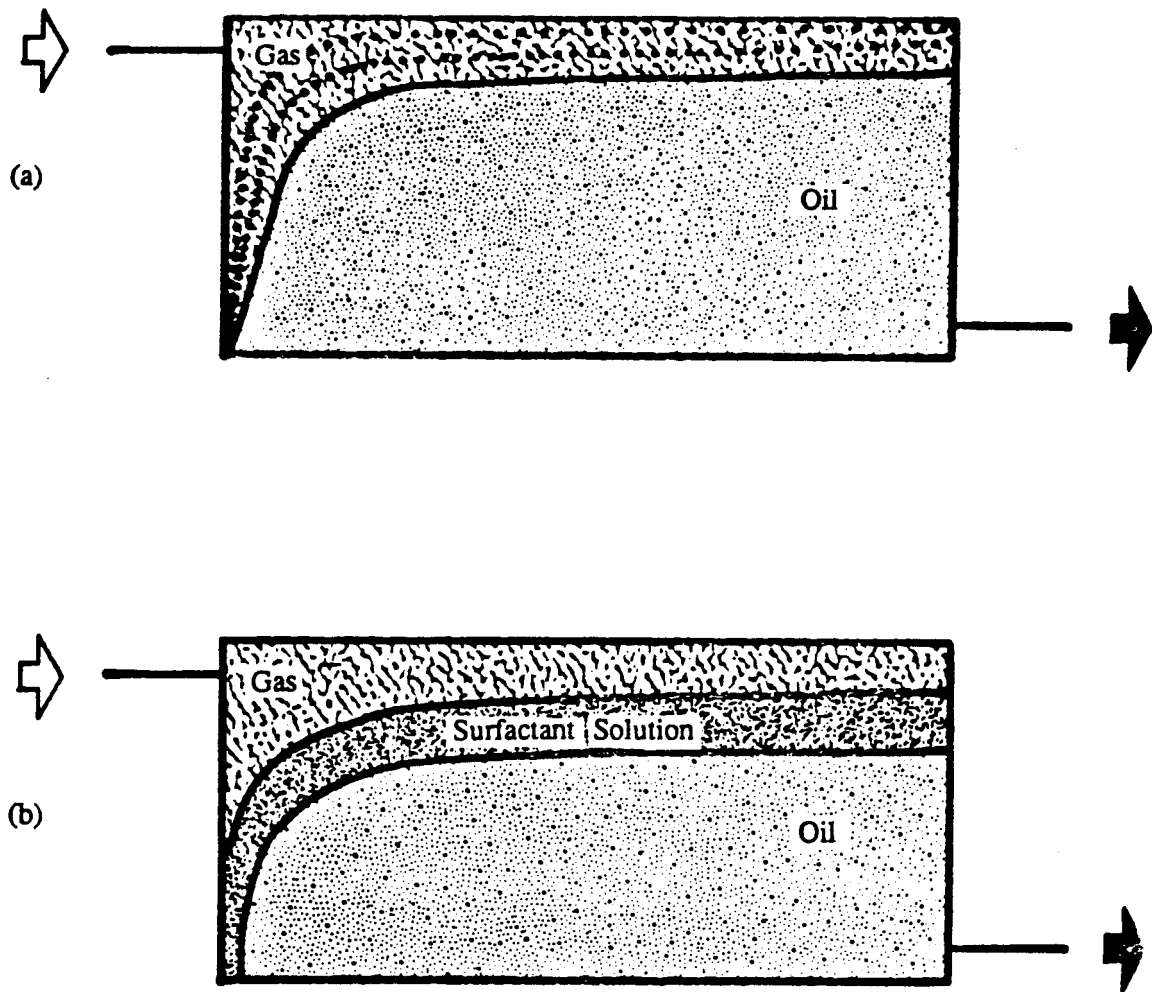


*Figure 4.12* An Idealized Diagram of Front Profiles During Preformed Foam Injection: (a) Early, (b) Later, showing Surfactant Bank.

The life of **this** simultaneous injection **run** can be divided into four stages (Fig. 4.13). The first stage is before the **start** of foam generation (Fig. 4.13(a) in which the gas and surfactant solution flowed in separate gravity tongues. The second stage **starts** when **the** foam generation initiates [Fig. 4.13(b)], and **lasts** until surfactant solution breaks through. The foam **front** advances in a piston-like shape, and both gas **and** surfactant solution tongues grow in size during **this** stage. The **third** stage is between the surfactant solution breakthrough and the finger interference [Fig. 4.13(c)], in which both the gas and the surfactant solution tongues **grow** in size. The fourth stage **starts** after these fingers interfere with each other [Fig. 4.13(d)] and the behavior becomes complex.

**This** method was seen to recover, in many **cases**, **twice** as much oil as the other **two** methods, since a substantial volume of oil could also be recovered after gas breakthrough. **A** delay in foam generation **was seen** in **this** method resulting in early **gas** breakthrough. **This** early breakthrough could possibly be reduced by injecting small slugs of highly concentrated surfactant solution alternated with small slugs of gas at the beginning of the displacement. If **this** were **med**, once foam generation **was** evidenced by a **sharp** decrease in injectivity, simultaneous injection could be started and continued until **the** end of the **flood**.

#### 4.42. Type of Surfactant

**This** is perhaps **the** most important decision in **the** process of proper slug design because **the** fate of the foam flood depends **on** it. The critical properties which must be considered include interfacial behavior, losses to reservoir rocks **and** in-situ **fluids**, and both chemical and thermal stabilities.

For good foamability, low CMC and low surface tension at CMC **is** required in a surfactant solution. **These** qualities **are** important for cyclic slug injection and simultaneous injection of gas **and** surfactant solution which depends on in-situ generation of **foam**, but **are** not critical for preformed foam injection.

Low interfacial tensions between surfactant solution and oil will reduce capillarity **thus** promoting emulsification and affecting trapped-oil saturation. Ultra-low interfacial tension may reduce residual oil saturation and **increase** recovery **on** a pore scale, **as** in some micellar floods, but ultra-low interfacial tensions **are** usually not encountered in a **foam flood**. On the other hand, **The** **reduction** of capillary forces may reduce vertical conformance, thereby lowering the recovery. Therefore, in reservoirs that have **high** initial water saturations, in cyclic slug injections where **aqueous** volumes **are** large, **or** other situations contributing to emulsification, low interfacial tensions should **be** avoided.

Spreading of oil on surfactant **solution** could **also** inhibit foam generation, hence low spreading is important for cyclic slug injection or simultaneous injection of gas and surfactant solution. For preformed foam injection, low adsorption and high mechanical stability are desirable to help the foam propagate **through** **the** **pres** without breakdown. **This** stability against **mechanical** breakdown could be checked by determining the **rate** of lowering of the surface tension or rate of attainment of equilibrium **at** a concentration just below the CMC. The ability of **a** surfactant solution **to** withstand **the** high temperatures and salinities generally found in reservoirs is also crucial for a preformed foam injection.

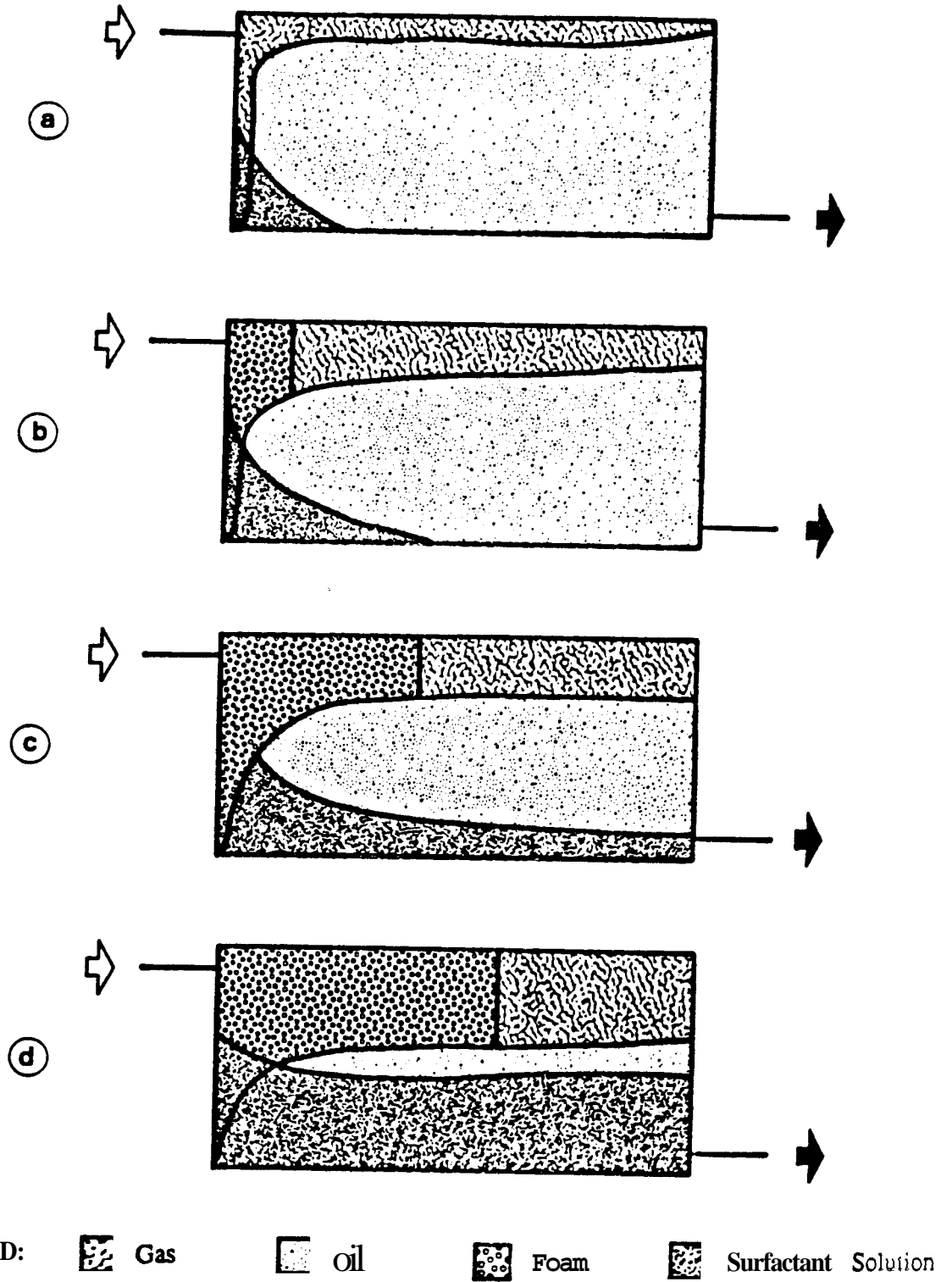


**Figure 4.13** Idealized Front Profiles for Different Stages of a Typical Gadsurfactant Solution Simultaneous Injection: (a) Before Foam Generation, (b) Foam

The most suitable surfactant for a foam **flood** may be defined as the one which has the lowest CMC, has the lowest surface tension to interfacial tension ratio at CMC, has the lowest spreading by oil, has the lowest losses, and is chemically and thermally stable in the reservoir conditions. Obviously, no single surfactant offers all these qualities and one has to compromise for optimizing the performance.

#### 4.4.3. Surfactant Concentration

Surfactant molecules, because of their unique hydrophobic-hydrophilic structure, are in the state of non-equilibrium when first introduced in an aqueous solution. The hydrophobic ends try to escape the bulk phase in order to reduce the free energy in the solution. Some of the molecules reach or form a surface or interface when they can orient themselves in such a way that their hydrophobic ends are away from the solution, satisfying the condition of minimum free energy. Eventually, orientation is completed and a state of equilibrium is reached. In surfactant solutions at or above the CMC, the bulk phase concentration is generally close to the surface concentration, since the excess molecules reorient themselves in the form of micelles. When a new surface is created, some molecules are transferred from the solution to the new surface thereby lowering the bulk phase concentration. In a reservoir, the surface areas are enormous, therefore, the adsorption of molecules on lamellae, on monolayers of aqueous-oil interfaces, and on rock surfaces can make bulk phase concentration much lower than injected concentration.

The injection of a dilute surfactant solution will tend to lower the foamability and foam stability. The injection of a concentrated solution, on the other hand, may cause emulsification of the oil. The optimum concentration is close to the CMC if there are no adsorption losses, but usually the concentration should be on the higher side to account for these losses.

#### 4.4.4. Surfactant Volume

The total volume of the surfactant injection is also an important design parameter. The cost effectiveness and the minimization of undemanded by surfactant solution should be the prime objectives. The relative volume of surfactant solution in a simultaneous injection process must be kept large because the effect of early surfactant breakthrough is small, as if a small portion of the reservoir was being water flooded instead of foam flooded. The volume of surfactant in a slug-type injection must be low because the early surfactant breakthrough will cause the subsequent slugs to merely flow through the same surfactant-swept zone without contributing further to the recovery. The volume of surfactant in a preformed foam injection can only be arbitrarily decided within the limits defined by the stability of the foam.

#### 4.4.5. Injection Location

The selection of the injection location depends on the mode of injection. In a slug-type process, surfactant solution should be injected at the top interval and the gas injected at the bottom interval so as to maximize the volume of surfactant solution coming in contact with the gas. In a preformed foam injection process, injection into an entire pay zone is desirable, whereas in a simultaneous injection process, injection into the top location is preferable. The injection at the top interval appears to be questionable because it could promote gas channeling, but the advantages of surfactant penetration into the gas channels are important for early foam generation.

The selection of an injection interval is more complex for heterogeneous reservoirs and requires a consideration of the permeability distribution. The objective should be to maximize the volume of surfactant solution coming in contact with gas. As a general rule, the aqueous slug should always be injected at the top interval except when low permeability streaks are encountered at the bottom of the reservoir, in which case injection at the bottom interval may be useful. By similar arguments, gas should always be injected at the bottom location, except where very low permeability streaks are present at the top. The interval into which gas is expected to be channeled must be selected for simultaneous injection method to minimize the delay in foam generation.

#### 4.4.6. Injection Rate

The effect of injection rate on the frontal behavior of a foam displacement is more pronounced than it is on waterflood or gas injection displacements. High injection rates favor displacement by lowering gravity segregation, but increase the mobility ratio due to a decrease in apparent viscosity of foam at higher flow rates. This is because of the pseudoplastic nature of foam. Therefore, flow rates should be as high as possible before gas breakthrough to minimize segregation, but afterwards should be lowered. However, high rates before breakthrough might cause the flow to be unstable resulting in a lower sweep efficiency, since the ability of capillary forces to resist fingering is minimized.

Many investigators have attempted to establish stability criteria for a variety of displacement conditions, but there has been no criterion established for deciding whether or not a gas/surfactant solution displacement under foaming conditions will be stable. In the experiments performed on the two-dimensional sandpack, the frontal behavior of gas was not changed much when injection rates were changed from 1 cm<sup>3</sup>/min to 200 cm<sup>3</sup>/min. Gas always segregated and moved through a thin gravity tongue on the top. However, the injection rate had a pronounced effect on the frontal behavior of the surfactant solution bank, and therefore, on the recovery and pressure behavior. Thus the author would suggest that an approximation of the critical rate for the onset of instability can be obtained by applying the stability criteria of a waterflood to the flow of surfactant solution, e.g. the one suggested by Peters and Flock (1981).

## 5. MATHEMATICAL FORMULATIONS FOR RECOVERY AND PRESSURE DROP

The theories of foam displacement through porous media are still in their infancy and a generally rigorous mathematical treatment is still not available. A few mathematical treatments have been proposed which fit with laboratory experiments under limited operating conditions, but a general theory applicable under a wide variety of conditions has not been proposed as described in Section 4, which are used here as a basis for mathematical treatment. An empirical relationship was found to describe the onset of foam generation and is described in the next section. The combination-drive model is described in Section 5.2. The approximate analytical equations for recovery and pressure drop of combination-drive displacement are derived in Sections 5.3 and 5.4, respectively. Another approximate model for displacement which does not resemble combination-drive behavior is derived in Section 5.5. These approximate analytical models are later compared with the experimental results in Section 6 and seem to be in good agreement.

### 5.1. ONSET OF FOAM GENERATION

A preformed foam injected into the sandpack had a tendency to break down initially. The same was also true for a gas surfactant in which foam did not generate in-situ at early times. Foam generation and propagation started only after large volume throughputs. This delay in foam generation was surmised to be due to neutralization of foamicidal surfaces and/or surfactant adsorption and has been termed the mass-effect.

The frontal behavior, recovery and pressure drops were appreciably changed by the generation of foam. Thus it became important to determine when foam generation would begin for recovery and pressure drop prediction. No guidelines are published in the literature to estimate the onset of in-situ foam generation. To make such an estimate, it would be important to understand the probable nature of losses and foam stability.

The reservoir rocks and fluids seem to have a foam breaking effect. The surfactant molecules migrate from foam lamellae to these newly-contacted surfaces and interfaces. This exchange causes weak spots of low surfactant concentration on the lamellae creating enough shock to break them. This foamcidal effect is reduced as more surfactant comes in contact with the foamcidal surfaces, and finally, a state of equilibrium is reached whereby foam can coexist with them. In the above hypothesis, the mass-effect has been assumed to be due to the attainment of dynamic equilibrium at the interfaces, hence it was inferred that the mass of surfactant contained in the injected fluids and the rate at which injection takes place would play prominent roles.

To investigate these two parameters, two sets of runs were performed in the two-dimensional sandpack. In OM set of runs the concentration of the surfactant was changed at a constant injection ratio and constant rate. In the other set of runs the rate of injection was changed at a constant injection ratio and concentration. For the first set of runs, the results indicated a linearity between the throughput required before foam generation began and the logarithm of concentration (Fig. 5.1). Similarly, there was a linearity between the required throughput and logarithm of injection rate for the second set of runs (Fig. 5.2). Combining these results, the following empirical relationship was developed, which was found to fit the onset of foam generation with the experimental data:

$$(G_i)_{fg} \cong \left[ 3 \ln \frac{1}{C} + \frac{1}{3} \ln q_s + 0.25 \right] \quad (5.1)$$

Where

$(G_i)_{fg}$  = Gas throughput required before foam generation was started, pore volumes

$C$  = The surfactant concentration, wt. % active

$q_s$  = The rate of surfactant solution injection,  $\text{cm}^3/\text{min}$ .

This equation was adequate to fit data from the above runs in which injected quality was constant, but later runs also indicated an influence of the gas-liquid injection ratio. The equation was found to be proportional to the injected quality. By trial-and-error, the following equation was found to approximate the volume of gas injection necessary for the on-set of foam generation:

$$(G_i)_{fg} = \left[ \frac{q_g}{q_g + q_s} \right] \left[ 3 \ln \frac{1}{C} + \frac{1}{3} \ln q_s + 0.25 \right] \quad (5.2)$$

where  $q_g$  is the ratio of gas injection, standard  $\text{cm}^3/\text{min}$ . Although the reasons for the mass-effect are not clear, it is possible to speculate on the role of each term in this equation. Perhaps absorption in the oil, adsorption on the sand grains and gravity segregation of the surfactant solution play key roles.

The terms in the first bracket indicate the volume ratio of the total surfactant solution which is injected with the gas. This is the injected quality; it is not the same as the flowing quality because of gravity segregation. The first term in the second bracket accounts for the availability of surfactant molecules per unit volume of surfactant solution. With a higher concentration, more surfactant molecules are available and less volume throughput will be required.

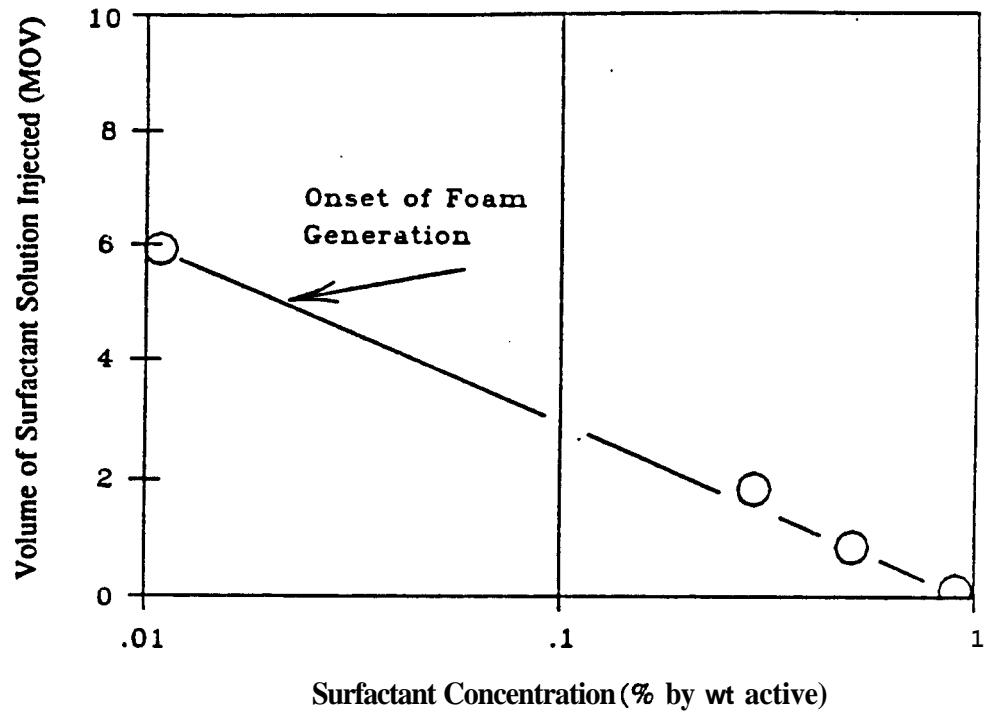


Figure 5.1 Effect of Surfactant Concentration on the Onset of Foam Generation.

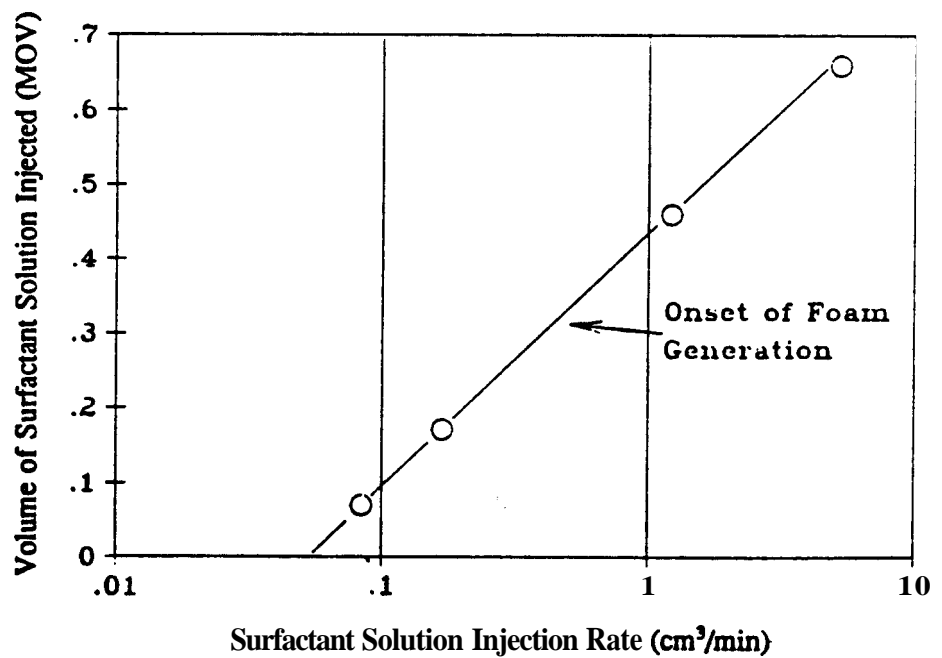


Figure 5.2 Effect of Surfactant Solution Rate on the Onset of Foam Generation.

The second term in the second bracket accounts for the proportion of surfactant mass retained in the sandpack. Most of the surfactant mass is produced, and only the small fraction retained in the sandpack is utilized in overcoming losses. This retention of the surfactant solution is a function of the injection rate. Less surfactant throughput is required at low rates because of a higher utilization, and vice versa.

Even though Eq. (5.2) in its present form satisfactorily predicted onset of foam generation, it is limited to this experimental system. It does not properly account for two-dimensional flow. In addition, this equation does not take into consideration the CMC, which is an important property on which equilibrium conditions depend. It is dimensionally incorrect also. Thus it is expected that systems with different geometry, different oils, different pore matrix and different surfactants will not be modeled by Eq. (5.2). It is recommended, therefore, that Eq. (5.2) should only be used as a basis for future research

## 5.2. DESCRIPTION OF THE COMBINATION-DRIVE MODEL

For modeling purposes, the life of the flood was divided in four stages. This division resembles closely the physical description of the four stages of a simultaneous injection run described in Section 4.4.1. and shown in Fig. 4.13. The only difference is the criterion for the end of the first stage which has been selected here to be the gas breakthrough instead of the onset of foam generation described previously. This change was necessary for the handling of the sharp mobility change which occurs as foam is generated.

The first stage [Fig. 4.13(a)] is from the start of injection until gas breakthrough. In this stage, recovery can be predicted by material balance. The pressure drop can be determined by applying Darcy's law after modifying it for the gravity segregation.

The second stage [Fig. 4.13(b)] is after gas breakthrough and includes displacement until surfactant breaks through. The total recovery during this stage is composed of two components, the recovery due to surfactant solution drive which can be obtained by simple material balance; and the recovery due to gas/foam drive which can be predicted using the Buckley-Leverett model.

In the third stage [Fig. 4.13(c)], which begins at surfactant breakthrough and lasts until the interference of gas and surfactant fronts, the recovery by gas/foam drive can be predicted as in the second stage, whereas the recovery by the surfactant solution drive can be computed using the Dietz model. It is assumed here that this drive meets the two important conditions of the Dietz model, namely the flow taking place in a gravity tongue and a sharp saturation gradient across the fronts. The total recovery is the sum of the recoveries by these two drives.

The fourth stage [Fig. 4.13(d)] begins when the surfactant and gas fronts interfere and lasts until the end of the life. This stage is complex, and its behavior is hard to predict, but the practical ultimate recoveries are obtained by the end of third stage.

Due to the losses described in Section 5.1, there is always some delay in foam generation. The onset of foam generation is approximated by the empirical relationship given in Eq. (5.2).

Foam advances through the gas tongue as a third front of low mobility and with a velocity much lower than the surfactant front. The movement of the foam front does not increase the pore-level displacement efficiency because it propagates only through the zone where oil

saturation has become low after large volumes of gas throughput. However, this foam front plays an important role in increasing the total pressure drop across the gas swept zone which is due to the composite effects of the pressure drop in the zone behind the foam front and the gas zone ahead. The increase in oil recovery is a result of this additional pressure drop.

### 5.3. RECOVERY FOR COMBINATION-DRIVE DISPLACEMENT

For approximate analytical modeling of a combination-drive process, the gas and surfactant flows are assumed to be taking place in separate gravity tongues. The gas tongue is handled in a fashion suggested by Dake (1978) in which a Buckley-Leverett displacement is modified for gravity. The surfactant solution tongue is treated as a Dietz (1953) tongue, and is coupled with the gas tongue in a manner that satisfies Darcy's law.

The producing life of a combination-drive flood is divided into the first three stages described in Section 5.2, whereas the fourth stage is nonproductive and is not included in this treatment.

#### 5.3.1. Scope and Limitations of Combination-Drive Model

The approximate analytical models derived in the following sections are inferred from visual observations through the two-dimensional sandpack, and are specifically related to this experimental system. The flow will probably not be the same near the wellbore in a reservoir, where the early flow is radial and the velocities vary with distance. Also the wellbore volume in comparison with the reservoir volume is much smaller than it was in this sandpack. The basic development is for a combination-drive displacement described in previous section. A range of other frontal behavior is expected when the operating conditions and the system are different. These models, however, provide guidelines for future developments.

The equations use a single value of mobility for gas-surfactant-foam flowing through the gas zone. In a typical gas-surfactant displacement, the mobility of gas changes as foam is generated, and thereafter, foam advances in the form of a third bank through the gas swept zone. It would be desirable to use a varying total mobility as the foam front moves through the system. To use a varying mobility, it would be necessary to estimate the onset of foam generation and then use a rheological model to take into account the advancing front. It was found that estimating the onset of foam generation by Eq. (5.2) and using an average value for the surfactant-gas-foam mobility in these approximate analytical models gave reasonable marches with the experimental data. The results are described and compared in Section 6.

#### 5.3.2. Assumptions for Approximate Analytic Modeling

The following are some of the simplifying assumptions made for the modeling:

- (1) Darcy's law is applicable and the gas velocity is low enough to neglect non-Darcy effects.
- (2) The flow is horizontal.
- (3) The flow is fully segregated, *i.e.*, gas and surfactant solution flow in different channels, and the mixed zone near the injection end is small.

- (4) The mobility ratios between gas/foam and oil, and between surfactant solution and oil are unfavorable, *i.e.*,  $m > 1$  and  $\bar{m} > 1$ .
- (5) The displacement through the gas tongue approximates the Buckley-Leverett mechanism, whereas the displacement through the surfactant solution tongue approximates the Dietz gravity tongue model. These two drives are mutually dependent and their effects must be calculated simultaneously.

### 533. Recovery Equations for Stage I

This stage starts at the start of injection and continues until gas breakthrough. The front profiles during this stage were shown in Fig. 4.13(a). It is assumed that the surfactant solution will not break through until long after gas breakthrough because of lower mobility and lower injection rate. The recovery during this stage is determined by material balance, *i.e.*, the volume of oil recovered is equal to the total volume of gas and surfactant solution injected. The recovery during this stage is thus given by:

$$N_{pD} = G_{iD} + W_{iD} = G_{iD} + \frac{G_{iD}}{R} \quad (5.3)$$

where

$$N_{pD} = \text{Cumulative oil produced, movable pore volumes} \\ = N_p / L h \phi (S_{oi} - S_{or})$$

$$W_{iD} = \text{Cumulative surfactant solution injected, movable pore volumes} \\ = W_i / L h \phi (S_{oi} - S_{or})$$

$$G_{iD} = \text{Cumulative gas injected, movable pore volumes} \\ = G_i / L h \phi (S_{oi} - S_{or})$$

$$R = \text{The ratio of gas injection to surfactant solution injection, } q_{ig} / q_{is}$$

The recovery at the time of gas breakthrough is determined from Eq. (5.27) derived in the development of the next stage.

### 53.4. Recovery Equations for Stage II

This stage starts after gas breakthrough and continues until surfactant solution breakthrough. The front profiles during this stage were shown in Fig. 4.13(b).

The recovery during this stage is assumed to be composed of two drives: gas/foam drive in the top zone, and surfactant solution drive in the bottom zone. This assumption is not rigorous, since there is a mixed zone near the injection well which will be included in both drives. The effect of this mixed zone included twice is a slightly higher recovery prediction than actually obtained. This mixed zone is generally negligible as indicated by visual observations and confirmed by comparison with the experimental results.

The recovery due to the gas drive is given by Buckley-Leverett frontal advance theory. The Buckley-Leverett equation in its standard form is given as:

$$V_{S_g} = \frac{dx}{dt} |_{S_g} = \frac{q_g}{A\phi} \frac{df_g}{dS_g} |_{S_g} \quad (5.4)$$

This equation relates the movement of the front to the fractional flow-saturation properties of the fluid/rock system. It simply states that the velocity of a constant gas saturation plane is directly proportional to the derivative of the fractional flow evaluated at the saturation of the plane. On integration and rearrangement, Eq. (5.4) becomes:

$$x_{S_g} = \frac{G_i}{A\phi} \frac{df_g}{dS_g} |_{S_g} \quad (5.5)$$

where  $G_i$  is the cumulative gas injected in volumetric units. After breakthrough,  $x_{S_g}$  equals  $L$  and Eq. (5.5) can be arranged to:

$$\frac{G_i}{LA\phi} = G_{id} = \frac{1}{\frac{df_g}{dS_g} |_{S_g}} \quad (5.6)$$

where  $G_{id}$  is the cumulative gas injection in pore volumes. Welge (1952) has derived an equation to determine the average saturation of a reservoir during a flood displacement based on Buckley-Leverett theory. The average gas saturation according to Welge is:

$$\bar{S}_g = S_{ge} + (1 - f_{ge}) \frac{1}{\frac{df_g}{dS_g} |_{S_{ge}}} \quad (5.7)$$

where subscript  $e$  denotes the producing end conditions. Equation (5.6) shows that the slope of the fractional flow curve,  $\frac{df_g}{dS_g} |_{S_{ge}}$  is the inverse of cumulative throughput, which reduces Eq. (5.7) to:

$$\bar{S}_g = S_{ge} + (1 - f_{ge}) G_{id} \quad (5.8)$$

By the principle of material balance,  $\Delta \bar{S}_g$  equals cumulative recovery, and when there is no initial gas saturation, it also implies that  $\bar{S}_g = N_{pd}$ . Thus Eq. (5.8) can be written as:

$$N_{pd} = \bar{S}_g = S_{ge} + (1 - f_{ge}) G_{id} \quad (5.9)$$

It will be more convenient later to express these terms in movable pore volume units as defined in Eq. (5.3). Rewriting Eq. (5.9) in terms of  $N_{pD}$  and  $G_{iD}$ , yields:

$$N_{pD} = \frac{S_{ge}}{1 - S_{or} - S_{wc}} + (1 - f_{ge}) G_{iD} \quad (5.10)$$

At this point in the development, an important assumption is made which is a key to the entire formulation. It is assumed that the displacement through the gas zone, whereas essentially following the Buckley-Leverett displacement, also meets one of the conditions of Dietz gravity tongue. It is not a true Dietz tongue, however, because it does not meet the criterion which requires that the saturation gradient across the front be sharp. What this assumption amounts to is that the displacement is Buckley-Leverett along the flow, whereas it has a shape similar to a Dietz gravity tongue in the direction normal to the flow.

This type of hybrid displacement can be handled in two ways. In one approach as taken by Dake (1978), the flow is essentially considered Buckley-Leverett but is linearized using a saturation-averaging technique in the flow-normal direction. In the other approach, which is used here, the flow is assumed to be taking place in the form of a tongue, similar in shape to Dietz gravity tongue but not necessarily similar in thickness. The thickness of this tongue is such that it satisfies the material balance obtained by a linear Buckley-Leverett displacement taking place through the entire pay zone. This point will be elaborated further as the development progresses.

For this type of displacement, the average saturation of gas,  $\bar{S}_{gx}$ , at a plane  $x$  where the thickness of the gas pseudotongue is  $\bar{y}_x$  can be given by a thickness-weighted average as follows:

$$\bar{S}_{gx} = \frac{(S_{gx})_{swept} \bar{y}_x + (S_{gx})_{unswept} (h - \bar{y}_x)}{\bar{y}_x + (h - \bar{y}_x)} \quad (5.11)$$

For a Dietz gravity tongue displacement, the saturation of gas anywhere in the swept zone is:

$$(S_g)_{swept} = 1 - S_{or} - S_{wc} \quad (5.12)$$

and the saturation of gas in the unswept zone is zero. On substitution of the gas saturation in the swept and unswept zones, Eq. (5.11) reduces to:

$$\bar{S}_{gx} = \frac{\bar{y}_x}{h} (1 - S_{or} - S_{wc}) \quad (5.13)$$

Let the fractional thickness of the gas tongue at plane  $x$ ,  $\bar{y}_x/h$ , be called  $b_x$ . Then the fractional thickness at the end is denoted as  $b_e$  and the average saturation at the producing end [(Eq. (5.13))] is rewritten as:

$$(\bar{S}_{ge}) = b_e (1 - S_{or} - S_{wc}) \quad (5.14)$$

To satisfy the material balance, the average saturation at the producing end of this pseudotongue must equal the producing end saturation as if it had been truly a linear Buckley-Leverett displacement from the entire formation. Hence the producing end saturations given by the pseudotongue [(Eq. (5.14))] and given by Buckley-Leverett [(Eq. (5.13))] must be equal. Thus  $\bar{S}_{ge}$  from Eq. (5.14) can be substituted into Eq. (5.10) resulting in:

$$N_{pD} = b_e + (1 - f_{ge}) G_{iD} \quad (5.15)$$

For a Dietz tongue, the fraction of gas flowing in the total stream can be determined by using the following definition of fractional flow:

$$f_{ge} = \frac{q_g}{q_g + q_o} \quad (5.16)$$

The gas and oil rates at the producing end can be determined by applying Darcy's Law to a unit width of porous medium:

$$\text{gas rate:} \quad q_g = -\bar{y}_e \frac{kk_{rg}}{\mu_g} \frac{\partial p_g^o}{\partial x} \quad (5.17)$$

$$\text{oil rate:} \quad q_o = -(h - \bar{y}_e) \frac{kk_{ro}}{\mu_o} \frac{\partial p_o^o}{\partial x} \quad (5.18)$$

where

- $\bar{y}_e$      ▪ Thickness of an equivalent gas tongue at the producing end
- $p_o^o$  and  $p_g^o$    ▪ Pressures in oil and gas zones, respectively, on the datum line at the producing end

When rates are substituted using Darcy's law [Eqs. (5.17) and (5.18)], and the horizontal pressure gradients are assumed to be the same in the oil and the gas tongues, the fractional flow equation [(Eq. (5.16))] becomes:

$$f_{ge} = \frac{\bar{y}_e \frac{k_{rg}}{\mu_g}}{\bar{y}_e \frac{k_{rg}}{\mu_g} + (h - \bar{y}_e) \frac{k_{ro}}{\mu_o}} \quad (5.19)$$

The mobility ratios are defined at the residual saturations of the displaced fluids, e.g., the mobility ratio of gas is given as:

$$\bar{m} = \frac{\left[ \frac{k_{rg}}{\mu_g} \right]_{S_{or}}}{\left[ \frac{k_{ro}}{\mu_o} \right]_{S_{oi}}} \quad (5.20)$$

Substituting the mobility ratio,  $\bar{m}$ , as defined above into Eq. (5.19) results in:

$$f_{ge} = \frac{\bar{y}_e \bar{m}}{\bar{y}_e \bar{m} + h - \bar{y}_e} = \frac{\bar{y}_e \bar{m}}{h + (\bar{m} - 1)\bar{y}_e} \quad (5.21)$$

Using the definition of the fractional thickness of the gas tongue,  $b_e = \bar{y}_e / h$ , this equation can be rewritten as:

$$f_{ge} = \frac{A b_e}{1 + (\bar{m} - 1) b_e} \quad (5.22)$$

This fractional flow of gas at the producing end obtained by applying the Dietz sharp saturation gradient concept to the pseudotongue must be equal to the fractional flow of a Buckley-Leverett displacement as defined by the fractional flow equation. Thus Eq. (5.22) can be substituted into Eq. (5.15):

$$N_{pD} = b_e + \left[ 1 - \frac{\bar{m} b_e}{1 + (\bar{m} - 1) b_e} \right] G_{iD} \quad (5.23)$$

The fractional thickness of the gas pseudotongue at the producing end,  $b_e$ , can be obtained from the following expression derived later in Stage III:

$$b_e = \frac{\sqrt{\bar{m} G_{iD}} - 1}{\bar{m} - 1} \quad (5.64)$$

On substitution of this value of  $b_e$ , Eq. (5.23) is simplified to:

$$N_{pD} = \frac{1}{\bar{m} - 1} (2\sqrt{\bar{m} G_{iD}} - 1 - G_{iD}) \quad (5.24)$$

This recovery equation is the same as Dake's (1978) mathematical treatment of a gravity segregated, horizontal and unfavorable mobility ratio displacement of oil by water. In his approach for calculating recovery for a segregated displacement, the Buckley-Leverett theory has been applied after reducing the displacement to one dimension by a saturation averaging technique. The fact that these equations are the same should not be surprising, since Dake has made assumptions which are the tenets of the Dietz gravity tongue model, i.e., a sharp saturation gradient and the use of end-point mobility ratios at residual saturations of the displaced fluids.

The above equation gives the recovery due to the gas drive only. Since the surfactant solution has not yet broken through, the recovery due to the surfactant solution drive is equal to the total surfactant solution injected,  $W_{iD}$ , which is defined as  $G_{iD} / R$ . The total recovery is thus given by adding the recoveries of these two independent drives:

$$N_{pD} = \frac{1}{\bar{m} - 1} (2\sqrt{\bar{m} G_{iD}} - 1 - G_{iD}) + \frac{G_{iD}}{R} \quad (5.25)$$

### 53.5. Recovery at Gas Breakthrough

Due to the material balance, the recovery due to the gas drive must be equal to the gas throughput up to the gas breakthrough. Thus the recovery at breakthrough due to gas drive,

$(N_{pD})_g$  can be determined from Eq. (5.24) after replacing both  $N_{pD}$  and  $G_{iD}$  with  $(N_{pD})_g$  and simplifying:

$$(N_{pD})_g = \frac{1}{\bar{m}} \quad (5.26)$$

The total recovery at gas breakthrough can be obtained by adding the recovery due to the gas drive given by Eq. (5.26) with the recovery due to the surfactant solution drive given by material balance:

$$N_{pD} = (N_{pD})_g + (N_{pD})_s = \frac{1}{\bar{m}} + \frac{(G_{iD})_{bt}}{R} = \frac{1}{\bar{m}} + \frac{1}{\bar{m}} \left( \frac{1}{R} \right) \quad (5.27)$$

### 53.6. Recovery at Surfactant Breakthrough

Up to surfactant breakthrough, the recovery due to surfactant solution drive is given by the following expression which is similar to the one for gas drive [Eq. (5.26)]:

$$(N_{pD})_s = \frac{1}{m} \quad (5.28)$$

However, due to the material balance, this recovery is also equal to the total surfactant solution throughput,  $W_{iD}$ , and is related to the total gas throughput by a factor R, which is defined as the ratio of gas and surfactant solution injection rates. Thus Eq. (5.28) can be written as:

$$(N_{pD})_s = 1/m = W_{iD} = (G_{iD})_{bt}/R \quad \text{or} \quad (G_{iD})_{bt} = R/m \quad (5.29)$$

Thus Eq. (5.25), after substitution for  $(G_{iD})_{bt}$  becomes:

$$(N_{pD})_{bt} = \frac{1}{m} + \frac{1}{(\bar{m} - 1)} \left[ 2\sqrt{\frac{\bar{m}}{m} R} - 1 - \frac{R}{m} \right] \quad (5.30)$$

Surfactant breakthrough occurs when oil production has reached the volume as given by Eq. (5.30).

### 53.7. Development of Recovery Equations for Stage III

This stage starts after the surfactant solution breakthrough and continues until the maximum recovery is obtained. The front profiles during this stage are shown in Fig. 4.13(c). This diagram is reproduced here as Fig. 5.3 including labels for the variables; and a detailed enlargement of the surfactant tongue is shown in Fig. 5.4.

The characteristic equation describing displacement can be obtained by considering a vertical cross-section at a distance  $x$  from the injection well at time  $t$ , as shown in Figs. 5.3 and 5.4. The pressure gradients in the oil and surfactant solution zones can be related by

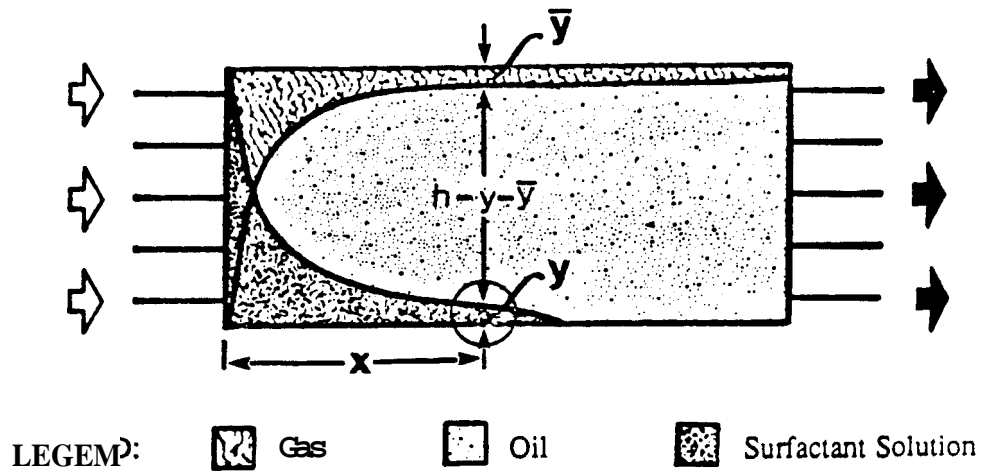


Figure 5.3 Front Profiles of a Combination-Drive Displacement During Stage III.

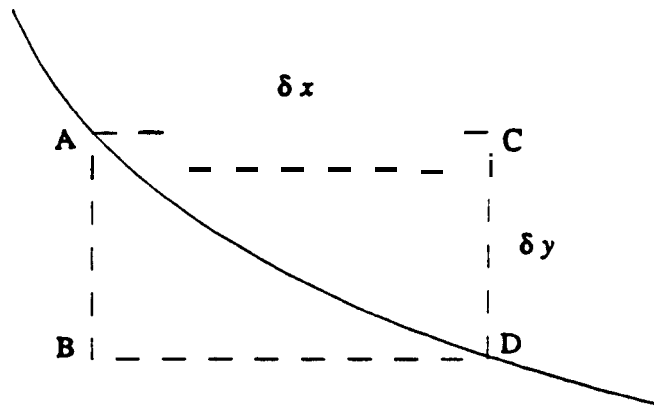


Figure 5.4 Enlarged View of the Surfactant Tongue at the Cross-section Encircled in Fig. 5.3.

considering the four points shown in Fig. 5.4. The pressures at any two points at the oil-water interface (front) can be related to each other by taking into account the gravity and viscous heads through the respective zones and accounting for the capillary pressure difference across the interface.

The pressure of the aqueous phase at point  $D$ ,  $p_s(D)$ , can be related to the pressure of the aqueous phase at point  $A$ ,  $p_s(A)$ , by taking into account the surfactant solution gravity head between points  $A$  and  $B$ , and the pressure gradient in the surfactant zone between points  $B$  to  $D$ . It can be written as:

$$p_s(D) = p_s(A) - \rho_s g dy + \frac{\partial p_s}{\partial x} dx \quad (5.31)$$

Similarly, the pressure of the aqueous phase at point  $D$  can be related to the pressure of the aqueous phase at point  $A$  by taking into account the pressure drop due to capillarity across the oil-surfactant solution interface at point  $A$ ,  $P_c(A)$ , the pressure gradient in the oil zone between points  $A$  and  $C$ , the oil gravity head between points  $C$  and  $D$ , and again the pressure drop due to capillarity across the oil-surfactant solution interface at point  $D$ ,  $P_c(D)$ :

$$p_s(D) = p_s(A) + P_c(A) + \frac{\partial p_0}{\partial x} dx - \rho_0 g dy - P_c(D) \quad (5.32)$$

It can be assumed that the capillary pressure gradient is small, which is generally the case for a Dietz gravity tongue having a sharp saturation gradient across the interface. Thus the capillary pressures at points  $A$  and  $D$  can be considered the same and cancelled. Equations (5.31) and (5.32) can then be equated and simplified, which results in:

$$\frac{dy}{dx} \Big|_x = \frac{\frac{\partial p_s}{\partial x} - \frac{\partial p_0}{\partial x}}{(\rho_s - \rho_0) g} \quad (5.33)$$

The gas flux, the surfactant solution flux and the oil flux per unit of cross-sectional width can be calculated by applying Darcy's law in the gas, the surfactant and the unswept zones individually:

$$q_g = \bar{y} \frac{k_g}{\mu_g} \frac{\partial p_g}{\partial x} \quad (5.34)$$

$$q_s = -y \frac{k_s}{\mu_s} \frac{\partial p_s}{\partial x} \quad (5.35)$$

$$q_0 = -(h - y - \bar{y}) \frac{k_0}{\mu_0} \frac{\partial p_0}{\partial x} \quad (5.36)$$

thickness and the gas zone thickness, respectively. The slope of the surfactant solution tongue is obtained by placing the pressure gradients from Eqs. (5.35) and (5.36) into Eq. (5.33):

$$\frac{\partial y}{\partial x} = - \frac{\left[ \frac{q_s}{y} \right] \left[ \frac{\mu_s}{k_s} \right] - \left[ \frac{q_0}{(h-y-\bar{y})} \right] \left[ \frac{\mu_0}{k_0} \right]}{g(\rho_s - \rho_0)} \quad (5.37)$$

The oil flow rate can be determined from material balance:

$$q_0 = q_t - q_s - q_g \quad (5.38)$$

where  $q_t$  is the total flow rate per unit cross-sectional width. The oil flow rate,  $q_0$  is replaced in Eq. (5.37) and rearranged:

$$\frac{\partial y}{\partial x} = \frac{\mu_0}{k_0 g (\rho_s - \rho_0)} \left[ - \left[ \frac{q_s}{y} \right] \frac{\mu_s / k_s}{\mu_0 / k_0} + \frac{q_t - q_s - q_g}{h - y - \bar{y}} \right] \quad (5.39)$$

Let the gas to oil mobility ratio, the surfactant solution to oil mobility ratio and the difference of density between oil and surfactant solution be defined as follows:

$$m = \left[ \frac{k_s / \mu_s}{k_0 / \mu_0} \right] \quad (5.40)$$

$$\bar{m} = \left[ \frac{k_g / \mu_g}{k_0 / \mu_0} \right] \quad (5.41)$$

$$\Delta\rho = (\rho_s - \rho_0) \quad (5.42)$$

These definitions of  $m$  and  $\Delta\rho$  are substituted into Eq. (5.39) which is then rearranged to:

$$\frac{k_0 g \Delta\rho}{\mu_0} \frac{\partial y}{\partial x} = \left[ \frac{q_t}{h - (y + \bar{y})} - \left[ \frac{1}{my} + \frac{1}{h - (y + \bar{y})} \right] q_s - \frac{q_g}{h - (y + \bar{y})} \right] \quad (5.43)$$

The ratio of gas to surfactant solution flux,  $R$  (defined earlier) is obtained by dividing the gas flux by the surfactant flux (as given by Darcy's law in Eqs. 5.34 and 5.35):

$$R = \frac{q_g}{q_s} = \frac{-\bar{y} \frac{k_g}{\mu_g} \frac{\partial p_g}{\partial x}}{-y \frac{k_s}{\mu_s} \frac{\partial p_s}{\partial x}} \quad (5.44)$$

This ratio, R, is difficult to determine at various cross-sections in the reservoir. It can be approximated, however, by the injection ratio of gas and surfactant solution, since in this stage both gas and surfactant solution have broken through. Thus the value of R being produced is close to the value being injected and is assumed to be nearly the same everywhere in the model. This assumption was tested by comparing the results from this development with the experiments and was found to be reasonable.

Dividing both the numerator and the denominator on the right-hand side of Eq. (5.44) by oil mobility,  $k_0/\mu_0$  and replacing the resulting mobility ratios with  $m$  and  $\bar{m}$  [Eqs. (5.40) and (5.41)] results in:

$$R = \frac{q_g}{q_s} = \frac{\bar{y} \bar{m}}{y m} \left[ \frac{\frac{\partial p_g}{\partial x}}{\frac{\partial p_s}{\partial x}} \right] \quad (5.45)$$

Since each zone is exposed to the same injection and producing well pressures, the pressure gradient in each zone has to be the same if the capillary pressure drop across the interface is negligible. Thus the last term on right hand side of Eq. (5.45) becomes unity, and it rearranges to:

$$\bar{y} = R (m / \bar{m}) y \quad (5.46)$$

For simplification, the expression,  $(1 + R m/\bar{m})$ , which appears rather frequently in the following developments, is defined as  $\beta$ , and substituted in Eq. (5.46):

$$y + \bar{y} = \beta y \quad (5.47)$$

This definition of  $(y + \bar{y})$  can be substituted in Eq. (5.43) to eliminate  $\bar{y}$ :

$$\frac{k_{0g}\Delta\rho}{\mu_0} \frac{\partial y}{\partial x} = \left[ \frac{q_i}{h - \beta y} - \left[ \frac{1}{my} + \frac{1}{h - \beta y} \right] \left| q_s - \frac{q_g}{h - \beta y} \right| \right] \quad (5.48)$$

Differentiating this equation with respect to  $x$  results in:

$$\begin{aligned} \frac{k_{0g}\Delta\rho}{\mu_0} \frac{\partial^2 y}{\partial x^2} &= \frac{q_i \beta}{(h - \beta y)^2} \frac{\partial y}{\partial x} + \frac{q_s}{my^2} \frac{\partial y}{\partial x} - \frac{1}{my} \frac{\partial q_s}{\partial x} - \frac{1}{(h - \beta y)} \frac{\partial q_s}{\partial x} \\ &\quad - \frac{\beta q_s}{(h - \beta y)^2} \frac{\partial y}{\partial x} - \frac{1}{h - \beta y} \frac{\partial q_g}{\partial x} - \frac{q_g \beta}{(h - \beta y)^2} \frac{\partial y}{\partial x} \end{aligned} \quad (5.49)$$

For fully segregated flow the curvatures of the gravity tongues may be assumed negligible near the producing end, i.e.,  $\partial^2 y/\partial x^2 = 0$ . This assumption is not valid near the injection well due to the sharp curvatures encountered there. The error in making this assumption for this development will be small, however, since it will be used only after surfactant solution breaks through.

Eq. (5.49) can be simplified by neglecting the second derivative and can be rearranged as follows:

$$\begin{aligned} & \frac{q_i \beta}{(h-\beta y)^2} \frac{\partial y}{\partial x} + \left[ \frac{1}{m y^2} - \frac{\beta}{(h-\beta y)^2} \right] q_s \frac{\partial y}{\partial x} \\ & - \frac{\beta q_g}{(h-\beta y)^2} \frac{\partial y}{\partial x} - \left[ \frac{1}{m y} + \frac{1}{h-\beta y} \right] \frac{\partial q_s}{\partial x} - \frac{1}{h-\beta y} \frac{\partial q_g}{\partial x} = 0 \end{aligned} \quad (5.50)$$

The gas and the surfactant solution rate gradients are also difficult to determine at various cross-sections, but they can be replaced by known and measurable parameters using the continuity equation. For the surfactant solution the equation can be given by:

$$\frac{\partial q_s}{\partial x} = -\phi \Delta S_s \frac{\partial y}{\partial r} \quad (5.51)$$

where

$\phi$  = porosity of the porous medium

$\Delta S_s$  = change in saturation of the surfactant solution

If the continuity equation for compressible fluids is used to determine the rate gradients of gas/foam, the resulting equation will be nonlinear, posing problems in analytical solution. However, foam generation has been fully established at this point and the pressure drops in the gas/foam zone have become almost constant in this stage of the flood (see pressure drop vs. gas volume injected graphs in Section 6). Thus the error introduced due to the assumption of incompressibility will be small and the same equation can be used for the gas zone:

$$\frac{\partial q_g}{\partial x} = -\phi \Delta S_g \frac{\partial \bar{y}}{\partial r} \quad (5.52)$$

where  $\Delta S_g$  is the change in saturation of the gas zone. This equation can be written in terms of  $y$  and  $\beta$  instead of  $\bar{y}$  using Eq. (5.47) in order to reduce the number of independent variables to one. Also,  $\beta$  can be eliminated from the time derivative since it only contains the ratio of gas and surfactant solution injection rates and the mobility ratios, all of which are independent of time. Thus Eq. (5.52) becomes:

$$\frac{\partial q_g}{\partial x} = -\phi \Delta S_g (\beta - 1) \frac{\partial y}{\partial r} \quad (5.53)$$

Equations (5.52) and (5.53) relate the rate gradients to the vertical velocities of the surfactant solution and gas/foam fronts. These rate gradients can be substituted in Eq. (5.50) to obtain:

$$\frac{q_i \beta}{(h-\beta)^2} \frac{\partial y}{\partial x} + \left[ \frac{1}{my^2} - \frac{\beta}{(h-\beta y)^2} \right] q_s \frac{\partial y}{\partial x} - \frac{\beta q_g}{(h-\beta y)^2} \frac{\partial y}{\partial x} - \left[ \frac{1}{my} + \frac{1}{h-\beta y} \right] \left[ -\phi \Delta S_s \frac{\partial y}{\partial t} \right] - \frac{1}{h-\beta y} \left[ -\phi \Delta S_g (\beta - 1) \frac{\partial y}{\partial t} \right] = 0 \quad (5.54)$$

It is also assumed here that the residual oil saturation in both gas/foam and surfactant solution tongues is equal. In the displacement runs performed in this study, the residual oil saturations were found to be almost equal in both the surfactant solution and the gas swept zones. This is not a limiting assumption since the two saturations would normally differ by a constant factor which could have been incorporated in the following developments if it had been necessary. However, based on the experimental data the saturation changes in both swept zones were assumed equal and the subscripts dropped. On rearrangement, Eq. (5.54) becomes:

$$\left\{ \frac{q_i \beta}{(h-\beta)^2} + \left[ \frac{1}{my^2} - \frac{\beta}{(h-\beta y)^2} \right] q_s - \frac{\beta q_g}{(h-\beta y)^2} \right\} \frac{\partial y}{\partial x} + \left[ \frac{1}{my} + \frac{1}{h-\beta y} + \frac{\beta-1}{h-\beta y} \right] \phi \Delta S \frac{\partial y}{\partial t} = 0 \quad (5.55)$$

The gas/foam and surfactant solution rates are other unknowns which must be replaced by known and measurable parameters, as shown in the next few steps which relate these rates to the total injection rate.

By applying the material balance as expressed in Eq. (5.38) and substituting for flow rates per unit cross-sectional width from Eqs. (5.34), (5.35) and (5.36), the ratio of surfactant solution rate to total rate can be written as:

$$\frac{q_s}{q_t} = \frac{-y \frac{k_s}{\mu_s} \frac{\partial p_s}{\partial x}}{-\bar{y} \frac{k_g}{\mu_g} \frac{\partial p_g}{\partial x} - y \frac{k_s}{\mu_s} \frac{\partial p_s}{\partial x} - (h-y-\bar{y}) \frac{k_0}{\mu_0} \frac{\partial p_0}{\partial x}} \quad (5.56)$$

The pressure gradients in each zone are assumed to be equal as discussed before. Thus the pressure gradient terms can be cancelled. The mobilities and  $\beta$ , as defined by Eqs. (5.40), (5.41), and (5.47), can be substituted in Eq. (5.56), which is then simplified to:

$$q_s = \frac{my}{(h-\beta y) + my + \bar{m}\beta y - \bar{m}y} q_t \quad (5.57)$$

The gas rate *can* also be related to the total rate in a fashion similar to that shown in Eqs. (5.56) and (5.57):

$$q_g = \frac{\bar{m}(\beta - 1)y}{(h - \beta y) + my + \bar{m}\beta y - \bar{m}y} q_t \quad (5.58)$$

Equation (5.55) *can* be rearranged after substituting for gas and surfactant solution flow rates from Eqs. (5.57) and (5.58) as follows:

$$\begin{aligned} & - \left[ \frac{1}{my} + \frac{1}{h - \beta y} + \frac{\beta - 1}{h - \beta y} \right] \phi \Delta S \frac{\partial y / \partial t}{\partial y / \partial x} \\ & = \left\{ \frac{\beta}{(h - \beta y)^2} + \left[ \frac{1}{my^2} - \frac{\beta}{(h - \beta y)^2} \right] \frac{my}{(h - \beta y) + my + \bar{m}\beta y - \bar{m}y} \right. \\ & \quad \left. - \frac{\beta \bar{m}(\beta - 1)y}{(h - \beta y)^2 [(h - \beta y) + my + \bar{m}\beta y - \bar{m}y]} \right\} q_t \quad (5.59) \end{aligned}$$

By the chain rule of partial derivatives:

$$\frac{\partial x}{\partial t} = - \frac{\partial y / \partial t}{\partial y / \partial x} \quad (5.60)$$

Substituting this in Eq. (5.59) gives:

$$\begin{aligned} & \left[ \frac{1}{my} + \frac{1}{h - \beta y} + \frac{\beta - 1}{h - \beta y} \right] \phi \Delta S \frac{\partial x}{\partial t} \\ & = \left\{ \frac{\beta}{(h - \beta y)^2} + \left[ \frac{1}{my^2} - \frac{\beta}{(h - \beta y)^2} \right] \frac{my}{(h - \beta y) + my + \bar{m}\beta y - \bar{m}y} \right. \\ & \quad \left. - \frac{\beta \bar{m}(\beta - 1)y}{(h - \beta y)^2 [(h - \beta y) + my + \bar{m}\beta y - \bar{m}y]} \right\} q_t \quad (5.61) \end{aligned}$$

This equation *can* be solved analytically without any further simplifying assumption. The solution technique is given in Appendix A. The solution is:

$$y = \frac{h \sqrt{(\alpha - \bar{\alpha} + \alpha\beta + \bar{\alpha}\beta)^2 - 4\alpha\beta(\alpha - \bar{\alpha} + \bar{\alpha}\beta) \left[ 1 - \frac{mQ}{Lh\phi\Delta S} \right]} - h(\alpha - \bar{\alpha} + \alpha\beta + \bar{\alpha}\beta)}{2\alpha\beta(\alpha - \bar{\alpha} + \bar{\alpha}\beta)} \quad (5.62)$$

where

- Q = cumulative total throughput in pore volumes
- a = m - 1
- $\bar{\alpha}$  =  $\bar{m} - 1$

It is interesting to note here that this expression basically represents the gadfoam and surfactant solution drives acting simultaneously as Dietz type gravity tongues. Therefore, if one drive is deactivated, by making proper substitutions this equation will give the thickness of the Dietz gravity tongue for the one which is active. For example, if the gas drive is deactivated by assuming  $\bar{m}$  and  $q_{ig}$  to be zero, the  $\alpha, \beta$  and R terms will become:

$$\alpha = -1, \quad R = 0, \quad \beta = 1.$$

When these values are substituted in Eq. (5.62) to deactivate the gas tongue, the fractional thickness of the Dietz tongue for surfactant solution drive acting alone will be obtained:

$$b_e = \frac{y}{h} = \frac{\sqrt{mW_D - 1}}{m - 1} \quad (5.63)$$

Similarly, if Eq. (5.62) is expressed in terms of fractional thickness of a gas tongue, and the surfactant solution drive is deactivated by making similar assumptions, the fractional thickness of the Dietz-type gravity tongue for gas drive will be obtained

$$\bar{b}_e = \frac{\bar{y}}{h} = \frac{\sqrt{\bar{m}G_D - 1}}{\bar{m} - 1} \quad (5.64)$$

Equations (5.63) and (5.64) were shown to emphasize the similarity of this development to the Dietz model and are not used in the development.

To continue the formulation, the recovery is related to the tongue thickness by the material balance which requires that the ratio of swept zone thickness to the total thickness must be the same as the ratio of oil recovery to the maximum possible recovery. This can be expressed as:

$$\frac{y + \bar{y}}{h} = N_{pD} \quad (5.65)$$

Using the definition of  $\bar{y}$  from Eq. (5.47), the equation becomes:

$$y = \beta \quad (5.66)$$

Substituting for  $\gamma$  in Eq. (5.62) results in:

$$N_{pD} = \frac{\sqrt{(\alpha - \bar{\alpha} + \alpha\beta + \bar{\alpha}\beta)^2 - 4\alpha\beta(\alpha - \bar{\alpha} + \bar{\alpha}\beta) \left[ 1 - \frac{mQ}{Lh\phi\Delta S} \right]} - (\alpha - \bar{\alpha} + \alpha\beta + \bar{\alpha}\beta)}{2\alpha(\alpha - \bar{\alpha} + \bar{\alpha}\beta)} \quad (5.67)$$

The throughput in movable pore volumes,  $Q_D$  is defined as:

$$Q_D = \frac{Q}{L h \phi \Delta S} \quad (5.68)$$

The following group of terms can be defined further for simplification:

$$C = \alpha - \bar{\alpha} + E \beta = (m - 1) + R (\bar{m} - 1) m/\bar{m} \quad (5.29)$$

Substituting  $C$  and  $Q_D$  into Eq. (5.67) results in:

$$N_{pD} = \frac{\sqrt{(C + \alpha\beta)^2 - 4\alpha\beta C(1 - mQ_D)} - (C + \alpha\beta)}{2\alpha C} \quad (5.30)$$

Maximum recovery is obtained by setting  $N_{pD}$  equal to 1.0, calling  $Q_D$  equal to  $(Q_D)_{\max}$  in Eq. (5.30), and solving for  $(Q_D)_{\max}$ :

$$(Q_D)_{\max} = \frac{\alpha\beta C(\alpha + 1)}{(\bar{\alpha} + a + 2)^2} - \frac{(\bar{\alpha} + 1)(C + \alpha\beta)}{(\alpha + 1)(\bar{\alpha} + a + 2)} + \frac{1}{(a + 1)} \quad (5.71)$$

### 5.3.8. Summary of Recovery Equations

Recovery up to gas breakthrough:

$$N_{pD} = G_{iD} + \frac{G_{iD}}{R} \quad (5.3)$$

Volume injected at gas breakthrough time:

$$(G_{iD})_{gbi} = (N_{pD})_{gbi} = \frac{1}{\bar{m}} + \frac{1}{\bar{m} R} \quad (5.27)$$

Recovery prior to surfactant solution breakthrough:

$$N_{pD} = \frac{G_{iD}}{R} + \frac{1}{(\bar{m} - 1)} (2\sqrt{\bar{m} G_{iD}} - 1 - G_{iD}) \quad (5.25)$$

Recovery at surfactant breakthrough time:

$$(N_{pD})_{stb} = \frac{1}{m} + \frac{1}{(\bar{m} - 1)} \left[ 2\sqrt{\frac{\bar{m}}{m}} R - 1 - \frac{R}{m} \right] \quad (5.30)$$

Recovery after surfactant breakthrough up to the end of flood:

$$N_{pD} = \frac{\sqrt{(C + \alpha\beta)^2 - 4\alpha\beta C(1 - mQ_D)} - (C + \alpha\beta)}{2\alpha C} \quad (5.70)$$

Volume injected at which maximum recovery is obtained:

$$(Q_D)_{max} = \frac{\alpha\beta C(\alpha + 1)}{(\alpha + \alpha + 2)^2} + \frac{(\alpha + 1)(C + \alpha\beta)}{(\alpha + 1)(\alpha + \alpha + 2)} + \frac{1}{(\alpha + 1)} \quad (5.71)$$

## 5.4. PRESSURE HISTORY FOR COMBINATION-DRIVE DISPLACEMENT

This section outlines the mathematical development for the prediction of pressure drop history for the combinationdrive flood. The following development is based on the assumption that the pressure gradients in all three zones are equal. This assumption is valid only when the capillary pressure at the interface is negligible, which is generally the case for surfactant and foam drives. It also assumes the flow is nearly horizontal. This assumption makes it possible to calculate only the pressure drop in the surfactant zone, which is then related to the overall pressure drop.

The combinationdrive model was found quite successful for predicting recovery, but it did not perform quite as well in predicting the pressure history. The predicted trends closely resembled the experimentally observed pressure history in most cases, as will be seen in Section 6, but the significant deviation observed in some other cases needs to be resolved in future studies.

It is possible that the inaccuracies in this formulation are due to the omission of foam bank, and its movement. Likely the abrupt change from gas mobility to average foam mobility is causing errors. A more realistic model would include the movement of the foam bank and treat the gas and foam as two separate banks existing in series. This approach should be tried in the future.

### 5.4.1. Development of Equations for Pressure Drops

The surfactant flux is given by applying Darcy's law in the surfactant swept zone, as shown in Eq. (5.35):

$$q_s = -y \frac{k_s}{\mu_s} \frac{\partial p_s}{\partial x} \quad (5.35)$$

The pressure drop in the surfactant **zone** between the injection well and the front can be given by rearranging and integrating this equation:

$$p_0 - p_x = - \frac{q_s \mu_s}{k_s} \int_0^x \frac{dx}{y} \quad (5.72)$$

This equation can not be explicitly solved for the pressure drop in its present form, until  $y$  is expressed as a function of  $x$  or vice versa. The relationship between  $x$  and  $y$  has already been established, and could be used to replace the  $dx$  as a function of  $y$ . This is done here in Eqs. (5.73) through (5.77). The location of the front is given by modifying the limit of integration ( $L$  changed to  $x$ ) in Eq. (A.4) of Appendix A:

$$\int_0^x dx = \frac{m h}{[(h - \beta y) + m\beta y] [(h - \beta y) + m y + \bar{m}\beta y - \bar{m}y]} \frac{1}{\phi \Delta S} \int_0^t q_t dt \quad (5.73)$$

Solving this equation for  $x$  results in:

$$x = \frac{m h}{[(h - \beta y) + m\beta y] [(h - \beta y) + m y + \bar{m}\beta y - \bar{m}y]} \frac{Q}{\phi \Delta S} \quad (5.74)$$

where  $Q$  is the cumulative total throughput. This relationship was derived by assuming that the gas/foam and surfactant tongues are acting simultaneously. For pressure drop prediction, each drive has to be considered independently, so that the total thickness  $h$  has to be replaced by the thickness of the surfactant tongue at the injection end,  $\bar{h}$ . Thus the previous equation becomes:

$$x = \frac{m \bar{h}}{[(\bar{h} - \beta y) + m\beta y] [(\bar{h} - \beta y) + m y + \bar{m}\beta y - \bar{m}y]} \frac{Q}{\phi \Delta S} \quad (5.75)$$

In previous development [Eq. (5.29)],  $C$  was defined as follows:

$$C = \alpha - \alpha + \alpha \beta = (m - 1) + R \frac{m}{\bar{m}} (\bar{m} - 1) \quad (5.29)$$

Equation (5.75) can be simplified by substituting for  $C$ :

$$x = \frac{m \bar{h} Q}{\phi \Delta S} \frac{1}{(\bar{h} + \alpha\beta y)(\bar{h} + C y)} \quad (5.76)$$

Differentiating this equation results in:

$$\frac{dx}{dy} = \frac{m \bar{h} Q}{\phi} \left[ \frac{C}{(K + \alpha\beta y)(\bar{h} + C y)^2} + \frac{\alpha\beta}{(K + \alpha\beta y)^2 (K + C y)} \right] \quad (5.77)$$

The value of  $\Delta x$  as a function of  $y$  is substituted into Eq. (5.72) to make it independent of  $x$ :

$$p_0 - p_x = - \frac{q_s \mu_s}{k_s} \int_{\frac{1}{h}}^y \frac{1}{h y} \left\{ \frac{m \bar{h} Q}{w \phi \Delta S} \left[ \frac{C}{(\bar{h} + \alpha \beta y)(\bar{h} + C y)^2} + \frac{\alpha \beta}{(\bar{h} + \alpha \beta y)^2 (\bar{h} + C y)} \right] \right\} dy \quad (5.78)$$

It may be noticed here that the limits of integration have also been changed accordingly to  $\bar{h}$ , the thickness of surfactant zone at injection well at  $x = 0$ , and,  $y$ , the thickness of surfactant zone at the front. The above equation is rearranged to:

$$- \frac{k_s}{q_s \mu_s} \frac{\phi \Delta S}{m \bar{h} Q} (p_0 - p_x) = \frac{C}{\bar{h}^3} \int_{\frac{1}{h}}^y \frac{dy}{\left(1 + \frac{\alpha \beta}{\bar{h}} y\right) \left(1 + \frac{C}{\bar{h}} y\right)^2 y} + \frac{\alpha \beta}{\bar{h}^3} \int_{\frac{1}{h}}^y \frac{dy}{\left(1 + \frac{\alpha \beta}{\bar{h}} y\right)^2 \left(1 + \frac{C}{\bar{h}} y\right) y} \quad (5.79)$$

In the following few steps, this equation is transformed to a **standard** form so that the solution can be written by comparison. Let us define  $a$  and  $b$  as follows:

$$a = \frac{\alpha \beta}{\bar{h}} \quad b = \frac{C}{\bar{h}} \quad (5.80)$$

After substitution for  $a$  and  $b$ , the right hand side of Eq. (5.79) becomes:

$$\text{R.H.S.} = \frac{C}{\bar{h}^3} \int_{\frac{1}{h}}^y \frac{dy}{(1 + ay)(1 + by)^2 y} + \frac{\alpha \beta}{\bar{h}^3} \int_{\frac{1}{h}}^y \frac{dy}{(1 + ay)^2 (1 + by) y} \quad (5.81)$$

The first and the **second** integrals in this equation can be defined as  $I_1$  and  $I_2$ . The **integral**  $I_1$  can be reduced to the following form using partial fraction expansion:

$$I_1 = \int_{\frac{1}{h}}^y \frac{dy}{(1 + ay)(1 + by)^2 y} = \frac{a^2}{(a - b)^2} \int_{\frac{1}{h}}^y \frac{dy}{y(1 + ay)} - \frac{ab}{(a - b)^2} \int_{\frac{1}{h}}^y \frac{dy}{y(1 + by)} - \frac{b}{(a - b)} \int_{\frac{1}{h}}^y \frac{dy}{y(1 + by)^2} \quad (5.82)$$

The integrals in Eq. (5.82) are standard integrals, whose solutions are readily available from handbooks (Spiegel, 1968):

$$I_1 = \frac{a^2}{(a-b)^2} \left[ \ln \frac{y}{(1+ay)} \right]_h^y - \frac{ab}{(a-b)^2} \left[ \ln \frac{y}{(1+by)} \right]_h^y - \frac{b}{(a-b)} \left[ \frac{1}{(1+by)} + \ln \frac{y}{(1+by)} \right]_h^y \quad (5.83)$$

Evaluating the above expression for the limits of integration results in:

$$I_1 = \frac{a^2}{(a-b)^2} \ln \frac{y(1+a\bar{h})}{\bar{h}(1+ay)} + \frac{b^2-2ab}{(a-b)^2} \ln \frac{y(1+b\bar{h})}{\bar{h}(1+by)} - \frac{b^2}{(a-b)} \frac{(K-y)}{(1+by)(1+b\bar{h})} \quad (5.84)$$

The solution of integral  $I_2$  can be written by inspection since integrals  $I_1$  and  $I_2$  are similar:

$$I_2 = \frac{b^2}{(b-a)^2} \ln \frac{y(1+b\bar{h})}{\bar{h}(1+by)} + \frac{a^2-2ab}{(b-a)^2} \ln \frac{y(1+a\bar{h})}{\bar{h}(1+ay)} - \frac{a^2}{(b-a)} \frac{(K-y)}{(1+ay)(1+a\bar{h})} \quad (5.85)$$

The values of these integrals  $I_1$  and  $I_2$  can now be substituted in Eq. (5.81), which is then simplified to:

$$\begin{aligned} \text{R.H.S.} = & \frac{1}{(a-b)^2} \left[ a(aC + a\alpha\beta - 2b\alpha\beta) \ln \frac{y(1+a\bar{h})}{ay} \right. \\ & + b(\alpha\beta b + bC - 2aC) \ln \frac{y(1+b\bar{h})}{\bar{h}(1+by)} \\ & \left. + \frac{a^2\alpha\beta(a-b)(\bar{h}-y)}{(1+ay)(1+a\bar{h})} - \frac{b^2C(a-b)(\bar{h}-y)}{(1+by)(1+b\bar{h})} \right] \quad (5.86) \end{aligned}$$

The values of  $a$  and  $b$  as defined in 4. (5.80) are substituted into Eq. (5.86) which simplifies it to:

$$\begin{aligned} \text{R.H.S.} = \frac{1}{\bar{h}^3 (\alpha\beta - C)} \left[ \alpha^2 \beta^2 \ln \frac{(y + \alpha\beta y)}{(\bar{h} + \alpha\beta y)} - C^2 \ln \frac{(y + Cy)}{(\bar{h} + Cy)} \right. \\ \left. + \frac{\alpha^3 \beta^3 (\bar{h} - y)}{(\bar{h} + \alpha\beta y) (1 + \alpha\beta)} - \frac{C^3 (\bar{h} - y)}{(\bar{h} + Cy) (1 + C)} \right] \end{aligned} \quad (5.87)$$

This expression can be substituted into Eq. (5.79), resulting in:

$$\begin{aligned} p_0 - p_x = - \frac{q_s \mu_s}{k_s} \frac{m \bar{h} Q}{\phi \Delta S} \frac{1}{\bar{h}^3 (\alpha\beta - C)} \left[ \alpha^2 \beta^2 \ln \frac{(y + \alpha\beta y)}{(\bar{h} + \alpha\beta y)} \right. \\ \left. - C^2 \ln \frac{(y + Cy)}{(\bar{h} + Cy)} + \frac{\alpha^3 \beta^3 (\bar{h} - y)}{(\bar{h} + \alpha\beta y) (1 + \alpha\beta)} - \frac{C^3 (\bar{h} - y)}{(\bar{h} + Cy) (1 + C)} \right] \end{aligned} \quad (5.88)$$

The cumulative throughput in movable oil volumes of surfactant swept zone  $Q_D$  is defined by material balance as:

$$Q_D = \frac{Q}{\bar{h} L \phi \Delta S} \quad (5.89)$$

After using this definition of  $Q_D$ , Eq. (5.88) is reduced to its final form:

$$\begin{aligned} p_0 - p_x = - \frac{q_s \mu_s}{k_s \bar{h}} \frac{m L Q_D}{(\alpha\beta - C)} \left[ \alpha^2 \beta^2 \ln \frac{(y + \alpha\beta y)}{(\bar{h} + \alpha\beta y)} - C^2 \ln \frac{(y + Cy)}{(\bar{h} + Cy)} \right. \\ \left. + \frac{\alpha^3 \beta^3 (\bar{h} - y)}{(\bar{h} + \alpha\beta y) (1 + \alpha\beta)} - \frac{C^3 (\bar{h} - y)}{(\bar{h} + Cy) (1 + C)} \right] \end{aligned} \quad (5.90)$$

The thickness of the surfactant tongue,  $y$ , is given by material balance in Eq. (5.66):

$$y = \frac{h N_{pD}}{\beta} \quad (5.66)$$

The cumulative oil recovery,  $N_{pD}$  to be used in determining  $y$  is given by Eq. (5.70):

$$N_{pD} = \frac{1}{2\alpha C} \left[ \sqrt{(C + \alpha\beta)^2 - 4\alpha\beta C (1 - mQ_D)} - (C + \alpha\beta) \right] \quad (5.70)$$

Replacing  $N_{pD}$  from Eq. (5.66) using Eq. (5.70) results in:

$$y = \frac{h}{2\alpha\beta C} \left[ \sqrt{(C + \alpha\beta)^2 - 4\alpha\beta C (1 - mQ_D)} - (C + \alpha\beta) \right] \quad (5.91)$$

This is the value of  $y$  to be used in conjunction with Eq. (5.90) to determine the pressure drops. These equations will be used in deriving the pressure drop relationships as shown in the following sections.

#### 5.4.2. Determination of Pressure Drop From Injector to Producer

Equation (5.90) gives the pressure drop across the surfactant front only. The total pressure drop across the injection well and the producing well can be found by arranging the surfactant and oil zones in series, in a manner described in the following.

During surfactant injection up to surfactant breakthrough, the pressure drop across the surfactant bank is given by Eq. (5.91). The total pressure drop during this interval is given by:

$$p_0 - p_1 = (p_0 - p_x) + \frac{q_s \mu_o (L - x)}{k_a y_b} \quad (5.92)$$

where  $x$  is the location of front given by Eq. (5.76), and  $y_b$  is the thickness of the Surfactant tongue at the front. The value of  $y_b$  is obtained from Eq. (5.66) after replacing for the oil recovery at slug breakthrough,  $(N_{pD})_{sbt}$  given by Eq. (5.70):

$$y_b = \frac{h (N_{pD})_{sbt}}{\beta} = \frac{h}{\beta} \left\{ \frac{1}{m} + \frac{1}{(\bar{m} - 1)} \left[ 2 \sqrt{\frac{\bar{m}}{m} R - 1} - \frac{R}{m} \right] \right\} \quad (5.93)$$

After surfactant breakthrough, the total pressure drop is given by Eq. (5.91).

### 5.5. RECOVERY FOR DISPLACEMENT OTHER THAN COMBINATION-DRIVE

In the following paragraphs, an approximate analytical model is proposed to predict the recovery for piston-like two-dimensional flow which behaves quite differently than a combination-drive behavior. Other flow behaviors are also expected in conditions drastically different than they were in this study. It is expected that approximate analytical models could be developed in a fashion similar to the method described here.

#### 5.5.1. Recovery for Piston-Like Displacement

When simultaneous injection of gas and surfactant solution is displacing a liquid, the flow cannot be truly piston-like because the mobility ratio between the gas and a liquid is always unfavorable. However, the mobility ratio between the injected surfactant solution and the in-situ oil can be favorable in some instances. In this situation, the upper part of the porous medium is driven by gas and the rest is driven by surfactant solution front with a vertical and piston-like profile. The recoveries can be obtained by adding the performance of these two drives as shown below.

The recovery due to gas drive can be obtained by using the Buckley-Leverett theory modified for gravity, as given by Eq. (5.24):

$$(N_{pD})_g = \frac{1}{(\bar{m} - 1)} (2 \sqrt{\bar{m} G_{iD}} - 1 - G_{iD}) \quad (5.24)$$

The recovery due to surfactant solution drive before surfactant breakthrough equals the surfactant injection volume, and must be added to the above equation:

$$N_{pD} = W_{iD} + \frac{1}{(\bar{m} - 1)} (2 \sqrt{\bar{m} G_{iD}} - 1 - G_{iD}) \quad (5.94)$$

where  $W_{iD}$  = cumulative surfactant solution injected, in movable oil volumes.

The volume of surfactant solution injected at breakthrough can be obtained by material balance. The location of the surfactant front,  $x$ , depends upon the thickness of the zone unswept by gas, and the surfactant solution throughput:

$$x = \frac{W_i}{y \phi \Delta S} \quad (5.95)$$

The expression for recovery by surfactant solution drive given by Eq. (5.15) can be used after modifying it for gas drive:

$$N_{pD} = \bar{y}_e + (1 - f_{ge}) G_{iD} = \frac{\bar{y}}{h} + (1 - f_{ge}) G_{iD} \quad (5.96)$$

The fractional flow of gas at the producing end,  $f_{ge}$ , can be obtained by substituting Eq. (5.64) into Eq. (5.22) after modifying for gas drive:

$$f_{ge} = \frac{\bar{m}}{\bar{m} - 1} \left[ 1 - \frac{1}{\sqrt{\bar{m} G_{iD}}} \right] \quad (5.97)$$

The thickness of the gas zone is obtained by substituting Eq. (5.96) into Eq. (5.15) and rearranging:

$$\bar{y} = h (N_{pD})_g + h \left\{ \frac{\bar{m}}{\bar{m} - 1} \left[ 1 - \frac{1}{\sqrt{\bar{m} G_{iD}}} \right] - 1 \right\} G_{iD} \quad (5.98)$$

The thickness of the surfactant zone,  $y$ , can be obtained by difference between the total thickness,  $h$ , and the thickness of the gas zone,  $\bar{y}$ . The surfactant breaks through when the front reaches the producing well, i.e., at  $x = L$  in Eq. 5.95.

After surfactant breakthrough, there is no recovery from the surfactant drive due to the sharp interfaces, and any additional recovery is merely due to the gas drive, which can be

obtained by adding the recovery due to the surfactant drive at surfactant breakthrough as calculated before:

$$N_{pD} = (N_{pD})_{sbt} + \frac{1}{(\bar{m} - 1)} (2 \sqrt{\bar{m} G_{iD}} - 1 - G_{iD}) \quad (5.99)$$

where  $(N_{pD})_{sbt}$  = recovery by surfactant drive at surfactant breakthrough.

The mobility of gas has to be modified after foam generation starts. The onset of foam generation can be estimated by the same empirical relationship proposed in Section 5.1 (Eq. 5.2). The above equations were used to analyze a run showing piston-like displacement, and the recovery predicted was found to be in good agreement with the laboratory data, as will be described in Section 6.

## 55.2. Viscous Dominated Flow

Flow can be classified as unstable when the viscous effects are overwhelming in the porous medium, in which case the front advances in the form of fingers. The number of these fingers and their thicknesses depend upon the degree of instability. The effect of these instabilities is pronounced in laboratory tests.

The combination drive and other models proposed previously are based on the concept of fully segregated stable flow, and therefore, are not valid for unstable displacement. No model has been developed as yet to describe such a system.

## 6. RESULTS AND DISCUSSION

The experimental results obtained in **this** study **are** analyzed in **this** section and **are** compared with the results obtained by using the modeling equations developed in Section 5. **Most** of these **results** were obtained when a liquid was displaced by gas/surfactant solution injection under foaming conditions. **These** experiments were performed in two stages. The **runs** were designed in the first stage to get a qualitative understanding of displacement, **and were** focussed **on** the frontal advance behavior **and** the identification of important operating parameters. **These** runs were, therefore, somewhat trial-and-error in nature. Once the displacement mechanism was understood, the **runs** in **the** later stages were performed with closely defined objectives, and under carefully controlled conditions.

In the first stage of obtaining a qualitative understanding, the study had to **be** started from a point where even the fundamental principles were not uniquely defined in the literature. Thus data obtained during **this** stage had little quantitative value, because the operational diversity made them difficult to analyze. These runs were not analyzed quantitatively and have **only** been referred to qualitatively. Quantitative analysis of the **runs** in the second stage is, however, presented in the following paragraphs.

The primary objective of **this** study was to get an understanding of **the** displacement. The number of **runs** performed are insufficient to completely prove or disprove **the** proposed conceptual models. However, it was hoped that they would give considerable insight and provide a good foundation for further studies.

### 6.1. RHEOLOGY OF FOAM

An investigation of the rheological behavior was not a major goal in **this** study, but due to the controversial nature of foam rheology, it was deemed necessary to **perform** some rheological tests. A series of three **runs** was performed in which **the** two-dimensional sandpack was initially **saturated** with only **fresh** water (no oil). **This** water was then displaced by **nitrogen** injection only, or by **nitrogen** and simultaneous injection of either fresh water or surfactant solution. The changes in apparent mobility behavior during these **three runs** are **shown** in Fig. 6.1.

The behavior of a **run** in which **fresh** water was displaced by simultaneous injection of nitrogen and surfactant solution is **shown** in line (a) of Fig. 6.1. The mobility was high at the **start** of the **run** due to a delay in foam generation for the reason described in Section 5.1 **as** the mass-effect. **Then** a **short** period of gradual decline in apparent mobility followed, which **was** also visually seen to **be** due to the propagation of foam through the gas tongue **as** a third **front**. The first straight line shown in line (a) of Fig. 6.1 represents **this** decline. After about **two** and a half **hours** of injection, the gas and surfactant began to produce finely dispersed foam and the apparent mobility decreased sharply by a ratio of about **250 to 1**. **This** was due to the foam front reaching the producing well. **Soon** after foam breakthrough, gas and surfactant solution started behaving **as** a single homogeneous fluid of very low mobility, whose **value** remained relatively constant, but never achieving a **truly** steady state condition.

The presence of a history-dependent **gel** strength was **also** noticed in **this** run. **After** the sandpack was thoroughly flooded with foam and flow approximated a steady **state** condition, the injection was stopped for several hours, and subsequently, resumed at a much higher **pressure** drop (at the maximum design of 20 psig), but it did not induce any flow. The rheology was also **Seen** to be time-dependent. After total blocking had **been** observed, the sandpack was

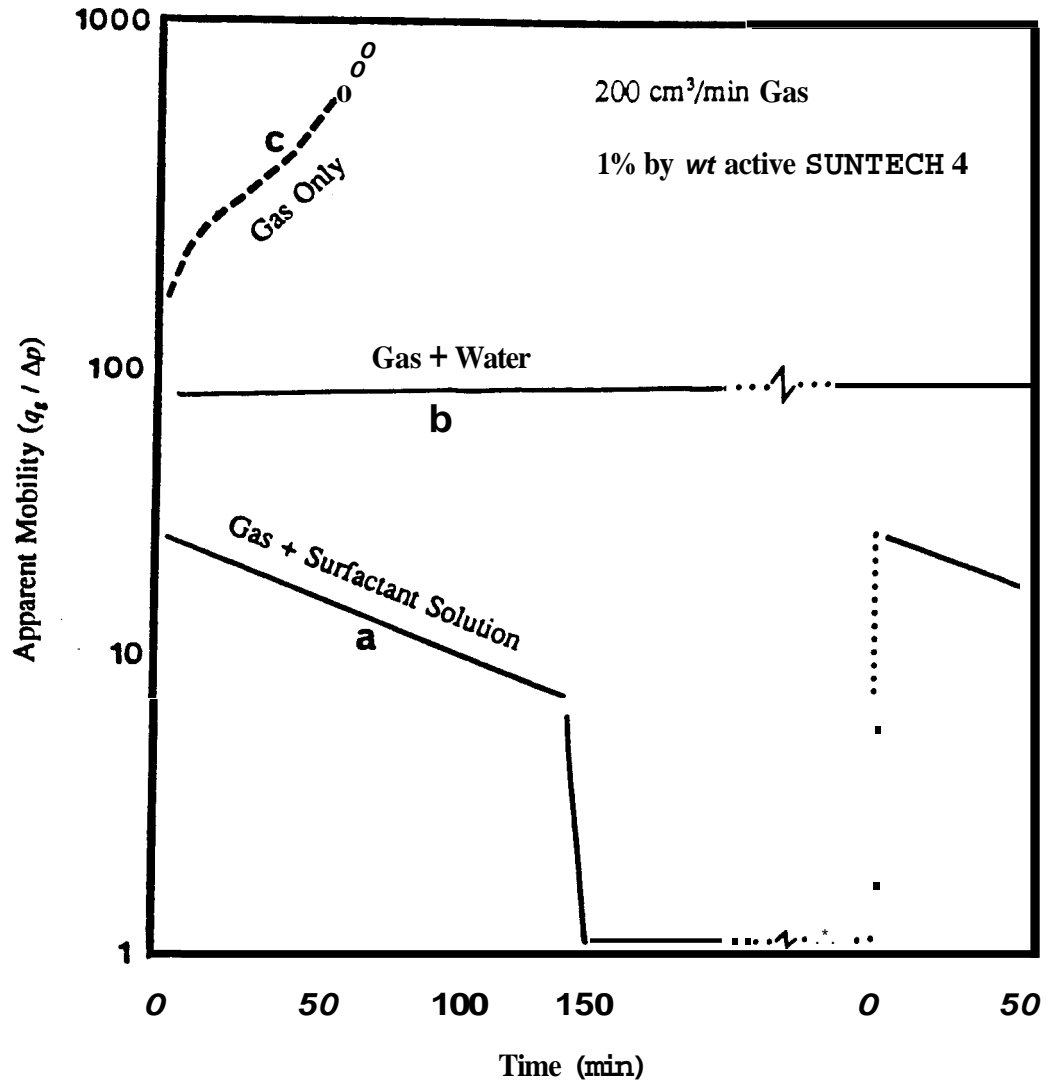


Figure 6.1 Effect of Time and Shear History for a Two-Dimensional Flow.

left undisturbed for several weeks. When injection was resumed, the initial mobility corresponded to the gas mobility. This was an indication that the foam had completely broken down. However, foam generation restarted rather quickly, suggesting that there were no losses encountered this time.

To see if this behavior was due to surfactant, another run was performed under the same operating conditions except that the surfactant solution was replaced with an equivalent volume of fresh water. The results were drastically different as shown in line (b) of Fig. 6.1. After a short early transient period, the flow stabilized at a high constant mobility indicating a steady state condition was reached. There was no change in mobility when the run was stopped and resumed after the same duration of shut-in as in the last run, except that another short transient period was noticed.

The third run in this series was performed to see the role of liquid, thus it was performed under identical operating conditions, except that no liquid was injected, only nitrogen. The results, shown in line (c) of Fig. 6.1, indicated a typical Buckley-Leverett displacement behavior with rapid increases in apparent mobility.

After the first three runs described above, later runs were performed with oil in-situ. An example of apparent mobility of some of these runs is graphed in Fig. 6.2. At first it looked like the rheology of foam is complex, changing from pseudoplastic at low rates to dilatant at high rates. Later, when the efforts to model the frontal behavior were made, it became clear that this complex mobility behavior was due to the two-dimensional nature of the flow, which was caused primarily by gravity segregation, and which made the displacement sensitive to rate changes.

### 63. SCALED-MODEL STUDIES

Scaled-model studies are useful for many flow problems specially those not amenable to analytical treatment. Displacement runs are performed on a laboratory scaled-model, and the performance is extrapolated for the prototype reservoir. The recovery performance obtained by a properly-scaled model is expected to approximate the performance of a prototype reservoir through the entire life of the flood.

The scaling approach was also tried in this study. The results obtained from such bench-scale laboratory models are valid only for the operating conditions for which they are designed. Nevertheless, it was hoped that some valid information of practical utility could be obtained by developing performance charts for oil displacement by gas-surfactant solution injection.

The same scaling laws were used which were originally derived for a water drive in a linear reservoir (Rapoport, 1955). The continuity equation was used to describe the flow. The scaling was performed on the same principles as described by Geertsma *et al.* (1956), where the important forces were also scaled along with the geometrical configuration.

The first step in this scaling attempt was to identify important parameters. Qualitative runs were performed on the two-dimensional sandpack which revealed that the oil displacement by gas-surfactant solution injection could be modeled using a combination-drive behavior (Section 5.5.2), in which flow is considered to be taking place in separate gravity tongues. The behavior of gas drive was not found to be sensitive in the range of experimental conditions,

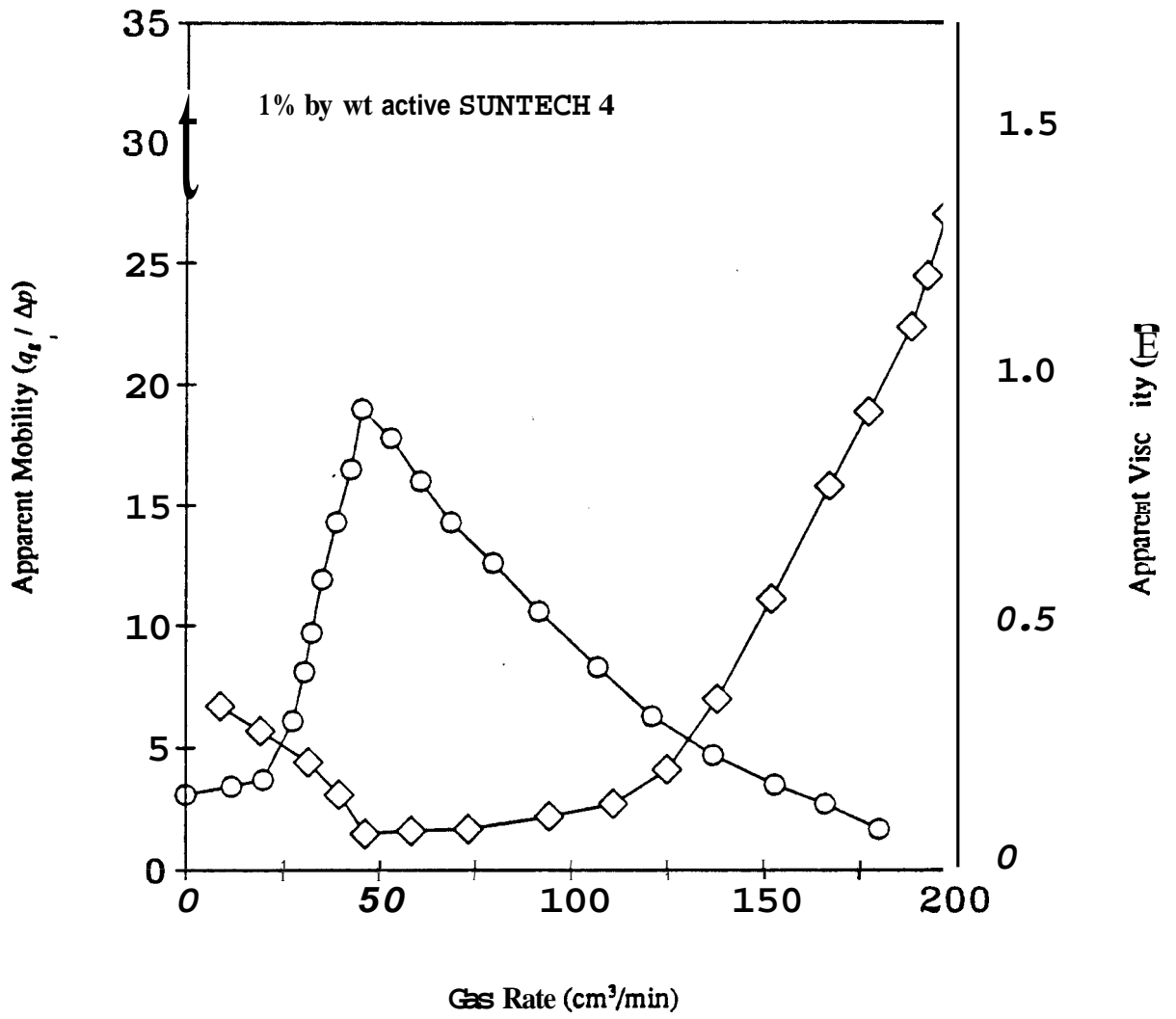


Figure 6.2 Effect of Rate on the Effective Mobility of Two-Dimensional Flow.

*i.e.*, it always formed a gravity tongue of more or less the same size. However, the recovery performance was found to be sensitive to the behavior of surfactant solution frontal movement.

The scaling groups should be established for both aqueous and gaseous phases for a combination-drive behavior, since both phases are flowing separately. However, the scaling laws are difficult to establish for gas drive due to the nonlinearity of the continuity equation for compressible fluids. This problem can be simplified by assuming that the compressibility effect of foam is small, and the same set of laws derived for liquid flow can be used without serious error. Based on this assumption, the scaling groups for the flow through two-dimensional laboratory sandpack were derived in Appendix C and were used for this part of the study. These scaling equations require that:

- (1) The product of length to height ratio and the square root of vertical to horizontal permeability must be the same in the model and prototype,
- (2) The ratio of capillary forces to the gravity forces (Bond No.) must be the same in the model and prototype.
- (3) The ratio of viscous to capillary forces (Capillary No.) must be the same in the model and prototype,
- (4) The mobility ratio must be the same in the model and prototype,
- (5) If conditions (2) and (3) above are met, it can also be deduced that the ratio of gravity forces to capillary forces (Gravity No.) must be the same in the model and prototype.

A series of runs were performed in which the values of similarity groups governing the performance were selectively changed in the range of practical interest, and the recovery data were graphed against these groups. These graphs are shown in Figs. 6.3 and 6.4, and a similar graph based on oil viscosity alone is shown in Fig. 6.5.

An interesting but discouraging observation was made as a result of developing these charts, that after a certain volume of injection, a significant jump in production takes place. An example of such behavior can be seen in each of these figures after about two pore volumes of throughput. This jump, which later was attributed to the mass-effect (Section 5.1), took place at different throughputs for different operating conditions. It was not clear at that time how to account for the increase in recovery caused by this jump. To make these performance charts useful, a large number of experiments would have been needed to cover all possible combinations of variables at which this jump takes place.

Research might have been pursued in the direction of finding appropriate methods of modifying the scaling groups, but this would not have served the main objective of this study which was to get a fundamental understanding of the displacement mechanism. The scaling approach was relinquished in favor of approximate mathematical modeling which was thought to be more promising (Section 5.2). Thus the later runs were performed in several series of small numbers of runs. Only one variable was changed in each of these series. The performance of these runs and the comparison with model equations are presented in the following sections.

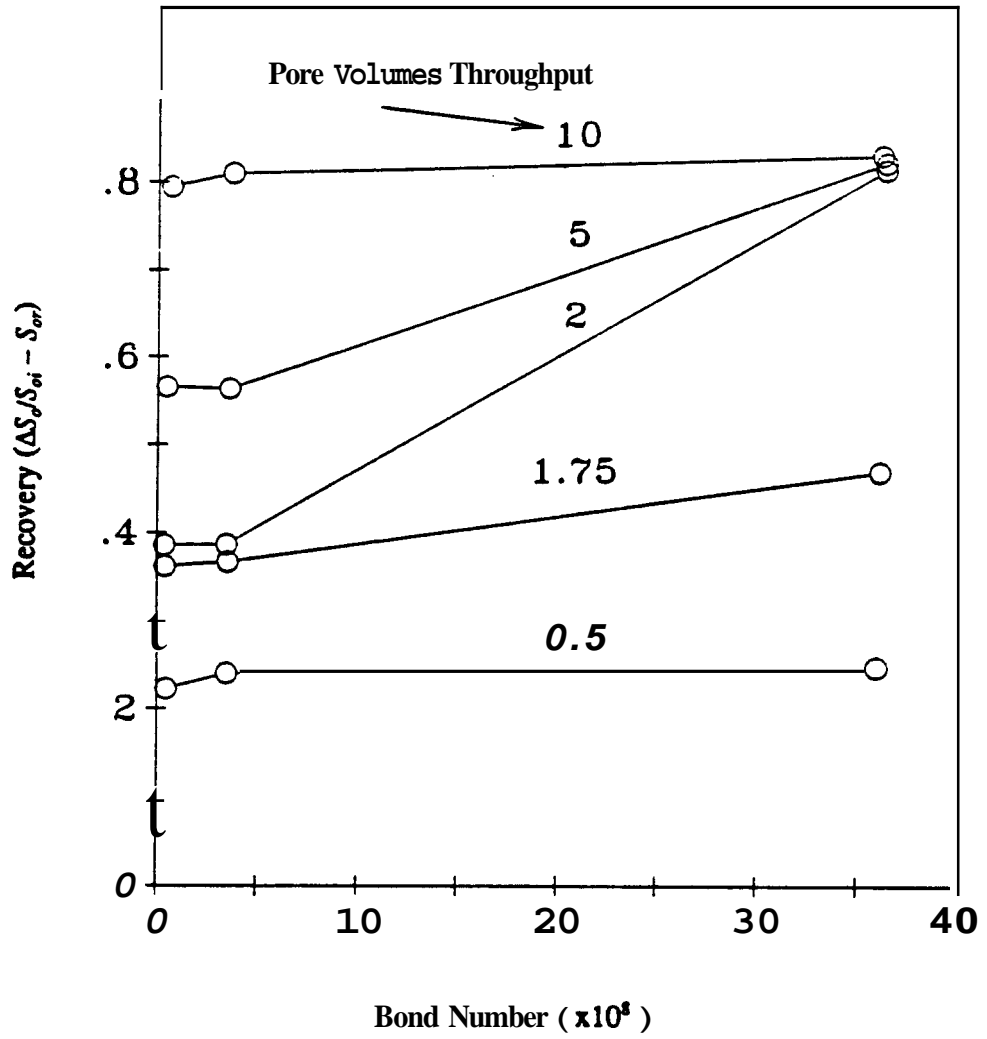


Figure 6.3 Typical Performance Chart Based on Bond Number.

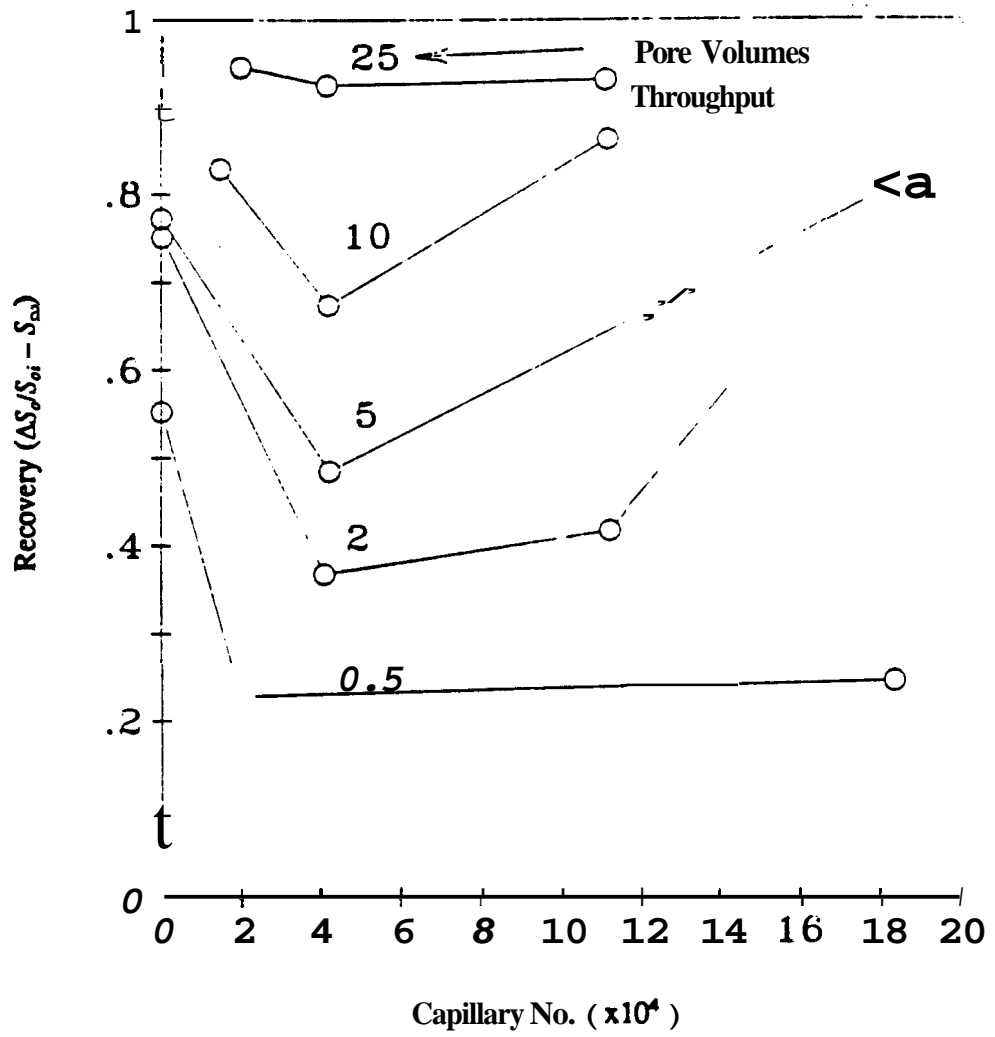


Figure 6.4 Typical Performance Chart Based on Capillary Number.

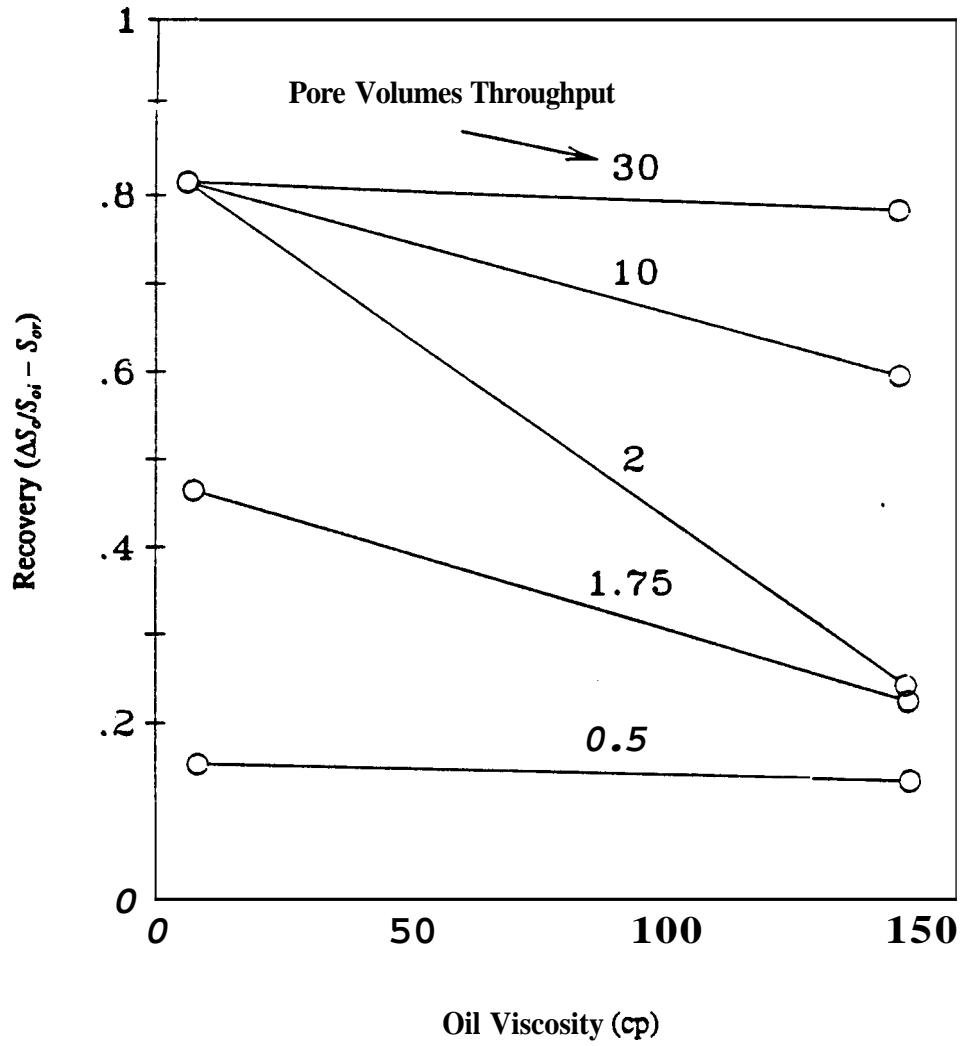


Figure 65 Typical Performance Chart Based on Oil Viscosity Alone.

### 63. EFFECT OF MODE OF INJECTION

A series of runs was performed to understand the effect of mode of injection on frontal behavior and on the flood performance. Nitrogen and surfactant solution were injected differently in each of these runs by either one of the following methods:

- (1) A single surfactant solution slug driven by gas,
- (2) Alternate slugs of surfactant solution and gas,
- (3) Preformed foam injection,
- (4) Simultaneous gas-surfactant solution injection.

The gas-to-oil and the surfactant-to-oil mobility ratios were unfavorable for these runs. The frontal behavior was noticeably different for each mode of injection, and consequentially, the production performance and the pressure histories were different. The behavior observed in each of these runs is described below:

#### 63.1. A Single Surfactant Slug Driven by Gas

In Run #8, the sandpack was initially saturated with decane (1 cp viscosity at S.T.P.) at imducible water saturation. A single surfactant slug of 0.2 pore volume was then injected. After the completion of surfactant slug injection, gas injection was started, and was continued until the end of the flood.

The surfactant front advanced through the two-dimensional sandpack in the form of a gravity tongue; the surfactant solution underrode and broke through during its injection as indicated in Fig. 4.10. The thickness of the tongue continued to increase after breakthrough until surfactant injection was stopped.

The mobility ratio between surfactant solution and oil was unfavorable but close to unity, and very little undemde would normally have taken place with pure water, but in this run it was aggravated due to the reduction in capillary forces caused by the surfactant. When gas injection was started, the gas severely overrode and broke through rapidly, in the form of a very thin finger. Later during gas injection, the gas finger slightly increased in thickness, while the surfactant profile remained intact. The run was abandoned when the rate of oil recovery became negligible, even though most of the middle section of the sandpack was still unswept.

Only a small fraction of total surfactant solution injected came in contact with the gas. This volume was not enough to overcome surfactant losses, and therefore, there was no evidence of foam generation, either direct (visual) or implied (through pressure drop data).

In summary, the behavior of a single surfactant solution slug which was injected before the start of gas injection could be described as if the lower part of the reservoir had been under surfactant flooding, and the upper part under gas injection. The recovery performance was predicted on the basis of this simplified model where the Dietz theory was used for surfactant drive and the gravity-modified Buckley-Leverett theory was used for the gas drive. Operating conditions of this run (Run #8) and the set of equations used for predicting the recovery behavior which are based on this model are listed in Table 6.1.

Note in Table 6.1 that the mobility ratio used for the gas was 200, and the mobility ratio used for the foam was 80. Although these are not theoretically the correct values for these mobilities, they were the ones that were found to fit the data best. Further these same values of mobility were used in all runs matched later. The reason why these somewhat incorrect

TABLE 6.1

**OPERATING CONDITIONS AND PREDICTIVE EQUATIONS FOR RUN #8  
(Single Slug of Surfactant Solution Followed by Gas Injection)**

Mode of injection	A single slug of 0.2 pore volumes of surf. solution followed by continuous gas
Type of oil in the porous medium	Decane (1 cp at room temp.)
Oil saturation	82% (at irreducible water saturation)
Type and concentration of surfactant	1% by weight of SUNTECH 4
Gas injection rate	1 standard cm <sup>3</sup> /min
Surfactant injection rate	0.167 standard cm <sup>3</sup> /min
Location of inj. and prod. intervals	Both inj. and prod. from bottom until gas breakthrough, then inj. into top
Injection and production history	Continuous, with no shut-in
Apparent mobility ratios	Gas to oil=200, Foam to oil=80, Surfactant to oil=5.
Recovery up to surf. breakthrough (Material Balance, Eq. 5.29)	$N_{pD} = W_{iD}$
Recovery at surf. breakthrough (Dietz Model, Eq. 5.28)	$(N_{pD})_{sbt} = \frac{1}{m}$
Recovery up to the end of surf. inj. (Dietz Model)	$N_{pD} = \frac{1}{m} + \frac{1}{m-1} (\sqrt{mW_{iD}} - 1)$
Recovery during gas injection (Modified Buckley-Leverett, Eq. 5.24)	$N_{pD} = \frac{1}{m-1} (2\sqrt{mG_{iD}} - 1 - G_{iD})$

values had to be used is not known. It is possible that it was due to the approximations used to formulate the combination-drive model equations.

The experimental data obtained during this run was graphed and compared against the data predicted by modeling in Fig. 6.6. Good agreement was obtained between experimental and predicted data.

### 63.2. Alternate slugs of Surfactant and Gas

This run (Run #6) was performed to observe the effect of injecting small surfactant slugs alternated with gas instead of a large single surfactant solution slug driven by gas injection. The total Surfactant solution injected was the same as in the previous run (0.2 pore volume) except that the injection strategy was changed. The rates, concentrations and fluids were also the same as in Run #8.

At the start of the run, a small surfactant solution slug (0.025 p.v.) was injected into the top zone, then a small gas slug was injected into the bottom zone, which was again followed by a small surfactant solution slug into the top. This sequence of small alternating slugs of surfactant solution and gas was continued throughout the life of the flood.

Due to this alternating small surfactant solution slugs injected between small gas slugs, the front profiles were improved. When the first surfactant slug was injected from the top zone, it underrode, but due to its smaller volume, it did not advance far. The gas injected subsequently from the bottom zone severely overrode in the form of a thin channel. When the second surfactant solution slug was injected at the end of first gas slug, it advanced the surfactant tongue slightly at the bottom, but it also partially invaded the gas swept zone, and in so doing, it slightly countered the effect of surfactant underrode.

When this cycle of injecting a small surfactant solution slug followed by a small gas slug was repeated, the surfactant front advanced in the form of a parabola, whereas the thickness of the gas finger also continuously increased. The curvature of the surfactant slug appeared to decrease with time, however, as shown in Fig. 4.11.

The operating conditions for the run (Run #6) are listed in Table 6.2 and the recovery performance is presented in Fig. 6.7. There is no predicted behavior in this graph, since the behavior does not resemble any of the models developed in this study.

### 63.3. Preformed Foam Injection

This run (Run #10) was performed to compare the performance of preformed foam injection to other modes of injection. In this run, the gas and surfactant were simultaneously injected into a Raza type foam generator (Raza, 1965). The excess surfactant was drained out whereas the dry foam was used to displace decane, which was initially in the model with imducible water under operating conditions similar to the previous runs.

In this run, the gas broke through very early through a thin gravity tongue at the top. As the preformed foam injection progressed, the size of this tongue grew gradually, at a continuously decreasing rate. At the bottom of this tongue, a liquid tongue of similar profile developed and started to grow in size (Fig. 4.12).

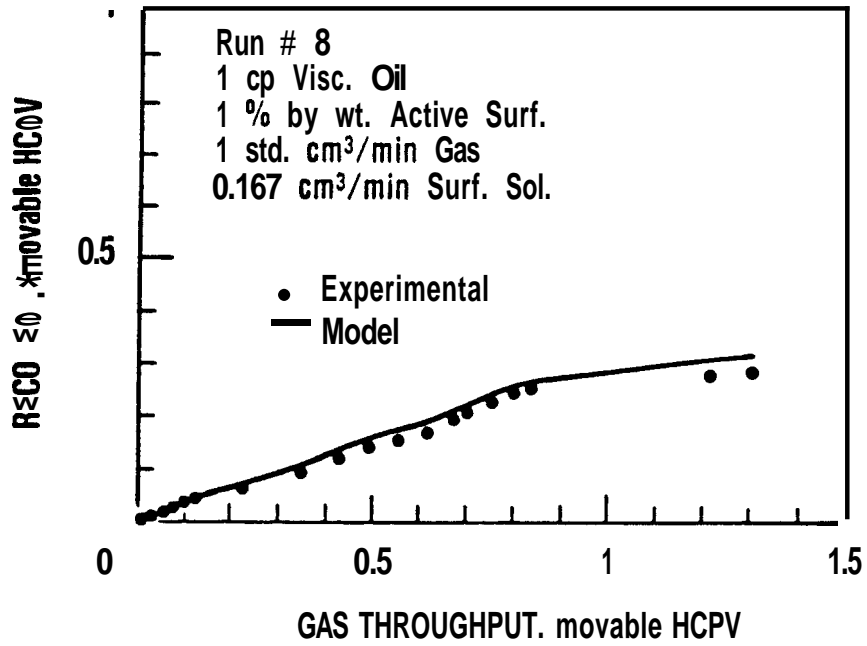


Figure 6.6 Comparison of Predicted and Experimental Recovery for Single Slug of Surfactant Solution Followed by Gas.

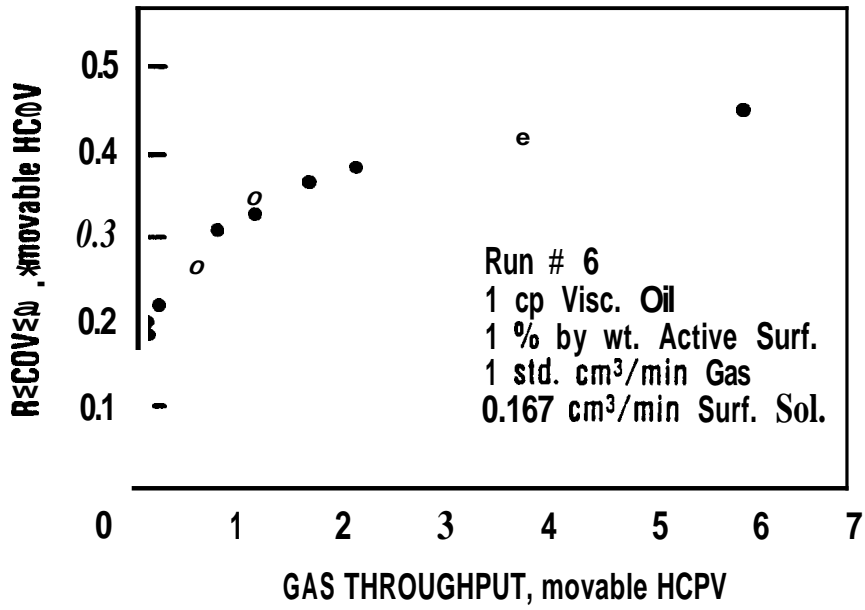


Figure 6.7 Experimental Recovery Data for Alternate Slugs of Gas and Surfactant Solution.

TABLE 6.2  
OPERATING **CONDITIONS** AND PREDICTIVE **EQUATIONS** FOR RUN #6  
(Alternate Slugs of Surfactant Solution and **Gas** Injection)

Mode of injection	Alternate slugs of <b>surf.</b> solution and gas
<b>Type</b> of oil in the porous medium	Decane (1 cp at <b>room</b> temp.)
Oil saturation	<b>82%</b> (at irreducible water saturation)
<b>Type</b> and concentration of surfactant	<b>1%</b> by weight of <b>SUNTECH 4</b>
<b>Gas</b> injection rate	1 standard cm <sup>3</sup> /min
Surfactant injection rate	<b>0.167</b> standard cm <sup>3</sup> /min
Location of inj. and prod. intervals	Both inj. and prod. from bottom until <b>gas breakthrough</b> , then <b>inj.</b> into top
Injection and production history	Continuous, with no shut-in

There was no evidence of in-situ foam generation or propagation either visually or through recovery and pressure behavior during the life of the flood. Foam eventually started to propagate through the sandpack, but only after many pore volumes of throughput beyond the useful producing life.

The production performance of this type of displacement could not be predicted using the combination-drive model, since there was not enough surfactant entering the formation to form a Dietz gravity tongue.

The recovery in this case was best predicted by assuming that gas and surfactant solution are flowing together as a single phase with a slight improvement in gas mobility. The operating conditions for this run (Run #10) and the set of equations used for predicting the recovery behavior are listed in Table 6.3. The predicted behavior obtained by using these equations is compared to the experimental data obtained during the run in Fig. 6.8. A good match was obtained by adjusting the apparent mobility.

An interesting point to note here is that the overall recovery performance of a preformed foam injection (Fig. 6.8) closely resembled a single surfactant slug followed by gas injection (Fig. 6.6). This would be expected since foam did not form in the model through the producing life, and therefore, there was no marked reduction in mobility. Early in the flood, the production was slightly higher in the preformed injection mode. This was perhaps due to a reduction in relative permeability because of the simultaneous liquid injection. This type of behavior is commonly observed in a water-alternating gas (WAG) type process.

#### 6.3.4. Simultaneous Gas-Surfactant Injection

In this strategy, both gas and surfactant solution were simultaneously introduced into the formation directly, and no mixing or foam generating device was used. The same oil, the same surfactant concentration, and the same injection rates were used as before.

In this run (Run #9), the gas overrode and advanced in the form of a thin finger. Gas breakthrough was rapid, as usual. The surfactant solution segregated from the gas and formed a surfactant solution bank along the bottom. A sharp saturation gradient was observed across the surfactant solution front. The surfactant finger broke through in the middle of the flood life. The frontal behavior was like a combination-drive, as has been described in Section 5.2.

A delay in foam generation and propagation through the porous medium was clearly observed. Foam generation started after the losses were overcome, and caused a considerable decrease in the apparent mobility of the injected gas. The mass of surfactant injection needed to start foam generation correlated well with the proposed empirical relationship. [See mass effect, Eq. (5.2).]

The foam bank was also seen to advance like a front but it propagated through the gas-swept zone only, and at a low speed (Fig. 4.13). The shape of this front was piston-like, as expected due to its low mobility, and it advanced to approximately one-fourth of the total length of the sandpack by the time most of the oil was produced. However, this foam bank kept advancing and did eventually reach the producing end long after the end of the effective flood life.

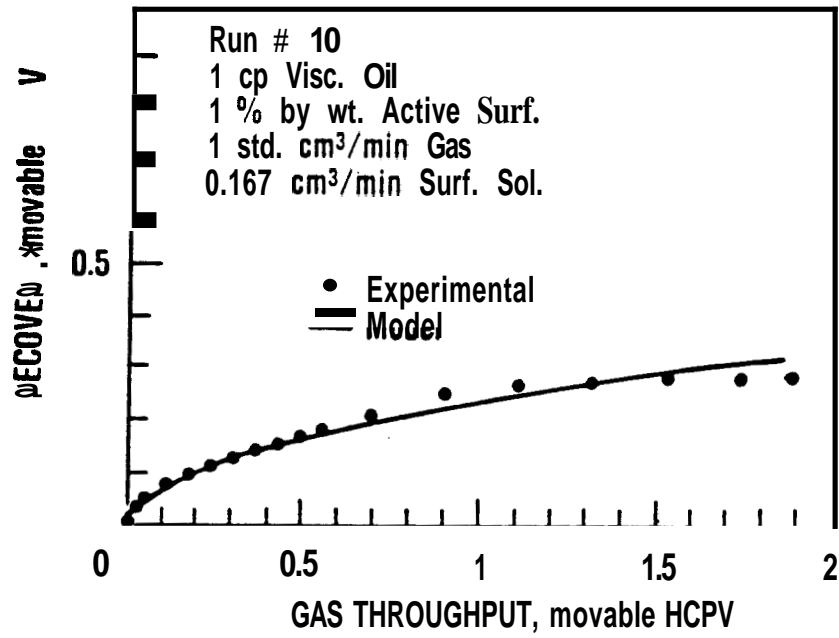


Figure 6.8 Comparison of Predicted and Experimental Recovery for Preformed Foam Injection.

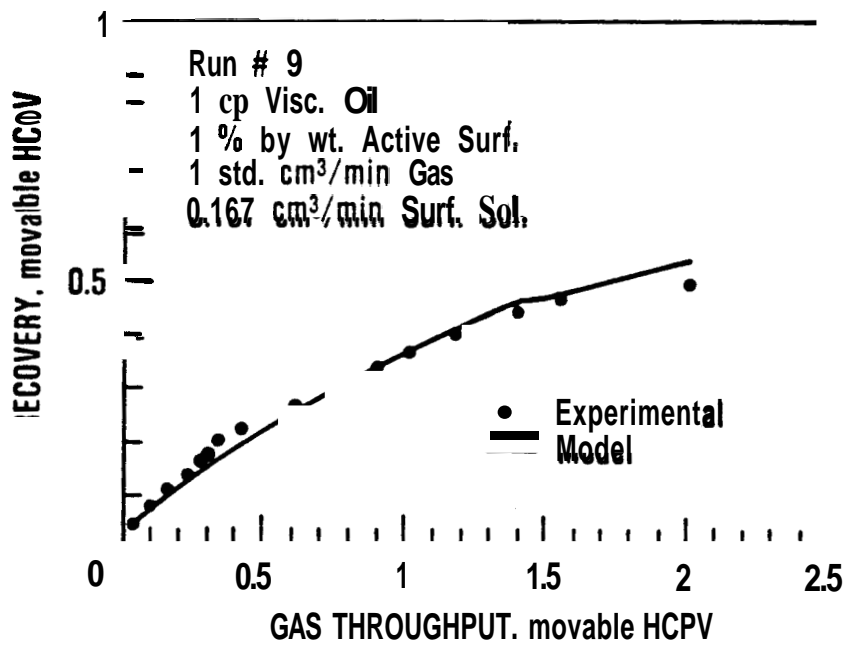


Figure 6.9 Comparison of Predicted and Experimental Recovery for Simultaneous Injection of Gas and Surfactant Solution.

**TABLE 6.3**  
**OPERATING CONDITIONS AND PREDICTIVE EQUATIONS FOR RUN # 10**  
**(Preformed Foam Injection)**

Mode of injection	Preformed foam injected to the sandpack through a Raza type foam generator
<b>Type</b> of <b>oil</b> in the porous medium	Decane (1 cp at mom temp.)
<b>oil</b> saturation	<b>82%</b> (at irreducible water saturation)
<b>Type</b> and concentration of surfactant	<b>1%</b> by weight of <b>SUNTECH 4</b>
Gas injection rate	1 standard cm <sup>3</sup> /min
Surfactant injection rate	<b>0.167</b> standard cm <sup>3</sup> /min into the foam generator
Location of inj. and prod. intervals	Both inj. and prod. from bottom until gas breakthrough then inj. is switched to top
Injection and production history	Continuous, with no shut-in
Apparent mobility ratios	Gas/surfactant mixture to oil, $m' = 100$
Recovery up to gas breakthrough material Balance, Eq. 5.3)	$N_{pD} = (1 / R + 1) G_{iD}$
Recovery at gas breakthrough (Modified Buckley-Leverett, Eq. 5.26)	$(G_{iD})_{gbi} = (N_{pD})_{gbi} = \frac{1}{\bar{m}}$
Recovery up to the end of flood (Modified Buckley-Leverett, after substituting $m'$ for $\bar{m}$ and $(G_{iD} + W_{iD})$ for $G_{iD}$ in Eq. 5.24)	$N_{pD} = \frac{2\sqrt{m'(G_{iD} + W_{iD})} - 1 - (G_{iD} + W_{iD})}{m' - 1}$

The production performance was predicted using the combination-drive model (Section 5.3). The operating conditions for the experimental run and the set of equations used are listed in Table 6.4. The predicted and the observed recoveries (Run#9) are compared in Fig. 6.9.

The agreement between experimental and predicted recoveries is excellent. There is a slight error near the end of the producing life. This may be because the mixed zone near the injection end is included twice in the combination-drive model and predicted recovery tends to be optimistic. The recovery in this run was higher throughout the producing life compared to either the slug type injection (Fig. 6.6) or preformed foam injection (Fig. 6.8). This was due to the earlier foam generation. The best recovery in the series was obtained with this mode of injection. Due to the superior performance demonstrated by simultaneous injection, all subsequent runs were performed using this method.

#### 6.4. EFFECT OF MOBILITY RATIOS

The two mobility ratios involved during gas-surfactant flooding are: the mobility ratio between injected gas and in-situ oil; and the ratio between surfactant solution injected and in-situ oil. Several runs were performed to see the effect of mobility ratios, and as expected, two distinct patterns were observed; one for favorable surfactant-to-oil mobility ratio and the other for unfavorable surfactant-to-oil mobility ratio.

The mobility of gas was always much higher than the oil so the gas-oil mobility ratio was very unfavorable, hence the gas bypassed and due to a large density difference, formed a gravity tongue on the top. The generation of foam improved the gas-oil mobility ratio, but, since the foam front lagged behind the gas front, it had a small effect on overall saturation changes. Foam did, however, induce crossflow which affected frontal behavior. This phenomenon has been explained in previous sections.

The mobility ratio between the surfactant injected and the reservoir oil was, on the other hand, important in determining the behavior of the surfactant bank front. The surfactant bank behavior for both unfavorable and favorable surfactant-oil mobility ratio is described in the following paragraphs. One run in each category has been selected to represent each type of behavior. The relative permeability-saturation relationship for the sandpack was not known due to the two-dimensional nature of the flow for each phase. In analyzing these runs, the effective permeabilities at imducible oil saturation were used.

##### 6.4.1. Favorable Surfactant Solution-To-Oil Mobility Ratio

In this run (Run #11) the surfactant solution-to-oil mobility ratio was favorable. Hexane (0.6 cp viscosity at S.T.P.) was initially saturated with irreducible water and displaced by simultaneous injection of nitrogen at 200 std cm<sup>3</sup>/min. and 1% Suntech 4 at 5 cm<sup>3</sup>/min. The gas to surfactant solution injection ratio was 40. The operating conditions for this run are listed in Table 6.5.

In this run, gas frontal behavior was similar to all other runs and gas broke through early. The surfactant solution front, on the other hand, was different; it had approximately a vertical profile and did not show significant gravity segregation (Fig. 45).

When the combinationdrive model was used to predict the behavior, it did not give a good match with the experimental results. Nor was it expected to, since this model is

**TABLE 6.4**  
**OPERATING CONDITIONS AND PREDICTIVE EQUATIONS FOR RUN # 9**  
**(Simultaneous Injection of Gas and Surfactant Solution)**

Mode of injection	Simultaneous gas and surfactant introduced directly without a mixing device
Type of oil in the porous medium	Decane (1 cp at room temp.)
Oil saturation	<b>82%</b> (at irreducible water saturation)
Type and concentration of surfactant	1% by weight of <b>SUNTECH 4</b>
Gas injection rate	1 standard cm <sup>3</sup> /min
Surfactant injection rate	0.167 standard cm <sup>3</sup> /min
Location of inj. and prod. intervals	Both inj. and prod. from bottom until gas breakthrough, then inj. into top
Injection and production history	Continuous, with no shut-in
Apparent mobility ratios	Gas to oil=200, Foam to oil=80 Surfactant to oil=5.
Recovery up to gas breakthrough (Material Balance, Eq. 5.3)	$N_{pD} = (1 / R + 1) G_{iD}$
Recovery at gas breakthrough (Modified Buckley-Leverett, Eq. 5.26)	$(G_{iD})_{gbi} = (N_{pD})_{gbi} = \frac{1}{\bar{m}}$
Recovery at surf. breakthrough (Modified Buckley-Leverett, Eq. 5.30)	$(N_{pD})_{sbi} = \frac{1}{\bar{m}} + \frac{1}{(\bar{m}-1)} (2\sqrt{\bar{m}R/m} - 1 - R/m)$
Recovery up to surf. breakthrough (Modified Buckley-Leverett, Eq. 5.25)	$N_{pD} = \frac{G_{iD}}{R} + \frac{1}{(\bar{m} - 1)} (2\sqrt{\bar{m}G_{iD}} - 1 - G_{iD})$
Recovery up to the end of flood (Combination-Drive Model, Eq. 5.70)	$N_{pD} = \frac{\sqrt{(C+\alpha\beta)^2 - 4\alpha\beta C(1-mQ_D)} - (C+\alpha\beta)}{2\alpha C}$
Max. recovery at the end of flood (Combination-Drive Model, Eq. 5.71)	$(N_{pD})_{max} = \frac{\alpha\beta C(\alpha+1)}{(\bar{\alpha}+\alpha+2)^2} + \frac{(\bar{\alpha}+1)(C+\alpha\beta)}{(\alpha+1)(\bar{\alpha}+\alpha+2)} + \frac{1}{(\alpha+1)}$

TABLE 6.5

OPERATING CONDITIONS AND PREDICTIVE EQUATIONS FOR RUN # 11  
(Favorable Mobility Ratio Between Oil and Surfactant Solution)

Mode of injection	Simultaneous <b>gas</b> and surfactant introduced directly without a mixing device
<b>Type of</b> oil in the porous medium	Hexane (0.6 cp at room temp.)
<b>Oil</b> saturation	90% (at irreducible water saturation)
<b>Type</b> and concentration of surfactant	1% by weight of <b>SUNTECH 4</b>
<b>Gas</b> injection rate	200 standard cm <sup>3</sup> /min
Surfactant injection rate	5 standard cm <sup>3</sup> /min
Location of inj. and prod. intervals	Both inj. and prod. from bottom until <b>gas</b> breakthrough, then inj. <b>into</b> top
Injection and production history	Continuous, with no shut-in
Apparent mobility ratios	Gas to oil=120, <b>Foam</b> to oil=80, Surfactant to oil=3
Recovery up to gas breakthrough (Material Balance, Eq. 5.3)	$N_{pD} = (1 / R + 1) G_{iD}$
Recovery at <b>gas</b> breakthrough (Modified Buckley-Leverett, Eq. 5.26)	$(G_{iD})_{gbr} = (N_{pD})_{gbr} = \frac{1}{\bar{m}}$
Recovery at <b>surf.</b> breakthrough (Noted from experimental data)	$(N_{pD})_{sbr} = 0.3$ Movable Pore Volumes
Recovery upto <b>surf.</b> breakthrough (Modified Buckley-Leverett, Eq. 5.25)	$N_{pD} = \frac{G_{iD}}{R} + \frac{1}{(\bar{m} - 1)} (2\sqrt{\bar{m}G_{iD}} - 1 - G_{iD})$
Recovery up to the end of flood (combination-Drive Model, Eq. 5.70)	$N_{pD} = \frac{\sqrt{(C+\alpha\beta)^2 - 4\alpha\beta C(1-mQ_D)} - (C+\alpha\beta)}{2\alpha C}$
Max. recovery at the end of flood (Combination-Drive Model, Eq. 5.71)	$(N_{pD})_{max} = \frac{\alpha\beta C(\alpha+1)}{(\bar{\alpha}+\alpha+2)^2} + \frac{(\bar{\alpha}+1)(C+\alpha\beta)}{(\alpha+1)(\bar{\alpha}+\alpha+2)} + \frac{1}{(\alpha+1)}$

applicable only for unfavorable mobility *ratio* displacement. The major difficulty was in predicting the time of surfactant solution breakthrough. The actual surfactant breakthrough time was used from the experimental run. Up to surfactant solution breakthrough, the recovery through the gas zone was assumed to follow the Buckley-Leverett model, modified to take into account the effect of gravity segregation, and the recovery due to surfactant drive was assumed to be equal to the surfactant solution volume injected. The recovery after surfactant breakthrough was found to approximately follow the combination-drive model.

The set of equations used to predict the recovery behavior are listed in Table 6.5. The recovery data obtained during the run and the predicted recovery are compared in Fig. 6.10. There was reasonably good match up to the surfactant solution breakthrough (at 0.5 pore volumes of recovery), then there was some disagreement. The reason for this is probably because the combination-drive model assumes the invasion of both gas and surfactant tongues into the oil zone in the middle of the vernal section due to the gravity drainage and vernal cross-flow, whereas in reality, no such unswept zone was seen in this run.

#### 6.4.2 Unfavorable Surfactant Solution-To-Oil Mobility Ratio

The mobility ratio between surfactant solution and oil is generally unfavorable under most reservoir conditions, therefore, most of the runs in this study were performed at this condition. Run #13 has been selected here to represent the performance of this type of displacement. In this run Blandol (15 cp viscosity) was initially saturated with irreducible water and was displaced by simultaneous injection of nitrogen at 200 std. cm<sup>3</sup>/min and Suntech 4 at 5 cm<sup>3</sup>/min. The operating conditions of the run are given in Table 6.6.

Two types of behavior were observed when the surfactant solution-to-oil mobility ratio was unfavorable: gravity dominated and viscous dominated. When the flow was gravity dominated, the displacement resembled a combination-drive model, in which both gas and surfactant solution advanced in separate gravity tongues. This was the most common behavior observed. The analysis of several gravity dominated runs can be found in Section 6.6.1. Viscous-dominated flow was generally encountered when the flow rates were very high, or the surfactant solution-to-oil mobility ratio was very unfavorable.

For viscousdominated displacement, the fingering of the surfactant solution bank was more prominent than the gravity effects. The surfactant solution bank advanced in the form of several thin fingers [Fig. 4.6(a)] which moved downward as they advanced and grew in size until they meshed with each other and thus swept the entire formation. Frontal behavior of gas was essentially the same as in any unfavorable mobility case, except that the thickness of gas tongue and its vernal growth rate were smaller. This was perhaps because of the overwhelming viscous effects rendering gravity drainage cross-flow insignificant. The time of breakthrough for each tongue and the increase in the thickness of the fingers were found to be functions of the mobility ratios.

The combination-drive model was not applicable for viscousdominated flow, since the surfactant fingers did not resemble the Dietz gravity tongue. The major error was in estimating the slug breakthrough time. It is interesting to note, however, that when the actually observed surfactant solution breakthrough time was used in the combination-drive model, it was able to predict the performance of this viscous-dominated flow with reasonable accuracy. With the above substitution, the recovery predicted for this run (Run #13) using the combination-drive model equations (Table 6.6) is compared in Fig. 6.11 with the experimentally observed recovery. The match between predicted results and the experimental data is excellent

TABLE 6.6

OPERATING CONDITIONS AND PREDICTIVE EQUATIONS FOR RUN # 13  
(Viscous-Dominated Surfactant Solution Front)

Mode of injection	Simultaneous gas and surfactant introduced directly without a mixing device
<b>Type</b> of oil in the porous medium	Blandol (15 cp at room temp.)
Oil saturation	85% (at irreducible water saturation)
<b>Type</b> and concentration of surfactant	1% by weight of SUNTECH 4
Gas injection rate	200 standard cm <sup>3</sup> /min
Surfactant injection rate	5 standard cm <sup>3</sup> /min
Location of inj. and prod. intervals	<b>Both</b> inj. and prod. from bottom until gas breakthrough, then inj. into top
Injection and production history	Continuous, with no shut-in
Apparent mobility ratios	<b>Gas to oil=300, Foam to oil=120, Surfactant to oil=15.</b>
Recovery up to gas breakthrough (Material Balance, Eq. 5.3)	$N_{pD} = (1 / R + 1) G_{iD}$
Recovery at gas breakthrough (Modified Buckley-Leverett, Eq. 5.26)	$(G_{iD})_{gbi} = (N_{pD})_{gbi} = \frac{1}{\bar{m}}$
Recovery at surf. breakthrough (Modified Buckley-Leverett, Eq. 5.30)	$(N_{pD})_{sbi} = \frac{1}{m} + \frac{1}{(\bar{m}-1)} (2\sqrt{\bar{m}R/m-1-R/m})$
Recovery upto surf. breakthrough (Modified Buckley-Leverett, Eq. 5.25)	$N_{pD} = \frac{G_{iD}}{R} + \frac{1}{(E-1)} (2\sqrt{\bar{m}G_{iD}} - 1 - G_{iD})$
Recovery up to the end of flood (Combination-Drive Model, Eq. 5.70)	$N_{pD} = \frac{\sqrt{(C+\alpha\beta)^2 - 4\alpha\beta C(1-mQ_D)} - (C+\alpha\beta)}{2\alpha C}$
<b>Max.</b> recovery at the end of flood (Combination-Drive Model, Eq. 5.71)	$(N_{pD})_{max} = \frac{\alpha\beta C(\alpha+1)}{(\bar{\alpha}+\alpha+2)^2} + \frac{(\bar{\alpha}+1)(C+\alpha\beta)}{(\alpha+1)(\bar{\alpha}+\alpha+2)} + \frac{1}{(\alpha+1)}$

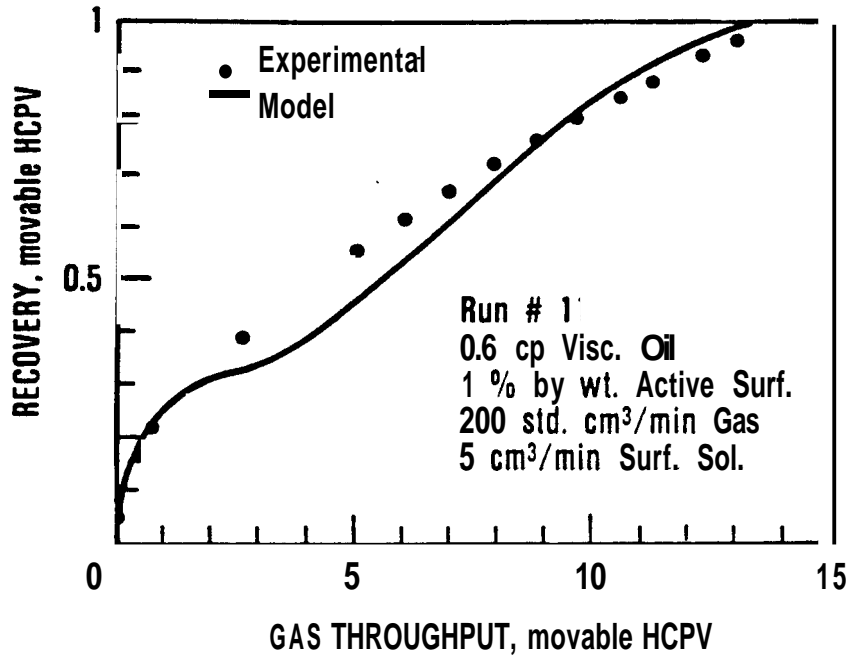


Figure 6.10 Comparison of Predicted and Experimental Recovery for Favorable Mobility Ratio Between Oil and Surfactant Solution.

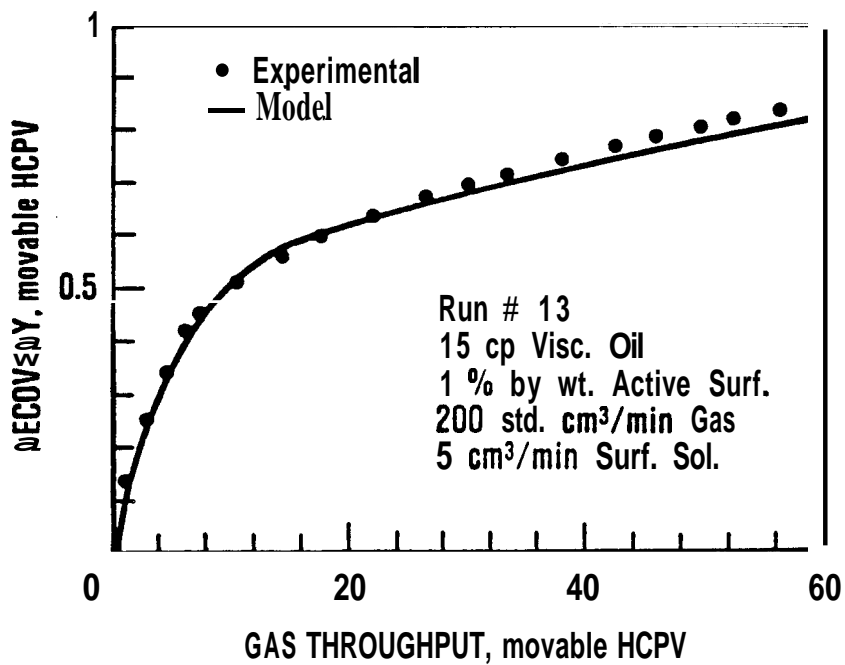


Figure 6.11 Comparison of Predicted and Experimental Recovery for Viscous-Dominated Surfactant Solution Front.

Another interesting observation was made while fitting the experimental data with modeling results. For this run, increasing the mobility ratio of surfactant solution-to-oil beyond the values listed in Table 6.6 did not make much difference. The reason for this insensitivity is not clear.

## 6.5. EFFECT OF SURFACTANT CONCENTRATION

Surfactant concentration affected the performance in two major ways: (1) in determining the initiation of foam generation and its physical characteristics, and (2) in determining the front profiles. Two characteristic behaviors were observed, one with surfactant concentrations above the CMC and the other with concentrations below or up to the CMC. Each of these are described below.

### 6.5.1. Performance Below and Up to the CMC

Two runs were performed to observe the effect of low surfactant concentrations on front profiles. One run (Run #16) was at the CMC concentration and the other run (Run #17) was at concentration much below the CMC. The operating conditions for these two runs are shown in Tables 6.7 and 6.8. Cyclohexane (1 cp viscosity at S.T.P.) was initially saturated at irreducible water saturation in these runs and was displaced by simultaneous injection of gas at 200 std. cm<sup>3</sup>/min. and surfactant solution at 5 cm<sup>3</sup>/min. Surfactant solution was Suntech 4 at concentrations of 0.3% or 0.01%, respectively. The injection ratio between the volumes of nitrogen and surfactant solution was 40 in both runs.

The frontal behavior of both runs was quite similar. Gas fingered through the top as usual and the finger thickness gradually increased. The surfactant solution bank also grew in size until it interfered with the gas channel, then it started advancing with a quite vertical profile at the front [Fig. 4.8(a)]. The effect of imbibition was quite noticeable. The saturation gradient across the surfactant solution front was not sharp, and as a result, the oil production continued even after the entire formation was swept. The decline in oil production was only gradual. However, since the surfactant profile was almost vertical due to imbibition, a considerable drop in recovery rate was noticed after surfactant broke through. An interesting point to note here is that foam was not generated for these runs during the useful life of the flood.

The combination drive model was not able to reasonably predict the recovery or pressure history for these runs, since this model is applicable only when the saturation gradient between oil and surfactant is sharp. The imbibition effects were so pronounced that a Dietz type gravity tongue did not form.

The recovery data are presented in Figs. 6.12 and 6.13. The recovery performance of both runs closely matched each other. There are no predicted recoveries in these figures, because no method to analyze this type of displacement is yet available. The profile of surfactant solution front was nearly vertical due to imbibition, and thus a considerable drop in recovery rate was observed.

### 6.5.2. Performance Above the CMC

Two runs (Run #20 and #21) were performed with surfactant concentrations higher than the CMC. Cyclohexane (1 cp viscosity) was initially present at irreducible water saturation, and was displaced by simultaneous injection of nitrogen at 200 std. cm<sup>3</sup>/min. and surfactant

TABLE 6.7  
**OPERATING CONDITIONS FOR RUN # 16**  
 (Near CMC Surfactant Concentration Displacement)

Mode of injection	<b>Simultaneous gas</b> and surfactant introduced directly without a mixing device
<b>Type</b> of <b>oil</b> in the porous medium	Cyclohexane (1 cp at room temp.)
Oil saturation	<b>87%</b> (at irreducible water saturation)
<b>Type</b> and concentration of surfactant	0.3% by weight of <b>SUNTECH 4</b>
<b>Gas</b> injection rate	<b>200</b> standard <b>cm<sup>3</sup>/min</b>
Surfactant injection rate	<b>5</b> standard <b>cm<sup>3</sup>/min</b>
Location of inj. and prod. intervals	<b>Both</b> inj. and <b>prod.</b> from bottom until <b>gas breakthrough</b> , then inj. <b>into</b> top
Injection and production history	Continuous, <b>with</b> no shut-in

**TABLE 6.8**  
**OPERATING CONDITIONS FOR RUN # 17**  
**(Below CMC Surfactant Concentration Displacement)**

Mode of injection	<b>Simultaneous</b> gas and surfactant introduced directly without a mixing device
Type of oil in the porous medium	Cyclohexane (1 cp at mom temp.)
<b>Oil</b> saturation	<b>88%</b> (at irreducible water saturation)
<b>Type</b> and concentration of surfactant	0.01% by weight of <b>SUNTECH 4</b>
<b>Gas</b> injection rate	<b>200</b> standard <b>cm<sup>3</sup>/min</b>
Surfactant injection rate	<b>5</b> standard <b>cm<sup>3</sup>/min</b>
Location of inj. and <b>prod.</b> intervals	<b>Both</b> inj. and prod. from bottom until <b>gas</b> breakthrough, then inj. <b>into</b> top
Injection and production history	Continuous, with no shut-in

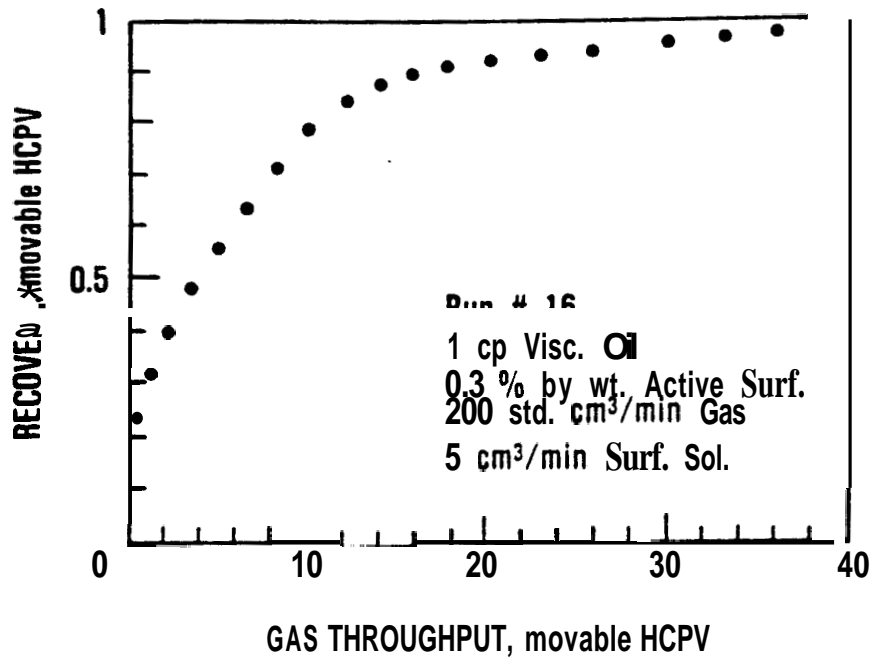


Figure 6.12 Experimental Recovery Data for a Low Concentration Displacement in which Surfactant Concentration was at CMC.

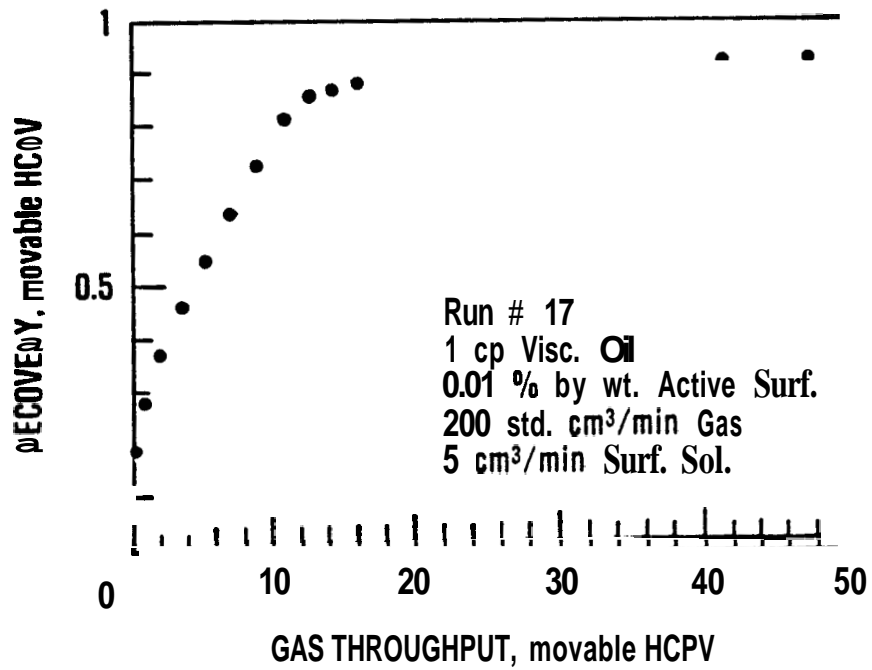


Figure 6.13 Experimental Recovery Data for a Low Concentration Displacement in which Surfactant Concentration was Much Below CMC.

solution at  $5 \text{ cm}^3/\text{min}$ . Surfactant concentrations in these two runs were 0.533% (Table 6.10, Run #20) and 0.767% (Table 6.9, Run #21) by weight of Suntech 4. The operating conditions for Run #20 and Run #21 are given in Tables 6.9 and 6.10 respectively.

In these runs, the surfactant solution bank formed a gravity tongue. Behavior of the gas finger was about the same as in the two low surfactant concentration runs (Run #16 and #17, below and up to the CMC) described in the previous section. Foam generated during the producing life and advanced through the gas channel as a third front (Fig. 4.8(b)).

The recovery for these runs was predicted using the combination-drive model as described previously in Section 5.3. The set of equations used for recovery prediction are given in Tables 6.9 and 6.10. The experimental data obtained during these runs, and the data obtained by modeling are all presented in Figs. 6.14 and 6.15. Agreement between the predicted behavior and the experimental results is generally good.

There is some inaccuracy late in the life of the flood for the 0.533% concentration run (Fig. 6.14), which is because the combination-drive equations were used beyond the expected practical life of the flood. However, for the second run shown in Fig. 6.15 (at 0.767% concentration) which was terminated at the end of the useful producing life, the agreement between model equations and experiment was good for the entire run.

The recovery was slightly higher for the 0.767% concentration run throughout the producing life, since foam was generated earlier. However, this difference in recovery was rather small.

## 6.6. EFFECT OF INJECTION RATE

For a simple gas or waterflood with no gravity segregation, the rate does not affect the frontal behavior or the recovery performance. Similarly, the performance is virtually independent of rate for a stable piston-like displacement, or for a fully segregated gravity-dominated flow. When instabilities such as viscous fingering are involved, the frontal behavior and production performance become strong functions of rate.

The effect of rate on the performance was similar to a simple waterflood prior to the onset of foam generation for displacement through the two-dimensional sandpack. But the throughput required to generate foam and the rate of advance of the foam front were rather sensitive to the rate of surfactant solution injection; both increased with increasing rate.

Two runs were performed to investigate the effect of flow rate on frontal behavior of a gravity-dominated flow. In these runs, decane or cyclohexane (1 cp viscosity at S.T.P.) was initially saturated with irreducible water and was displaced by simultaneous injection of nitrogen and 1% surfactant solution. The gas to surfactant solution volume injection ratio was 40 in both runs. Gas rates were 24 and 124 std.  $\text{cm}^3/\text{min}$ , as shown in Table 6.11 (Run #19) and Table 6.12 (Run #18), respectively, along with other operating conditions.

The gas front was found to be gravity dominated for both flow rates and operating conditions, because of the large density difference between the injected gas and the reservoir fluids. The gravity effects were overwhelming such that any change in the frontal behavior of the gas was unnoticeable from one gas rate to the other.

TABLE 6.9

OPERATING CONDITIONS AND PREDICTIVE EQUATIONS FOR RUN # 20  
(Slightly higher than CMC Surfactant Concentration Displacement)

Mode of injection	Simultaneous gas and surfactant introduced directly without a mixing device
Type of oil in the porous medium	Cyclohexane (1 cp at room temp.)
Oil saturation	88% (at irreducible water saturation)
Type and concentration of surfactant	0.533% by weight of SUNTECH 4
Gas injection rate	200 standard cm <sup>3</sup> /min
Surfactant injection rate	5 standard cm <sup>3</sup> /min
Location of inj. and prod. intervals	Both inj. and prod. from bottom until gas breakthrough, then inj. into top
Injection and production history	Continuous, with no shut-in
Apparent mobility ratios	Gas to oil=200, Foam to oil=80, Surfactant to oil=5 .
Recovery up to gas breakthrough (Material Balance, Eq. 5.3)	$N_{pD} = (1 / R + 1) G_{iD}$
Recovery at gas breakthrough (Modified Buckley-Levem, Eq. 5.26)	$(G_{iD})_{bt} = (N_{pD})_{bt} = \frac{1}{\bar{m}}$
Recovery at surf. breakthrough (Modified Buckley-Leverett, Eq. 5.30)	$(N_{pD})_{bt} = \frac{1}{m} + \frac{1}{(\bar{m}-1)} (2\sqrt{\bar{m}R/m-1}-R/m)$
Recovery up to surf. breakthrough [Modified Buckley-Leverett, Eq. 5.25)	$N_{pD} = \frac{G_{iD}}{R} + \frac{1}{(\bar{m}-1)} (2\sqrt{\bar{m}G_{iD}-1}-G_{iD})$
Recovery up to the end of flood (Combination-Drive Model, Eq. 5.70)	$N_{pD} = \frac{\sqrt{(C+\alpha\beta)^2-4\alpha\beta C(1-mQ_D)} - (C+\alpha\beta)}{2\alpha C}$
Max. recovery at the end of flood (Combination-Drive Model, Eq. 5.71)	$(N_{pD})_{max} = \frac{\alpha\beta C(\alpha+1)}{(\bar{\alpha}+\alpha+2)^2} + \frac{(\bar{\alpha}+1)(C+\alpha\beta)}{(\alpha+1)(\bar{\alpha}+\alpha+2)} + \frac{1}{(\alpha+1)}$

TABLE 6.10

OPERATING CONDITIONS AND PREDICTIVE EQUATIONS FOR RUN # 21  
(Quite Higher Than CMC Surfactant Concentration Displacement)

Mode of injection	<b>Simultaneous</b> gas and surfactant introduced directly without a mixing device
<b>Type</b> of oil in the porous medium	Cyclohexane (1 <b>cp</b> at room temp.)
Oil saturation	<b>88%</b> (at irreducible water saturation)
<b>Type</b> and concentration of surfactant	0.767% <b>by weight</b> of <b>SUNTECH 4</b>
Gas injection rate	<b>200</b> standard <b>cm<sup>3</sup>/min</b>
Surfactant injection rate	<b>5</b> standard <b>cm<sup>3</sup>/min</b>
Location of <b>inj.</b> and prod. intervals	<b>Both</b> inj. and prod. from bottom until gas breakthrough, then inj. into top
Injection <b>and</b> production history	Continuous, <b>with</b> no shut-in
Apparent mobility ratios	<b>Gas to oil=200, Foam to oil=80, Surfactant to oil=5 .</b>
Recovery up to gas breakthrough (Material <b>Balance</b> , Eq. 5.3)	$N_{pD} = (1/R + 1) G_{iD}$
Recovery at gas breakthrough (Modified Buckley-Leverett, Eq. 5.26)	$(G_{iD})_{gbr} = (N_{pD})_{gbr} = \frac{1}{\bar{m}}$
Recovery at <b>surf.</b> breakthrough (Modified Buckley-Leverett, Eq. 5.30)	$(N_{pD})_{sbt} = \frac{1}{m} + \frac{1}{(\bar{m}-1)} (2\sqrt{\bar{m}R/m-1}-R/m)$
Recovery up to surf. breakthrough (Modified Buckley-Leverett, Eq. 5.25)	$N_{pD} = \frac{G_{iD}}{R} + \frac{1}{(\bar{m}-1)} (2\sqrt{\bar{m}G_{iD}-1}-G_{iD})$
Recovery up to the end of flood (Combination-Drive Model, Eq. 5.70)	$N_{pD} = \frac{\sqrt{(C+\alpha\beta)^2-4\alpha\beta C(1-mQ_D)} - (C+\alpha\beta)}{2\alpha C}$
Max. recovery at the end of flood (Combination-Drive Model, Eq. 5.71)	$(N_{pD})_{max} = \frac{\alpha\beta C(\alpha+1)}{(\bar{\alpha}+\alpha+2)^2} + \frac{(\bar{\alpha}+1)(C+\alpha\beta)}{(\alpha+1)(\bar{\alpha}+\alpha+2)} + \frac{1}{(\alpha+1)}$

TABLE 6.11

OPERATING CONDITIONS AND PREDICTIVE EQUATIONS FOR RUN # 19  
(Displacement at Surfactant Solution Rate of 24 cm<sup>3</sup>/min)

Mode of injection	Simultaneous <b>gas</b> and surfactant introduced directly without a mixing device
<b>Type</b> of <b>oil</b> in the porous medium	Decane (1 cp at room temp.)
<b>Oil</b> saturation	88% (at irreducible water saturation)
<b>Type</b> and concentration of surfactant	1% by weight of <b>SUNTECH 4</b>
Gas injection rate	24 standard cm <sup>3</sup> /min
Surfactant injection rate	0.6 standard cm <sup>3</sup> /min
Location of inj. and prod. intervals	<b>Both</b> inj. and prod. from <b>bottom</b> until <b>gas</b> breakthrough, then inj. into top
Injection and production history	Continuous, with no shut-in
Apparent mobility ratios	<b>Gas</b> to <b>oil</b> =200, <b>Foam</b> to <b>oil</b> =80, surfactant to <b>oil</b> =5.
Recovery up to gas breakthrough (Material Balance, Eq. 5.3)	$N_{pD} = (1 / R + 1) G_{iD}$
Recovery at gas breakthrough (Modified Buckley-Leverett, Eq. 5.26)	$(G_{iD})_{gt} = (N_{pD})_{gt} = \frac{1}{\bar{m}}$
Recovery at surf. breakthrough (Modified Buckley-Leverett, Eq. 5.30)	$(N_{pD})_{st} = \frac{1}{\bar{m}} + \frac{1}{(\bar{m}-1)} (2\sqrt{\bar{m}R/\bar{m}-1}-R/\bar{m})$
Recovery up to surf. breakthrough (Modified Buckley-Leverett, Eq. 5.25)	$N_{pD} = \frac{G_{iD}}{R} + \frac{1}{(\bar{m}-1)} (2\sqrt{\bar{m}G_{iD}} - 1 - G_{iD})$
Recovery up to the end of flood (Combination-Drive Model, Eq. 5.70)	$N_{pD} = \frac{\sqrt{(C+\alpha\beta)^2 - 4\alpha\beta C(1-mQ_D)} - (C+\alpha\beta)}{2\alpha C}$
<b>Max.</b> recovery at the end of flood (Combination-Drive Model, Eq. 5.71)	$(N_{pD})_{max} = \frac{\alpha\beta C(\alpha+1)}{(\bar{\alpha}+\alpha+2)^2} + \frac{(\bar{\alpha}+1)(C+\alpha\beta)}{(\alpha+1)(\bar{\alpha}+\alpha+2)} + \frac{1}{(\alpha+1)}$

TABLE 6.12

OPERATING CONDITIONS AND PREDICTIVE EQUATIONS FOR RUN # 18  
(Displacement at Surfactant Solution Rate of 124 cm<sup>3</sup>/min)

Mode of injection	Simultaneous gas and surfactant introduced directly without a mixing device
<b>Type</b> of oil in the porous medium	Decane (1 cp at room temp.)
Oil saturation	88% (at irreducible water saturation)
<b>Type</b> and concentration of surfactant	1% by weight of <b>SUNTECH 4</b>
Gas injection rate	124 standard cm <sup>3</sup> /min
Surfactant injection rate	3.09 standard cm <sup>3</sup> /min
Location of inj. and prod. intervals	Both inj. and prod. from boam until gas breakthrough. then inj. into top
Injection and production history	Continuous, with no shut-in
Apparent mobility ratios	Gas to oil=200, Foam to oil=80, Surfactant to oil=5.
Recovery up to gas breakthrough (Material Balance, Eq. 5.3)	$N_{pD} = (1 / R + 1) G_{iD}$
Recovery at gas breakthrough (Modified Buckley-Levem, Eq. 5.26)	$(G_{iD})_{gbt} = (N_{pD})_{gbt} = \frac{1}{\bar{m}}$
Recovery at surf. breakthrough (Modified Buckley-Leverett, Eq. 5.30)	$(N_{pD})_{sbt} = \frac{1}{m} + \frac{1}{(\bar{m}-1)} (2\sqrt{\bar{m}R/m-1}-R/m)$
Recovery up to surf. breakthrough (Modified Buckley-Leverett, Eq. 5.25)	$N_{pD} = \frac{G_{iD}}{R} + \frac{1}{(\bar{m}-1)} (2\sqrt{\bar{m}G_{iD}-1}-G_{iD})$
Recovery up to the end of flood (Combination-Drive Model, Eq. 5.70)	$N_{pD} = \frac{\sqrt{(C+\alpha\beta)^2-4\alpha\beta C(1-mQ_D)} - (C+\alpha\beta)}{2\alpha C}$
<b>Max. recovery</b> at the end of flood (Combination-Drive Model, Eq. 5.71)	$(N_{pD})_{max} = \frac{\alpha\beta C(\alpha+1)}{(\bar{\alpha}+\alpha+2)^2} + \frac{(\bar{\alpha}+1)(C+\alpha\beta)}{(\alpha+1)(\bar{\alpha}+\alpha+2)} + \frac{1}{(\alpha+1)}$

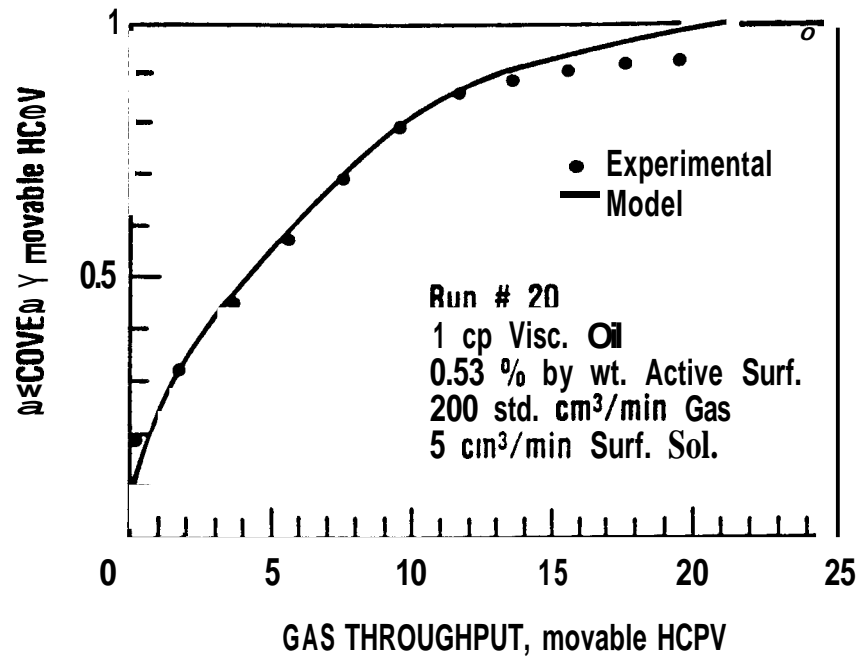


Figure 6.14 Comparison of Predicted and Experimental Recovery for Displacement in which Surfactant Concentration was Slightly Higher Than CMC.

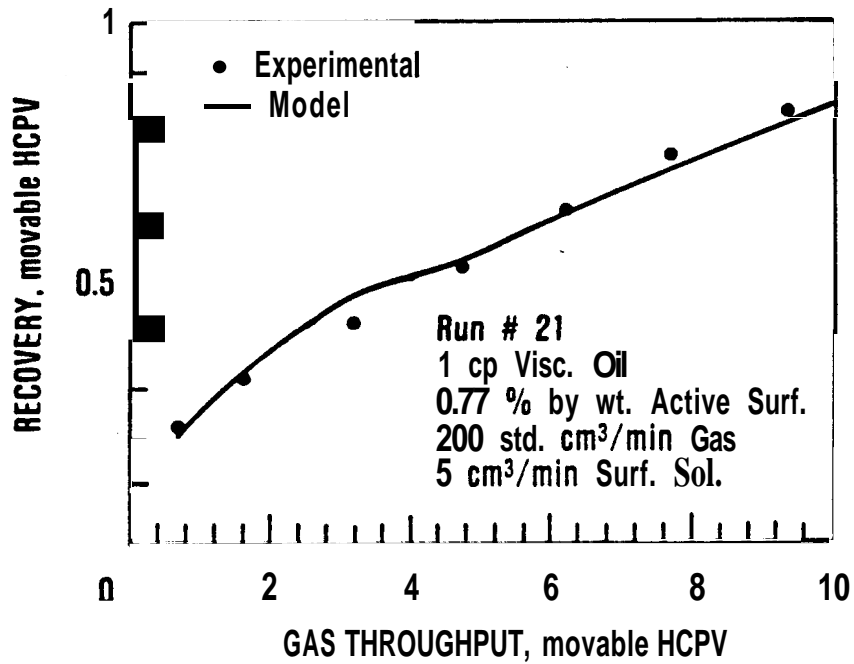


Figure 6.15 Comparison of Predicted and Experimental Recovery for Displacement in which Surfactant Concentration was Quite Higher Than CMC.

For the gas rate of  $24 \text{ std cm}^3/\text{min}$  and surfactant rate of  $0.6 \text{ cm}^3/\text{min}$  (Table 6.11, Run #19), foam generation was quite late in the run and the surfactant solution bank was fully dominated by gravity effects. The flow of gas and surfactant solution was in two different thin fingers, growing in size with the progress of the flood, and finally interfering with each other. Only a small volume of surfactant solution came in contact with gas.

For the gas rate of  $124 \text{ std cm}^3/\text{min}$  and surfactant solution rate of  $3.09 \text{ cm}^3/\text{min}$ , the evidence of foam generation was earlier and stronger; thus the gravity tonguing of surfactant solution was less severe. The entire height of sandpack near the injection well was swept by the surfactant solution. This improved sweep caused more surfactant solution volume to come in contact with gas and help in foam generation.

The rate did not seem to change the basic recovery mechanism, other than the time of foam generation. The combinationdrive model was used effectively to predict the recovery behavior of these runs and a good agreement was obtained between modeling equations and the experimental results. The set of equations used for predicting the recovery behavior are given in Tables 6.11 and 6.12 and these results are presented in Figs. 6.16 and 6.17.

## 6.7. EFFECT OF GAS/SURFACTANT SOLUTION VOLUME RATIO

The ratio between the volumes of surfactant solution and gas injection is another important parameter in determining the performance. This ratio is important for the flood performance for two reasons: (1) it affects the time of foam generation, and (2) it affects the rheology of foam after the foam generation has started.

The effect of the gas/surfactant solution volume ratio was investigated for the following four defined categories: Balanced, Low, High, Variable. These four distinct behaviors are described in the following sections.

### 6.7.1. Balanced Gadsurfactant Solution Volumetric Ratio

The balanced ratio is defined here as the volume proportion of surfactant and gas which can be sustained by the foam body. In the runs with this condition (gadsurfactant solution volumetric ratio = 40:1), the combinationdrive behavior was observed. The surfactant solution which entered the sandpack with gas, segregated and advanced in the form of a bank. The recovery and pressure histories were estimated using the combinationdrive model.

Most of the runs in this study were performed with balanced gadsurfactant solution volumetric ratio (40:1), and therefore, have been extensively discussed in many sections. To avoid duplication, these runs would not be discussed here. For analysis and discussion of these types of runs, the reader is referred to Sections 6.3 through 6.6 (Figs. 6.6 through 6.17) already discussed, and Section 6.8 (Fig. 6.20).

### 6.7.2. High Gas/Surfactant Solution Volumetric Ratio

One run was performed with a volume ratio which was too high to generate continuous foam. The gadsurfactant solution volumetric ratio in this run (Run #14) was 60:1. Cyclohexane (1 cp viscosity) was initially present at irreducible water saturation and was displaced by

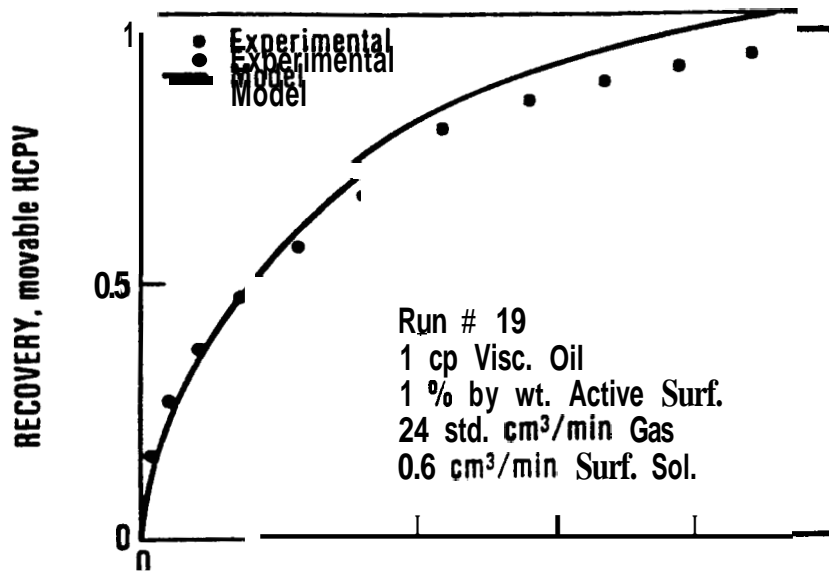


Figure 6.16 Comparison of Predicted and Experimental Recovery for Surfactant Solution Rate of 24 cm<sup>3</sup>/min.

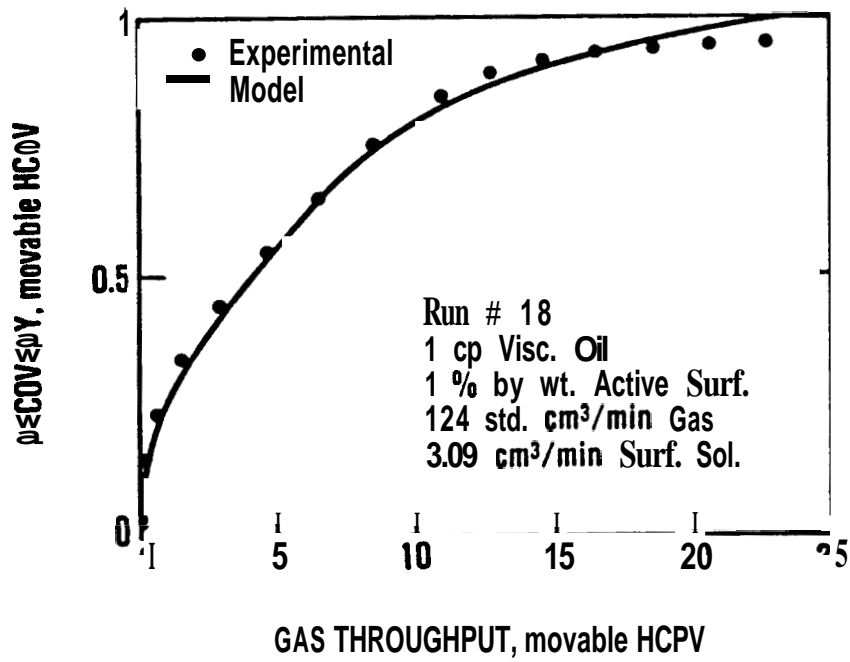


Figure 6.17 Comparison of Predicted and Experimental Recovery for Surfactant Solution Rate of 124 cm<sup>3</sup>/min.

simultaneous injection of nitrogen at 10 std cm<sup>3</sup>/min and 1% Suntech 4 at 0.167 cm<sup>3</sup>/min. The operating conditions for this run are listed in Table 6.13.

The frontal advance behavior was very similar to the runs performed with balanced gas/surfactant solution volumetric ratio runs mentioned in earlier sections. Foam generation was comparatively late in the life of the flood, as would be expected due to the mass effect, hence the recovery performance was lower, as expected.

Recovery and pressure history were predicted by the combination-drive model and the time of foam generation was determined by the empirical relationship for the mass-effect (Eq. (5.2)). The set of equations used for predicting the production performance are given in Table 6.13. The experimental recovery data and the recovery predicted by model equations are both graphed in Fig. 6.18. A good agreement between predicted results and experimental data was obtained.

### 6.7.3. Low Gas/Surfactant Solution Volumetric Ratio

This run was performed with a gas/surfactant solution volumetric ratio of 6:1. The sandpack was initially saturated with Decane (1 cp viscosity) at irreducible water saturation, which was then displaced by simultaneous injection of nitrogen at 1 std cm<sup>3</sup>/min and surfactant solution (1% Suntech 4) at 0.167 cm<sup>3</sup>/min.

The recovery for low gas/surfactant solution volumetric ratio was successfully estimated using the combination-drive model. This run (Run #9) has also been analyzed in Section 6.3.4 (Fig. 6.9). A good agreement between the sandpack results and modeling equation prediction was seen. The production performance of the lower gas/surfactant solution volumetric ratio run was seen to be superior to that of a higher gas/surfactant solution volumetric ratio.

### 6.7.4. Variable Gas/Surfactant Solution Volumetric Ratio

One run was performed in which the surfactant solution rate was kept constant, and the gas was injected at variable rate but at constant pressure (20 psig). After foam generation started, the gas mobility was reduced, which also lowered the gas injectivity. Since the surfactant solution rate was kept constant, the gradually decreasing gas rate caused the gas/surfactant solution volumetric ratio to continuously decrease. The operating conditions for this run (Run X12) are described in Table 6.14. Cyclohexane (1 cp viscosity) was initially saturated with irreducible water and was then displaced by simultaneous injection of nitrogen and surfactant solution (1% Suntech 4). The nitrogen rate was 200 std cm<sup>3</sup>/min until the pressure limitation was reached, and then it became variable, whereas the surfactant solution rate was constant at 5 cm<sup>3</sup>/min.

The frontal behavior in this run resembled a low-tension flood more than it resembled the combination flood. The gas broke through from the top as in any combination flood, but soon after foam generation started, the foam front advanced rapidly. After foam front breakthrough, the foam virtually blocked the gas channel, reducing the gas injection rate to a negligible value. The surfactant bank advanced in the form of a Dietz tongue, but with a strong cross-flow in the upward direction. The production behavior up to 2.2 pore volumes of throughput was between that expected for a high gas/surfactant solution volumetric ratio run and that for a low gas/surfactant solution volumetric ratio run. After 2.2 pore volumes of throughput, foam generation started and blocked the gas flow, resulting in a "kick" in recovery versus volume injected. The recovery levelled off sharply after surfactant breakthrough.

TABLE 6.13

OPERATING CONDITIONS AND PREDICTIVE EQUATIONS FOR RUN # 14  
(High Gas to Surfactant Solution Volumetric Ratio Displacement)

Mode of injection	Simultaneous gas and surfactant introduced directly without a mixing device
Type of oil in the porous medium	Cyclohexane (1 cp at room temp.)
Oil saturation	826 (at irreducible water saturation)
Type and concentration of surfactant	1% by weight of SUNTECH 4
Gas injection rate	10 standard cm <sup>3</sup> /min
Surfactant injection rate	0.167 standard cm <sup>3</sup> /min
Location of inj. and prod. intervals	Both inj. and prod. from bottom until gas breakthrough, then inj. into top
Injection and production history	Continuous, with no shut-in
Apparent mobility ratios	Gas to oil=200, Foam to oil=80, Surfactant to oil=5 .
Recovery up to gas breakthrough (Material Balance, Eq. 5.3)	$N_{pD} = (1 / R + 1) G_{ID}$
Recovery at gas breakthrough (Modified Buckley-Leverett, Eq. 5.26)	$(G_{ID})_{gt} = (N_{pD})_{gt} = \frac{1}{\bar{m}}$
Recovery at surf. breakthrough (Modified Buckley-Leverett, Eq. 5.30)	$(N_{pD})_{st} = \frac{1}{m} + \frac{1}{(\bar{m}-1)} (2\sqrt{\bar{m}R/m-1}-R/m)$
Recovery up to surf. breakthrough (Modified Buckley-Leverett, Eq. 5.25)	$N_{pD} = \frac{G_{ID}}{R} + \frac{1}{(\bar{m}-1)} (2\sqrt{\bar{m}G_{ID}-1}-G_{ID})$
Recovery up to the end of flood (Combination-Drive Model, Eq. 5.70)	$N_{pD} = \frac{\sqrt{(C+\alpha\beta)^2-4\alpha\beta C(1-mQ_D)} - (C+\alpha\beta)}{2\alpha C}$
Max. recovery at the end of flood (Combination-Drive Model, Eq. 5.71)	$(N_{pD})_{max} = \frac{\alpha\beta C(\alpha+1)}{(\bar{\alpha}+\alpha+2)^2} + \frac{(\bar{\alpha}+1)(C+\alpha\beta)}{(\alpha+1)(\bar{\alpha}+\alpha+2)} + \frac{1}{(\alpha+1)}$

TABLE 6.14

**OPERATING CONDITIONS AND PREDICTIVE EQUATIONS FOR RUN # 12**  
(Variable Gas to Surfactant Solution Volumetric Ratio Displacement)

Mode of injection	<b>Simultaneous gas and surfactant</b> introduced directly without a mixing device
Type of oil in the porous medium	Cyclohexane (1 cp at room temp.)
Oil saturation	87% (at irreducible water saturation)
<b>Type and concentration</b> of surfactant	1% by weight of SUNTECH 4
Gas injection rate	200 standard cm <sup>3</sup> /min at start, then maintained at 20 psig constant pressure
Surfactant injection rate	5 standard cm <sup>3</sup> /min
Location of inj. and prod. intervals	<b>Both inj. and prod. from bottom</b> until gas breakthrough, then <b>inj.</b> into top
Injection and production history	Continuous, with <b>no</b> shut-in
Apparent mobility ratios	<b>Gas to oil=200, Foam to oil=80, surfactant to oil=5 .</b>
Recovery up to gas breakthrough (Material Balance, Eq. 5.3)	$N_{pD} = G_{iD} + W_{iD}$
Recovery at gas breakthrough (Modified Buckley-Leverett, Eq. 5.26)	$(G_{iD})_{gt} = (N_{pD})_{gt} = \frac{1}{\bar{m}}$
Recovery at surf. breakthrough (Modified Buckley-Leverett, after substituting $G_{iD}/W_{iD}$ for $R$ in Eq. 5.30)	$\frac{1}{m} + \frac{1}{(\bar{m}-1)} (2\sqrt{\bar{m}G_{iD}/mW_{iD}} - 1 - G_{iD}/W_{iD}m)$
Recovery up to surf. breakthrough (Modified Buckley-Leverett, Eq. 5.94)	$N_{pD} = W_{iD} + \frac{1}{(\bar{m}-1)} (2\sqrt{\bar{m}G_{iD}} - 1 - G_{iD})$
Recovery up to the end of flood (Combination-Drive Model, after substituting $(q_w/q_g+1)G_{iD}$ for $Q_{iD}$ in Eq. 5.70)	$\frac{\sqrt{(C+\alpha\beta)^2 - 4\alpha\beta C(1-m(q_w/q_g+1)G_{iD})} - (C+\alpha\beta)}{2\alpha C}$
Max. recovery at the end of flood (Combination-Drive Model, Eq. 5.71)	$(N_{pD})_{max} = \frac{\alpha\beta C(\alpha+1)}{(\bar{\alpha}+\alpha+2)^2} - \frac{(\bar{\alpha}+1)(C+\alpha\beta)}{(\alpha+1)(\bar{\alpha}+\alpha+2)} - \frac{1}{(\alpha+1)}$

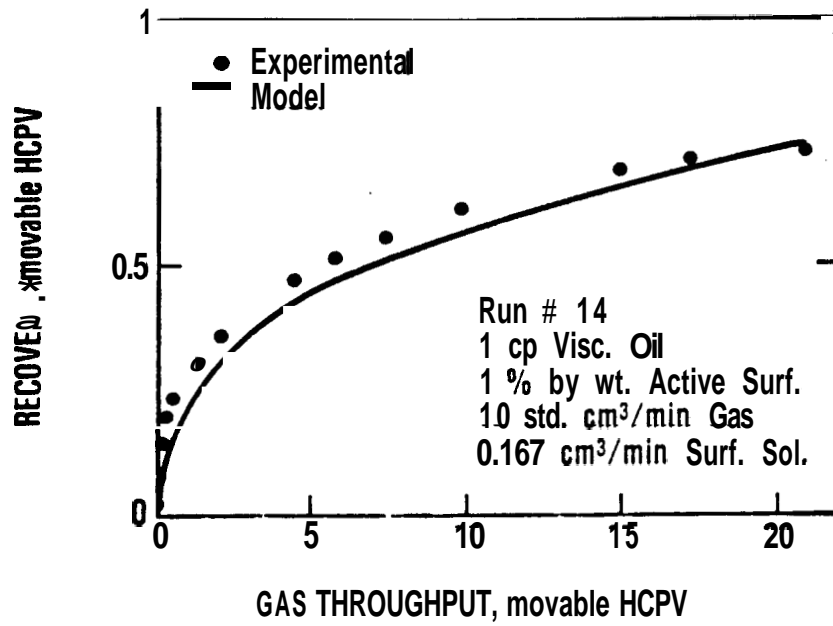


Figure 6.18 Comparison of Predicted and Experimental Recovery for High Gas to Surfactant Solution Volumetric Ratio.

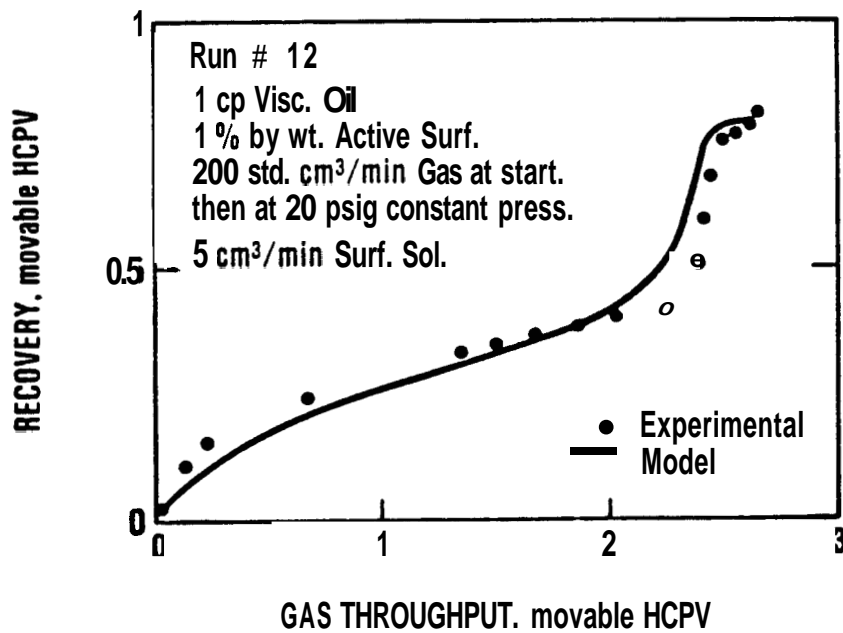


Figure 6.19 Comparison of Predicted and Experimental Recovery for Variable Gas to Surfactant Solution Volumetric Ratio.

Despite these deviations **observed** in the frontal behavior, it was possible **to** match the production performance in **this case** also by using the combination-drive model, except that the ratio of cumulative volumes **had to be** used in the equations instead of rate ratios **to take into account** the changing rate of gas injection.

The set of equations used for matching the recovery behavior **are** given in Table 6.14. The experimental data and the data obtained by modeling **are** graphed in Fig. 6.19. The agreement between predicted results **and** the experimental data is quite reasonable.

## 6.8. GRAVITY-DOMINATED DISPLACEMENT WITH A LONG SHUT-IN

Run #15 was **performed to see** the effect of a long shut-in on recovery and was performed under the operating conditions **described** in Table 6.15. **This run** was very similar **to** the other gravity-dominated runs (Section 6.5.3), except that it was shut-in for considerable time (2 days) **after** in-situ foam generation **had started**. The performance before shut-in was the same **as** for other gravity-dominated runs described in Section 6.5.3. During shut-in, the foam collapsed and gravity segregation continued. **This** was evidenced when the displacement was resumed by a higher initial mobility and more segregated conditions. Foam generation began **again** after **only** a small surfactant volume injection. **Also** the foam front advanced rapidly toward the producing end.

Since gravity segregation of surfactant solution continued during shut-in, and the shut-in was long, the surfactant solution gravity tongue reached the producing well. **On restart** of injection, surfactant solution breakthrough **took** place immediately. Therefore, the effect of shut-in was **to reduce** the recovery by lowering the "effective" surfactant solution breakthrough time. However, the overall effect of long shut-in on oil recovery and foam collapse was rather small.

For prediction of the performance for **this** run, the surfactant breakthrough time was not calculated by the equation **given** in the combination-drive model; rather the breakthrough time was assumed **to coincide** with the time the run was resumed, as **seen** from the experiment. The equations used for predicting the recovery behavior **are** given in Table 6.15. The predicted recovery is **compared** with the experiment in Fig. 6.20. **The** match is quite **good**.

## 6.9. PRESSURE HISTORY MATCHING

The mathematical development for the prediction of **pressure** history for **this** two-dimensional vertical sandpack was **tested on** the experimental data. The agreement between predicted and experimental results was reasonable for those runs in which the combination-drive behavior was expected. But the agreement was not generally **as good** for predicting the **pressure** as it was for the **recovery**.

**This** is perhaps not **too surprising**. The combination-drive model presented in Section 5 neglects the effect of the gradual **advancement** of the foam front. For recovery prediction; an instantaneous change from no-foaming **to** full-foaming condition is assumed **and** an average value of foam mobility is used. This assumption **has** only a small effect on recovery calculations, **since the foam front is** advancing in the zone already swept by gas. In that zone the remaining oil saturation is small, such that the oil recovery from the gas/foam swept zone is almost entirely due to the oil displacement by gas. However, the same is not **true** for the pressure drops, since the **pressure drop across** the gas zone is due **to** a composite effect of **both** the

**TABLE 6.15**  
**OPERATING CONDITIONS AND PREDICTIVE EQUATIONS FOR RUN # 15**  
**(Gravity-Dominated Displacement with a Long Shut-in)**

Mode of injection	Simultaneous gas and surfactant introduced directly without a mixing device
Type of oil in the porous medium	Cyclohexane (1 cp at room temp.)
Oil saturation	86% (at irreducible water saturation)
Type and concentration of surfactant	1% by weight of SUNTECH 4
Gas injection rate	47 standard cm <sup>3</sup> /min
Surfactant injection rate	1.175 standard cm <sup>3</sup> /min
Location of inj. and prod. intervals	Both inj. and prod. from bottom until gas breakthrough, then inj. into top
Injection and production history	Long shut-in at 30% of movable oil volume recovered, then reinjection
Apparent mobility ratios	Gas to oil=200, Foam to oil=80, Surfactant to oil=5
Recovery up to gas breakthrough (Material Balance, Eq. 5.3)	$N_{pD} = (1 / R + 1) G_{iD}$
Recovery at gas breakthrough (Modified Buckley-Leverett, Eq. 5.26)	$(G_{iD})_{gbt} = (N_{pD})_{gbt} = \frac{1}{\bar{m}}$
Recovery at surf. breakthrough (Recovery at the time of shut down)	$(N_{pD})_{sbt} = 0.3$ Movable Pore Volumes
Recovery up to surf. breakthrough (Modified Buckley-Leverett, Eq. 5.25)	$N_{pD} = \frac{G_{iD}}{R} + \frac{1}{(\bar{m} - 1)} (2\sqrt{\bar{m}G_{iD}} - 1 - G_{iD})$
Recovery up to the end of flood (Combination-Drive Model, Eq. 5.70)	$N_{pD} = \frac{\sqrt{(C+\alpha\beta)^2 - 4\alpha\beta C(1-mQ_D)} - (C+\alpha\beta)}{2\alpha C}$
Max. recovery at the end of flood (Combination-Drive Model, Eq. 5.71)	$(N_{pD})_{max} = \frac{\alpha\beta C(\alpha+1)}{(\bar{\alpha}+\alpha+2)^2} + \frac{(\bar{\alpha}+1)(C+\alpha\beta)}{(\alpha+1)(\bar{\alpha}+\alpha+2)} + \frac{1}{(\alpha+1)}$

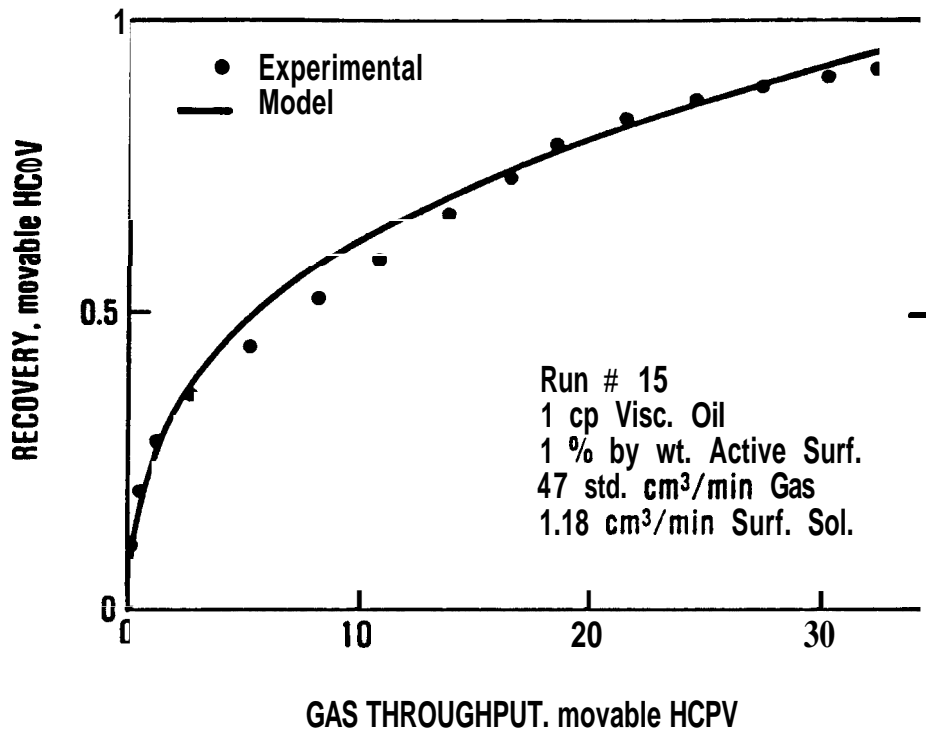


Figure 6.20 Comparison of Predicted and Experimental Recovery for Gravity-Dominated Displacement with Long Shut-in.

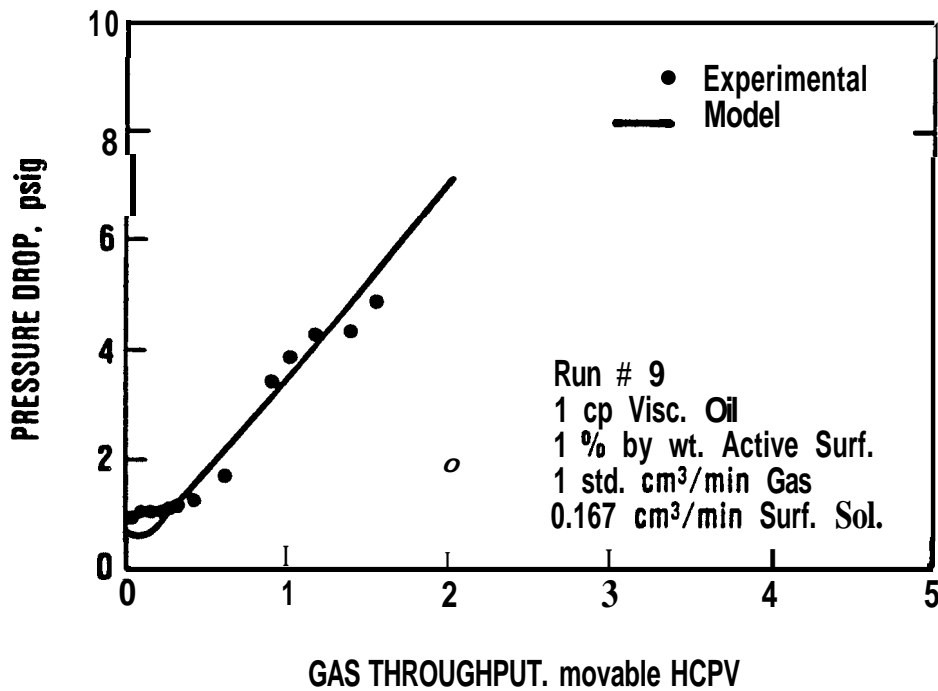


Figure 6.21 Comparison of Predicted and Experimental Pressure Drops for Simultaneous Injection of Gas and Surfactant Solution.

pressure drop in the foam zone and in the gas zone. Thus the effect of foam front advance is critical for predicting the pressure history.

If the rate of advance of the foam front could somehow be accurately predicted and incorporated in this model, a more accurate pressure prediction would likely be possible. However, no attempts were made in this study to describe the velocity of the foam front.

For runs in which the frontal behavior did not resemble the combination-drive model, the recovery was predicted using alternate models. However, the pressure history was calculated using the same mathematical development for all runs. Therefore, as expected, the pressure drop match was poor for runs in which the combination-drive behavior was not observed.

In the following sections the results of all runs are discussed for which prediction of pressure history was attempted. Not every run was analyzed, since as mentioned earlier, the frontal behavior in some runs was so different from a combination-drive model that even a rough approximation was not expected.

### 6.9.1. Runs with Combination-Drive Behavior

In the series of runs performed to see the effect of mode of injection (Section 6.4), only the run with simultaneous injection of gas and surfactant solution seemed to give a good match with the experimental results, as expected, since the frontal behavior in other modes of injection did not resemble the combinationdrive. In Run #9, decane at irreducible water saturation was displaced by simultaneous injection of nitrogen at a rate of 1 std cm<sup>3</sup>/min and surfactant solution (1% Suntech 4) at a rate of 0.167 std cm<sup>3</sup>/min. The operating conditions for this run are given in Table 6.4 and the recovery match is shown in Fig. 6.9. The pressure history match is shown in Fig. 6.21. The agreement was good as long as the initial operating conditions were maintained. After two pore volumes of throughput, injection of surfactant solution was stopped, which resulted in a sharp decrease of pressure in the experiment.

Among the runs performed to see the effect of surfactant concentration in the solution (Section 6.7), only those runs performed with surfactant concentrations higher than the CMC showed combinationdrive behavior. In run #21, cyclohexane with irreducible water saturation was displaced by simultaneous injection of nitrogen at a rate of 200 std cm<sup>3</sup>/min and surfactant solution (0.767% Suntech 4) at a rate of 5 std cm<sup>3</sup>/min. The operating conditions for this run are given in Table 6.10 and the recovery match is shown in Fig. 6.15. The pressure performance of this run is shown in Fig. 6.22. The agreement between the predicted and the experimental results is reasonable. There are increases and decreases in the model equation prediction of pressure drops. It is surmised that this curve shape resulted because the value of gas mobility was changed abruptly to the value of foam mobility after foam generation, whereas the actual mobility change took place gradually in the experiment.

The pressure history and the model predictions for another run similar to the one described above is shown in Fig. 6.23. The recovery performance of this run (Run #20) was shown in Fig. 6.14 and the operating conditions were listed in Table 6.9. The only difference in this run from the previous one was a lower concentration, i.e., 0.533% instead of 0.767%. The agreement between the model prediction and the experimental result is reasonable until 6-8 pore volumes of gas were injected, after which the agreement became rather poor. The reason for this disagreement is not clear.

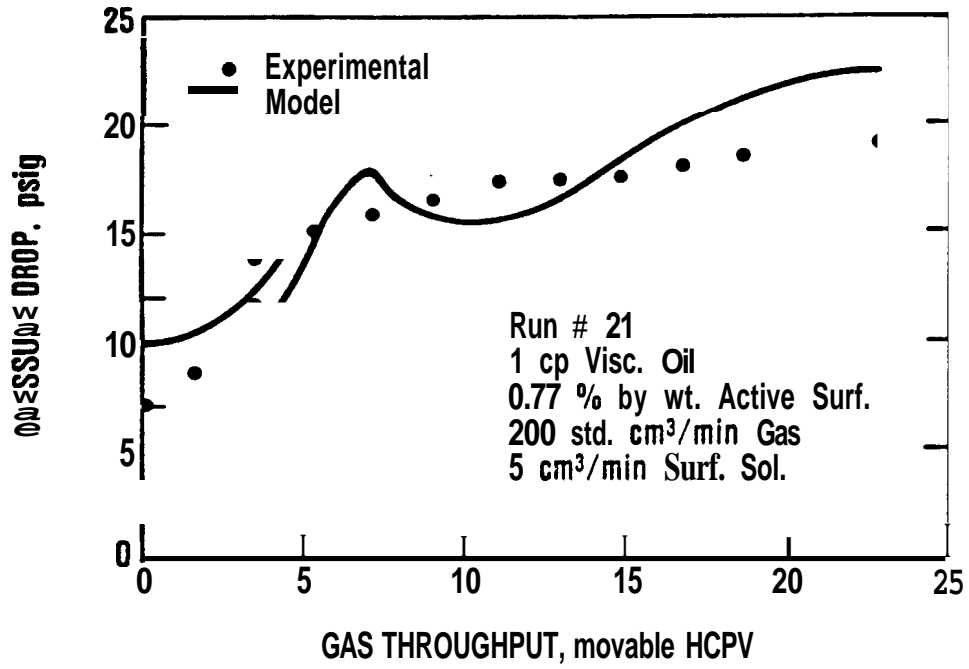


Figure 6.22 Comparison of Predicted and Experimental Pressure Drops for Displacement in which Surfactant Concentration was Quite Higher Than CMC.

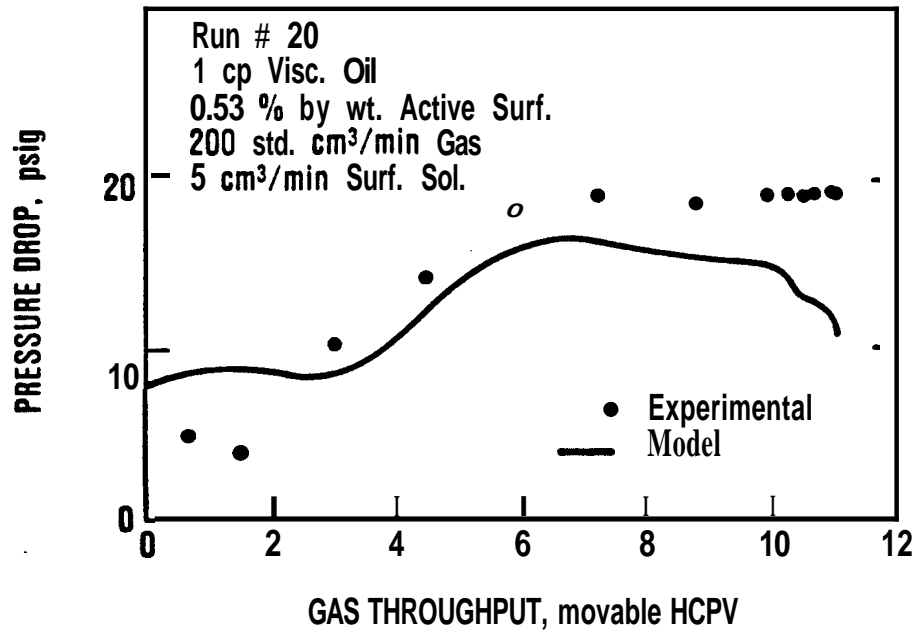


Figure 6.23 Comparison of Predicted and Experimental Pressure Drops for Displacement in which Surfactant Concentration was Slightly Higher Than CMC.

Two runs were performed to see the effect of rate on displacement behavior (Section 6.8). Nitrogen was injected at the rates of 24 and 124 std cm<sup>3</sup>/min. Combination-drive model behavior was observed in both runs, and therefore the pressure history of both the runs was similar. Due to the similarity, only one run is discussed here.

In Run #18, decane at irreducible water saturation was displaced by simultaneous injection of nitrogen at a rate of 124 std cm<sup>3</sup>/min and surfactant solution (1% Suntech 4) at a rate of 3.09 std cm<sup>3</sup>/min. The operating conditions for this run are given in Table 6.12 and the recovery performance is shown in Fig. 6.17. The pressure behavior is shown in Fig. 6.24 and is compared with the predicted pressures. The agreement between the predicted and the experimental pressure results is not very good at low throughputs but is better at higher throughput. The reason for this discrepancy in early life is the same as described before, i.e., it is due to using a different value of gas mobility at the time of foam generation. It is interesting to note, however, that the shape of the predicted pressure drop curve is similar to the one shown in Fig. 6.22 except that the deviation started earlier in this run due to the earlier foam generation.

## 69.2. Runs without Resemblance to the Combination-Drive Behavior

The modeling equation derived for the prediction of pressure drops was based on the combination-drive model behavior, hence it was not directly applicable to other types of frontal behavior. Nevertheless, this equation was also used for the prediction of other types of behavior observed in this study. This was done to get some insight to the scope and limitations of the pressure modeling equation. These attempts are discussed here to show the variety of pressure behavior observed. Sometimes it was possible to use the same pressure equation successfully with minor modifications. Some of these modifications which allow reasonable pressure predictions are also described in the following paragraphs.

The pressure behavior for Run #11 (Section 6.5.1) in which the surfactant solution-to-oil mobility ratio was favorable is shown in Fig. 6.25. The operating conditions for this run are given in Table 6.5 and the recovery behavior is shown in Fig. 6.10. The agreement between experimental pressure drop and model equation predictions is not good. The surfactant solution frontal behavior was piston-like in this run due to the favorable mobility ratio, and therefore, foam generation started earlier than predicted by the mass-effect empirical relationship. Also, the value of predicted pressure drop decreased up to 5 pore volumes of gas injection, due to the built-in model assumption that the injected fluid has higher mobility, whereas in reality the pressure drop should have increased due to the injection of a lower mobility fluid. Both these assumptions caused the predicted pressure drops to be lower than the observed values. However, after foam initiation the rate of increase of calculated pressure drop is close to the actual one.

Run #13 was another run in which the frontal behavior was significantly different from combination-drive behavior. The surfactant solution front was viscous-dominated in this run, which resulted in an earlier breakthrough than expected in a stable figures 6.24 and 6.25 displacement. However, as the flood progressed, these fingers became diffuse and formed a tongue similar to a Dietz tongue. The operating conditions for this run were given in Table 6.6 and the recovery behavior was presented in Fig. 6.11. The predicted pressure drops and experimental pressure drops are both graphed in Fig. 6.26, where it can be seen that the agreement is not good up to about 10 pore volumes of gas injection, after which it becomes reasonable. The reason for this error in matching is clear. The model assumes a gradual decline in pressure drop due to the encroachment of a higher mobility injection fluid (surfactant solution), whereas this decline in pressure was rapid during the experimental run due to the early breakthrough of surfactant solution fingers. After about 10 pore volumes of injection, these fingers were diffuse and thereafter the behavior resembled a combination-drive model behavior in agreement with the model equation.

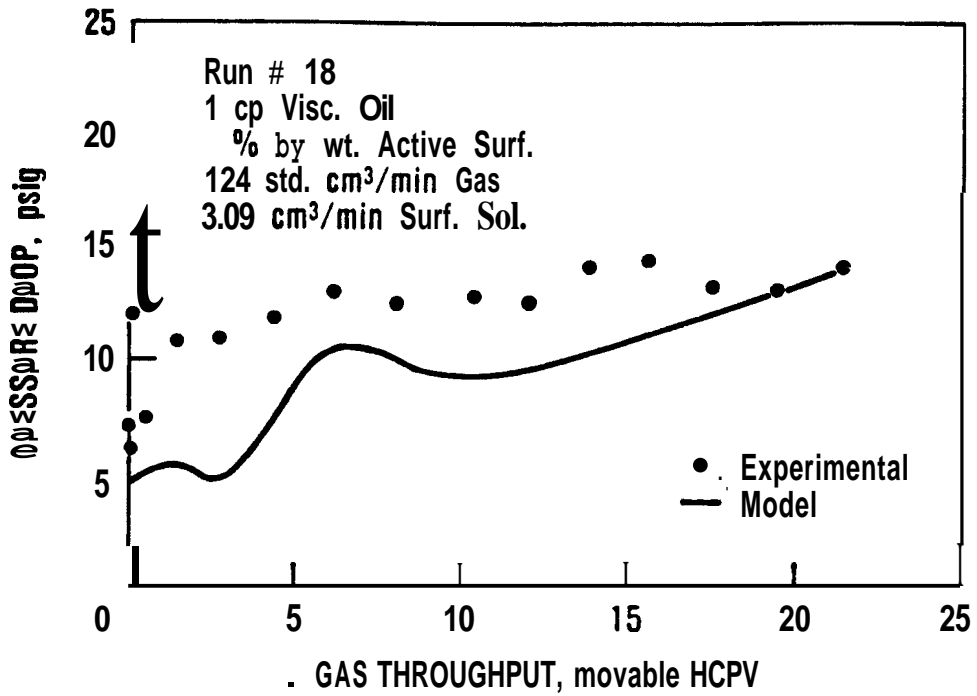


Figure 6.24 Comparison of Predicted and Experimental Pressure Drops for Surfactant Solution Rate of 124 cm<sup>3</sup>/min.

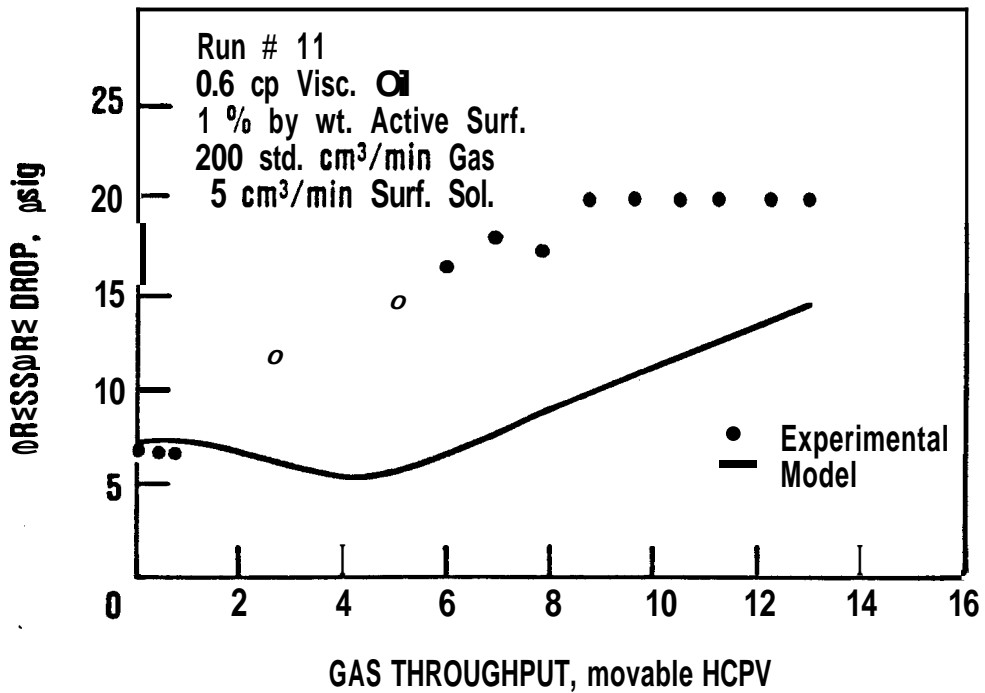


Figure 6.25 Comparison of Predicted and Experimental Pressure Drops for Favorable Mobility Ratio Between Oil and Surfactant Solution.

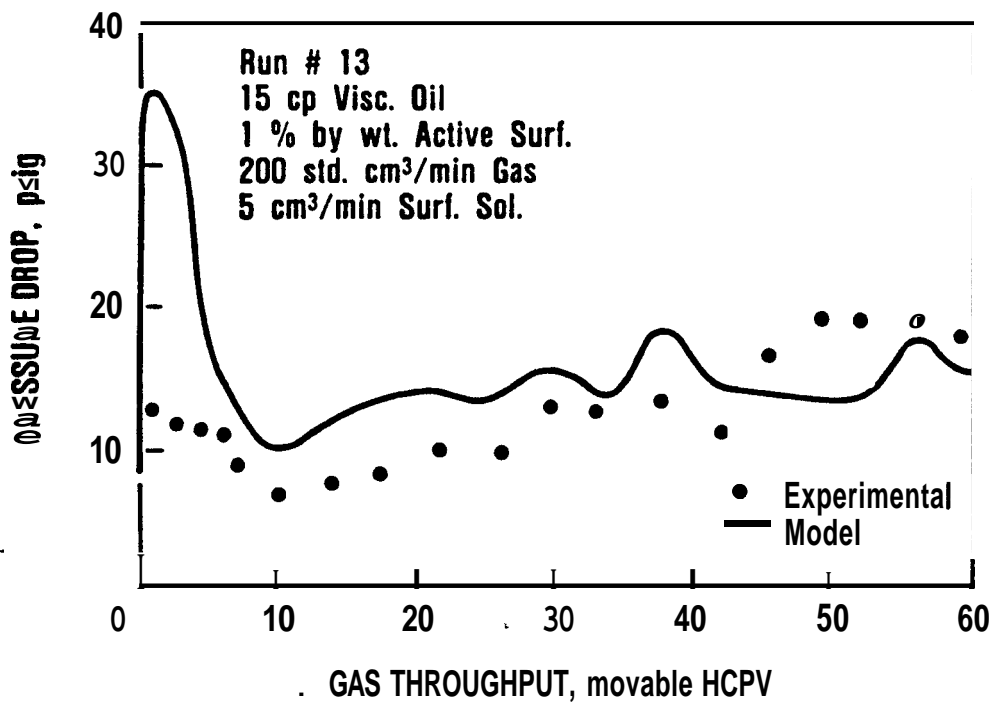


Figure 6.26 Comparison of Predicted and Experimental Pressure Drops for Viscous-Dominated Surfactant Solution Front.

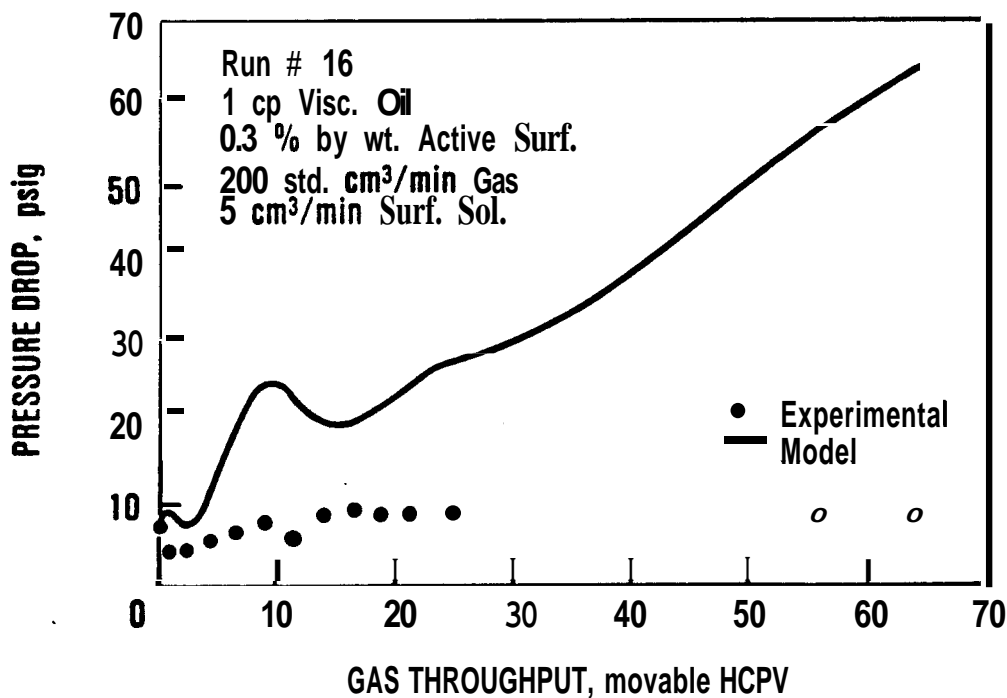


Figure 6.27 Comparison of Predicted and Experimental Pressure Drops for a Low Concentration Displacement in which Surfactant Concentration was at CMC.

The prediction of pressure drops by the model equation was worst for runs performed with concentrations lower than CMC. The surfactant concentrations of these runs were 0.3% (Run #16) and 0.01% (Run #17) by weight. The operating conditions for these runs were given in Tables 6.7 and 6.8, and the recovery behavior was shown in Figs. 6.12 and 6.13, respectively. The imbibition effects were quite pronounced and a Dietz type sharp front did not form. The time of foam generation as predicted by the mass-effect empirical relationship was grossly incorrect, since foam did not generate at all during the producing life of the flood. Also the model equation incorrectly predicted the surfactant solution breakthrough time and the velocity of the front. Due to these major differences between the experimentally observed behavior and the combination-drive model behavior, gross errors in the model equation were expected. The result can be seen in Figs. 6.27 and 6.28, where predicted pressure drops are compared with observed behavior. In both these figures, the experimental pressure drops remain almost constant during the entire run, whereas the model pressure drops show a continuous increase due to the assumption of foam generation and propagation.

The combination-drive model equations were also not able to predict the pressure behavior for Run #15 in which the displacement was shut-in for a long duration. This run was performed with the operating conditions listed in Table 6.15, and its recovery behavior was graphed in Fig. 6.20. During shut-in, the foam collapsed and the surfactant solution bank became fully segregated. When the run was resumed, the surfactant bank broke through immediately and also the foam regenerated and advanced rapidly. Both of these events were caused by shut-in and would not have been observed in a continuous injection. The model equations assumed a slower rate of foam advance and thus predicted lower pressure drops throughout the run (Fig. 6.29), whereas the experimental pressure drops became constant after foam bank breakthrough. However, as the flood progressed and approached the condition of foam breakthrough, the error was reduced.

Run #14 is another example of a run in which the front did not behave like the combination-drive model. This run was performed with low surfactant solution to gas volume ratio. The pressure behavior of this run is shown in Fig. 6.30. The operating conditions for this run were given in Table 6.13 and the recovery behavior was shown in Fig. 6.18.

The agreement between the experimental pressure drop and model prediction was good up to 5 pore volumes of gas injection, after which the predicted pressure drop steadily increased whereas the experimental pressure drop remained nearly constant. The mass-effect empirical relationship gave an erroneous prediction, as it did for concentrations below the CMC. The equation predicted foam generation at about 4 pore volumes of gas injection, whereas in the experimental run, foam generation was quite late.

Finally, the pressure history of a run that operated in a completely different injection mode is shown in Fig. 6.31. The operating conditions for this run were shown in Table 6.14 (Run #12) and the recovery performance was shown in Fig. 6.19. Cyclohexane (1 cp viscosity) was originally displaced in this run by simultaneous injection of nitrogen at 200 std cm<sup>3</sup>/min and surfactant solution (1% Suntech 4) at 5 std cm<sup>3</sup>/min until the injection pressure rose due to foam generation to 30 psig at about two pore volumes injection. After that the injection pressure was held constant, and as a result, the gas injection rate dropped due to the lowered gas mobility. To model this it was necessary to take into account that the gas/surfactant solution ratio varied. The model was able to predict the pressure reasonably well as long as the rates were kept constant. However, after that the model prediction showed a continuous increase in pressure drop, whereas the pressure drop was kept constant in the experiment. It is possible that the model might have been able to predict the pressure drop during the period the pressure was held constant, provided that the gradually decreasing rate are used in the model. However, this was not attempted in this study.

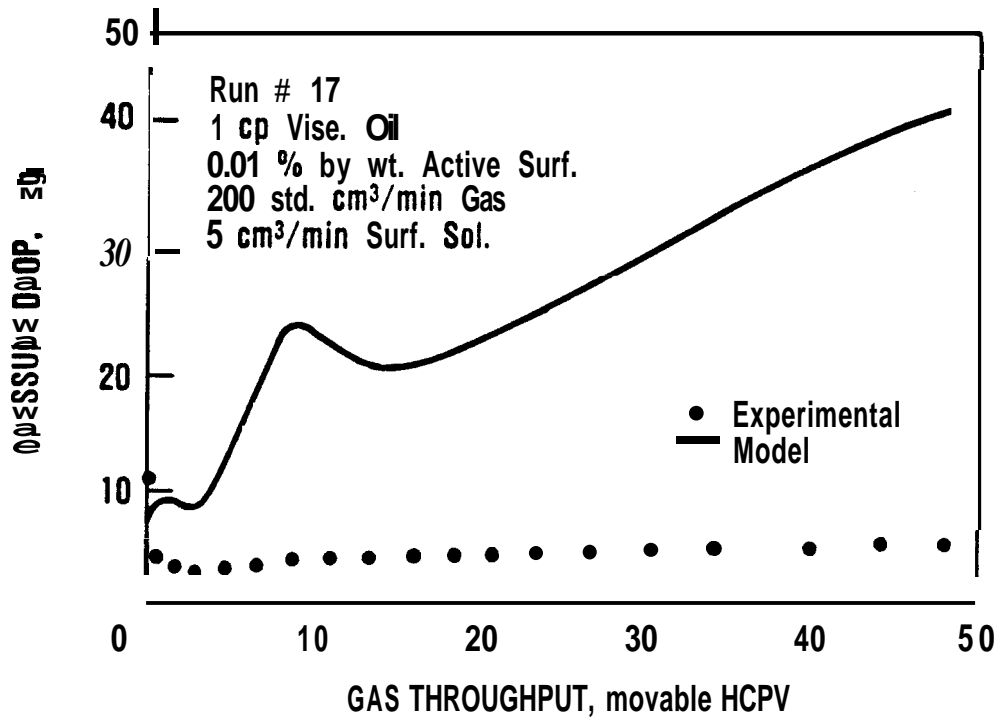


Figure 6.28 Comparison of Predicted and Experimental Pressure Drops for a Low Concentration Displacement in which Surfactant Concentration was Much Below CMC.

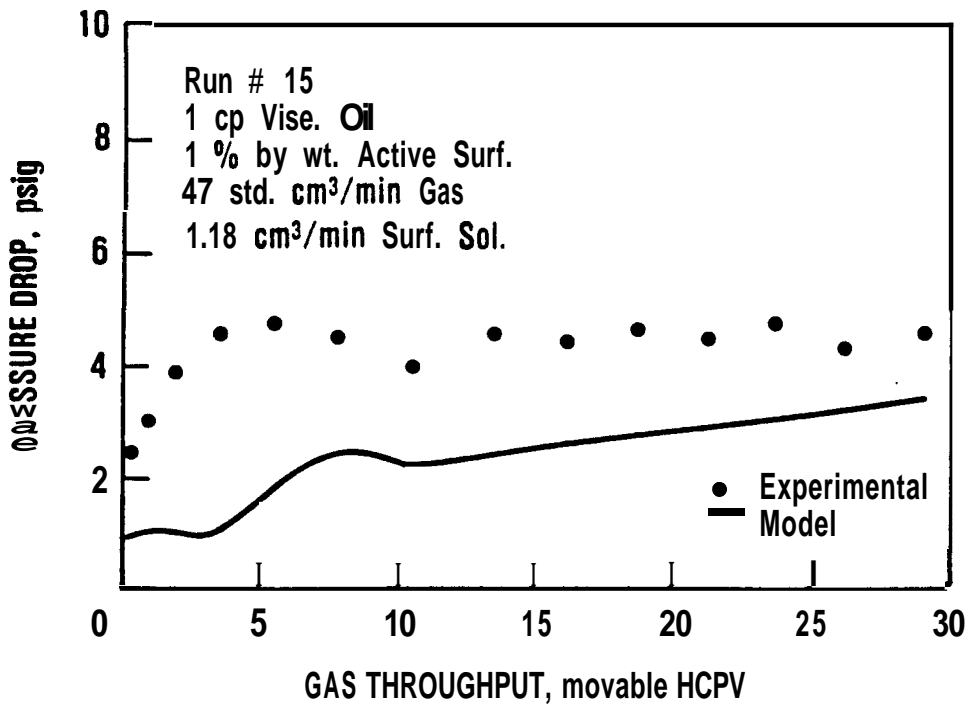


Figure 6.29 Comparison of Predicted and Experimental Pressure Drops for Gravity-Dominated Displacement with Long Shut-in.

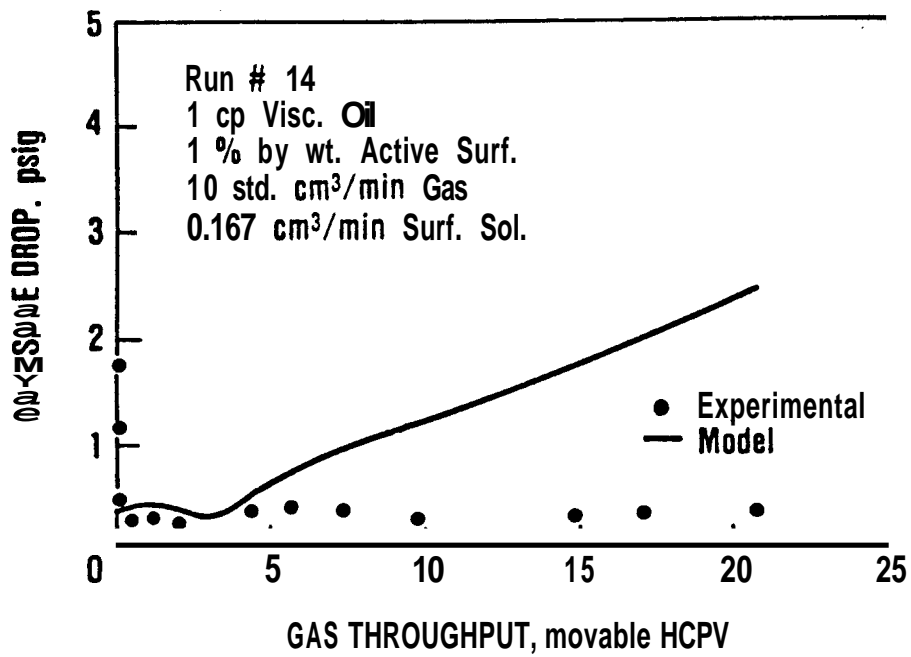


Figure 6.30 Comparison of Predicted and Experimental Pressure Drops for High Gas to Surfactant Solution Volumetric Ratio.

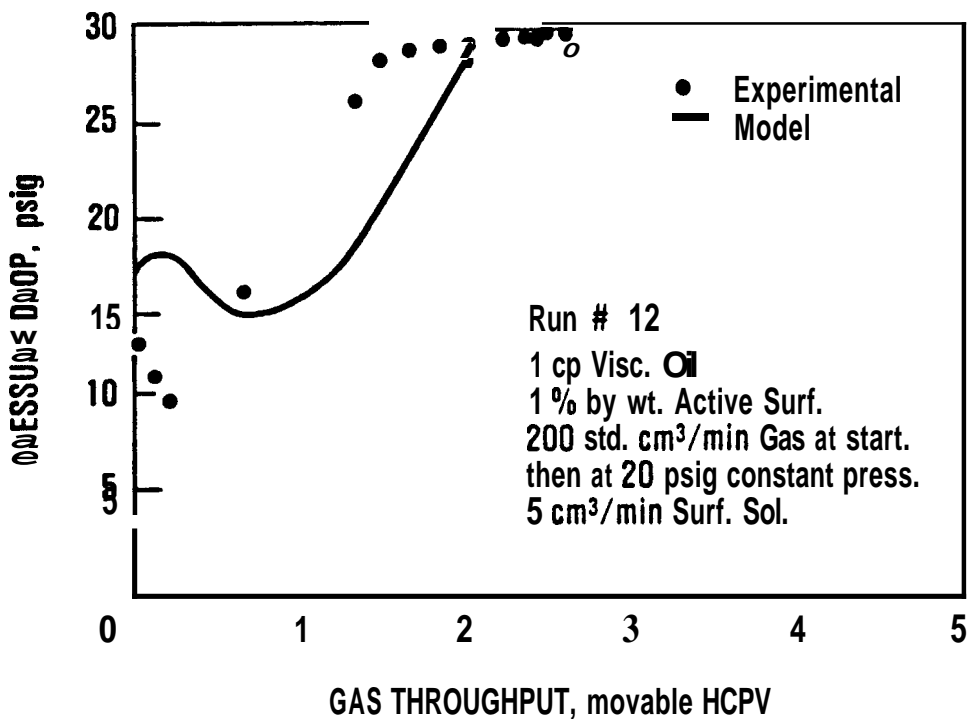


Figure 6.31 Comparison of Predicted and Experimental Pressure Drops for Variable Gas to Surfactant Solution Volumetric Ratio.

## 7. CONCLUSIONS AND RECOMMENDATIONS

A number of conclusions, both qualitative and quantitative have been arrived at as a result of this research. The qualitative conclusions are somewhat speculative in nature and thus lead to the recommendations (Section 7.2) for further research to better define the general nature of foam flow behavior when gravity force is also important.

### 7.1. CONCLUSIONS

In this two-dimensional sandpack, gravity was always an important force for all injection rates. The rates used were in the range that would scale to the rates of typical oil field reservoirs. In all cases it was found that the gas rose to the top of the sandpack and rapidly formed a thin Dietz-type tongue extending up to the producing end. The rate of gas injection had virtually no effect on the behavior of this gas finger.

The surfactant solution always segregated toward the lower part of the model. The nature of its flow depended on the rate, the surfactant concentration and the mobility ratio between the surfactant solution and the oil. When the mobility ratio was favorable, the surfactant moved as a nearly vertical front at the rates tested.

When the mobility ratio was unfavorable, and the surfactant solution rate was low, it moved along the bottom as a Dietz tongue. When the mobility ratio was unfavorable, and the surfactant solution injection rate was high, viscous fingers were formed at the surfactant solution-oil displacement front.

The surfactant concentration affected these liquid fronts, apparently due to the reduction in capillary forces. Low concentration surfactant solutions showed a more diffused interface, while higher concentration solutions showed sharper fronts.

Many different modes of injection and production were tried initially in an attempt to reduce gravity segregation and to cause foam flow to begin sooner in the reservoir. These included:

- (1) A single slug of surfactant solution followed by gas,
- (2) Alternate slugs of surfactant solution and gas with the surfactant solution injected into the top and the gas into the bottom,
- (3) Preformed foam injection, and
- (4) Simultaneous injection of surfactant solution with gas.

In all cases segregation occurred, but the best recovery was found when the surfactant and gas were injected simultaneously. Thus all subsequent experiments were run in this mode.

An attempt was made to model these subsequent runs using the scaling laws and dimensionless groups which relate capillary, viscous and gravity forces. The results were inconsistent. In particular it could be seen that, in the middle of many runs, the oil production rate began to rise rapidly. This always occurred at the time when foam generation was seen to begin in the sandpack, forming a third front in the gas-swept zone. It became clear that this delay in foam generation was a key to understanding the behavior, and was also the reason that the simple dimensionless variables did not adequately define the system.

This delay in the onset of in-situ foam generation has been termed the mass effect. It was speculated that the foamicidal behavior would be a function of the rates of gas and surfactant solution injection, the surfactant concentration, and the geometry of the system; and also the natures of the porous medium, the in-place fluids, and the surfactant solution. Although several oils were used in this experimental work, they were all refined oils of different viscosities which seemed to have similar behavior. Also the porous medium and geometry were constant in this work and the same surfactant was always used. Thus the variables of importance found for these experiments were the gas and surfactant injection rates and the surfactant concentration. All three variables affected the time of in-situ foam generation. An empirical equation was developed which successfully predicted the onset of foam generation in the sandpack.

Most of the data indicated two gravity tongues, gas and surfactant solution; and after the mass effect was overcome, a third foam front formed in the gas tongue. A simplified equation was derived to calculate the recovery from these tongues using a modified Buckley-Leverett formulation combined with a Dietz tongue in the gas, and a simple Dietz tongue in the surfactant solution. This is called the Combination-Drive Model herein. Once in-situ foam started to flow in the gas tongue, mobility in the model was modified to take the reduced gas mobility into account. This model was successful in predicting the recovery history of most of the runs. The exceptions occurred only in those runs where the displacement behavior differed markedly from the model. To make these calculations, the terms that were inserted into the equation were the oil saturation change in the gas and surfactant solution tongues, and the mobilities of surfactant solution, gas and foam. The same values could be used in all cases.

This same formulation concept was used to calculate the pressure drop history of the mass, and the success was far less pronounced. For several runs, the pressure drop history was well matched, but the behavior differed widely for many others. The poorer matches are probably due to the assumptions used in the model that the gas foam mobility was constant once foam was formed. Actually, as the foam moved through the model, the gas foam mobility decreased with time. No method was found to predict the rate of movement of the foam front; however, it is expected to be a complex function of the same variables which affect the onset of in-situ foam generation.

## 72. RECOMMENDATIONS

Since only one surfactant, and one porous medium with one geometry were used in the experiments, it would be useful to pursue other experiments where these factors were varied. With such systems, both the mass effect equation and the combinationdrive displacement model could be tested, and modified if necessary.

A series of runs should be made to better define the foam front movement in the gas finger. From these data an equation of foam movement should be developed. Pressure drop measurements near the top of the model could help define these mobilities. The same variables mentioned in the paragraph above could be included in the foam front equation. If this were successful, the pressure drop history of foam floods could be better matched.

**a NOMENCLATURE**

- $a = m - 1$   
 $\alpha = \bar{m} - 1$   
 $\beta = 1 + R m / \bar{m}$   
 $C = \alpha - \bar{\alpha} + \bar{\alpha} \beta$   
 $G_{iD}$  = Cumulative **gas** throughput, movable pore volumes  
 $(G_{iD})_{gbt}$  = Cumulative **gas** throughput at gas breakthrough, movable pore volumes  
 $h$  = The vertical height of the porous medium, **cm**  
 $T$  = Thickness of the surfactant tongue at the injection well, **cm**  

$$= \frac{h}{1 + R m / \bar{m}}$$
  
 $m = \frac{k_s / \mu_s}{k_o / \mu_o}$   
 $\bar{m} = \frac{k_g / \mu_g}{k_o / \mu_o}$   
 $N_{pD}$  = Cumulative oil recovery, movable pore volumes  
 $(N_{pD})_{gbt}$  = Cumulative oil recovery at **gas** breakthrough, movable pore volumes  
 $(N_{pD})_{sbt}$  = Cumulative **oil** recovery at surfactant breakthrough, movable pore volumes  
 $P_o$  = Absolute **pressure at the** injection well, atm.  
 $P_x$  = Absolute **pressure** at the surfactant front,  $x$ , **atm.**  
 $P_1$  = Absolute pressure at **the** producing well, am.  
 $q_g$  = Gas injection rate per unit **cross** sectional width,  $\text{cm}^3/\text{sec-cm}$   
 $q_s$  = Surfactant injection rate per unit **cross** sectional width,  $\text{cm}^3/\text{sec-cm}$   
 $(Q_{pD})_{max}$  = Maximum cumulative throughput up to **which** this model is valid, movable **pore** volumes  
 $Q_D$  = Cumulative **total** throughput, movable **pore** volumes =  $( 1 + 1/R ) G_{iD}$   
 $R$  = Ratio of **gas** to surfactant injection rates =  $q_{ig}/q_{is}$   
 $x$  = Location of **the** front **before** slug breakthrough.

## 9. REFERENCES

1. Abernathy, C.K. and Eerligh, J.J.P.: "**An** Investigation of Several Properties of Foam in **Flow** through **Short Connected** Porous Media," **MS** report, Petroleum Eng. Dept., **Stanford U., Stanford, CA (1966)**.
2. Ahmed, G.: "**An** Experimental Study of Recovery **from a 2-D Layered Sand** model," **MS report**, Petroleum Eng. Dept., Stanford U., Stanford, CA (1984).
3. Ahmed, G., Castanier, L.M., and Brigham, W.E.: "An Experimental Study of Waterflooding in Layered Reservoirs," paper SPE **13599** presented at the **SPE Calif. Regional Meeting, Bakersfield, CA, Mar. 27-29 (1985)**.
4. Aizad, T., and Okandan, E.: "Flow Equation for Foam **Flowing** Through **Porous** Media and Its Application as a Secondary Recovery Fluid," paper SPE **6599** presented at the Int. SPE Oilfield & Geothermal Chem. Symp., San Diego, CA June **27-29 (1977)**.
5. **Al-Attar, H.H.:** "The Evaluation of Oil Foam for Use as a Displacing Medium for Oil Recovery in Porous Medium," **Ph.D. Thesis**, Dept. of Petroleum Eng., Colorado School of **Mines**, Golden (1976).
6. Albrecht, R.A., and Marsden, S.S.: "Foams as **Blocking Agents** in Porous Media," *Soc. Per. Eng. J.* p. 51-55, March (1970).
7. Ali, J.: "Foam as an Enhanced **Oil** Recovery Agent," **Ph.D. Thesis**, Dept. of Chemical and **Process** Engineering, Heriot-Watt U., **Edinburgh, Scotland (1983)**.
8. Ali, J., Burley, R.W., and Nutt, C.W.: "Foam Enhanced Oil Recovery From Sand Packs," *Chem. Eng. Res. Des.*, Vol. **63**, p. 101-111, March (1985).
9. Amiyan, A.V.: "A Study of Two-Phase Foam **Rheology**," *Nepte Promyslovoe Delo* No. **8**, p. 14-17 (1971).
10. Augsburger, L.A.: "Aerosol Foams: The Relationship of Bubble Size to Foam Rheology and a Preliminary Study of the **Rheology** of Pressurized Emulsions," **Ph.D. Thesis**, Dept. of **Chemical** Eng., U. of Maryland (1967).
11. Badalov, A.A., and Khasaev, A.M.: "Structuro-Mechanical Properties of Foam," *IV. Vyssh. Ucheb. Zavedenii, Neft I. Gaz.*, Vol. **9**, No. **5**, p. 32-38 (1966).
12. Bernard, G.G.: "Effect of Foam on Recovery of Oil by Gas-Drive," *Producers Monthly* Vo. **27**, No. **1**, p. 18-21, **Jan.** (1963).
13. Bernard, G.G.: "**Foam Drive Oil Recovery Process**," **U.S. Patent No. 3,529,668 (1974)**.
14. **Bernard, G.G.:** "**Use** of Gas-Driven **Foam Bank** in a **Secondary** Recovery Process," *Can. Pat. Office Rec.*, Vol. **79**, No. **50**, P. 8773, 121 (1969).

15. Bernard, **G.G.**, and Holm, L.W.: "Effect of Foam on Permeability of Porous Media to **Gas**," *Soc. Pet. Eng. J.* p. **267-274**, Sept. (1964).
16. Bernard, **G.G.**, and Holm, L.W.: "Model Study of Foam as a Sealant for **Leaks** in **Gas** Storage Reservoirs," *Soc. Pet. Eng. J.* p. **9-15**, **Mar.** (1970).
17. Bernard, G.G., Holm, L.W., and Jacobs, W.L.: "Effect of Foam on Trapped **Gas** Saturation and on Permeability of Porous Media to Water," paper SPE **1204** presented at the SPE 40th Annual Meeting, Denver, CO, **Oct. 3** (1965). Trans., **AIME**, Vol. **234**, p. **295-300** (1966).
18. Beyer, A.H., Millhone, **R.S.**, and Foote, R.W.: "Flow Behavior of Foam as a Well Circulating Fluid," paper SPE **3986** presented at the SPE Annual Meeting, San Antonio, TX, Oct. **2-5** (1972).
19. Bikerman, J.J.: "**Foams**," *Appl. Phys. & Engr.*, No. **10**, Springer-Verlag, New York (1973).
20. Bird, R.B., Stewart, W.E., and Lightfoot, E.N.: *Transport Phenomena*, p. **48-50, 460-462 and 467-469**, John Wiley & Sons, New York (1960).
21. Blauer, R.E., and Kohlhaas, C.A.: "Formation Fracturing with Foam," paper SPE 5003 presented at the SPE **49th** Annual Meeting, Houston, TX, Oct. **6-9** (1974).
22. Blauer, R.E., Mitchell, B.J., and Kohlhaas, C.A.: "Determination of Laminar, Turbulent, and Transitional Foam **Losses** in Pipes," paper SPE **4885** presented at the SPE **44th** Annual California Regional Meeting, San Francisco, CA, April **4-5** (1974).
23. Bond, D.C.: "**Secondary** Recovery Method with Surfactant in Fracturing Fluid," U.S. Patent No. **3,335,794**, Union Oil Co., Calif. (1965).
24. Bond, D.C., and Bernard, G.G.: "Rheology of Foams in Porous Media," presented at **SPE-AIChE** Joint Symp., Dallas, TX, Feb. (1966).
25. Bond, D.C., and Holbrook, O.C.: "**Gas** Drive Oil Recovery Process," U.S. Patent No. **2,866,507** (1958).
26. Brigham, W.E., Marcou, J.A., Sanyal, **S.K.**, Malito, O.P., and Castanier, L.M.: "A Field Experiment of Improved Steam Drive with *In Situ* Foaming," paper SPE **12784** presented at the **55th** SPE Calif. Regional Meeting, Bakersfield, CA, March **27-29** (1985).
27. Buckley, S.E., and Leverett, M.C.: "Mechanism of Fluid Displacement in Sands," Trans., **AIME**, Vol. **146**, p. **107-116** (1942).
28. Chang, R.C., Schoen, H.M., and Groves, C.S.: "Bubble **Size** and Bubble Size Determination," *Ind. Eng. Chem.*, Vol. **48**, p. **2035** (1956).
29. Chiang, J.C.: "Foam as an Agent to Reduce Gravity **Override**," Engineer's thesis, Dept of Petroleum Engineering, Stanford U., Stanford, CA (1979).

30. Chiang, J.C., Mahmood, S., Sufi, A., and Castanier, L.: "Foam as a Mobility Control Agent for **Steam Injection**," paper SPE 8912 presented at the 50th SPE Annual California Regional Meeting, Pasadena, CA, Apr. 9-11 (1980).
31. Chuoke, R.L., Meurs, P.Y., and Van der Poel, C.: "The Instability of Slow, Immiscible, Viscous Liquid-Liquid Displacements in Permeable Media," Trans., AIME, Vol. 216, p. 188-194 (1959).
32. Clark, N.O.: *Special Report No. 6*, D.S.I.R., Home Ministry Stationary office, London, England (1947).
33. Craig, F.F., Jr., Sanderlin, J.L., Moore, D.W., and Geffen, T.M.: "A Laboratory Study of Gravity Segregation in Frontal Drives," Trans., AIME, Vol. 210, p. 275-282 (1957).
34. Craig, F.F., Jr.: "The Reservoir Engineering Aspects of Waterflooding," SPE Monograph, vol. 3, Henry L. Doherty Series, (1971).
35. Croissant, R.: *Developpement des Instabilites en Milieu poreux, Influence de la Pression Capillaire*, Revue IFP Vol. 25, p. 227 (1970).
36. Daalen, F.V., and Domselaar, H.R.: "Scaled Fluid-Flow Models with Geometry Differing from that of Prototype," paper SPE 3359, Trans., AIME, Vol. 253 (1972).
37. Dake, L.P.: *Fundamentals of Reservoir Engineering*, Developments in Petroleum Science, vol. 8, Elsevier Scientific Publishing Company, New York (1978).
38. Darcy, H.: *Les fontaines publiques de la ville de Dijon*, Victor Dalmont (1856).
39. David, A., and Marsden, S.S., Jr.: "The Rheology of Foam," paper SPE 2544 presented at the SPE 44th Annual Meeting, Denver, CO, Sept 23-Oct. 1 (1969).
40. David, A.: "The Rheology of Foam," Ph.D. Thesis, Stanford U., Stanford, CA (1969).
41. Dietz, D.N.: "A Theoretical Approach to the Problem of Encroaching and Bypassing Edge Water," Proc., Koninkl. Ned. Akad. Wetenschap B56, 38 (1953).
42. Dilgren, R.E., Deemer, A.R., and Owens, K.B.: "The Laboratory Development and Field Testing of Steam/Non-Condensable Gas Foams for Mobility Control in Heavy Oil Recovery," paper SPE 10774 presented at the 52nd WE Calif. Regional Meeting, San Francisco, CA, March 24-26 (1982).
43. Doscher, T.M., and Hammershamb, E.C.: "Field Demonstration of Steam Drive with Ancillary Materials," paper SPE/DOE 9777 presented at 2nd Joint SPE/DOE Symp. on EOR, Tulsa, OK, April 4-8 (1981).
44. Drew, D.A., and Segel, L.A.: "An Averaging Approach to the Theory of Two-Phase Flows," Proc., Int. IChE, AIChE & ASME Two-Phase Syst. Symp., Technion City, Haifa, Aug. 29-Sept. 2 (1971).

45. Engelberts, W.L., and Klinkenberg, L.J.: "Laboratory Experiments on the Displacement of Oil by Water from Packs of Granular Materials," Proc., Third World Pet. Cong., Vol. II, p. 544 (1951).
46. Eson, R.L., Fitch, J.P., and Shannon, A.M.: "North Kern Front Field Steam Drive with Ancillary Materials," paper SPE/DOE 9778 presented at the 2nd Joint SPE/DOE Symp. on EOR, Tulsa, OK, April 5 (1985).
47. Evgenev, A.E.: "Questions Concerning Rheological Properties of Foam in a Porous Medium," *Izv. Vyssh. Ucheb. Zavedenii, Neft Got. No. 7*, p. 81-84 (1973).
48. Evgenev, A.E., and Turnier, V.N.: "Rheological Properties of Foam in a Porous Medium," *Int. Chun. Eng.*, Vol. 9, No. 2, p. 261-262, (1973).
49. Fried, A.N.: "The Foam-hive Process for Increasing the Recovery of Oil," report of investigation, No. 5866:65 pp; USBM (1961).
50. Gangoli, N., and Thudos, G.: "Enhanced Oil Recovery Techniques — State-of-the-Art Review," *J. Can. Per. Tech.*, Vol. 16:4, p. 13-20, Oct.-Dec. (1977).
51. Grove, C.S. Jr., Wise, G.E., March, W.C., and Gray, J.B.: "Viscosity of Fire-Fighting Foam," *Ind. Eng. Chem.* Vol. 43, No. 5, p. 1120 (1951).
52. Gurbanov, R.S., Guliev, B.B., Mekhtiev, K.G., and Kerimov, R.G.: "Study of Two-Phase Foam Flow," *Nefteprom. Delo* Vol. 9, p. 14-16, USSR (1970).
53. Handy, L.L.: "Non-Darcy Flow in Porous Media," 16th Annual Report. Pet. Rec. Fundam., 41 (1971).
54. Hatschek, E.: "Die Viskositat Der Dispersoide," *Kolloid Z.* Vol. 8, p. 34, (1911).
55. Heller, J.P.: "Enhanced Oil Recovery by CO<sub>2</sub> Foam Flooding," Second annual report, Report No. DOE/MC/03259-10, Dept. of Chemical Engineering, New Mexico State U., Las Cruces, NM., Feb. (1980).
56. Hoffer, M.S., and Rubin, E.: "Flow Regimes of Stable Foams," *Ind. Eng. Chem.* Vol. 8, No. 3, p. 483-490, Aug. (1969).
57. Holbrook, S.,T., Patton, J.T., and Hsu, W.: "Rheology of Mobility Control Foam," paper SPE/DOE 9809 presented at the 2nd Joint Symp. on Enhanced Oil Recovery, Tulsa, OK, Apr. 5 (1981).
58. Holcomb, D.L., Callaway, E., and Curry, L.: "The Chemistry, Physical Nature and Rheology of an Aqueous Stimulation Foam," paper SPE 9530 presented at the SPE Eastern Regional Meeting, Morgantown, WV, Nov. 5-7 (1980).
59. Holditch, S.A., and Plummer, R.A.: "The Design of Stable Foam Fracturing Treatments," Proc., 23rd Annual Southwestern Petroleum Short Course, Lubbock, TX (1976).

60. Holm, L.W.: "Foam Injection Test in ~~the~~ Siggins Field, Illinois, *J. Per. Tech.* p. 1499, Dec. (1970).
61. Holm, L.W.: "The Mechanism of **Gas** and Liquid Flow **Through** Porous Media in the Presence of Foam," paper SPE 1846 presented at the SPE 42nd Annual Meeting, Houston, TX, Oct. 1 (1967). *Soc. Per. Eng. J.* p. 359-369, Dec. (1968).
62. Hooker, P.R., and Marsden, S.S. Jr.: "The Stratified Flow of Foam and Liquid in a Horizontal Tube — A Preliminary Study of a New Pipeline Concept," MS report, Dept. of Petroleum Eng., Stanford U., Stanford, CA (1972).
63. Hubbert, M.K.: "Entrapment of Petroleum under Hydrodynamic Conditions," *Bull. Am. Assoc. Petrol. Geologists* p. 1954, Aug. (1953).
64. Ikoku, C.U.: "Transient Flow of Non-Newtonian Power-Law Fluids in Porous Media," Ph.D. Thesis, Dept. of Petroleum Eng., Stanford U., Stanford, CA (1978).
65. Kanda, M., and Schechter, R.S.: "On the Mechanism of Foam Formation in Porous Media," paper SPE 6200 presented at the SPE 51st Annual Technical Conference and Exhibition, New Orleans, LA, Oct. 3-6 (1976).
66. Khan, S.A.: "The Flow of **Foam** Through Porous Media," Engineer's report, Dept. of Petroleum Engineering, Stanford U., Stanford, CA (1965).
67. Kolb, G.E.: "Several Parameters Affecting the Foam Drive **Process** for the Removal of Water from Consolidated Porous Media," MS thesis, Dept. of Petroleum and Natural **Gas** Eng., Pennsylvania State U., University Park, PA (1964).
68. Kopalinsky, E.M., and Bryant, R.A.: "Friction Coefficients for Bubbly Two-Phase **Flow** in Horizontal Pipes," *AIChE J.* Vol. 22, p. 82 (1976).
69. Kozeny, J.: "Über Kapillare Leitung des Wassers in Boden (Aufstieg, Versickerung und Anwendung auf die Bewässerung), *S.d. Wiener A M . d. Wissenschaften*, Abt. II a, 136, p. 271-306, (1927).
70. Krug, J.A.: "Foam **Pressure Loss** in Vertical Tubing," *Oil and Gas J.* Vol. 73, No. 40, p. 74-76, 78 (1975).
71. Krug, J.A. and Mitchell, B.J.: "Charts Help Find Volume, **Pressure** Needed for Foam Drilling," *Oil and Gas J.* p. 61-64, Feb 7 (1972).
72. Lemlich, R.: "Prediction of **Changes** in Bubble Size Distribution due to Interbubble **Gas** Diffusion in Foam," *Ind. Eng. Chem., Fundam.*, Vol. 17:2, p. 89-93, U. of Cincinnati, Ohio (1965).
73. Lord, D.L.: "Mathematical Analysis of Dynamic and Static Foam Behavior," *J. Pet. Tech.* Vol. 33, No. 1, Jan. (1981).

74. Mahmood, S.M.: "Recovery Optimization of Gas/Surfactant Displacement under Foaming Conditions," MS report, Dept. of Petroleum Engineering, Stanford U., **Stanford, CA (1983)**.
75. Mahmood, S.M., Castanier, **L.M.** and Brigham, W.E.: "An Approximate Model for 2-D Displacement of Oil by Foam," Proc., IEA Collaborative Project on Enhanced Oil Recovery Meeting, Tokyo, Japan, **Oct. 7-9 (1985)**.
76. Mahmood, S.M., Owete, **O.S.**, Al-Khafaji, A., and Wang, F.: "Improvement of Steam Injection through the Use of Foaming Additives," Proc., Heavy Oil and West Coast Contractors EOR Meeting, July **28-30 (1981)**.
77. Mahmood, S.M., **Tarig**, S.M. and Brigham, W.E.: "A Model for Prediction of Recovery and Pressure History for 2-D Displacement of Oil through Porous Media by Gas/Surfactant," paper SPE **15076** presented at the **56th California Regional Meeting**, Oakland, CA, Apr. **2 4 (1986)**.
78. Mannheimer, R.J.: "Anomalous Rheological Characteristics of a High-Internal-Phase-Ratio Emulsion," *J. of Colloid and Interface Science* Vol. **40**, No. **3**, p. **370-382**, Sept. **(1972)**.
79. Marsden, **S.S.**: "Foams in Porous Media," Stanford U. Pet. Res. **Trs.** (SUPRI) Topical Report **TR-49**, U.S. DOE Publication No. **DE8600290**, May **(1986)**.
80. Marsden, **S.S.**, and Khan, **S.A.**: "The Flow of Foam Through Short Porous Media and Apparent Viscosity Measurements," *Soc. Pet. Eng. J.* p. **17-25**, Mar. **(1966)**.
81. Marsden, **S.S.** Jr., Eerligh, J.J.P., Albrecht, R.A., and David, A: "Use of Foam in Petroleum Operations," Proc.. **7th World Pet. Cong.**, Vol. **3 (1967)**.
82. Mast, **R.F.**: "Microscopic Behavior of Foam in Porous Media," paper SPE **3997** presented at the **SPE 47th Annual Meeting**, San Antonio, **TX, Oct. 8 (1972)**.
83. Mendez, A.P.: "**An** investigation of the effectiveness of foamed-crude displacement in porous media," MS report, Dept. of Petroleum Engineering, Colorado School of Mines, Golden, CO **(1975)**.
84. Meurs, P.V.: "The Use of Transparent Three-Dimensional Models for Studying the Mechanism of Flow Processes in Oil Reservoirs," Trans., **AIME**, p. **295**, Vol. **210 (1957)**.
85. Meurs, P.V., and Poel, C.V.: "A Theoretical Description of Water-Drive Processes Involving Viscous Fingering," Trans., **AIME**, p. **103**, Vol. **213 (1958)**.
86. Minssieux, L.: "Oil Displacement by Foams in Relation to Their Physical Properties in Porous Media," *J. Pet. Tech.* p. **100-108**, Jan. **(1974)**.
87. Mitchell, B.J.: "Viscosity of Foam," Ph.D. Thesis, Dept. of Petroleum Eng., U. of Oklahoma, Norman, OK **(1970)**.

88. Nahid, **B.H.**: "Non-Darcy Flow of Gas Through Porous Media in the Presence of Surface Active Agents," Ph.D. Thesis, U. of Southern California, Los Angeles, CA (1971).
89. Owete, **O.S.**: "Flow of Foam Through Porous Media," Ph.D. Thesis, Petroleum Eng. Dept., Stanford U., Stanford, CA (1982).
90. Owete, O.S., Mahmood, S., Riley, M., Castanier, L.M., and Brigham, W.E.: "Foam for Gas Drive Improvement," Proc., No. DOE/CONF/820712, Annual Heavy Oil/E.O.R. Contractors Meeting, San Francisco, CA, July 27-29 (1982).
91. Patton, J.T., Holbrook, S., Roubicek, R., and Phelan, P.F.: "Enhanced Oil Recovery by CO<sub>2</sub> Flooding," DOE/MC/16551-6, First Annual Report (1983).
92. Penny, W.G., and Blackman, M.: *Ministry of Home Security (F Division) Report*, England, REN 282 (1943).
93. Perkins, T.K., and Johnston, O.C.: "A Study of Immiscible Fingering in Linear Models," *Soc. Pet. Eng. J.* p. 39, Mar. (1969).
94. Peters, E.J., and Flock, D.L.: "The Onset of Instability During Two-Phase Immiscible Displacement in Porous Media," *Soc. Pet. Eng. J.* p. 249-257, Apr. (1981).
95. Plateau, J.: *Mem. Acad. Roy. Sci., Belgique* Vol. 37, p. 49, (1869).
96. Ploeg, J.F. and Duerksen, J.H.: "Two Successful Steam/Foam Field Tests, Sections 15A and 26C, Midway-Sunset Field," paper SPE 13609 presented at the Calif. Regional Meeting, Bakersfield, CA, Mar. 27-29 (1985).
97. Quintero, Douglas A.A.: "The Flow of Macroemulsions Through Porous Media," Ph.D. Thesis, Dept. of Chemical Engineering, Stanford U., Stanford, CA (1975).
98. Rapoport, L.A.: "Scaling Laws for Use in Design and Operation of Water-Oil Flow Models," paper SPE T.P. 4121 presented at the SPE Petroleum Branch Fall Meeting, San Antonio, TX, Oct. 17-20 (1954). *Trans.*, AIME, 204, 143-150.
99. Raza, S.H.: "Foam in Porous Media: Characteristics and Potential Applications," paper SPE 2421, Proc., Int. SPE Mid-Continent Sect. Improved Oil Rec. Symp., Tulsa, OK, Apr. 13-15 (1969). Also published in *Soc. Pet. Eng. J.*, p. 328-336 (1970).
100. Raza, S.H.: "Plugging Formations with Foam," U.S. Patent No. 3,491,832 (1968).
101. Raza, S.H.: "The Streaming Potential of Foam," Ph.D. Thesis, Petroleum Eng. Dept., Stanford U., Stanford, CA (1965).
102. Raza, S.H., and Marsden, S.S.: "The Flow of Foam: 1. Rheology and Streaming Potential," paper presented at SPE Annual Meeting, Denver, CO, Oct. 3-6 (1965).
103. Raza, S.H., and Marsden, S.S. Jr.: "The Streaming Potential and the Rheology of Foam," *Soc. Pet. Eng. J.* Vol. 7, No. 4, p. 359-368, Dec. (1967).

104. Richman, **M.D.**: "A Study of Pressurized Foams with Emphasis on Rheological Evaluation," Ph.D. Thesis, Dept. of Chemical Eng., U. of Maryland (1966).
105. Rojas, **G.**, and Farouq Ali, **S.M.**: "Dynamics of Subcritical CO<sub>2</sub>/Brine Floods for Heavy Oil Recovery," paper SPE 13598 presented at the SPE California Regional Meeting, Bakersfield, CA, March 27-29 (1985).
106. Root, P.J.: "Foam Recovery Process," U.S. Patent No. 3,893,511 (1971).
107. Rosen, M.J.: *Surfactants and Interfacial Phenomena*, John Wiley & Sons, p. 200-223 (1978).
108. Ross, **S.**: "Foams and Emulsion Stability," *J. Phys. Chem.* p. 266, Vol. 47 (1953).
109. Ross, **S.**: "Mechanisms of Foam Stabilization and Antifoaming Action," *Chem. Eng. Progr. No. 9*, p. 41-47, Vol. 63 (1967);
110. Ross, **S.**: "Bubbles and Foam," *Ind. Eng. Chem.*, 61.48 (1969).
111. Roszelle, W.O.: "Use of Surfactant Foam for Recovery of Petroleum," U.S. Patent No. 3,599,715 (1971).
112. Sharma, **S.K.**: "The Study of the Microscopic Behavior of the Foam Drive Method," MS report, Petroleum Eng. Dept., Stanford U., Stanford, CA (1965).
113. Sharma, **M.K.**, Shah, D.O., and Brigham, W.E.: "The Chain Length Compatibility and Surface Properties of Foaming Solutions in Relation to Fluid Displacement Efficiency in Porous Media," paper SPE 10612 presented at Int. Symp. Oilfield and Geothermal Chem., Dallas, TX, Jan (1982).
114. Sibree, T.O.: "The Viscosity of Froth Emulsions," *Trans., Farad Soc.*, 30, 325, (1943).
115. Smith, C.L., Anderson, J.L., and Ro, P.G.: "New Diverting Technique for Acidizing and Fracturing," paper SPE 2741 presented at the 40th Calif. Regional Meeting, San Francisco, CA, Nov. 6-9 (1969).
116. Smith, David "Flow of Foam through 2-D Layered Model," MS report, Dept. of Petroleum Engineering, Stanford U., Stanford, CA (1983).
117. Spiegel, M.R.: *Handbook of Formulas and Tables*, McGraw-Hill Book Company, New York (1968). *Schaum's* Outline Series in Mathematics.
118. Starkey, P.E.: "The Flow Properties of Foam," Ph.D. Thesis, U. of London, (1975).
119. Stenuf, T.J.: "A Study of the Variables Affecting the Fluid Dynamics of Foam," Ph.D. Thesis, Dept. of Chemical Engineering, Syracuse U., Syracuse, NY (1953).
120. Wang, G.C.: "A Laboratory Study of CO<sub>2</sub> Foam Properties and Displacement Mechanism," paper SPWDOE 12645 presented at SPWDOE Symp. on EOR, Tulsa, OK, April (1984).

121. Wang, P.F., Al-Khafaji, A., Castanier, L.M., and Brigham, W.E.: "Steam surfactant systems at reservoir conditions," Proc., No. DOE/CONF/820712, Annual Heavy Oil/E.O.R. Contractors Meeting, San Francisco, CA, July 27-29, p. 219-226, (1982).
122. Welge, H.J.: "A Simplified Method for Computing Oil Recovery by Gas or Water Drive," *Trans., AIME* Vol. 195, 91-98 (1952).
123. Wenzel, H.G. Jr., Stelson, T.E., and Brungraber, R.J.: "Flow of High Expansion Foam in Pipes," Proc., J. Eng. Mech. Div., Amer. Soc. Civil Eng., Vol. 93, No. EM6, page 153-165, Dec. (1967).
124. Wise, G.E. Jr.: "Fluid Dynamics and Other Studies of Mechanical Fire Fighting Foams," PhD dissertation, Dept. of Chemical Engineering, Syracuse U., Syracuse, NY (1951).
125. Zirritz, J.L., and Rancel, C.: "Report on Literature Survey of Foam for Use in Steam Injection," progress report, United States DOE-Venezuelan Ministry of Mines Agreement, Annex 4 (1983).

APPENDIX A  
ANALYTICAL SOLUTION OF THE RECOVERY EQUATION

This appendix outlines the steps taken in solving Eq. (5.58) which is reproduced below:

$$\begin{aligned} & \left[ \frac{1}{my} + \frac{1}{h - \beta y} + \frac{\beta - 1}{h - \beta y} \right] \phi \Delta S \frac{\partial x}{\partial t} \\ & = \left\{ \frac{\beta}{(h - \beta y)^2} + \left[ \frac{1}{my^2} - \frac{\beta}{(h - \beta y)^2} \right] \frac{my}{(h - \beta y) + my + \bar{m}\beta y - \bar{m}y} \right. \\ & \quad \left. - \frac{\beta \bar{m}(\beta - 1)y}{(h - \beta y)^2 [(h - \beta y) + my + \bar{m}\beta y - \bar{m}y]} \right\} q_t \end{aligned} \quad (A.1)$$

Simplifying the L.H.S. of (A.1) and rearranging yields:

$$\begin{aligned} \frac{\partial x}{\partial t} & = \left\{ \frac{m\beta y}{(h - \beta y)} + \left[ \frac{h - \beta y}{y} - \frac{\beta my}{h - \beta y} \right] \frac{my}{(h - \beta y) + my + \bar{m}\beta y - \bar{m}y} \right. \\ & \quad \left. - \frac{\beta \bar{m}(\beta - 1)my^2}{(h - \beta y)[(h - \beta y) + my + \bar{m}\beta y - \bar{m}y]} \right\} \frac{1}{[(h - \beta y) + m\beta y]} \frac{q_t}{\phi \Delta S} \end{aligned} \quad (A.2)$$

This equation can be algebraically reduced to:

$$\frac{\partial x}{\partial t} = \left\{ \frac{mh}{[(h - \beta y) + m\beta y][(h - \beta y) + my + \bar{m}\beta y - \bar{m}y]} \right\} \frac{q_t}{\phi \Delta S} \quad (A.3)$$

Equation (A.3) can be integrated within the appropriate limits as follows:

$$\int_0^L \partial x = \frac{mh}{[(h - \beta y) + m\beta y][(h - \beta y) + my + \bar{m}\beta y - \bar{m}y]} \cdot \frac{1}{\phi \Delta S} \int_0^t q_t \partial t \quad (A.4)$$

The solution of Eq. (A.4) can be written as:

$$L = \frac{mh}{[(h - \beta y) + m\beta y][(h - \beta y) + my + \bar{m}\beta y - \bar{m}y]} \frac{Q}{\phi \Delta S} \quad (A.5)$$

where Q is the cumulative total throughput in pore volumes. Equation (A.5) can be written in quadratic form in powers of y, which results in:

$$\frac{[\beta^2(m-1)(\bar{m}-1) - \beta(m-1)(\bar{m}-m)]}{[\beta(\bar{m}-1) - (\bar{m}-m) + \beta(m-1)]h} y^2 + y + \frac{h^2 - (mhQ/L\phi\Delta S)}{[\beta(\bar{m}-1) - (ET-m) + \beta(m-1)]h} = 0 \quad (A.6)$$

Equation (A.6) is a standard quadratic equation whose solution is:

$$y = \frac{-1 \pm \sqrt{1 - \frac{4(m-1)[\beta(\bar{m}-1) - (\bar{m}-m)]\beta[h^2 - (mhQ/L\phi\Delta S)]}{[\beta(\bar{m}-1) + \beta(m-1) - (\bar{m}-m)]^2 h^2}}}{\frac{2(m-1)[\beta(\bar{m}-1) - (\bar{m}-m)]\beta}{[\beta(\bar{m}-1) + \beta(m-1) - (\bar{m}-m)]h}} \quad (A.7)$$

This equation can be simplified if the following definitions are used:

$$\bar{m} - 1 = \bar{\alpha}; \quad m - 1 = \alpha; \quad \text{so that} \quad \bar{m} - m = \bar{\alpha} - \alpha \quad (A.8)$$

Using these definitions, Eq. (A.7) is reduced to:

$$y = \frac{h \sqrt{(\alpha - \bar{\alpha} + \alpha\beta + \bar{\alpha}\beta)^2 - 4\alpha\beta(\alpha - \bar{\alpha} + \bar{\alpha}\beta)} \left[ 1 - \frac{mQ}{Lh\phi\Delta S} \right] - h(\alpha - \bar{\alpha} + \alpha\beta + \bar{\alpha}\beta)}{2\alpha\beta(\alpha - \bar{\alpha} + \bar{\alpha}\beta)} \quad (A.9)$$

The solution of Eq. (A.1) given as Eq. (A.9) has been used in Section 5 [Eq. (5.59)] for recovery predictions of the combination-drive displacement

## APPENDIX B APPLICATION OF SCALING AND MODELING LAWS

### B.1 INTRODUCTION

The application of scaling laws for scaled-model studies is well-established in the literature. The scaling groups have been derived by many investigators for similar two dimensional models. These scaling groups are not unique in most cases but the basic concept is the same, i.e., the ratio of important forces and geometrical configuration must be the same in the model as in the prototype. The variations seen in these scaling groups from one study to another come from the simplifying assumptions and the selection of the variables to be arbitrarily fixed.

At the time when these scaling groups were derived, the description of the flow mechanism and the frontal behavior of a foam flood was somewhat speculative. For the purpose of scaling the model, the foam was assumed to be propagating through the porous medium as a single phase homogeneous fluid. The dimensionless groups derived here were used to run a series of experiments to determine whether the scaling laws were applicable with foam in the system. Thus the values of these groups were varied and recovery results were graphed to see their effect (Figs. 6.3, 6.4 and 6.5). Later it was seen from the observations (Section 6.2) that flow in the two-dimensional sandpack did not support this assumption. Thus approximate analytical modeling was pursued (Section 5).

### B.2 ASSUMPTIONS

The following assumptions have been made in deriving the scaling groups:

- (1) Foam propagates through the porous medium as a single phase homogeneous fluid of low compressibility.
- (2) Foam has high stability so that it can propagate through the entire formation without breakdown.

### B.3 MATHEMATICAL FORMULATION

The two-dimensional displacement of oil by the injection of an incompressible fluid through a porous medium is governed by the continuity equation:

$$\frac{\partial}{\partial x} (v_x f_x) + \frac{\partial}{\partial z} (v_z f_z) = -\phi \frac{\partial S}{\partial t} \quad (\text{B.1})$$

where  $v_x$  and  $v_z$  are total flow rates per unit bulk cross-section in the directions of  $x$  and  $z$ , respectively; and  $f_x$  and  $f_z$  are the fraction of oil in the total fluid stream flowing in the corresponding direction as defined by Leverett (1941) in the fractional flow equation:

$$f_u = \frac{1 + k_u \frac{k_{r0}}{v_{iu} \mu_0} \left[ \frac{\partial P_c}{\partial u} - g \Delta \rho \sin \alpha_d \right]}{1 + \frac{k_0}{k_d} \frac{\mu_d}{\mu_0}} \quad (\text{B.2})$$

where subscript  $d$  denotes the properties of injected fluid which was surfactant solution in this study, and  $u$  denotes the direction of flow. This equation can be simplified by defining the permeability and mobility functions as follows:

$$\xi = \frac{1}{1 + \frac{k_0}{k_d} \frac{\mu_d}{\mu_0}} \quad (\text{B.3})$$

$$\psi = \xi k_{r0} \quad (\text{B.4})$$

Substituting  $\xi$  and  $\psi$  into Eq. (B.2) and rearranging gives:

$$f_u = \xi + \psi \frac{k_u}{v_{iu} \mu_0} \left[ \frac{\partial P_c}{\partial u} - g \Delta \rho \sin \alpha_d \right] \quad (\text{B.5})$$

For flow in the  $x$  direction,  $f_u = f_x$ ,  $\sin \alpha_d = 0$ , and Eq. (B.5) reduces to:

$$f_x = \xi + \psi \frac{k_x}{v_{ix} \mu_0} \frac{\partial P_c}{\partial x} \quad (\text{B.6})$$

Multiplying both sides by  $v_{ix}$  gives:

$$v_{ix} f_x = \xi v_{ix} + \psi \frac{k_x}{\mu_0} \frac{\partial P_c}{\partial x} \quad (\text{B.7})$$

Differentiating this equation along the  $x$  direction yields:

$$\frac{\partial}{\partial x} \left[ v_{ix} f_x \right] = \frac{\partial}{\partial x} \left[ \xi v_{ix} \right] + \frac{k_x}{\mu_0} \frac{\partial}{\partial x} \left[ \psi \frac{\partial P_c}{\partial x} \right] \quad (\text{B.8})$$

Similarly, for flow in the  $z$  direction,  $\sin \alpha_d = 1$ , and Eq. (B.5) becomes:

$$v_{iz} f_z = \xi v_{iz} + \psi \frac{k_z}{\mu_0} \frac{\partial P_c}{\partial z} - \psi \frac{k_z}{\mu_0} g \Delta \rho \quad (\text{B.9})$$

which on differentiation along the  $z$  direction becomes:

$$\frac{\partial}{\partial z} \left[ v_{iz} f_z \right] = \frac{\partial}{\partial z} \left[ \xi v_{iz} \right] + \frac{k_z}{\mu_0} \frac{\partial}{\partial z} \left[ \psi \frac{\partial P_c}{\partial z} \right] - \frac{k_z}{\mu_0} g \Delta \rho \frac{\partial \psi}{\partial z} \quad (\text{B.10})$$

When the first and second terms in the continuity equation, Eq. (B.1), are replaced by Eqs. (B.8) and (B.10), the following flow equation for a prototype porous medium is obtained:

$$\begin{aligned} \phi \frac{\partial S_d}{\partial t} + \frac{\partial}{\partial x} \left[ \xi v_x \right] + \frac{\partial}{\partial z} \left[ \xi v_z \right] + \frac{k_x}{\mu_0} \frac{\partial}{\partial x} \left[ \psi \frac{\partial P_c}{\partial x} \right] \\ + \frac{k_z}{\mu_0} \frac{\partial}{\partial z} \left[ \psi \frac{\partial P_c}{\partial z} \right] - \frac{k_z g \Delta \rho}{\mu_0} \left[ \frac{\partial \psi}{\partial z} \right] = 0 \end{aligned} \quad (B.11)$$

The flow equation for the model can be written immediately due to the similarity involved:

$$\begin{aligned} \phi' \frac{\partial S'_d}{\partial t'} + \frac{\partial}{\partial x'} \left[ \xi' v'_x \right] + \frac{\partial}{\partial z'} \left[ \xi' v'_z \right] + \frac{k'_x}{\mu_0} \frac{\partial}{\partial x'} \left[ \psi' \frac{\partial P'_c}{\partial x'} \right] \\ + \frac{k'_z}{\mu_0} \frac{\partial}{\partial z'} \left[ \psi' \frac{\partial P'_c}{\partial z'} \right] - \frac{k'_z g \Delta \rho'}{\mu_0} \left[ \frac{\partial \psi'}{\partial z'} \right] = 0 \end{aligned} \quad (B.12)$$

The variables are primed for the model equation to indicate they are different than in the prototype.

#### B4 DEFINING THE FUNCTIONAL CONSTANTS

The scaling factors are determined after the flow equation is transformed by replacing the model parameters with expressions containing the reservoir parameters and appropriate constants which relate the model and reservoir parameters. The method of transformation is described in next section, whereas these constants are arbitrary defined here as follows:

$$\frac{x'}{x} = A_x \quad (B.13), \quad \frac{z'}{z} = A_z \quad (B.14), \quad \frac{k'_x}{k_x} = B_x \quad (B.15),$$

$$\frac{k'_z}{k_z} = B_z \quad (B.16), \quad \frac{\mu_0'}{\mu_0} = E \quad (B.17), \quad \frac{\mu_d'}{\mu_d} = r \quad (B.18),$$

$$\frac{k'_{rd}}{k_{rd}} = m \quad (B.19), \quad \frac{S_0'}{k'_{r0}} = n \quad (B.20), \quad \frac{\xi'}{\xi} = b \quad (B.21),$$

$$\frac{\psi'}{\psi} = \frac{\xi k_{r0}}{\xi' k'^0} = b n \quad (B.22), \quad \frac{\phi'}{\phi} = C \quad (B.23),$$

$$\frac{q'}{q} = G \quad (B.24), \quad \frac{\Delta \rho'}{\Delta \rho} = D \quad (B.25)$$

It is **assumed** here **that the saturation** changes of the displacing phase **are the** same in the model and the reservoir **to simplify the derivation of the scaling groups**. **This** assumption is valid only when **high** concentrations of surfactants **are** involved, Eq. (B.26) holds, and where the **pore geometries are similar** in model and reservoir

$$\frac{\partial S_d}{\partial x} = \frac{\partial S'_d}{\partial x'} \quad (\text{B.26})$$

$$(S_d)_x = (S'_d)_{x'} \quad (\text{B.27})$$

The ratio between **some** parameters can be deduced **from** the fundamental **constants** defined in **Eqs. (B.13) through (B.25)**. **Thus the** ratios between velocities and volumes **are** given as:

$$\frac{v_x}{v'_x} = \frac{q / yz}{q' / yz'} = \frac{G}{A_z} \quad (\text{B.28})$$

$$\frac{v_z}{v'_z} = \frac{q / yz}{q' / yz'} = \frac{G}{A_x} \quad (\text{B.29})$$

$$\frac{\Delta V}{\Delta V'} = \frac{q t}{q' t'} = \frac{x y z \phi}{x' y' z' \phi'} \quad (\text{B.30})$$

Equation (B.30) can be rearranged, and after substitutions **from** Eqs. (B.13), (B.14), (B.23) and (B.24) it **becomes**:

$$\frac{t}{t'} = \frac{x y z \phi / q}{x' y' z' \phi' / q'} = \frac{A_x A_z C}{G} \quad (\text{B.31})$$

The capillary **pressure** gradients in both the **x** and the **z** direction **are** complex functions of pore geometries of **each** individual porous medium, and can not be correlated. The capillary **pressure** gradients can, however, be related indirectly as described below. By **the chain** rule of differentiation, the capillary **pressure** gradients in the **x** direction can be written as:

$$\frac{\partial P_c}{\partial x} = - \left[ \frac{dP_c}{dS_d} \right] \frac{\partial S_d}{\partial x} \quad (\text{B.32})$$

Similarly, for the **z** direction:

$$\frac{\partial P_c}{\partial z} = - \left[ \frac{dP_c}{dS_d} \right] \frac{\partial S_d}{\partial z} \quad (\text{B.33})$$

The capillary pressure as a function of saturation can thus be related by a constant  $F$ :

$$F = \frac{\left[ \frac{dP_c}{dS_d} \right]}{\left[ \frac{dP'_c}{dS'_d} \right]} \quad (\text{B.34})$$

It is also assumed here that the capillary pressure-saturation relationship can be correlated by using the following form of the Leverett J-function:

$$J(S_w) = \frac{P_c}{\sigma \cos \theta} \sqrt{k/\phi} \quad (\text{B.35})$$

Thus differentiating this J-function with saturation, substituting in Eq. (B.34), and recognizing from Eq. (B.27) that the saturation changes are the same in model and prototype, Eq. (B.34) becomes:

$$F = \frac{1/\sigma \cos \theta \sqrt{\phi/k}}{1/\sigma' \cos \theta' \sqrt{\phi'/k}} \quad (\text{B.36})$$

## B.5 TRANSFORMING THE FLOW EQUATION

Modeling Eq. (B.12) can now be transformed to the reservoir equation, Eq. (B.11), by substituting the reservoir parameters and appropriate constants as defined by Eqs. B.13 through B.36. The step-by-step procedure to transform each term individually is shown below. Substituting for  $\phi' S'_d$  and  $t$  in the first term of Eq. (B.12), from Eqs. (B.23), (B.27) and (B.31) results in:

$$\phi' \frac{\partial S'_d}{\partial t'} = \frac{\phi}{C} \frac{\partial (S_d)}{\partial \left[ \frac{G}{A_x A_z C} t \right]} = \frac{A_x A_z}{G} \phi \frac{\partial S_d}{\partial t} \quad (\text{B.37})$$

Substituting for  $x' \xi'$  and  $v'_x$  in the second term of Eq. (B.12), from Eqs. (B.13), (B.21) and (B.28) results in:

$$\frac{\partial}{\partial x'} \left[ \xi' v'_x \right] = \frac{\partial \left[ \frac{1}{b} \frac{A_z}{G} \xi v_x \right]}{\partial \left[ \frac{1}{A_x} x \right]} = \frac{A_x A_z}{b G} \frac{\partial}{\partial x} \left[ \xi v_x \right] \quad (\text{B.38})$$

Substituting for  $z' \xi'$  and  $v'_z$  in the third term of Eq. (B.12), from Eqs. (B.14), (B.21) and (B.29) results in:

$$\frac{\partial}{\partial z'} \left[ \xi' v'_z \right] = \frac{\partial \left[ \frac{1}{b} \frac{A_x}{G} \xi v_z \right]}{\partial \left[ \frac{1}{A_z} z \right]} = \frac{A_x A_z}{b G} \frac{\partial}{\partial z} \left[ \xi v_z \right] \quad (\text{B.39})$$

The terms  $x'$ ,  $k_x$ ,  $\mu_o$ ,  $\psi'$  and  $P_c'$  in the fourth term from Eq. (B.12) can be replaced by Eqs. (B.13), (B.15), (B.17), (B.22) and (B.34). The capillary pressure gradient in this term can be expanded using the chain rule of differentiation [Eq. (B.32)]. These substitutions result in:

$$\frac{k_x'}{\mu_o} \frac{\partial}{\partial x'} \left[ \psi' \frac{\partial P_c'}{\partial x'} \right] = - \frac{E A_x A_x}{b n F B_x} \frac{k_x}{\mu_o} \frac{\partial}{\partial x} \left[ \psi \frac{dP_c}{dS_d} \frac{\partial S_d}{\partial x} \right] \quad (\text{B.40})$$

Similarly, substituting for  $z'$ ,  $k_z$ ,  $\mu_o$ ,  $\psi'$  and  $P_c'$  in the fifth term of Eq. (B.12), from Eqs. (B.14), (B.16), (B.17), (B.22) and (B.34); and using the chain rule of differentiation [Eq. (B.33)] yields:

$$\frac{k_z'}{\mu_o} \frac{\partial}{\partial z'} \left[ \psi' \frac{\partial P_c'}{\partial z'} \right] = - \frac{E A_z A_z}{b n F B_z} \frac{k_z}{\mu_o} \frac{\partial}{\partial z} \left[ \psi \frac{dP_c}{dS_d} \frac{\partial S_d}{\partial z} \right] \quad (\text{B.41})$$

Substituting for  $z'$ ,  $k_z$ ,  $\mu_o$ ,  $\psi'$  and  $\Delta\rho'$  in the last term of Eq. (B.12), from Eqs. (B.14), (B.16), (B.17), (B.22) and (B.25) results in:

$$\frac{k_z' g \Delta\rho'}{\mu_o} \left[ \frac{\partial \psi'}{\partial z'} \right] = \frac{k_z}{B_z} g \frac{\Delta\rho}{D} \frac{E}{\mu_o} \left[ \frac{\partial \left[ \frac{\psi}{b n} \right]}{\partial \left[ \frac{z}{B_z} \right]} \right] = \frac{E A_z}{b n B_z D} \frac{k_z g \Delta\rho}{\mu_o} \left[ \frac{\partial \psi}{\partial z} \right] \quad (\text{B.42})$$

The basic modeling equation [Eq. (B.12)] is transformed to prototype variables by substituting these transformed terms given in Eqs. (B.37) through (B.42) as follows:

$$\begin{aligned} & \left[ \frac{A_x A_x}{G} \right] \phi \frac{\partial S_d}{\partial t} + \left[ \frac{A_x A_x}{b G} \right] \frac{\partial}{\partial x} \left[ \xi v_x \right] + \left[ \frac{A_z A_x}{b G} \right] \frac{\partial}{\partial z} \left[ \xi v_z \right] \\ & - \left[ \frac{E A_x A_x}{b n B_x F} \right] \frac{k_x}{\mu_o} \frac{\partial}{\partial x} \left[ \psi \frac{dP_c}{dS_d} \frac{\partial S_d}{\partial x} \right] \\ & - \left[ \frac{E A_z A_z}{b n B_z F} \right] \frac{k_z}{\mu_o} \frac{\partial}{\partial z} \left[ \psi \frac{dP_c}{dS_d} \frac{\partial S_d}{\partial z} \right] \\ & - \left[ \frac{E A_z}{b n B_z D} \right] \frac{k_z g \Delta\rho}{\mu_o} \left[ \frac{\partial \psi}{\partial z} \right] = 0 \end{aligned} \quad (\text{B.43})$$

This equation can be simplified by multiplying by  $G/A_x A_z$  and rearranging:

$$\begin{aligned}
 \phi \frac{\partial S_d}{\partial t} + \left[ \frac{1}{b} \right] \frac{\partial}{\partial x} \left[ \xi v_x \right] + \left[ \frac{1}{b} \right] \frac{\partial}{\partial z} \left[ \xi v_z \right] \\
 - \frac{E G A_x}{B_x F A_z b n} \frac{k_x}{\mu_0} \frac{\partial}{\partial x} \left[ \psi \frac{dP_c}{dS_d} \frac{\partial S_d}{\partial x} \right] \\
 - \frac{E G A_z}{B_z F A_x b n} \frac{k_z}{\mu_0} \frac{\partial}{\partial z} \left[ \psi \frac{dP_c}{dS_d} \frac{\partial S_d}{\partial z} \right] \\
 - \frac{E G}{B_z D A_x b n} \frac{k_z g \Delta \rho}{\mu_0} \left[ \frac{\partial \psi}{\partial z} \right] = 0
 \end{aligned} \tag{B.44}$$

Equation (B.44) is the transformed flow equation for the model; and is expressed in terms of the reservoir parameters and the arbitrarily defined constants.

## B.6 THE DETERMINATION OF SCALING GROUPS

The performance in the model is expected to be the same as in the prototype reservoir, provided the coefficients of all the terms in the transformed flow equation [Eq. (B.44)] are equal to the corresponding coefficients of the prototype flow equation [Eq. (B.11)]. In the following steps, the nonequal coefficients of Eq. (B.44) are set equal to the corresponding coefficients of Eq. (B.11). The relationships thus obtained are used to identify the scaling groups. This process is performed in the following steps.

Comparing the coefficients of the second and third terms of Eq. (B.11) and (B.44):

$$\frac{1}{b} = 1 \quad \rightarrow \quad b = 1 \quad \rightarrow \quad \xi = \xi' \tag{B.45}$$

From the definition of  $\xi$  [Eq. (B.3)], it can be inferred from the above equation that:

$$\left[ \frac{k_{ro}}{k_{rd}} \frac{\mu_d}{\mu_0} \right]_{model} = \left[ \frac{k_{ro}}{k_{rd}} \frac{\mu_d}{\mu_0} \right]_{prototype} \tag{B.46}$$

The ratios of model and prototype parameters contained in the above equation can be replaced by their definitions given in Eqs. (B.17) through (B.20), which reduces Eq. (46) to:

$$n = \frac{m E}{r} \tag{B.47}$$

Comparing the coefficients of the fourth terms of Eq. (B.11) and (B.44); replacing  $n$  in the resulting expression from Eq. (B.47) results in:

$$\frac{E G A_x}{B_x F A_x b n} = 1, \quad \rightarrow \quad E G A_x = B_x F A_x b n = B_x F A_x b \frac{m E}{r} \quad (\text{B.48})$$

Taking  $b$  as unity [Eq. (B.45)], the above expression reduces to:

$$r G A_x = B_x F A_x m \quad (\text{B.49})$$

The constants in this equation are replaced by their definitions given in Eqs. (B.13), (B.14), (B.15), (B.18), (B.19), (B.24) and (B.36), resulting in:

$$\left[ \frac{q \mu_d x}{z k_{rd} \sigma \cos \theta k_x \sqrt{\phi / k}} \right]_{\text{model}} = \left[ \frac{q \mu_d x}{z k_{rd} \sigma \cos \theta k_x \sqrt{\phi / k}} \right]_{\text{prototype}} \quad (\text{B.50})$$

The coefficients of the fifth term can be compared in a similar fashion to yield:

$$\frac{E G A_x}{B_x F A_x b n} = 1 \quad \rightarrow \quad E G A_x = B_x F A_x b n = B_x F A_x \frac{m E}{r} \quad (\text{B.51})$$

After substituting for  $b$  from Eq. (B.3) and  $n$  from Eq. (B.47) as done in the previous equations, the above equation is reduced to:

$$r G A_x = B_x F A_x m \quad (\text{B.52})$$

Due to the similarity of this equation with Eq. (B.49), the group obtained from this equation will closely resemble the one given in Eq. (B.50). One possibility is to simplify the above equation by combining with Eq. (B.49):

$$B_x A_x^2 = A_x^2 B_x \quad (\text{B.53})$$

Substituting for the definitions from Eqs. (B.13) through (B.16), this equation becomes:

$$\left[ \frac{x}{z} \sqrt{\frac{k_z}{k_x}} \right]_{\text{model}} = \left[ \frac{x}{z} \sqrt{\frac{k_z}{k_x}} \right]_{\text{prototype}} \quad (\text{B.54})$$

Similarly, the coefficients of the last term have to be compared. Also the values of  $b$  and  $n$  have to be substituted from Eq. (B.3) and (B.4) as before. These two steps result in:

$$\frac{E G}{B_x D A_x b n} = 1 \quad \rightarrow \quad E G = B_x D A_x \frac{m E}{r} \quad \rightarrow \quad r G = B_x D A_x m \quad (\text{B.55})$$

For simplification, Eqs. (B.52) and (B.55) can be combined to yield:

$$F = D A_z \quad (B.56)$$

Substituting for the definitions from Eqs. (B.13), (B.25) and (B.36) as &ne before, this equation becomes:

$$\left[ \frac{\sigma \cos \theta}{z \Delta \rho} \sqrt{\frac{\phi}{k}} \right]_{model} = \left[ \frac{\sigma \cos \theta}{z \Delta \rho} \sqrt{\frac{\phi}{k}} \right]_{prototype} \quad (B.57)$$

## B.7 SUMMARY OF THE SCALING GROUPS

The following is the *summary* of the scaling groups determined in this section. If a close approximation of the performance is desired, the values of these scaling groups for the model should be the same as for the reservoir.

$$\left[ \frac{k_{ro} \mu_d}{k_{rd} \mu_o} \right]_{model} = \left[ \frac{k_{ro} \mu_d}{k_{rd} \mu_o} \right]_{prototype} \quad (B.46)$$

$$\left[ \frac{q \mu_d x}{z k_{rd} \sigma \cos \theta k_x \sqrt{\phi / k}} \right]_{model} = \left[ \frac{q \mu_d x}{z k_{rd} \sigma \cos \theta k_x \sqrt{\phi / k}} \right]_{prototype} \quad (B.50)$$

$$\left[ \frac{x}{z} \sqrt{\frac{k_z}{k_x}} \right]_{model} = \left[ \frac{x}{z} \sqrt{\frac{k_z}{k_x}} \right]_{prototype} \quad (B.54)$$

$$\left[ \frac{\sigma \cos \theta}{z \Delta \rho} \sqrt{\frac{\phi}{k}} \right]_{model} = \left[ \frac{\sigma \cos \theta}{z \Delta \rho} \sqrt{\frac{\phi}{k}} \right]_{prototype} \quad (B.57)$$

## APPENDIX C OPERATIONAL DETAILS OF FLOW LINES USED IN THE GLASS SANDPACK

The apparatus used for the experimental part of this study was described in Section 3. The material presented in this appendix is specifically focused on the flow line design of this apparatus.

The flow network can be essentially subdivided into: (1) the flow lines used for cleaning, (2) the flow lines used when the model is being saturated with water or oil, and (3) the flow lines used when a run is in progress. Each of these operations is described in the following sections.

### C.1 FLOW LINES USED FOR CLEANING THE MODEL

The cleaning process consists of injecting large volumes of nitrogen, carbon dioxide, water, mineral spirits and tertiary butyl alcohol. To avoid contamination, non-miscible fluids had to be kept and transported separately. Thus separate flow lines were provided for gas, aqueous and nonaqueous phases. The step-by-step procedures for gas injection, water injection and other liquids (non-aqueous) injection are given below. All numbers and letters within parenthesis in the following description refer to Fig. 3.1.

#### C.1.1 Method of Gas Injection

The gas was obtained from a carbon dioxide cylinder by opening the pressure regulator Valves 1 to the desirable pressure setting. The filter was checked and replaced occasionally, otherwise some dirt, moisture and condensate could have entered the sandpack, permanently damaging it.

The following valves were opened in the following order: Valve 2 and Valve 3 towards the right, Valve 4 towards the right, injection end Valves 16 through 20, producing end Valves 21 through 25, and, the main outlet Valve 26 towards the right.

The gas coming out of the sandpack was exhausted to the air whereas any liquids present in the model were collected in the waste collector (S).

#### C.1.2 Method of Water Injection

The injection of a liquid directly in the sandpack was avoided because excessive pressures could have been reached if flow was somehow hindered which happened quite often when foam was generated. An indirect injection method was designed in which the water was first filled from the distilled water container (X), into the aqueous slug vessel (L) through a pump (K), and then was driven into the sandpack by nitrogen at a constant pressure instead of a constant rate.

The systematic procedure was as follows. The slug vessel Valve 8 and the gas bleed Valve 10 were opened. Container (X) was filled with distilled water and the water pump (K) was operated to fill the water slug vessel (L). After the vessel had been filled, the slug vessel Valve 8 and the gas bleed Valve 10 were closed. The nitrogen regulator was opened and set to a desirable pressure (not to exceed 25 psig). The filter was checked and replaced when necessary. Valve 3 was opened towards the bottom, Valve 4 towards the left, Valve 5 towards

the right, Valve 6 towards the right; the main outlet Valve 26 and the producing end Valve 21 were opened towards the right, and all the pressure was bled. Then these two valves were closed again, the injection end Valves 16 through 20 were opened very slowly [Caution: opening the injection valves suddenly damaged the sandpack], the main producing end Valves 21 through 25 were opened, and finally, the outlet Valve 26 was opened towards the right to initiate continuous flow. The nitrogen coming out of the sandpack was being exhausted in the air, whereas the liquids were collected in the waste collector (S).

### C.13 Method of Nonaqueous Phase Injection

The procedure for mineral spirits, tertiary butyl alcohol and oil injection was very similar to the procedure for injecting water, except that a separate slug vessel (M), a separate pump (J) and separate flow lines were used. The same slug vessel, pump and flow lines were used, however, for each non-aqueous phase. Thus it was imperative to rinse the lines thoroughly before filling the tank.

The systematic procedure was as follows: The slug vessel Valve 7 and the gas bleed Valve 9 were opened, the nonaqueous phase pump (J) was operated to fill the nonaqueous phase slug vessel (M). After the slug had been filled, the slug vessel Valve 7 and the gas bleed Valve 9 were closed. The nitrogen regulator was opened and set to the desired pressure (not to exceed 25 psig). The filter was checked and replaced when necessary. Valve 3 was opened towards the bottom, Valve 4 towards the left, Valve 5 towards the left, Valve 6 towards the left, the main outlet Valve 26 and the producing end Valve 21 towards the right and all the pressure bled. Then these two valves were closed again, the injection end Valves 16 through 20 were opened very slowly, and the producing end Valves 21 through 25, and finally, the main outlet Valve 26 was opened towards the right to initiate continuous flow.

## C.2 FLOW LINES USED FOR SATURATING THE MODEL

After cleaning was completed, the model was first saturated with distilled water, then oil injection began. Several pore volumes of oil had to be injected before the water saturation reached the irreducible saturation level. The procedure for saturating with water was the same as described in Section C.1.2, and the procedure for saturating with oil was the same as described in Section C.1.3.

## C.3 FLOW LINES USED FOR MAKING RUNS

These flow lines were used whenever a run was in progress. Since the mode of injection was variable, a combination of different flow lines had to be used. Depending on the location of injection and/or production intervals chosen, certain of injection Valves 16 through 20 and producing end Valves 21 through 25 were opened or closed. All the auxiliary equipment, such as the pressure transducer, the chart recorder, the timers, the automatic camera and the fraction collector had to be turned on and set properly before opening the flow lines. Metering Valves 13 through 15 on the pressure line were also opened before the runs were started. The procedure used for opening the flow lines for each type of injection mode is as follows:

### C.3.1 For Simultaneous Surfactant-Gas Injection Runs

First the gas was bled from the sandpack by opening the main outlet Valve 26 and producing end Valve 21 for a few minutes and closing them again. The nitrogen regulator (R1) was set to the desired pressure. The filter was checked and replaced when necessary. The gas metering pump control was set to the desired values; the foam generator Valve 27 and 28 were opened towards the left, and the injection Valves 16 through 20 were opened towards bleed; then the metering pump (E) was turned on. Both gas and surfactant were then mixed and drained out. Draining was continued until the lines had been thoroughly rinsed and flow conditions stabilized. To start the run, only those injection end Valves 16 through 20 and producing end Valves 21 through 25 were opened which were prescribed for the run. The main outlet Valve 26 was opened towards the bottom to initiate production.

### C.3.2 For Preformed Foam Injection Runs

The procedure for preformed foam flow was exactly the same as the simultaneous surfactant-gas injection method described in the previous section (C.3.1), except that the gas from the gas metering pump (D) and the surfactant from the liquid metering pump (E) were injected simultaneously into the foam generator (C), and the preformed foam from the generator was injected into the model. The only difference, therefore, was that the Valves 27 and 28 were opened towards the right instead of the left. If a dry foam injection was desirable, the excess surfactant solution was drained out from the bottom of the foam generator (C) by opening Valve 29 and collecting the excess surfactant solution in vessel (W).

### C.3.3 For Slug Type Injection Runs

In this type of run, one or more surfactant slugs were injected during the run. When a liquid slug was to be injected, the gas injection through the model was terminated, and resumed after the liquid slug injection had been completed. The procedure for the slug injection was simple. The water pump (K) was connected to the surfactant source instead of a water source, and exactly the same procedure was followed as described in the section for water injection (C.1.2). When slug injection was over, all valves were closed and the procedure for gas injection was followed (C.1.1).